

**Joint Contact Modelling of Articular Cartilage
in
Synovial Joints**

Sainath Shrikant Pawaskar

Submitted in accordance with the requirements for the degree of
Doctor of Philosophy

The University of Leeds
School of Mechanical Engineering

April 2010

The candidate confirms that the work submitted is his own, except where work which has formed part of jointly-authored publications has been included. The contribution of the candidate and the other authors to this work has been explicitly indicated below. The candidate confirms that appropriate credit has been given within the thesis where reference has been made to the work of others.

This copy has been supplied on the understanding that it is copyright material and that no quotation from the thesis may be published without proper acknowledgement

The right of Sainath Shrikant Pawaskar to be identified as Author of this work has been asserted by him in accordance with the Copyright, Designs and Patents Act 1988.

© 2010 The University of Leeds and Sainath Shrikant Pawaskar

Jointly Authored Publications

- 1) Pawaskar, S.S., Jin, Z., Ingham, E., and Fisher, J. A novel, generic and robust approach to the contact analysis of articular cartilage. In *Journal of Biomechanics, 16th Congress, European Society of Biomechanics* (Eds. R. Huiskes and Guilak, F.), Lucerne, Switzerland, 2008, S302, Presentation O-299.

This forms the basis of **Chapter 2** and was carried out by the author of this thesis in its entirety.

- 2) Pawaskar, S. S., Fisher, J., and Jin, Z., 2010, "Robust and General Method for Determining Surface Fluid Flow Boundary Conditions in Articular Cartilage Contact Mechanics Modeling," *Journal of Biomechanical Engineering*, 132(3), pp. 8 (031001).

This was a more exhaustive study based on the publication mentioned in **1)**. This work was carried out the current author and **Chapter 2** is based on it.

- 3) Pawaskar, S. S., Ingham, E., Fisher, J., and Jin, Z. M. Importance of clearance on contact mechanics of hemiarthroplasty in hip joints. In: *55th Annual Meeting of the Orthopaedic Research Society*. 2009, Las Vegas, NV, **34**. Poster No.: 2405.

This investigation was carried out by the current author and forms a part of **Chapter 5**.

Acknowledgement

Even though hard work, dedication and perseverance are important in shaping one's career, it is the help from others and generosity of those around you which are often easily forgotten, that make up the fundamental building blocks in that endeavour.

I am grateful to my parents, Shrikant and Shrimati who are no longer with us, for all the efforts they put so that I can have a decent shot at life, even when it was beyond their means. I thank my brother Ajit, sisters Shraddha and Leena, and friends Prasad and Deepali who were patient and stood by me in whatever I chose to do. I sincerely thank Mr. Joseph M. Fernandes who always encouraged me to do the right thing and without his balanced views on my plans to pursue PhD, I would not have come to the UK in the first place.

The expertise of technicians Adrian, Phillip, Irwin, Lee, Amisha, Jane and Mr Stephen Terry was important to my research and so was help from Louise, Sophie and Jia. Alison and Nagitha were always helpful whenever I approached them. I am grateful to Qingen, Nic, Stewart, Simon, Mazen, Jayantha, Peter and Adam for helping me in whatever way possible and for some of the intelligent conversations we have had. I am honoured to have had this opportunity to work with my supervisors Professor Zhongmin Jin, Professor Eileen Ingham and Professor John Fisher in this centre of excellence. Their inputs, ideas, support and guidance were invaluable and helped me remain on the track. Debra and Cheryl were helpful both in their administrative role as well as a means of decoding John's handwriting.

It was a pleasure to have been associated with Assistant Professor Salvatore Federico from University of Calgary, Ms. Kathryn E. Keenan from Stanford University, Associate Professor Nicole M. Grosland from University of Iowa, Research Assistant Professor Andrew E. Anderson from University of Utah, Professor Gerard A. Ateshian from Columbia University, Dr. Patrick Knupp from Sandia National Laboratories, Dr. Jason A. Kraftcheck from University of Wisconsin-Madison and Dr. Ross Cotton from Simpleware Ltd. Their invaluable help, in-depth discussions and tips from their personal experiences steered my research towards the desired goals.

Devonshire Hall has been my home for almost 4 years. I thank my wardens Dr. Darron Dixon-Hardy and Dr. Joanna Drugan as well as Hall Managers Mrs. Hilary Collins and Miss Catherine Miller for making my stay memorable and comfortable. I am thankful to sub-wardens and the students on my floor all these years and had to let a few of their fun filled gatherings go because of me. The presence of Nandan, Atul and Chandra Shekhar in Leeds helped me avoid home sickness and some of the experiments we performed with cooking were quite amusing.

I am also thankful to all the others whose names have not appeared here but I am sure, have contributed to this work in one way or the other. Lastly, I am grateful to Overseas Research Students Awards Scheme and School of Mechanical Engineering, University of Leeds for funding my research.

In Loving Memory of My Parents

Abstract

Hip joint is one of the important load bearing joints and has been extensively studied to investigate contact mechanics and tribology. It has known to experience high contact forces and stresses. However, cartilage shows remarkable lubricating and wear properties, and survives the lifetime of a person. Biphasic lubrication based on the principle of fluid load support has provided an explanation for this. However, when, the cartilage fails the part or whole of the joint needs to be replaced and hemiarthroplasty is one such remedy.

Three-dimensional finite element models with elastic/hyperelastic cartilage have been used to investigate contact mechanics of the hip joint. However, to understand the role of interstitial fluid in contact mechanics and tribology, cartilage has to be modelled as biphasic material. Interventions such as hemiarthroplasty may alter this phenomenon and hence it is also important to know the extent of this effect. This study was thus an attempt to address these issues.

An algorithm developed earlier for 2-D problems was refined, adapted and tested for 3-D problems to detect nodes in contact to impose surface fluid flow conditions. This was then used in natural hip joint where fluid load support was found to be very high (~94%). Three-dimensional hemiarthroplasty was then experimentally verified using porcine hips. The methodology was then used to investigate the effect of clearance in hemiarthroplasty which confirmed the earlier findings that undersizing of the femoral head increases both contact and shear stresses probably leading to cartilage erosion. The investigation of the activities of daily living showed lower contact stresses when compared to the outcomes of clinical studies and depended not only on the magnitude of the load but also on their locations. In all the models the total fluid load support was very high and was between ~90% which supported the biphasic lubrication hypothesis.

Contents

Jointly Authored Publications	iii
Acknowledgement	iv
Abstract	vi
Contents	vii
Figures.....	x
Tables	xiv
Abbreviations/Terms Used.....	xvi
Chapter 1 Introduction and Literature Review	1
1.1 Background.....	1
1.2 Hip Joint.....	3
1.2.1 Joint Structure	3
1.2.2 Proximal Femur	4
1.2.3 Acetabulum.....	4
1.3 Articular Cartilage.....	7
1.3.1 Structure.....	7
1.3.2 Constitutive Formulations	9
1.4 Hip Joint: Kinematics.....	10
1.5 Hip Joint: Kinetics.....	12
1.5.1 Theoretical Studies	13
1.5.2 Experimental and Clinical Studies.....	21
1.6 Biotribology	24
1.6.1 Friction.....	24
1.6.2 Wear.....	26
1.6.3 Lubrication	26
1.6.3.1 Biphasic Lubrication	26
1.6.3.2 Other Lubrication Mechanisms.....	28
1.7 Osteoarthritis.....	30
1.7.1 The Disease and its Etiology	30
1.7.2 Interventions	30

1.7.3 Hemiarthroplasty.....	32
1.8 Contact Mechanics of Hip Joint	36
1.8.1 Theoretical Studies	37
1.8.2 Experimental and Clinical Studies.....	40
1.8.3 Finite Element/Numerical Studies	46
1.9 Aims and Objectives.....	54
1.9.1 Aims	54
1.9.2 Objectives.....	54
Chapter 2 Contact Mechanics of Articular Cartilage	55
2.1 Introduction	55
2.2 Models and Methods	56
2.2.1 Contact formulation, detection and imposition of fluid flow boundary conditions.....	56
2.2.2 A Rigid Impervious Surface against Cartilage Surface.....	61
2.2.3 Cartilage Surface against Cartilage Surface	63
2.3 Results.....	66
2.4 Discussion.....	73
Chapter 3 Natural Human Hip Joint: Contact Mechanics and Fluid Load Support	77
3.1 Introduction	77
3.2 Model and Methods.....	77
3.3 Results	82
3.4 Discussion.....	84
Chapter 4 Porcine Hip Joint: Hemiarthroplasty Validation	88
4.1 Introduction	88
4.2 Model and Methods.....	88
4.2.1 Material properties derivation.....	89
4.2.2 Porcine acetabular cup – validation process.....	96
4.2.2.1 Experimental Measurement of Contact Stress and Area	96
4.2.2.2 μ CT Scanning and Segmentation.....	100
4.2.2.3 FE model	102
4.3 Results.....	105

4.4 Discussion.....	108
Chapter 5 Human Hip Joint with Hemiarthroplasty: Effect of Clearance on Fluid Load Support	113
5.1 Introduction	113
5.2 Model and Methods.....	114
5.3 Results	116
5.4 Discussion.....	119
Chapter 6 Applications of Hemiarthroplasty Model - Gait Analysis	123
6.1 Introduction	123
6.2 Models and Methods	123
6.3 Results	127
6.4 Discussion.....	134
Chapter 7 Overall Discussion and Conclusions	139
7.1 FE modelling of Natural Hip Joint and Hemiarthroplasty.....	139
7.2 Conclusions.....	145
7.3 Promising Potential	146
References	148
Appendix A Sample Input Files.....	182
A.1 Natural Hip Joint	182
A.2 Hip Joint with Hemiarthroplasty.....	186
Appendix B Pseudo Code of FORTRAN User Subroutines	190
B.1 Cartilage Surface against Cartilage Surface.....	190
B.2 A rigid Impervious Surface against Cartilage Surface	200
Appendix C Verification of Biphasic Jump Condition.....	201
Appendix D Mesh Sensitivity Analysis.....	204
Appendix E Publications	206
E.1 Published.....	206
E.1.1 Journals	206
E.1.2 Conferences.....	206
E.2 Under Review/Submitted	206
E.2.1 Journals	206
E.3 To be Submitted	207
E.3.1 Journals/Conferences	207

Figures

Figure 1.1 Hip Joint (Orthopaedics, 2007).....	3
Figure 1.2 Left Proximal Femur (Palastanga <i>et al.</i> , 2006)	4
Figure 1.3 Left Hip Bone in Lateral View (Palastanga <i>et al.</i> , 2006).....	5
Figure 1.4 Acetabulum (Palastanga <i>et al.</i> , 2006)	6
Figure 1.5 Acetabulum with labrum (Palastanga <i>et al.</i> , 2006)	6
Figure 1.6 Layered structure of Articular Cartilage (Mow and Huiskes, 2005)	8
Figure 1.7 Cartilage structure showing surface lamina and boundary layer (Forster and Fisher, 1999).....	9
Figure 1.8 Range of motion during one cycle of normal walking (Bergmann, 2001)	12
Figure 1.9 Typical two peak variation of resultant hip joint force versus time for normal walking (Bergmann, 2001)	13
Figure 1.10 Unipolar Head (Courtesy: DePuy).....	33
Figure 1.11 Bipolar Head (Courtesy: DePuy)	35
Figure 2.1 Flowchart of the proposed algorithm	59
Figure 2.2 Finite element mesh of axisymmetric model of articular cartilage with a rigid spherical indenter.....	63
Figure 2.3 Finite element mesh of axisymmetric model of joint contact mechanics of identical articular cartilages with node N1 0.2 mm below lower cartilage surface.....	64
Figure 2.4 Distribution of contact pressure at the cartilage surface after (a) 2 seconds and (b) 1000 seconds for different surface flow conditions.....	67
Figure 2.5 Distribution of pore pressure at the cartilage surface after (a) 2 seconds and (b) 1000 seconds for different surface flow conditions.....	68
Figure 2.6 Fluid velocity directions after 1000 seconds for (a) contact dependent, (b) free flow and (c) sealed surface flow conditions.....	69
Figure 2.7 Distribution of contact pressure at the cartilage surface after (a) 2 seconds and (b) 1000 seconds with contact dependent surface flow conditions for different element types.....	70

Figure 2.8 Distribution of pore pressure at the cartilage surface after (a) 2 seconds and (b) 1000 seconds with contact dependent surface flow conditions for different element types.....	71
Figure 2.9 Fluid pore pressure and solid compressive axial stress over time at node N1 cartilage-cartilage and equivalent models when non-linear geometry was not considered	72
Figure 2.10 Fluid pore pressure and solid compressive axial stress over time at node N1 cartilage-cartilage and equivalent models when non-linear geometry was considered.....	72
Figure 2.11 Fluid velocity directions after 300 seconds (a) in the contact zone (b) at the end of the contact zone; of the lower cartilage	73
Figure 3.1 FE model of natural hip joint.....	78
Figure 3.2 Axisymmetric and three-dimensional model of ball and cup	81
Figure 3.3 Contour plots of fluid pressure (MPa) after 1 second of loading in a) axisymmetric and b) 3D models.....	83
Figure 3.4 The contour of fluid pressure (MPa) on acetabular cartilage contact surface after 1 second of loading	83
Figure 3.5 Fluid velocity vectors after 1 second of loading	84
Figure 4.1 Flowchart for experimental validation of hemiarthroplasty	89
Figure 4.2 Porcine acetabular cartilage pin of 9 mm diameter.....	91
Figure 4.3 Location of porcine acetabular cup pins	91
Figure 4.4 Radius of curvature measurement using Talysurf	91
Figure 4.5 Thickness measurement of cartilage using Nikon profile projector	92
Figure 4.6 Indentation of porcine acetabular cartilage pin	93
Figure 4.7 Mean deformation curve for cartilage pins (n=21, Mean±SD).....	94
Figure 4.8 Geometry and FE Model of average cartilage pin	95
Figure 4.9 Vertical loading of acetabular cup using Instron and the use of Fuji film to measure contact stress and contact area.....	97
Figure 4.10 Typical loading curve on Instron.....	98
Figure 4.11 Measuring acetabular cup orientation using CMM.....	100
Figure 4.12 Flowchart for converting μ CT data into FE model.....	100
Figure 4.13 A typical μ CT slice	101

Figure 4.14 Segmented acetabular cup from μ CT.....	102
Figure 4.15 A typical FE model of acetabular bone.....	103
Figure 4.16 Acetabular cartilage mesh generation using blocks in IA-FEMesh (Grosland <i>et al.</i> , 2009).....	103
Figure 4.17 A typical final porcine acetabular cup FE model.....	104
Figure 4.18 FE Curve fitting to experimental deformation plot.....	105
Figure 4.19 FE deformation curve for a longer duration corresponding to the one in Figure 4.18.....	106
Figure 4.20 Rosette pattern of Fuji film after the removal of load.....	106
Figure 4.21 FE model prediction of the contact stresses in MPa (Refer Table 4-6 for specimen numbers).....	107
Figure 5.1 FE model of hip hemiarthroplasty.....	114
Figure 5.2 Contour plots of contact stresses and fluid pressure (MPa) after 3 seconds of loading for radial clearance of (a) 0.0 (b) 0.5, (c) 1.0 and (d) 2.0 mm.....	116
Figure 5.3 Variation of peak contact pressure with time for different radial clearances.....	117
Figure 5.4 Variation of peak fluid pressure with time for different radial clearances	118
Figure 5.5 Variation of percentage contact area with time for different radial clearances.....	118
Figure 5.6 Variation of total fluid load support with time for different radial clearances.....	119
Figure 6.1 Anatomic regions of acetabular cartilage (A) Lateral roof, (B) anterior horn, (C) medial roof, (D) posterior horn (Yoshida <i>et al.</i> , 2006).....	124
Figure 6.2 Node N1 at which fluid velocity was monitored during first cycle of slow, normal and fast walking.....	125
Figure 6.3 Hip joint contact forces during different activities of daily living (Bergmann, 2001).....	126
Figure 6.4 (a) Peak contact pressure, (b) peak fluid pressure, (c), (d) acetabular contact area and (e) total fluid load support during first cycle of slow, normal and fast walking.....	128
Figure 6.5 Total fluid load support for five normal walking cycles.....	129

Figure 6.6 Contours of contact stresses (MPa) in acetabular cup during different phases of first cycle of normal walking (A – Anterior; P – Posterior; M – Medial; L – Lateral)	130
Figure 6.7 Contours of contact stresses at 84% of first walking cycle	131
Figure 6.8 Fluid velocity at node N1 during first cycle of slow, normal and fast walking	131
Figure 6.9 (a) Peak contact pressure, (b) peak fluid pressure, (c), (d) acetabular contact area and (e) total fluid load support during first cycle of standing up and sitting down.....	132
Figure 6.10 (a) Peak contact pressure, (b) peak fluid pressure, (c), (d) acetabular contact area and (e) total fluid load support during first cycle of going down stairs and climbing stairs.....	133
Figure 6.11 (a) Peak contact pressure, (b) peak fluid pressure, (c), (d) acetabular contact area and (e) total fluid load support during first cycle of knee bending and standing on one leg.....	134
Figure C.1 Two-dimensional plane strain model of contact mechanics of poroelastic elements.....	201
Figure C.2 Fluid velocity vectors after 1 second of loading for (a) free flow, (b) sealed surface flow and (c) contact dependent surface fluid flow conditions	203
Figure D.1 First uniform mesh used for mesh sensitivity analysis discussion	204

Tables

Table 1-1 Publications and the methods used for deriving hip joint forces	15
Table 1-2 Peak hip joint forces predicted by different analytical studies	16
Table 1-3 List of objective functions/constraints in optimisation models used by different researchers	18
Table 1-4 Peak hip joint forces measured in different experimental and clinical studies	22
Table 1-5 Peak hip contact stresses predicted by different analytical studies in normal joints	38
Table 1-6 Peak hip contact stresses measured in different experimental and clinical studies	41
Table 1-7 Peak hip contact stresses predicted by different finite element/numerical studies	49
Table 2-1 Material properties used in the model of cartilage indentation with spherical indenter (Spilker <i>et al.</i> , 1992; Goldsmith <i>et al.</i> , 1995; Warner, 2000)	62
Table 2-2 Material properties used in the model of joint contact mechanics of articular cartilages (Federico <i>et al.</i> , 2004)	65
Table 3-1 Elements used for the cup and ball model.....	81
Table 3-2 Comparison of two- and three-dimensional cup and ball model for validation	82
Table 4-1 Accuracy and Resolution of the instrumentation/machines used for experimental validation	90
Table 4-2 Weights of the individual components of indenter loading assembly	93
Table 4-3 Parameters used to convert colour intensity into contact stresses	98
Table 4-4 Percentage of body Weight (with reference to 400 N) used in the validation process of FE models	99
Table 4-5 Number of elements used in FE models of each specimen.....	105
Table 4-6 Experimental results and FE predictions of contact area.....	107
Table 4-7 Experimental results and corresponding FE predictions of peak contact stresses	107

Table 4-8 FE predictions of total fluid load support (TFLS).....	108
Table 5-1 Elements used in Hemiarthroplasty Model	115
Table 6-1 List of activities with their start and end (Bergmann <i>et al.</i> , 2001).....	124
Table 6-2 Maximum peak contact pressure with corresponding peak fluid pressure, contact area and total fluid load support (TFLS) for different activities and where and when they occurred	127
Table 6-3 Average total fluid load support (TFLS) for different activities.....	128
Table C.1 Material properties used in the biphasic jump condition model (ABAQUS., 2007 and Federico <i>et al.</i> , 2004)	202
Table D.1 Predictions in mesh sensitivity analysis	205

Abbreviations/Terms Used

AVN – AVascular Necrosis

BW – Body Weight

DMOAD – Disease-Modifying OA Drug

ECM – Extra-Cellular Matrix

FE – Finite Element

HA – Hyaluronic Acid

NSAID – Non-Steroidal Anti-Inflammatory Drug

OA – OsteoArthritis

PEEK – PolyEtherEtherKetone

RA – Rheumatoid Arthritis

CAX4 – Four-node bilinear

CAX4P – Four-node bilinear displacement and pore pressure

C3D4 – Four-node linear tetrahedral elements

C3D6 – Six-node linear triangular prism

C3D8 – Eight-node linear brick

C3D8RP – Eight-node trilinear displacement and pore pressure, reduced integration

Chapter 1 Introduction and Literature Review

1.1 Background

Diarthrodial synovial joints allow free movement of the bones and are characterized by a synovial cavity, connective tissue and the cartilage covering each of the articulating ends of the bones (Tortora and Grabowski, 2004) acting as a bearing material. For example, articular cartilages in the hip joint cover the acetabular cavity and the femoral head. This articular cartilage has remarkable lubricating properties with a very low coefficient of friction in the range of 0.001 to 0.02 (Mow and Lai, 1980; Macirowski *et al.*, 1994; Persson, 2000) and low wear rates (Lipshitz and Glimcher, 1979; Mow and Lai, 1980; Mow and Huijskes, 2005). Though, it normally survives the life time of a person, sometimes it suffers degradation and wear due to many factors including age, improper use like extreme sports, injury, trauma, wear and tear, and congenital diseases (Meachim, 1980; Yang, 2003).

The healthy cartilage supports a wide range of complex loads, as high as 7 – 9 times body weight (BW) (Crowninshield *et al.*, 1978; Bergmann *et al.*, 1993) and motions at different speeds ranging from 0.06 m/s to 0.6 m/s (Mow, 1969) and yet is able to provide excellent lubrication mechanism over these differing and at times conflicting loading regimes. Different lubrication mechanisms such as hydrodynamic, elasto-hydrodynamic, boundary, boosted, weeping and biphasic lubrication have been hypothesised to explain the remarkable tribological performance under a wide variety of operating conditions in synovial joints. Biphasic lubrication which is due to the load partitioning between solid and fluid phases was proposed in 1980s as a potential explanation for wide variety of cartilage lubricating properties (Mow and Lai, 1980). However, the role of interstitial fluid in lubrication was hypothesised long before cartilage properties were explained using biphasic theory (Lewis and McCutchen, 1959; McCutchen, 1959).

In unhealthy cartilage, these lubricating and wear properties are compromised, e.g. as in osteoarthritic cartilage. Osteoarthritis (OA) is a degenerative disease of the articular cartilage in which it gets degraded ultimately leading to a complete breakdown thus initiating bone to bone contact causing pain. The initiation of cartilage breakdown is still unknown; however, it is thought to be induced due the mechanical factors causing structural as well as biochemical changes (Radin *et al.*, 1978; Muehleman and Arsenis, 1995; Aigner and McKenna,

2002). There are many ways of treating OA and treatment generally falls into three broad categories; non-pharmacological, pharmacological and surgical treatments (Carrabba and Sarzi-Puttini, 2004).

Hemiarthroplasty is one of the surgical treatments often preferred by surgeons; e.g. in hip joint the diseased or damaged femoral head is replaced with a metallic prosthesis which then articulates with the natural acetabular articular cartilage. This may alter the tribology of the joint leading to complications.

The hip joint is one of the most studied human diarthrodial joints owing to its relative simplicity in geometry (ball and socket) and kinematics apart from it being “one of the largest and most heavily loaded joints” (Dowson *et al.*, 1981a). Most of the studies on the hip joint have been *in vitro* or *in situ* under laboratory conditions (Rushfeldt *et al.*, 1981a; Brown and Shaw, 1982; Brown and Shaw, 1983; Ferguson *et al.*, 2003) or *in vivo* using instrumented prosthesis (Rydell, 1966; Hodge *et al.*, 1986; Bergmann *et al.*, 1988; Hodge *et al.*, 1989; Carlson, 1993; Park *et al.*, 1999; Bergmann *et al.*, 2001; Morrell *et al.*, 2005). However, these are mostly invasive techniques. The use of CT, MRI and ultrasound is on the rise but mostly in morphological *in vivo* studies or for fracture determination (Jonsson *et al.*, 1992; Nakanishi *et al.*, 2001; Naish *et al.*, 2006; Barkmann *et al.*, 2009; Keller and Nijs, 2009).

However, contact mechanics and tribological studies, especially those involving parametric evaluations, are time-consuming and difficult to be carried out experimentally and clinically. Moreover, non-invasive studies are not possible using these models and always one or both the cartilages are sacrificed in clinical studies involving instrumented prosthesis. One of the ways to overcome this problem is to use mathematical models (Paul, 1967; Seireg and Arvikar, 1975; Ipavec *et al.*, 1999; Daniel *et al.*, 2001; Mavcic *et al.*, 2002) which have become more accurate over time (Brand *et al.*, 1994; Stansfield *et al.*, 2003).

Numerical modelling such as finite/discrete element modelling is another alternative to study joints non-invasively (Rapperport *et al.*, 1985; Ferguson *et al.*, 2000a; Bachtar *et al.*, 2006; Yoshida *et al.*, 2006; Anderson *et al.*, 2008; Harris *et al.*, 2009). However, some of these models are geometrically simplified and most do not take into account the effects of biphasic lubrication which is known to reduce the coefficient of friction due to load partitioning (Mow and Lai, 1980). Moreover, these models have not investigated the relationship between fluid load support in the cartilage and contact mechanics in a whole hip joint within physiological loading regimes. This study thus aims to correct this anomaly by proposing a methodology to model three-dimensional human hip joint with natural cartilages as well as hemiarthroplasty joints.

1.2 Hip Joint

1.2.1 Joint Structure

The hip joint is a synovial and diarthrodial joint in the pelvic region. It is enclosed in a synovial cavity and is capable of rendering free movements of the bones forming the joint (Tortora and Grabowski, 2004). It is typically a ball and socket joint as shown in **Figure 1.1**. It is the joint formed by the ball at proximal end of the femur and the acetabulum in the hip bone. It joins the superior and inferior parts of the body.

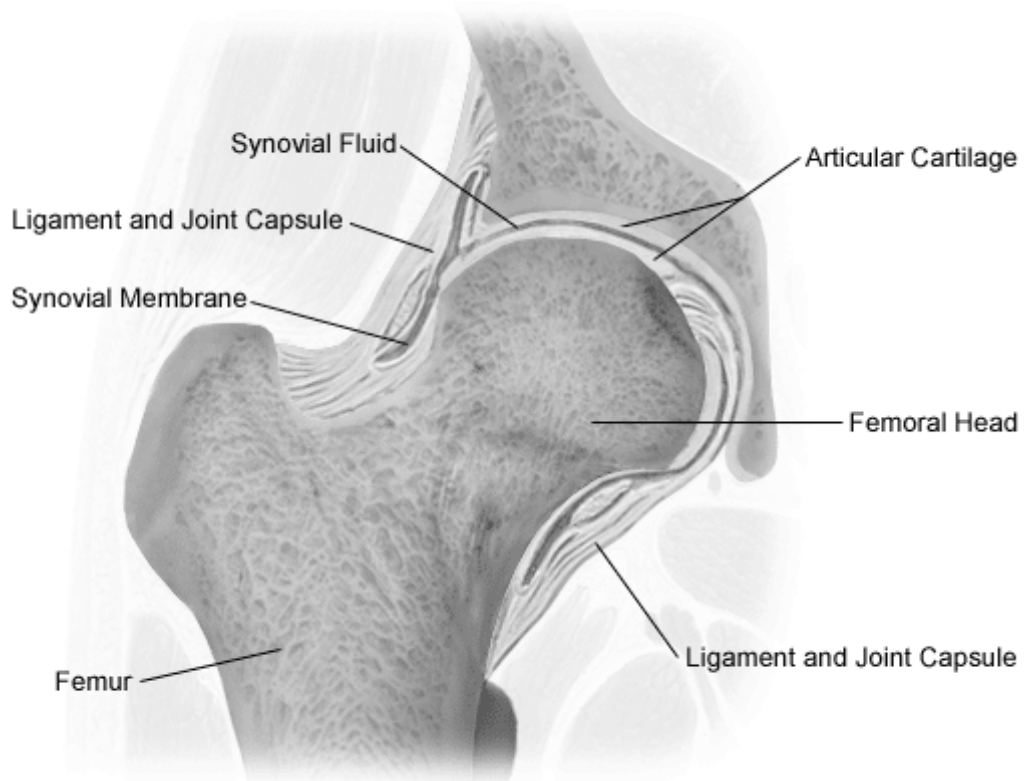


Figure 1.1 Hip Joint (Orthopaedics, 2007)

It is designed more for stability and withstanding high loads rather than mobility (Drake *et al.*, 2005). The moving ends of the bones are covered with hyaline articular cartilages. The joint has two articulating components; proximal femur and acetabulum.

1.2.2 Proximal Femur

The femur is the longest and the strongest bone in the body and its proximal end has a head which is connected to the bone shaft by a neck (Gray, 2000; Drake *et al.*, 2005) (**Figure 1.2**). The head of the femur is approximately spherical and is covered with articular cartilage except for a small area called fovea on the medial surface for ligament attachment (Gray, 2000; Drake *et al.*, 2005). The neck of the femur is inclined at approximately 125° to the shaft (Drake *et al.*, 2005) in males and is almost at right angle to the shaft in females (Gray, 2000). Apart from superior-medial projection, the neck is also inclined anteriorly to the shaft by an angle of around $12^\circ - 14^\circ$ (Gray, 2000).

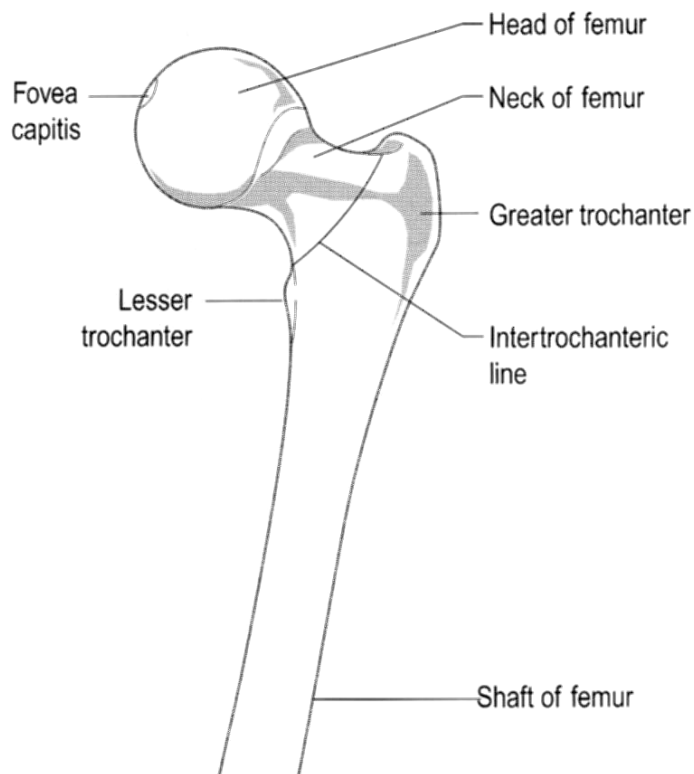


Figure 1.2 Left Proximal Femur (Palastanga *et al.*, 2006)

1.2.3 Acetabulum

The pelvic bone or the hip bone is the fusion of three different bones; ilium, ischium and pubis (Gray, 2000; Drake *et al.*, 2005) as shown in **Figure 1.3**. The acetabulum is “a deep, cup-shaped, hemispherical depression” (Gray, 2000) in the pelvic bone where its three constituent bones fuse (Drake *et al.*, 2005) and is directed inferiorly and anterolaterally (Gray, 2000).

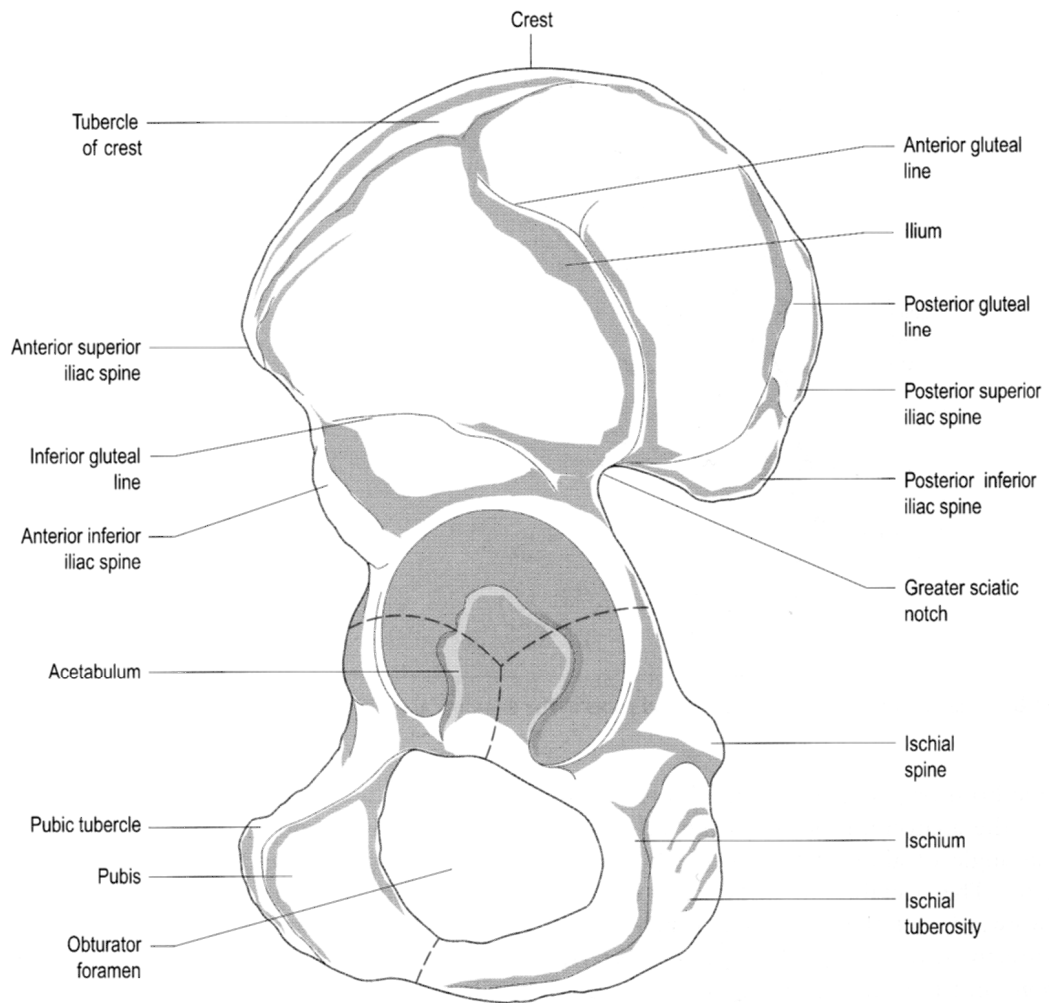


Figure 1.3 Left Hip Bone in Lateral View (Palastanga *et al.*, 2006)

The deep notch at the inferior acetabular margin called the acetabular notch is continuous with a rough non-articular depression called acetabular fossa which is located in the central inferior part of the acetabulum and provides for femoral head ligament attachment (Gray, 2000; Drake *et al.*, 2005). The remaining surface also called the lunate surface of the acetabulum is covered with “crescent-shaped” articular cartilage and covers “anterior, superior and posterior margins of the acetabular fossa” (Drake *et al.*, 2005). The lunate surface is the broadest at the superior part “where most of the body’s weight is transmitted through the pelvis to the femur” (Drake *et al.*, 2005). See **Figure 1.4**.

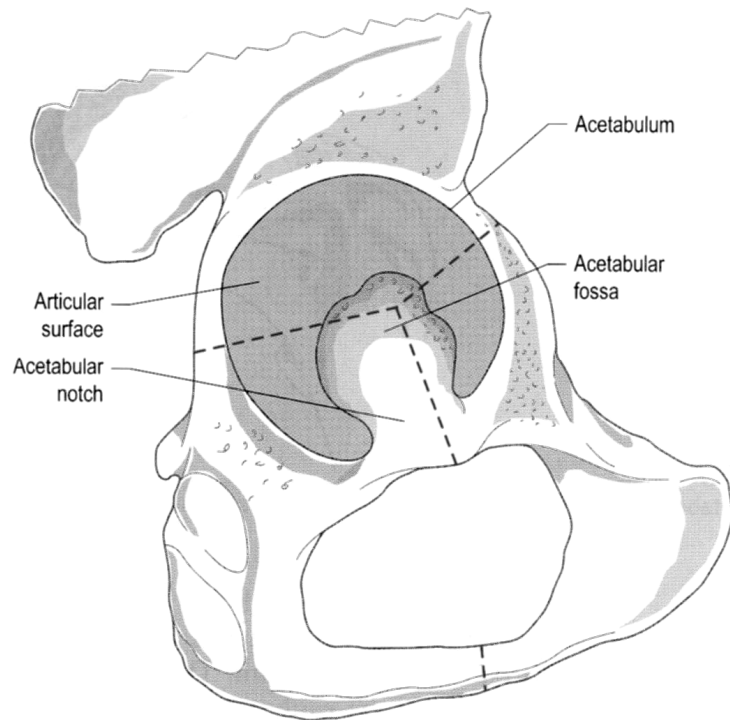


Figure 1.4 Acetabulum (Palastanga *et al.*, 2006)

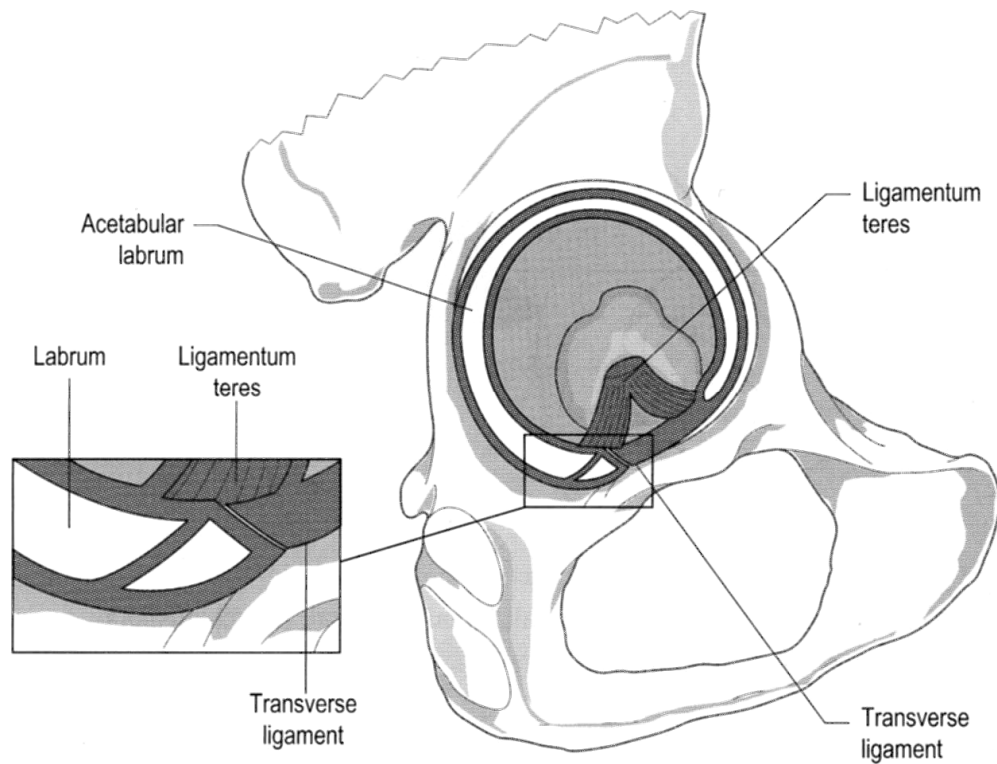


Figure 1.5 Acetabulum with labrum (Palastanga *et al.*, 2006)

Fibrocartilage called acetabular labrum is attached to the superiorly thick and strong uneven rim of the acetabular cavity thus deepening it (Gray, 2000) as shown in **Figure 1.5**. This “labrum bridges across the acetabular notch”, forming the transverse acetabular ligament (Drake *et al.*, 2005). The femoral head ligament (ligamentum teres) is a flat band-like tissue with one end attached to the fovea and “the other end to the acetabular fossa, transverse acetabular ligament and margins of the acetabular notch” (Drake *et al.*, 2005). This entire assembly is then covered by the synovial membrane to form the synovial cavity.

1.3 Articular Cartilage

The articular cartilage covering each of the moving ends of the bones in synovial joint is avascular, aneural and an excellent bearing material with exceptional tribological properties.

1.3.1 Structure

The cartilage is made up of extra-cellular matrix (ECM), chondrocytes and water. The interstitial water containing dissolved electrolytes is around 60 – 80% of the total wet weight (Linn and Sokoloff, 1965; Mankin and Thrasher, 1975; Lipshitz *et al.*, 1976; Lai and Mow, 1980; Armstrong and Mow, 1982; Macirowski *et al.*, 1994; Olsen and Oloyede, 2002). The ECM is a reinforced structure consisting of a dense network of collagen type II fibres and proteoglycan gel with a high degree of cross-linking. The cartilage structure is inhomogeneous, non-linear, anisotropic and exhibits time-dependent behaviour (Elmore *et al.*, 1963; Edwards, 1966; Kempson, 1979; Lai and Mow, 1980; Mow *et al.*, 1980; Mow and Huiskes, 2005).

Its thickness varies depending upon species, joints, location within joints and age. The range of values in the literature is quite high; from 0.023 mm (mouse ankle) to 6.25 mm (human knee) (Simon, 1970; Ateshian *et al.*, 1991). In the human hip joint, the cartilage thickness in the acetabulum and on the femoral head range approximately from 1 – 3 mm (Armstrong and Gardner, 1977; Rushfeldt *et al.*, 1981a; Adam *et al.*, 1998; Nakanishi *et al.*, 2001; Wyler *et al.*, 2009). However, cartilages thinner than 1 mm and thicker than 3 mm have also been found (Armstrong and Gardner, 1977; von Eisenhart *et al.*, 1999; Naish *et al.*, 2006; Wyler *et al.*, 2009). Average thickness of the femoral head cartilage has been found to be significantly greater than the acetabular cartilage but the same does not apply to maximum thickness (Adam *et al.*, 1998; von Eisenhart *et al.*, 1999). Moreover, the

thickest cartilage in both acetabulum and femoral head is mostly ventral in the acetabular dome and it is thought to be related to the dynamic weight-bearing areas (Adam *et al.*, 1998; von Eisenhart *et al.*, 1999). A decrease in cartilage thickness with age has also been observed (Adam *et al.*, 1998; von Eisenhart *et al.*, 1999). Techniques such as needle indentation (Shepherd and Seedhom, 1999), microscope (Kurrat and Oberlander, 1978), X-rays (Armstrong and Gardner, 1977), CT (Wyler *et al.*, 2009), MRI (Naish *et al.*, 2006) and ultrasound (Adam *et al.*, 1998) have been used to calculate the cartilage thickness,

Articular cartilage shows a layered structure along its depth with 4 primary zones; superficial tangential zone (STZ), middle zone, deep zone and calcified zone (**Figure 1.6**). The water and collagen contents decrease from STZ to deep zone. Proteoglycan content is the maximum in the middle zone. The chondrocyte shape and size also vary with the depth. The collagen fibrils are densely packed and arranged parallel to the surface in the STZ. They are oriented randomly in the mid zone whereas in the deep zone they are bundled together and are perpendicular to the tide mark thus anchoring the cartilage onto the bone (Davies *et al.*, 1962; Stockwell and Scott, 1967; Weiss *et al.*, 1968; Muir *et al.*, 1970; Clarke, 1971; Mow *et al.*, 1974; Lane and Weiss, 1975; Redler *et al.*, 1975; Lipshitz *et al.*, 1976; Torzilli, 1985; Torzilli, 1988; Mow and Huiskes, 2005).

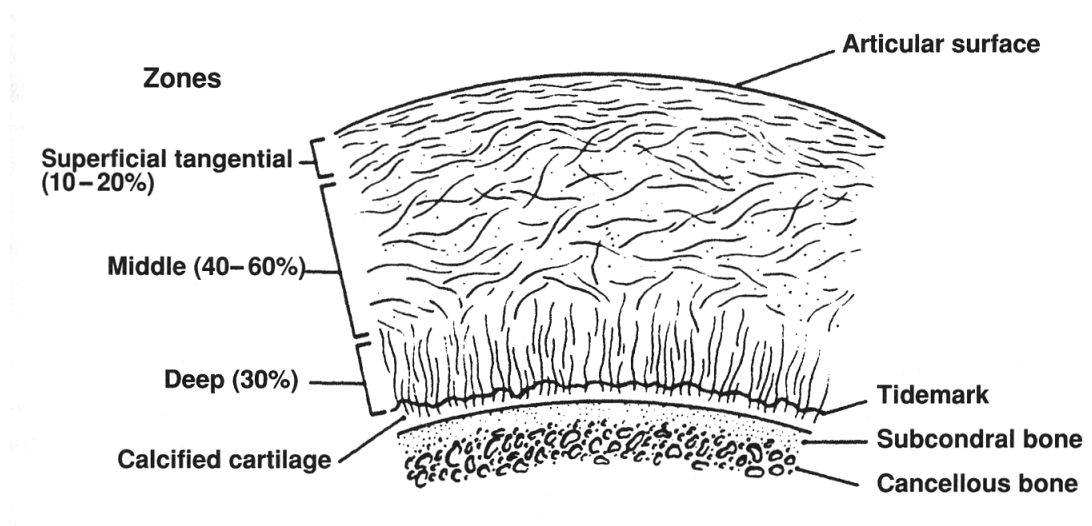


Figure 1.6 Layered structure of Articular Cartilage (Mow and Huiskes, 2005)

It has been shown in various forms that two more layers (**Figure 1.7**); viz. surface lamina of proteoglycans and boundary layer of phospholipids and glycoproteins are present above the STZ (MacConaill, 1951; Balazs *et al.*, 1966; Weiss *et al.*, 1968; Wilkins, 1968; Walker *et al.*, 1969; Swann *et al.*, 1981; Ghadially

et al., 1982; Stanescu and Leibovich, 1982; Orford *et al.*, 1983; Orford and Gardner, 1985; Forster and Fisher, 1999). Both these layers are acellular and non-collagenous.

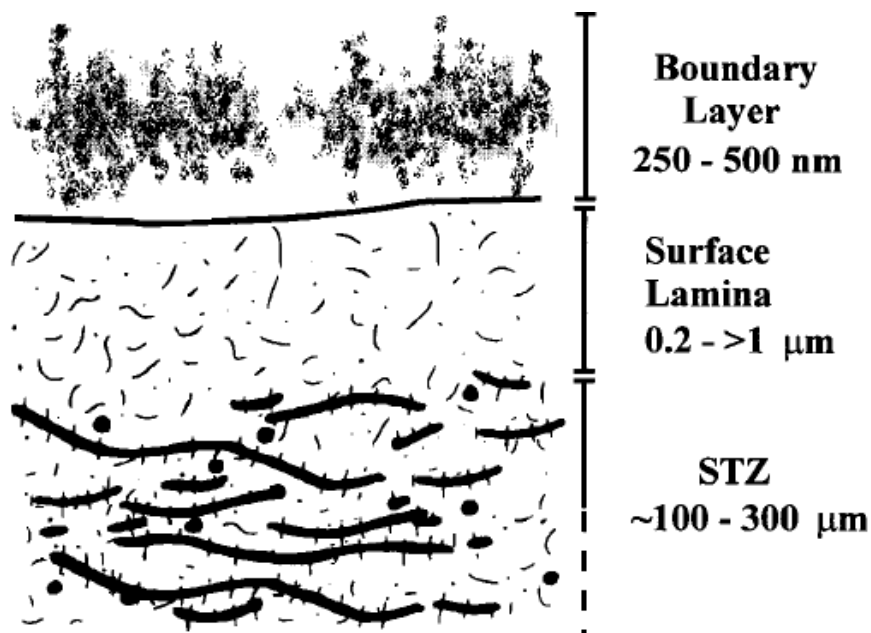


Figure 1.7 Cartilage structure showing surface lamina and boundary layer (Forster and Fisher, 1999)

1.3.2 Constitutive Formulations

Articular cartilage is inhomogeneous, non-linear, anisotropic and multiphasic (Goldsmith *et al.*, 1996; Sun *et al.*, 1999). However the earliest models were linearly elastic (Elmore *et al.*, 1963; Sokoloff, 1966; Kempson *et al.*, 1971; Hori and Mockros, 1976). This formulation was sufficient to predict static, instantaneous and equilibrium conditions but failed to take into account the time-dependent behaviour of the cartilage. Thus, viscoelastic models were proposed (Hayes and Mockros, 1971; Parsons and Black, 1977; Hayes and Bodine, 1978). However, these models could not explain the effect of fluid present in the cartilage.

Biphasic theory was proposed in 1980 (Mow *et al.*, 1980) according to which cartilage was composed of two phases; a fluid phase representing water and dissolved electrolytes and a solid phase representing collagen fibres, proteoglycans, chondrocytes and other components. Both the phases were immiscible and incompressible individually. The solid phase was porous and permeable and the compression of the cartilage was due to the fluid flow within the porous permeable solid phase and its exudation. Due to the very low permeability

of the cartilage, high resistance is offered to the fluid flow and this in turn induces large drag forces (Lai and Mow, 1980; Kwan *et al.*, 1984; Mow and Huijskes, 2005) thus maintaining high fluid pressure over a long period of time.

With infinitesimal strain and constant permeability, this theory becomes linear biphasic theory. However, cartilage deformation is non-linear with finite strains and its permeability is dependent on compaction. Thus, Strain-dependent permeability (Lai and Mow, 1980; Lai *et al.*, 1981; Mow *et al.*, 1984; Holmes, 1985; Holmes *et al.*, 1985; Holmes, 1986) and non-linear finite deformation (Kwan, 1985; Holmes, 1986; Holmes and Mow, 1990; Kwan *et al.*, 1990) were incorporated in the biphasic theory.

Biphasic theory is capable of explaining only the flow-dependent viscoelasticity. Flow-independent viscoelasticity which is due to the ECM (Hayes and Bodine, 1978) also contributes to the time-dependent behaviour of the cartilage. Mak studied and incorporated this in the biphasic theory (Mak, 1986). Through their uniaxial creep compression experiments, Setton and colleagues showed that this flow-independent viscoelasticity plays an important role in damaged cartilage (Setton *et al.*, 1993) with high permeability where the fluid is unable to support very high loads.

Subsequently triphasic theory (Lai *et al.*, 1991) with separate phase for anions and cations and quadriphasic theory (Huyghe and Janssen, 1997) with individual anion and cation phases were also proposed.

1.4 Hip Joint: Kinematics

Gait analysis or locomotion of the hip joint and its component parts is essential in the investigation of contact mechanics. A person goes through many routine activities such as walking, climbing stairs, sitting or standing up on a daily basis. The forces and stresses within the joint will differ based on these activities. Hence, the temporal and spatial movements of the femoral head within the acetabular cup need to be understood before attempting to investigate contact forces, contact pressure, fluid load support and many other functional parameters of interest. Apart from this, understanding locomotion of joints helps in “proper diagnosis and surgical treatment of joint disease”, and designing better prosthesis (An and Chao, 1984). It will also help in post-operative rehabilitation of the patients.

From the mechanical engineering perspective, the individual segments of the joint can be represented as rigid bodies attached together at the joint and

undergoing relative angular motion.

The hip joint renders a wide variety of motions to the body though limited in extent to which it does this when compared to the shoulder joint. The hip joint is capable of movements such as flexion, extension, adduction, abduction, medial/inner and lateral/outer rotation and circumduction (Drake *et al.*, 2005). These movements are explained in the following paragraph assuming the person is standing.

The flexion is the upward/forward motion of the femur relative to the upper part of the pelvis whereas extension is the downward/backward motion (Gray, 2000). The more flexion, the lesser will be the angle between the femur and the upper part of the pelvis. The opposite is the case for extension. Abduction and adduction are the angular movements of the femur about a horizontal anteroposterior axis. Abduction is the movement away from the medial plane whereas adduction is towards it (Gray, 2000). The medial and lateral rotations are rotary motions but are about the vertical/longitudinal axis. Medial rotation is towards the centre of the body whereas lateral rotation is away from it. Circumduction is the circular motion of the femur. In this motion the femur circumscribes a cone (Gray, 2000).

However, there is a limit on the range of motion involving these movements due to different muscles and the structure of the joint and body itself. Normal hip joint flexion is around 120° and extension is approximately 20° (Dowson *et al.*, 1981a; Palastanga *et al.*, 2006). However, with external help these motions can be extended further to 130° and 30° respectively (Palastanga *et al.*, 2006). Abduction and adduction are 45° each whereas total of medial and lateral rotation is around 90° (Dowson *et al.*, 1981a; Palastanga *et al.*, 2006).

The typical range of motion curves over one cycle of normal walking for an average patient (Bergmann, 2001) are shown in **Figure 1.8**. The positive angles are for flexion, abduction and outer/lateral rotation. The cycle starts at the heel strike.

To record the gait, skin markers are attached to the skin nearer the bony landmarks. They are mostly flashing LEDs (Crowninshield *et al.*, 1978; Rohrle *et al.*, 1984) or reflective markers (Heller *et al.*, 2001). The movement of joints through time is recorded using photographic cameras (Crowninshield *et al.*, 1978) or movie cameras (Paul, 1967) which capture the motion of the markers. In modern systems these have been replaced by infrared cameras (Heller *et al.*, 2001).

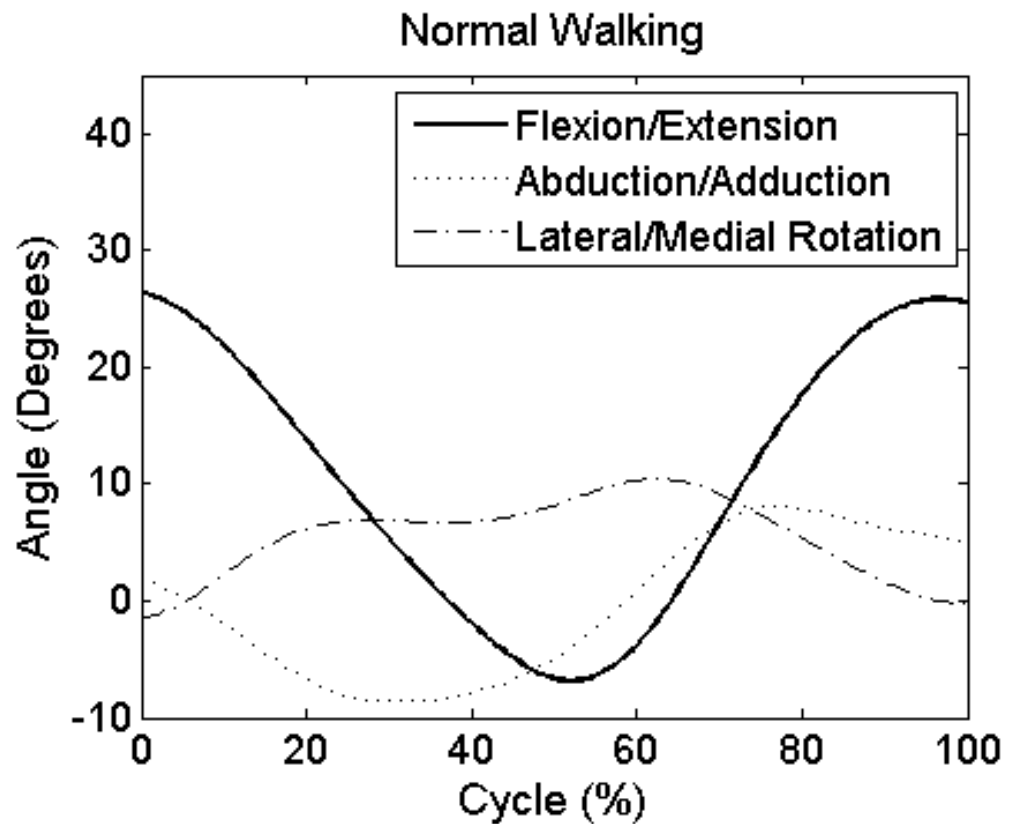


Figure 1.8 Range of motion during one cycle of normal walking (Bergmann, 2001)

1.5 Hip Joint: Kinetics

The motion of the femoral head within the acetabular cup is accompanied by forces which are introduced due to these motions, body weight and muscles. These forces, particularly those within the contacting zone, have implications to the long term survival of the joint and smooth functioning of the articular cartilage.

It is important to understand these forces for two reasons: 1) to understand diseases like OA which are attributed to mechanical factors and 2) to help design new prostheses which not only replace joint function but also give structural stability to the whole musculoskeletal system (Paul, 1967). The first attempts to understand joint kinetics date back to the late nineteenth and early twentieth century (Braune and Fischer, 1890; Elftman, 1939; Paul, 1966; Paul, 1967). These joint forces comprise of external forces as well as those exerted by the muscles. They are typically calculated or measured from gait analysis studies (Bergmann *et al.*, 1993;

Brand *et al.*, 1994). The forces had to be calculated in the earlier studies, using mass and acceleration of the body parts, and mass itself was predicted from corpses (Braune and Fischer, 1890; Paul, 1967). It was possible to measure the foot-ground forces only after the development of the foot plate in the 1950s (Cunningham and Brown, 1952). These along with the joint kinematics captured using cameras are used to predict the joint forces (Paul, 1967). Instrumented prosthesis have been used in several cases to measure these forces directly (Rydell, 1965; English and Kilvington, 1979; Bergmann *et al.*, 1988; Davy *et al.*, 1988; Brand *et al.*, 1994; Bergmann *et al.*, 2001).

A typical resultant hip joint force versus time curve for normal walking shows two distinct peaks. The first of these peaks is just after the heel strike and the second one is just before toe off (**Figure 1.9**).

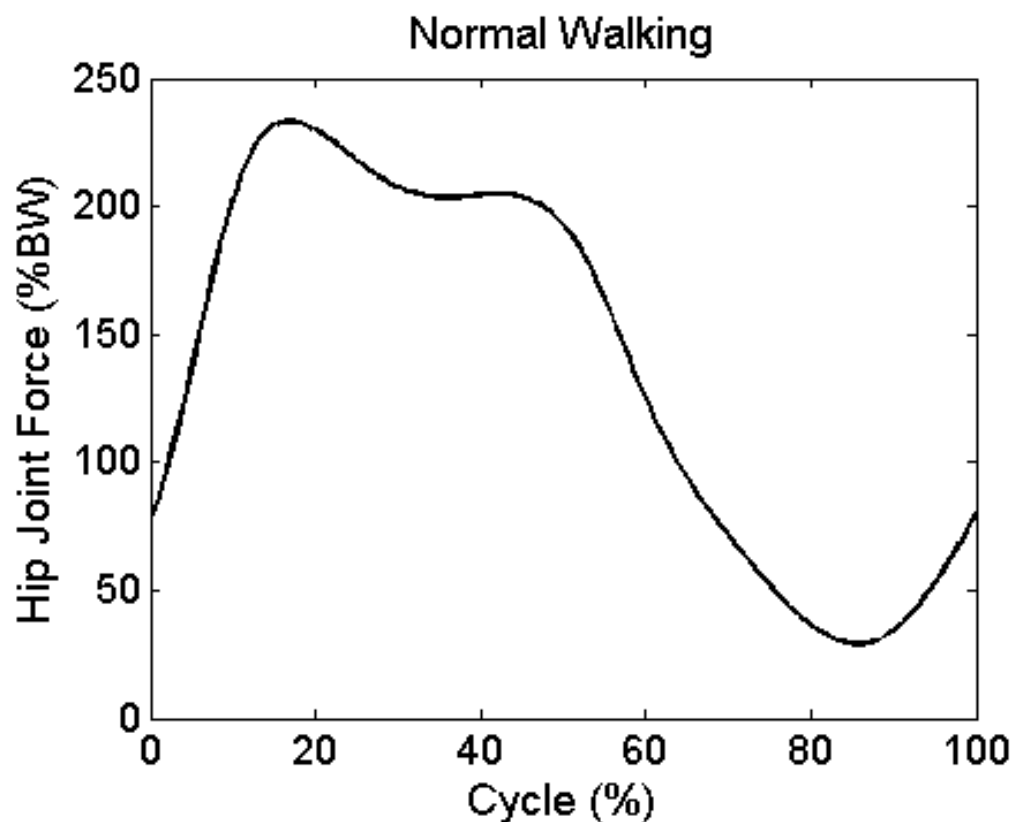


Figure 1.9 Typical two peak variation of resultant hip joint force versus time for normal walking (Bergmann, 2001)

1.5.1 Theoretical Studies

Several mathematical/analytical gait mechanics studies have been conducted over the years which gave insight into the function of the hip joint (Paul, 1967;

Seireg and Arvikar, 1975; Crowninshield *et al.*, 1978; Johnston *et al.*, 1979; Rohrle *et al.*, 1984; Brand *et al.*, 1994; Duda *et al.*, 1997; Pedersen *et al.*, 1997; Stansfield *et al.*, 2003). They have been successfully used in predicting the hip joint forces along with those applied by muscle. However, one needs to exercise caution while interpreting the predicted forces mentioned in different studies. In many cases, the resultant hip joint force through the centre of the femur has already accounted for the moments and forces due to the muscles (Rohrle *et al.*, 1984). In some studies, this is not done and so hip resultant forces will seem too low to be of physiological significance (Crowninshield *et al.*, 1978).

These mathematical models are inverse dynamics problems and hence require kinematic and kinetic data as input, to predict joint forces, stresses, etc. The geometrical parameters, masses, centre of masses and moments of inertia of the bony segments of the joint are required in order to accurately model the joints. These can be obtained from regression equations (Crowninshield *et al.*, 1978; Park *et al.*, 1999) derived from statistical analysis of cadavers (Clauser *et al.*, 1969; Chandler *et al.*, 1975) or living subject data (Young *et al.*, 1983). Another way of deriving these inertial properties is geometrical approximation (Jensen, 1978; Hatze, 1980) or by using MRI techniques (Martin *et al.*, 1989; Mungiole and Martin, 1990). Video-based systems (Sarfaty and Ladin, 1993) or 3-D laser scanning (Wang *et al.*, 2007) could also be used to measure the anthropometric data directly. They are non-invasive and subject specific. The dimensional data have also been derived from radiographs such as CT or X-ray (Heller *et al.*, 2001; Stansfield *et al.*, 2003). This data is then used along with skin markers data to get the positions of bony landmarks of the lower limbs during gait (Heller *et al.*, 2001). The external forces are captured using force plates (Paul, 1967; Crowninshield *et al.*, 1978; Heller *et al.*, 2001). They measure foot-ground reaction forces in sync with camera measurements. This data is then used to calculate internal joint forces.

Musculoskeletal mathematical model is an indeterminate problem as there are usually more number of unknowns than the equations available to solve them (Iglie *et al.*, 2002). As such, they will have an infinite number of possible solutions. Two methods have been primarily used in solving this indeterminate problem (Andriacchi and Hurwitz, 1997); viz. the reduction method (Paul, 1967; Iglie *et al.*, 1993c) and the optimisation method (Seireg and Arvikar, 1973; Crowninshield *et al.*, 1978). Various publications which have used one of these two methods in deriving the hip joint forces are listed in **Table 1-1**.

Table 1-1 Publications and the methods used for deriving hip joint forces

Reference	Method Used
(Paul, 1967)	Reduction
(Duda <i>et al.</i> , 1997)	Reduction
(Igljic <i>et al.</i> , 1993c)	Reduction
(Seireg and Arvikar, 1973)	Optimisation
(Seireg and Arvikar, 1975)	Optimisation
(Crowninshield <i>et al.</i> , 1978)	Optimisation
(Johnston <i>et al.</i> , 1979)	Optimisation
(Crowninshield and Brand, 1981)	Optimisation
(Rohrle <i>et al.</i> , 1984)	Optimisation
(Heller <i>et al.</i> , 2001)	Optimisation
(Stansfield <i>et al.</i> , 2003)	Optimisation
(Frayssse <i>et al.</i> , 2009)	Optimisation

In the reduction method, the number of unknowns in equilibrium equations is reduced, so that the problem becomes determinate. To do this, e.g., Paul grouped 22 hip muscles into 6 groups and then ignored antagonistic muscle activities as he was only interested in the activity between heel strike to the next heel strike when these muscle activities are not significant (Paul, 1967). This reduced the number of unknowns to six. The grouping of muscles was done based on an electromyographic study in which the electrodes attached to the skin generated electric signals based on activated muscles. The set of five equations of equilibrium were then solved for level walking for limiting cases of joint forces by considering the muscles with either the longest or shortest moment arm. Though the true value would lie between these two values, the lower of the two was reported in the absence of any verifiable criteria (Paul, 1967). The maximum of the first and second peaks of hip joint force curve in normal walking (cycle time: 1.02 – 1.24 seconds; average 1.13 seconds) were found to be 5.8 and 6.4 times the BW respectively. The corresponding average values were 3.29 and 3.88 times BW respectively (**Table 1-2**). In a more exhaustive study, a mean hip joint force of 4.9 times BW was predicted for normal walking (Paul, 1976).

Table 1-2 Peak hip joint forces predicted by different analytical studies

Reference	Peak Hip Joint Force (× BW)		Activity
	Max	Average	
(Paul, 1967)	6.4	3.88	Walking (0.81 – 0.98 Hz) (avg - 0.88 Hz)
(Seireg and Arvikar, 1973)	3.3	--	Stooping
(Seireg and Arvikar, 1975)	5.4	--	Level walking
(Paul, 1976)	--	4.9	Slow walking (1.10 m/s)
	--	4.9	Normal walking (1.48 m/s)
	--	7.6	Fast walking (2.01 m/s)
	--	7.2	Ascending stairs
	--	7.1	Descending stairs
(Crowninshield <i>et al.</i> , 1978)	5.0	4.3	Walking (0.95 – 1.05 m/s)
	7.6	--	Ascending stairs
	3.9	--	Descending stairs
	3.7	--	Rising from chair (chair height – 440 mm)
(Crowninshield and Brand, 1981)	5.0	--	Walking
(Rohrle <i>et al.</i> , 1984)	--	4.1	Walking (0.8 m/s)
	--	5.5	Walking (1.2 m/s)
	--	6.9	Walking (1.6 m/s)
(Iglıc <i>et al.</i> , 1993c)	2.4	--	One legged stance
(Brand <i>et al.</i> , 1994)	4.0	3.5	Walking (1.11 – 1.36 m/s)
(Duda <i>et al.</i> , 1997)	3.8	--	Level walking
(Heller <i>et al.</i> , 2001)	3.1	2.7	Walking (1.08 m/s)
	3.2	2.7	Ascending stairs (step height – 170 mm)
(Stansfield <i>et al.</i> , 2003)	3.1	3.0	Walking (avg - 1.00 m/s)
	3.2	3.1	Walking (avg - 1.43 m/s)
	4.4	4.0	Walking (avg - 1.86 m/s)
	2.8	2.6	Rising from chair
	2.2	2.2	Sitting on chair
	4.5	3.8	2-1-2 leg stance
(Frayssé <i>et al.</i> , 2009)	--	4.0	Walking

Duda and colleagues used the muscle forces and points of muscle insertions obtained from earlier studies (Brand *et al.*, 1982; Brand *et al.*, 1986) in their quasi-static walking model using force and moment equilibrium equations (Duda *et al.*, 1997). Their estimate of peak contact force was around 3.8 times BW just before

toe-off. Though their model was not purely a reduction model, they did reduce the number of unknowns by using the published values of muscle forces.

Iglic and colleagues reduced the number of unknowns by dividing nine muscle segments into three groups and then assuming that the mean tension in a muscle in any group was equal (Iglic *et al.*, 1993c). The individual muscle force was proportional to its relative cross-sectional area and average tension. There were six equilibrium equations to solve for six unknowns; three for resultant hip joint force components and three for muscle groups (Iglic *et al.*, 1993c; Iglic *et al.*, 2002). In one legged stance, the hip joint resultant force was 2.4 times BW for an optimum configuration of the pelvis with respect to its interhip half distance (84.5 mm - neutral) and muscle insertion point on the iliac crest (Dostal and Andrews, 1981; Iglic *et al.*, 1993c).

Optimisation was used in 1973 to predict joint reaction forces and muscle forces for the first time (Seireg and Arvikar, 1973). In this method, an objective function is either minimised or maximised depending upon the problem to be solved and can be formulated as either a linear or non-linear function. Since, the problem is indeterminate, its solution space is infinite and in the musculoskeletal problem it is continuous as well. Hence, there is a need to reduce the solution space. The force/moment equilibrium equations are the constraints imposed on the system by the need for the system to be in static/dynamic equilibrium (Seireg and Arvikar, 1973) and most of the time these are the only ones required. However, sometimes additional constraints are needed. Objective functions and constraints used in different studies are listed in **Table 1-3**.

Several functions such as minimizing muscle forces, muscle work to attain a particular posture, vertical reaction forces at joints, ligament moments at joints and the weighted sum of these parameters were investigated by Seireg and Arvikar to study their feasibility using activities like standing, leaning and stooping (Seireg and Arvikar, 1973). For stooping e.g., they found the maximum joint forces of 3.3 times BW using ligament moment minimisation and, sum of muscle forces and weighted moment minimisation criteria. This method was then extended to analyse normal walking using minimisation of weighted sum of muscle forces and ligament moments at the three joints of the lower extremity (Seireg and Arvikar, 1975). The maximum resultant hip force, in the study, was found to be 5.4 times the BW. Unlike in Paul's model, where a group of muscles was represented by a line between centroid of insertions areas, this model used more realistic representation of the individual muscles as the lines joining the point of origin and insertion point. The limitation of this study was that no additional realistic constraints (other than equilibrium equations and the values of all the variables to be non-negative) were

placed on muscle forces (Seireg and Arvikar, 1973; Seireg and Arvikar, 1975).

Table 1-3 List of objective functions/constraints in optimisation models used by different researchers

Reference	Objective function	Constraints
(Seireg and Arvikar, 1973)	Minimizing muscle forces, muscle work to attain a particular posture, vertical reaction forces at joints, ligament moments at joints and the weighted sum of these parameters	1) Force/moment equilibrium 2) All variables ≥ 0
(Seireg and Arvikar, 1975)	Minimisation of weighted sum of muscle forces and ligament moments	1) Force/moment equilibrium 2) All variables ≥ 0
(Crowninshield <i>et al.</i> , 1978)	Minimise muscle forces	1) Force/moment equilibrium 2) Only tensile muscle forces 3) Maximum muscle forces not to exceed those proportional to physiological cross-sectional area of that muscle
(Crowninshield and Brand, 1981)	Minimisation of sum of muscle stresses to the n^{th} power	1) Force/moment equilibrium
(Rohrle <i>et al.</i> , 1984)	Minimisation of total muscle forces	1) Force/moment equilibrium
(Brand <i>et al.</i> , 1994)	Minimisation of sum of muscle stresses to the power '3'	1) Force/moment equilibrium
(Heller <i>et al.</i> , 2001)	Minimisation of total muscle forces	1) Force/moment equilibrium 2) Muscle forces less than 85% of physiological muscle force
(Stansfield <i>et al.</i> , 2003)	1) Minimise maximum muscle stresses 2) Minimise sum of muscle and joint forces.	1) Force/moment equilibrium 2) Muscle stress/intensity less than maximum value
(Frayssé <i>et al.</i> , 2009)	Minimisation of sum of muscle stresses to the power '2'	1) Force/moment equilibrium

Penrod and colleagues used the minimization of total weighted muscle forces with the inequality constraint on muscle forces such that they could not be compressive (Penrod *et al.*, 1974). This was later used by Crowninshield and

colleagues to minimise total muscle forces along with an additional constraint that the maximum muscle force was not to exceed the value proportional to physiological cross-sectional area of that muscle (Crowninshield *et al.*, 1978). They found the hip contact forces during walking (0.95 – 1.05 m/s) in normal patients to be between 3.3 to 5 times BW (average 4.3 times BW) and were higher than those reported clinically for patients with abnormal gait at that time (3.3 times BW) (Rydell, 1966). They also reported contact forces of 7.6 times BW during stair climbing.

In a somewhat similar study to that of Crowninshield and colleagues, a linear optimization model was analysed by Heller and colleagues to compare measured and calculated cycle-to-cycle hip contact forces (Heller *et al.*, 2001). They used minimisation of muscle forces as the objective function with the constraints placed on maximum muscle forces. 85% of the physiologically possible forces were used in the study as the maximum allowed. Normal walking (speed 1.08 m/s) and stair climbing were modelled. The hip contact forces in both activities were between 2 – 3 times BW and calculated forces were both overestimated as well as underestimated though the tendency was towards the former. The means of contact forces differed by around 12% and 14% respectively for walking and stair climbing.

Minimisation of total muscle forces was also used as the objective function by Rohrle and colleagues (Rohrle *et al.*, 1984). The dependence of the hip joint forces on walking speed was investigated by varying it between 0.8 – 1.6 m/s. Mean hip joint forces of 2.9 – 6.9 times the BW were reported for varying gait speed. A linear relationship was observed between the forces and the gait speed with the hip joint forces increasing with the walking speed. The dependence of the hip resultant forces, contact forces and other parameters on velocity has also been shown previously (Paul, 1970; Crowninshield *et al.*, 1978). Similar observations have been reported for ground reaction forces (Andriacchi *et al.*, 1977).

Crowninshield and Brand extended their study (Crowninshield *et al.*, 1978) by removing inequality constraints and instead using non-linear relationship of muscle forces and their endurance. This was considered physiologically more relevant to predict the muscle forces. They hypothesized that since the joint contact force depended on the muscle forces, the selection of the muscles for different activities may be such that the sum of muscle stresses to a power was minimized thus allowing the activity to be carried out over longer time duration. This hypothesis was used in the mathematical model for predicting the muscle forces rather than an arbitrary criterion. However, the hip contact forces were still very high (maximum around 3500 N) for walking. Assuming a subject of around 69 kg (used in the previous study), this will be around 5.0 times the BW. However, they found an

agreement between predicted muscle activity and those seen during Electromyography studies monitored during gait (Crowninshield and Brand, 1981).

The endurance mathematical model was then used by Brand and colleagues to compare hip joint forces with those from instrumented prosthesis (Brand *et al.*, 1994). The steady state free level walking speeds of 1.11 – 1.36 m/s were investigated. The mean peak resultant forces were found to be in the range of 2.5 – 3.5 times the BW which compared well with those from instrumented prosthesis (peak predicted forces were only 0.5 times BW higher than measured values). However, the measurements with prosthesis implanted in one patient and mathematical predictions were carried out at different times.

Optimisation techniques used in hip kinetics have improved since they were first used. Objective functions and constraints have become more complex. Some have also used a two-staged optimisation process in which maximum muscle stresses were first minimized and then the sum of muscle and joint forces were minimised. (Bean *et al.*, 1988; Stansfield *et al.*, 2003). This method ensured that muscle forces were distributed in such a way that no particular muscle carried excessive stress.

Stansfield and colleagues used this two-stage optimization process to derive joint forces (Stansfield *et al.*, 2003). Activities like walking with speeds 0.97 – 2.01 m/s, rising from a chair, sitting on a chair and 2-1-2 leg stance were modelled. The forces were subject-specific (two subjects) and the mean differences in the calculated and measured values were 13.45% and 18.11% for the two subjects investigated. For the normal walk (1.43 m/s) the mean peak hip joint contact force was around 3.1 times BW. The measured forces using instrumented prosthesis during initial loading, early and late swing and late stance were found to be higher than the calculated values. This was thought to be due to antagonistic muscles contributing towards measured forces and not being modelled.

Fraysse and colleagues predicted joint contact force of 4.0 times BW for a walking cycle (Fraysse *et al.*, 2009). They used inverse dynamics to derive the joint reaction forces and then an optimization scheme to derive hip contact forces for 9 healthy subjects by considering the muscle contractions. They used minimization of the sum of squared muscle stresses as the objective function which was proposed earlier Crowninshield and Brand (Crowninshield and Brand, 1981).

The optimization models discussed above used polynomial forms of objective function along with additional constraints to ensure that the solution represented physiological phenomenon. Soft saturation criterion proposed by Siemienski, on the other hand, does not require such additional constraints as the objective function

itself ensures that none of the muscles are maximally loaded “if another, less-loaded, muscle can contribute to carrying the external load “(Siemienski, 1992). However, both these criteria face numerical problems as the power of objective function increases. Rasmussen and colleagues thus proposed min/max criteria which can be transformed into a linear problem using bound formulation and thus numerically easier and efficient to solve (Rasmussen *et al.*, 2001; Damsgaard *et al.*, 2006). The objective here is to minimize “maximal muscle activity” without having to need any additional constraints (Damsgaard *et al.*, 2006).

The usefulness of the mathematical models does not lie merely in the fact that they can verify the experimental/clinical outcomes but also in parametric studies (Johnston *et al.*, 1979; Rohrle *et al.*, 1984; Iglic *et al.*, 1993a) as is already seen in dependence of hip joint forces on walking speed. Johnston and colleagues created a mathematical model of the hip joint to study the effects of joint replacement and its variations on the joint load (Johnston *et al.*, 1979). They noticed that the contact forces increased with the increase in femoral shaft-prosthetic neck angle. The angles between 130° and 140° gave minimum bending moment about the stem-neck junction of the prosthesis and 130° was found to be the optimal angle. The placement of the acetabular component was found to be of prime importance in reducing the loads with the optimum position being placing the centre “as medially, inferiorly and anteriorly as was anatomically possible”. The effect of moving the greater trochanter laterally was found to be insignificant.

Iglic and colleagues have also shown using their reduction model, in one-legged stance, that the hip muscle resultant force and the hip joint contact forces depend upon the pelvic shape (Iglic *et al.*, 1993c). Both these parameters increased with the half inter-hip distance as well as for higher laterally inclined hips.

Neural networks is also gaining acceptance in clinical biomechanics at least as a classification tool; e.g. to diagnose the healthy and diseased walking patterns by estimating speed and inclination of walking (Aminian *et al.*, 1995; Schöllhorn, 2004).

1.5.2 Experimental and Clinical Studies

Rydell was the first to use instrumented prosthesis with strain gauges to measure *in vivo* (Rydell, 1965) contact forces. He observed the typical double peak for walking and found an increase in contact forces with increasing walking speed as predicted in the mathematical models discussed earlier. He found contact forces as high as ~1766N which was about 2.5 times BW during fast walking with a speed of 1.3 m/sec (**Table 1-4**). This was same as the force acting during standing on one

leg. In a study with two patients Rydell found peak forces of 2.3 and 2.9 times BW in one legged stance (Rydell, 1966). For walking speeds of 1.1 m/s and 1.4 m/s, the values at first peak were 3.0 and 3.3 times BW. The disadvantage of this prosthesis was that the contact had to be kept inside the connective tissue and hence needed to be opened up again in order to take measurements.

Table 1-4 Peak hip joint forces measured in different experimental and clinical studies

Reference	Peak Hip Joint Force (× BW)		Activity
	Max	Average	
(Rydell, 1965)	1.8	--	Walking (0.9 m/s)
	2.5	--	Walking (1.3 m/s)
	2.5	--	One-legged stance
(Rydell, 1966)	3.0	--	Walking (1.1 m/s)
	3.3	--	Walking (1.4 m/s)
	2.9	--	One-legged stance
(English and Kilvington, 1979)	2.7	--	Walking (0.73 m/s)
	3.59	--	One-legged stance
(Davy <i>et al.</i> , 1988)	2.8	2.64	Walking (0.5 m/s)
	2.6	--	Stair climbing (step height – 170 mm)
	2.1	--	One-legged stance
(Kotzar <i>et al.</i> , 1991)	--	2.4	Walking (0.9 m/s)
	--	2.5	Walking (1.1 m/s)
	--	2.8	Walking (1.3 m/s)
	--	3.6	Walking (1.8 m/s)
	--	2.6	One-legged stance
	5.5	--	Instability during one-legged stance
	--	2.6	Ascending stairs
--	1.23	Rising from chair (chair height – 445 mm)	
(Bergmann <i>et al.</i> , 1993)	8.7	--	Stumbling
(Brand <i>et al.</i> , 1994)	3.5	--	Walking (0.94 – 0.97 m/s)
	3.3	--	Walking (1.11 – 1.36 m/s)
(Bergmann, 2001; Bergmann <i>et al.</i> , 2001)	--	2.33	Walking (1.08 m/s)
	--	2.32	One-legged stance
	--	2.52	Ascending stairs (step height – 170 mm)
	--	2.60	Descending stairs (step height – 170 mm)
	--	1.90	Rising from chair (chair height – 500 mm)

English and Kilvington were the first to use a telemetric instrumented prosthesis (English and Kilvington, 1979). They found the hip forces of 2.7 and 1.25 times BW in stance and swing phase respectively 42 days after the operation and patient walking at a speed of 0.73 m/s. Twelve days post-operatively, the forces

were as high as 3.59 times BW in one-legged stance with hand support. Davy and colleagues recorded the forces active on the hip joint using a telemetric prosthesis in one patient within a month of operation and found the forces of around 2.6 to 2.8 times BW in stance phase of gait at 0.5 m/s (Davy *et al.*, 1988). In one-legged stance they found the contact force to be 2.1 times BW which increased to 2.6 times BW during stair climbing.

Kotzar and colleagues reported on two patients undergoing various activities like walking, rising from chair, ascending stairs, etc. (Kotzar *et al.*, 1991). The maximum peak of 5.5 times BW was found during instability when one of the patients was trying to stand on one leg. The dependence of contact forces on speed was also highlighted by this study.

Bergmann and colleagues have conducted several studies on the hip joint (Bergmann *et al.*, 1993; Bergmann *et al.*, 1995a; Bergmann *et al.*, 1995b; Bergmann *et al.*, 1997; Bergmann *et al.*, 2001) using instrumented prostheses. Their pioneering work has enabled not only them but other researchers to successfully advance the field to the point where it is today. They have found the forces to be as low as 0.26 times BW (rising from a chair) and as high as 2.6 times BW (going down the stairs).

The dependence of forces on the speed of gait was also observed in their studies (Bergmann *et al.*, 1993). They observed an increase in the median peak forces with an increase in walking speed. The angle made by the peak forces with the vertical axis in the frontal plane was found to remain almost constant during activities such as walking, running, stumbling, etc. (Bergmann *et al.*, 1993; Bergmann *et al.*, 2001). Gait analysis data along with hip joint contact forces and ground reactions forces have been documented for the most common human activities like walking, stair climbing, standing up, etc. by Bergmann and colleagues (Bergmann, 2001; Bergmann *et al.*, 2001). They found the average peak force of 233% of BW (2.33 times BW) during normal walking with a speed of 1.08 m/s. They have also reported the joint contact forces of 2.52 times BW while climbing stairs. For going downstairs they were 2.60 times BW. An extremely high magnitude load of 870% of BW (~9 times BW) was observed in the hip joint by Bergmann and colleagues (Bergmann *et al.*, 1993) during stumbling in their clinical study.

It should be noted that these clinical studies were carried out on patients with medical conditions and hence cannot be classified as normal hips. Either both the acetabulum and femoral head or just the femoral head are usually replaced thus compromising the natural configuration of the joints. Having said that, it was observed that the clinical studies gave qualitatively similar results as those predicted by analytical studies, however, the contact forces at the hip, measured

using instrumented prosthesis have usually been found to be lower than those found by analytical studies (Bergmann *et al.*, 1993; Brand *et al.*, 1994) as can be seen from **Table 1-2** and **Table 1-4**. However, the mathematical models are becoming increasingly complex and have become more accurate over time (Brand *et al.*, 1994; Stansfield *et al.*, 2003).

1.6 Biotribology

Friction, lubrication and wear in living systems is referred to as biotribology. The human or animal joints possess exceptional lubrication properties with very low coefficient of friction and show remarkably low wear rates.

1.6.1 Friction

Friction is the resistance to motion when two surfaces move relative to each other. This resistance may be due to the microscopic asperities on two surfaces touching each other or because of shear resistance due to the viscosity of the lubricating fluid present between the surfaces. The surface of articular cartilage is microscopically rough (arithmetic mean deviation under unloaded conditions, $R_a = 1$ to $6 \mu\text{m}$) when compared to a metal femoral head ($R_a = 0.025 \mu\text{m}$ (Dowson, 1981)) or ceramic surface ($R_a = 0.005 \mu\text{m}$ (Jin *et al.*, 1997)). In spite of this, the coefficient of friction of cartilage has been found to be extremely low and is in the range of 0.001 – 0.02 (Mow and Lai, 1980; Macirowski *et al.*, 1994; Persson, 2000).

When cartilage is loaded with another cartilage or with a rigid prosthesis/indenter, more than 90% of the load is sustained by interstitial fluid resulting in minimal solid to solid contact (Macirowski *et al.*, 1994; Ateshian and Wang, 1995; Ateshian, 1997). However, as the cartilage gets consolidated, load is increasingly sustained by the solid phase resulting in increased solid-to-solid contact. This, in turn, increases the coefficient of friction. To account for this increase in coefficient of friction, it has been described as “effective coefficient of friction”. On the other hand “equilibrium coefficient of friction” describes when the cartilage consolidation has reached its equilibrium and the entire load is carried by the solid phase. Thus, even if the equilibrium coefficient of friction is high, the effective coefficient of friction will depend on the load partitioning between fluid and solid phases and will be very low when the load sustained by the fluid phase is very high. The typical creep equilibrium time for human/bovine cartilage of thickness 2 – 4 mm is between 4 – 16 hours whereas less than 1 mm thick rabbit cartilage will take around 1 hour (Mow *et al.*, 1980; Mow and Hung, 2001). From this it is clear

that the low coefficient of friction will prevail over a very long time periods.

It follows from this discussion that, if W is the total normal load with the fluid and solid phases sustaining W_f and W_s respectively, then

$$W = W_f + W_s \quad (1.1)$$

and,

$$\mu_{\text{eff}} = \mu_{\text{eq}} \frac{W_s}{W} \quad (1.2)$$

where,

μ_{eff} – Effective coefficient of friction

μ_{eq} – Equilibrium coefficient of friction

As can be seen from **Equations (1.1) and (1.2)**, effective coefficient of friction will be very low even if the equilibrium value is high as long as the load supported by the fluid phase is very high. **Equation (1.2)** is valid when the cartilage is loaded with a rigid prosthesis/indenter or with another cartilage when solid area fraction is neglected (Ateshian, 1997).

However, when solid area fraction, ϕ , is taken into account, **Equation (1.2)** can be written as (Ateshian *et al.*, 1998; Park *et al.*, 2003):

$$\mu_{\text{eff}} = \mu_{\text{eq}} \left[1 - (1 - \phi) \frac{W_f}{W} \right] \quad (1.3)$$

If μ_{eq} is 0.3 and fluid load support is 90%, then without accounting for solid area fraction, μ_{eff} would be 0.03. However, if the articulating cartilages are assumed to be made up of 70% water, then the maximum solid area fraction would be 0.09 (0.3×0.3). This would increase effective coefficient of friction to 0.05.

1.6.2 Wear

Wear of articular cartilage is “the amount and rate at which the organic phase of the tissue is lost from joint surfaces” (Lipshitz and Glimcher, 1979) as it moves in contact with other surfaces. The wear can be broadly classified as interfacial, like adhesion and abrasion, which is due to the interaction between the two contacting solid surfaces and fatigue which is due to the “accumulation of microscopic damage” due to cyclic stresses and strains (Armstrong and Mow, 1980; Ateshian and Mow, 2005). Wear rates of cartilage are low and are extremely difficult to measure due to the swelling of the cartilage owing to its hydrophilic nature (Armstrong and Mow, 1980; Ateshian and Mow, 2005). Several techniques, such as optical profilometer, measuring PG content in the tissue before and after tests, and analysing lubricating fluid after the test for collagen and PG contents have been used to measure wear (Lipshitz *et al.*, 1975; Verberne *et al.*, 2009). Lipshitz and his colleagues quantified the wear rates by sliding a stainless steel plate against a bovine cartilage surface and then measuring the hydroxyproline and hexosamine contents in the debris. Hydroxyproline and hexosamine were used as collagen and proteoglycan markers respectively (Lipshitz *et al.*, 1975; Lipshitz and Glimcher, 1979). Their general observations were that the wear rates increased with increasing normal load and relative speed of the surfaces; decreased with time attaining an equilibrium value. The dependence of wear on normal load and test duration (increasing with increase in both parameters) was also recently shown (Verberne *et al.*, 2009). The wear rates have also been shown to increase with contact stresses (Katta *et al.*, 2009; McCann *et al.*, 2009) and decrease with increasing conformity between the bearing surfaces (McCann *et al.*, 2009).

1.6.3 Lubrication

Lubrication reduces friction and wear by separating the contacting surfaces. The lubrication mechanism in natural joints is very complex but very efficient and effective, and different theories have been proposed to explain the same. The loads exerted on the joint are varied in nature with respect to space and time. The kinematics of the joint is also complex. Any single proposed theory has failed to explain the lubrication mechanism in each and every loading scenario.

1.6.3.1 Biphasic Lubrication

The hypothesis that the interstitial fluid exuding from the cartilage surface in the loaded region may have a role to play in lubrication was first expounded by

McCutchen and Lewis (Lewis and McCutchen, 1959; McCutchen, 1959). Weeping or hydrostatic lubrication exists when the two articular surfaces come in contact or a cartilage surface comes in contact with another glass/metal counterface, exuding interstitial fluid enough to provide the fluid film of around 15 – 35 μm thus keeping the surfaces separated and lubricated. This has also been demonstrated experimentally (Lewis and McCutchen, 1959; McCutchen, 1962; Macirowski *et al.*, 1994).

It was, however, not until 1980 that the biphasic theory was proposed (Mow *et al.*, 1980) which considered the cartilage to be made up of immiscible and incompressible, fluid and solid phases. Based on this theory, biphasic lubrication was explained (Mow and Lai, 1980). According to this, the load partitioning between solid and fluid phases, and more specifically the larger proportion of load being sustained by the fluid phase (interstitial fluid pressurization) resulted in a lower effective coefficient of friction.

Over the years it has been found that the interstitial fluid pressurisation is the most significant factor in reducing the effective coefficient of friction (McCutchen, 1962; Mow *et al.*, 1992; Macirowski *et al.*, 1994; Forster *et al.*, 1995; Forster and Fisher, 1996; Ateshian, 1997; Ateshian and Wang, 1997; Ateshian *et al.*, 1998; Forster and Fisher, 1999; Katta *et al.*, 2007; Ateshian, 2009). It has not only been directly measured (Soltz and Ateshian, 1998; Park *et al.*, 2003; Krishnan *et al.*, 2004) but has also been shown to be linearly correlated with coefficient of friction in sliding experiments of cartilage against glass under constant loading (Krishnan *et al.*, 2004). However, Oloyede and Broom were the first to experimentally measure interstitial fluid pressurization in one-dimensional static loading in confined compression (Oloyede and Broom, 1991). As mentioned in **section 1.3.2**, the low permeability of the cartilage offers resistance to the fluid flow inducing large drag forces which helps in maintaining high interstitial fluid pressure. It has been found that the fluid phase is capable of supporting more than 90% of the load thus resulting in lesser solid-to-solid contact and hence a lower effective coefficient of friction (Macirowski *et al.*, 1994; Ateshian, 1997; Soltz and Ateshian, 1998; Park *et al.*, 2003). However, this fluid load support increases with congruence (Ateshian and Wang, 1995; Kelkar and Ateshian, 1995; Ateshian, 1997) and is higher when tension-compression non-linearity at the surface of the cartilage is considered (Soltz and Ateshian, 2000; Ateshian, 2009).

In the case of a migrating contact this fluid pressurization is sustainable due to continuous fluid replenishment (Pawaskar *et al.*, 2007; Katta *et al.*, 2009) Moreover, if the contact moves faster than the diffusive velocity of the interstitial fluid ($\sim 10^{-4}$ – 10^{-6} mm/s), higher fluid pressurisation may be maintained over longer time duration

(Caligaris and Ateshian, 2008; Ateshian, 2009). It is thus possible to maintain a very low coefficient of friction over a long time period. However, in the case of stationary contact area or where the sliding distance was such that most of the initial contact area always remained loaded, the coefficient of friction was found to increase over time as the load was slowly transferred to the solid phase (Bell *et al.*, 2006; Caligaris and Ateshian, 2008). The sustainability of high interstitial fluid pressurization has also been analysed using the finite element method (Pawaskar *et al.*, 2007) and the FE predictions agreed well with the experimental results.

The biphasic amorphous layer which is above the superficial tangential zone and composed of mostly fluid has been found to support more load than the bulk of the cartilage (Graindorge *et al.*, 2005; Graindorge *et al.*, 2006).

1.6.3.2 Other Lubrication Mechanisms

Lubrication mechanisms which are not due to the load partitioning have been classified in this category. This includes all the conventional lubrication types along with boosted lubrication.

Sometimes when the two cartilage surfaces move at relatively high speeds such that the fluid is drawn into the converging wedge-shaped gap, the fluid pressure generated can be high enough to lift up the two surfaces away from each other. This is hydrodynamic lubrication and may be present in joints experiencing high speeds and lighter loads as in the glenohumeral joint of the shoulder of the baseball pitcher when he is throwing the ball and also may be during swing phase of walking (Mow, 1969; Ateshian and Mow, 2005). However, to maintain this lubrication the surfaces will have to be continuously moving at relatively high speeds.

When elastic deformation of the contacting surfaces takes place due to the high fluid pressure generated between the surfaces or due to the low elastic modulus of the engaging surfaces, it is called as elastohydrodynamic lubrication. Dowson and Jin showed that due to this fluid pressurization, the asperities were flattened out and the fluid film thickness to R_a ratio was found to increase to 19 (Dowson and Jin, 1986). They called it micro-elastohydrodynamic lubrication.

In the squeeze film lubrication mechanism, the viscosity of the fluid trapped between the two approaching cartilage surfaces does not allow it to be squeezed out giving rise to time-varying pressure fields which can withstand high loads (Hou *et al.*, 1992; Ateshian and Mow, 2005). However, for this lubrication mechanism to exist, the theoretical time required to reduce the fluid film thickness before asperity

contacts occur should be greater than the physiological loading times of the joint (Higginson and Unsworth, 1981; Ateshian and Mow, 2005).

Self-generating lubrication mechanism has been observed under slow and moderate loading in analytical models as well as experimental studies (Mow and Lai, 1979; Mow and Lai, 1980; Kwan *et al.*, 1984; Ateshian and Mow, 2005). Synovial fluid hydrodynamic pressure was modelled with parabolic distribution of normal load sliding over the cartilage surface with physiological speeds and it was observed that the fluid exuded from the leading and trailing edges of this load. It was concluded that the fluid exuding from the leading edge must be providing the lubricant needed to maintain the fluid film.

In some cases, it was noticed that as the two cartilages approach each other, the synovial fluid was filtered through the porous cartilage structures (pore size - 20 – 70 Å) leaving behind a hyaluronic acid - protein complex (size > 4000 Å) which was gel like and was believed to provide lubrication (Balazs *et al.*, 1967; Ateshian and Mow, 2005). This was called boosted lubrication and was proposed in the late 1960s (Maroudas, 1966; Walker *et al.*, 1968). This complex was also observed under scanning electron microscopy (Seller *et al.*, 1971).

Synovial fluid secreted by the synovium in synovial joints has long been studied and debated for its possible role in joint lubrication (Dintenfuss, 1963; Davies, 1966; Dowson, 1966; McCutchen, 1966; Radin, 1968; Ikeuchi, 1995). Synovial fluid is a “dialysate of blood plasma without clotting factors, erythrocytes or haemoglobin”. However, it contains hyaluronate, lubricating glycoprotein and wear-retarding phospholipids (Ateshian and Mow, 2005). These constituents are thought to make synovial fluid an exceptionally good lubricating medium. The effectiveness of synovial fluid as a lubricating fluid has been experimentally shown and found to be better than PBS and Ringer’s solution in lowering the static coefficient of friction (Forster and Fisher, 1996; Schmidt *et al.*, 2007; Schmidt and Sah, 2007; Caligaris *et al.*, 2009).

In the boundary lubrication regime this lubricant layer thickness reduces to a monolayer or more thus increasing asperity contacts which will result in increased wear. In natural synovial joints this monolayer could be either of hyaluronic acid (Bell *et al.*, 2002; Bell *et al.*, 2006; Schmidt *et al.*, 2007) or lubricin (Swann *et al.*, 1979; Swann *et al.*, 1985; Rhee *et al.*, 2005; Schmidt *et al.*, 2007; Gleghorn *et al.*, 2009) or surface-active phospholipids (Hills, 1989; Hills, 2000; Hills and Crawford, 2003; Schmidt *et al.*, 2007) or a several molecule thick “structured water” layer (Davis *et al.*, 1979).

However, given the complexities of the joints it is most likely that various

combinations of these different lubrication modes exist depending upon the operating conditions (Dowson *et al.*, 1981b).

1.7 Osteoarthritis

1.7.1 The Disease and its Etiology

Osteoarthritis (OA), rheumatoid arthritis (RA), impingement of femoral and acetabular bones, avascular necrosis (AVN) and femoral neck fractures are the major conditions that can occur in a hip joint. OA is a degenerative disease of the load-bearing joint wherein the articular cartilage becomes degraded and may ultimately break down completely, bringing two articulating bones into contact causing pain. The cartilage degradation may be caused due to several reasons such as age, injury, improper use or load, trauma, congenital and other joint diseases (Meachim, 1980; Yang, 2003). Its exact etiology is still unknown; however, it is thought to be induced due the mechanical factors causing structural as well as biochemical changes (Radin *et al.*, 1978; Muehleman and Arsenis, 1995; Aigner and McKenna, 2002; Morrell *et al.*, 2005). These structural failures along with altered metabolic activities may cause further cartilage damage (Setton *et al.*, 1999). Osteoarthritis manifests itself as cartilage surface fibrillation, fissures and cracks inside the cartilage, cracks at the cartilage-bone interface and partial or complete loss of the cartilage (Meachim, 1980; Guilak *et al.*, 1994; Atkinson and Haut, 1995; Setton *et al.*, 1999). Apart from the structural changes, compositional and biochemical changes can also be seen such as increased water content and increased synthesis of proteoglycan and collagen (Mankin and Thrasher, 1975; McDevitt and Muir, 1976; Eyre *et al.*, 1980; Carney *et al.*, 1984; Ratcliffe *et al.*, 1994; Setton *et al.*, 1999). Though the proteoglycan synthesis has been found to increase in OA cartilage, its content has been observed to decrease (McDevitt and Muir, 1976; Setton *et al.*, 1999).

1.7.2 Interventions

The treatment for osteoarthritis can be broadly categorised into non-pharmacological, pharmacological and surgical (Carrabba and Sarzi-Puttini, 2004). Exercise, weight control, physiotherapy, acupuncture and homeopathy are some of the non-pharmacological treatments (Hurley and Walsh, 2001; Carrabba and Sarzi-Puttini, 2004). Folk remedies such as mud baths and drinking herbal tea have also been tried (Lester *et al.*, 2006). The aerobic and strengthening exercises coupled with diet can be helpful in alleviating pain and improving joint functions. Bracings

and footwear have also been used for their simplicity and cost-effectiveness (Pollo, 1998). Thermal therapies, ultrasound, electromagnetic fields have all been used before with limited success along with socio-behavioural interventions (Sarzi-Puttini *et al.*, 2005).

Pharmacological treatments include analgesic and anti-inflammatory drugs, hyaluronic acid (HA) supplements, structure modifying drugs, etc. (Hochberg and Dougados, 2001; Carrabba and Sarzi-Puttini, 2004; Sarzi-Puttini *et al.*, 2005). Analgesic like 'acetaminophen' has been recommended for mild to moderate pain (Shamoon and Hochberg, 2001) and as has ibuprofen (Altman, 1999). Non-steroidal anti-inflammatory drugs (NSAID) are often used to reduce the pain and inflammation but may cause 'upper gastrointestinal complications' (Hochberg and Dougados, 2001). HA supplements have been used to increase the viscoelastic properties of synovial fluid. DMOADs or disease-modifying OA drugs such as glucosamine sulphate dosages and others have been investigated and their efficacy is yet to be fully established (Qvist *et al.*, 2008).

The last group of treatments is invasive surgical techniques which includes arthroscopy, osteotomy, cartilage transplant, resurfacing arthroplasty, hemiarthroplasty and arthroplasty (Ilfeld, 1953; Carrabba and Sarzi-Puttini, 2004; Smith *et al.*, 2005; Peltier, 2007). Arthroscopy involves using an arthroscope to look inside the joint to either evaluate the cartilage or repair it using techniques such as suturing (Sekiya *et al.*, 2009) or removing loose particles or cartilage by shaving (Carrabba and Sarzi-Puttini, 2004). In osteotomy, the bones such as the tibia, femur or acetabulum are reshaped or moved to correct deformity or improve alignment between the components. It is also carried out to improve joint congruity and in the case of the hip joint improve femoral head coverage (Matsuo *et al.*, 2009). Cartilage transplantation includes such techniques as autologous osteochondral transplant (osteochondral plugs taken from the non weight bearing areas of the same subject) (Brittberg *et al.*, 1994) and osteochondral allograft transplant (grafts taken from a donor) (Williams *et al.*, 2007). Autologous chondrocyte implantation (ACI) is another such technique in which chondrocytes from the subject's cartilage are separated and harvested in a laboratory conditions. They are then implanted in the defect zones and allowed to integrate with the native tissue (Ruano-Ravina and Jato Díaz, 2006). However, the success with these treatments is limited and in the case of ACI which is a relatively newer intervention (Brittberg *et al.*, 1994), there is a lack of long term data to analyse its efficacy. Moreover, in the advanced stages of OA, these treatments may not be as effective.

Hence, joint replacement techniques such as hemiarthroplasty, resurfacing and total arthroplasty are being preferred by more and more people. In hip

resurfacing, the articulating surface is generally replaced either with a metallic (femoral/acetabular) or polyethylene/polyetheretherketone (acetabular) surface (Wagner, 1978; Kurtz and Devine, 2007; Patil *et al.*, 2008). Polyetheretherketone is widely known as PEEK. The neck and head of the femur are left intact in this procedure with minimal of bone removal. The second conservative approach is hemiarthroplasty which will be described in more detail in **Section 1.7.3**. Total arthroplasty involves replacing both the articulating surfaces with artificial prostheses. The femoral head and neck have to be sacrificed in this kind of joint replacement in addition to drilling into the femoral shaft to accommodate prosthetic shaft. Femoral components are usually rigid metallic or ceramic materials (Wang *et al.*, 1998). The acetabular cavity needs to be reamed to fit in polyethylene/metallic/ceramic /polyurethane/PEEK acetabular cup (Livermore *et al.*, 1990; Clarke, 1992; Wang *et al.*, 1998; Smith *et al.*, 2000; Liu *et al.*, 2005).

1.7.3 Hemiarthroplasty

Hemiarthroplasty, as the name suggests is a conservative approach for joint replacement in which only one articulating surface is replaced by a rigid metallic prosthesis. Though it is mainly used for femoral neck fractures (Gebhard *et al.*, 1992; van der Meulen *et al.*, 2002), it can also be used to treat osteoarthritis if it is localised to the femoral head cartilage and the acetabular cartilage is intact (Ilfeld, 1953; Devas and Hinves, 1983; Phillips, 1987). In this kind of arthroplasty, the acetabular cartilage is kept as it is. One of the advantages of first performing hemiarthroplasty is that, if the acetabular cartilage gets severely damaged for any reason, it can be revised to some form of total arthroplasty (Sharkey *et al.*, 1998; Sen *et al.*, 2009). There are two kinds of hemiarthroplasty as follows:

Unipolar Hemiarthroplasty

Unipolar hemiarthroplasty was developed in the 1940s and 1950s mainly to reduce the instances of reoperation after internal fixation complications such as osteonecrosis (Parker *et al.*, 2002; Levine *et al.*, 2007). Two major designs in this category were the Austin-Moore prosthesis with “a solid polished unipolar head with a collared, straight, fenestrated stem designed for noncemented use” and the Thompson prosthesis with “a solid unipolar head and a collared, shorter, curved, nonfenestrated stem”, the latter being available both in noncemented as well as cemented configurations (Levine *et al.*, 2007). Long term survivorship between 5 and 10 years in 94% percent of the unipolar prostheses has been observed in a study done on 162 women subjects over 70 years old, though only 6% of the

patients survived at 10 years (Wachtl *et al.*, 2003).



Figure 1.10 Unipolar Head (Courtesy: DePuy)

However, femoral shaft penetration and dislocations were reported in many patients with this type of prosthesis (D'Arcy and Devas, 1976; Blewitt and Mortimore, 1992). However, the major concern has been the cartilage undergoing erosion accompanied by pain as a consequence of the metallic prosthesis articulating with the native acetabular cartilage, impact loading or due to the mismatch of prosthetic head and native acetabular cavity (D'Arcy and Devas, 1976; Devas and Hinves, 1983; Dalldorf *et al.*, 1995). In an age related study, it was observed that younger patients (< 70 years) tend to have more erosion related complications (D'Arcy and Devas, 1976). The unipolar hemiarthroplasty should be avoided not only in younger patients but also in those patients who have a life expectancy of greater than 5 years (Chandrasekar *et al.*, 2009) and who are active (Kofoed and Kofod, 1983; Phillips, 1989). The duration of which an implant has been in body, is a factor in increasing cases of erosion (Phillips, 1989; Dalldorf *et al.*, 1995). Recently, it has been suggested that coating the prosthetic head with a biocompatible polymer prevents the cartilage erosion due to a significant reduction in friction (Kyomoto *et al.*, 2010).

Another complication with these prostheses is acetabular protrusion in which the medial wall of the acetabulum gets pushed further into the pelvic bone (Berend, 2008). This has also been observed in clinical studies (Whittaker *et al.*, 1972; Soreide *et al.*, 1982; Kofoed and Kofod, 1983).

Cemented prosthesis has been found to be better as they have been shown

to reduce the number of intraoperative periprosthetic fracture incidents (Weinrauch *et al.*, 2006).

In one unique study carried out in canines, it was found that low-temperature isotropic pyrolytic carbon implants had 92% cartilage survivorship compared to 20% with metal alloy (Co-Cr-Mo and titanium) implants for the period of 18 months (Cook *et al.*, 1989). This was thought to be due to lower elastic modulus of carbon and lower stiffness of implant-carbon interface. The resulting cushioning effect would lower shear and contact stresses thus reducing cartilage wear.

Bipolar Hemiarthroplasty

The acetabular cartilage erosion and pain associated with unipolar prosthesis forced the change in design of the prosthesis. Out of this rethinking, two bipolar prosthesis designs emerged in the early 1970s: the Bateman and the Giliberty (Levine *et al.*, 2007). The Hastings design was another such prosthesis that was widely used (Stewart and Papagiannopoulos, 1986). These were born out of an idea that the relative motion between prosthesis and acetabular cartilage needed to be reduced in order to prevent/reduce erosion. These mainly consisted of three components (Levine *et al.*, 2007): 1) modular femoral stem with varying head sizes making it easier to convert it to total hip arthroplasty whenever required; 2) an intermediate bearing of either ultrahigh molecular weight polyethylene (UHMWPE) which articulates with the femoral head; and 3) press-fitted metallic head which is mounted over the intermediate bearing and articulates with acetabular cartilage. The relative motion between intermediate bearing and femoral head mounted on the stem was designed to reduce that between outer metallic head and the cartilage. However, it has been found that the design goals of this prosthesis are not fully met. It has been suggested that bipolar hemiarthroplasty does not offer any advantages over unipolar hemiarthroplasty (Ong *et al.*, 2002; Bhattacharyya and Koval, 2009) and that the inner bearing motion is limited thus causing greater relative motion of the cartilage-outer head bearing resulting in erosion (Drinker and Murray, 1979; Verberne, 1983; Phillips, 1987). However, there have been equally convincing clinical studies showing very little erosion and both the bearings working as designed (Bochner *et al.*, 1988; Goldhill *et al.*, 1991; James and Gallannaugh, 1991). Long term survivorship of around 15 years was observed in 99.4% prostheses with as little as 4.7% revisions/removals in a study of 212 bipolar hemiarthroplasties (Haidukewych *et al.*, 2002).



Figure 1.11 Bipolar Head (Courtesy: DePuy)

However, bipolar hemiarthroplasty has its unique set of complications not found in unipolar hemiarthroplasty. Dislocation or disassembly of modular components is one such complication (Georgiou *et al.*, 2006; Guo *et al.*, 2008; Lee *et al.*, 2008). Apart from better design, careful preoperative planning and meticulous placement of components during the operation may be required in order to avoid such cases. Another complication is osteolysis mostly due to polyethylene wear debris (Bose *et al.*, 1995; Coleman *et al.*, 2001; Rizzo and Pace, 2003). In osteolysis, due to the reaction of wear particles, bone resorption takes place resulting in the loosening of implant. In one particular case this polyethylene wear has been found to be as high as 0.7 mm per year resulting in 56% of cases having osteolysis around the stem after an average of 38 months (Coleman *et al.*, 2001). This was very high compared to 0.13 mm per year observed in polyethylene acetabular component in total hip replacement (Livermore *et al.*, 1990). Metallosis due to metal debris can also result from such a system (Matsuda and Yamamuro, 1994).

Irrespective of whether unipolar or bipolar hemiarthroplasty is used and apart from surgeon training as suggested earlier (Georgiou *et al.*, 2006), using the correct femoral head size also plays an important role in avoiding complications of hemiarthroplasty (van der Meulen *et al.*, 2002). In a non-clinical study it has been shown that the calliper measurement method used by surgeons to measure femoral head diameter has a tendency to undersize it which is further aggravated by “downward rounding” of the implant diameter (Kosashvili *et al.*, 2008). The smaller prosthetic size will lead to increased clearance and reduced contact area resulting

in increased stresses leading to cartilage erosion and pain, and potentially migration of the implant (Harris *et al.*, 1975; Kosashvili *et al.*, 2008). However, an oversized head affects the entire pelvis and tends to increase the periacetabular stresses and those towards the medial side (Finlay *et al.*, 1986). Thus the selection of the correct femoral head size for congruent acetabular fit is an important parameter to be considered when hemiarthroplasty is the chosen intervention (Yamagata *et al.*, 1987; Jeffery and Ong, 2000).

It has also been hypothesised that the cartilage degeneration is not necessarily due to the metallic prosthesis articulating with soft tissue but also due to repetitive stresses (McGibbon *et al.*, 1999).

Femoral components with a non-spherical head have also been investigated (Cathcart, 1971; Cathcart, 1972). Cathcart hypothesised that this type of head shape helps in proper nutrient transportation. He also noticed reduced cartilage erosion and found the patients with full or approaching full range of motions without the use of support.

1.8 Contact Mechanics of Hip Joint

Contact mechanics of articular cartilage plays an important role in the tribology and maintenance of the diarthrodial joint. It is mainly concerned with what happens at the contacting surfaces and its implications to tribology and structural stability of the cartilage. It will typically include investigations of contact forces, contact stresses and contact areas. Though contact pressure has a role to play in cartilage damage and repair; it is not the static pressure that matters but its temporal and spatial distribution and history (Brand, 2005).

Contact stresses are usually calculated from contact forces and corresponding contact area. They have also been directly measured using instrumented prosthesis (Hodge *et al.*, 1986; McGibbon *et al.*, 1999). They play an important role in the tribology of the cartilage (Hodge *et al.*, 1986; Katta *et al.*, 2009), cartilage degradation (Hadley *et al.*, 1990; Maxian *et al.*, 1995; Mavcic *et al.*, 2002), wear of the implants, “preoperative planning and postoperative rehabilitation” (Yoshida *et al.*, 2006). These stresses can be so high in some of the activities of daily living, that they have the potential of inducing several complications in the joint. Excessive wear of the cartilage may result from very high contact stresses. It should be noted that it is not just the high stresses that are damaging to the cartilage but under-loading can have an adverse effect as well due to lesser use of the cartilage (Harrison *et al.*, 1953). The contact stresses are also indicative of the

load distribution within the articulating surfaces which may give an indication of the acetabular areas which are most susceptible to breakdown.

1.8.1 Theoretical Studies

Theoretical models were simple to begin with. The contacting articular surfaces were modelled as elastic spheres (Eberhardt *et al.*, 1990; Eberhardt *et al.*, 1991a; Eberhardt *et al.*, 1991b) mainly for parametric studies of contact stress distribution (such as the effect of cartilage thickness and stiffness, joint curvature and radius of contact). Frictionless rolling contact models of cylindrical biphasic cartilage layers have shown that most of the load is sustained by the fluid phase (Ateshian *et al.*, 1994b; Ateshian and Wang, 1995). The interstitial fluid pressurisation increases with the increase in the joint congruity (Ateshian and Wang, 1995) and is higher when articular surface tension-compression nonlinearity is accounted for (Soltz and Ateshian, 2000). This shields the solid phase from stresses thus protecting the cartilage. These biphasic cartilage models (Ateshian and Wang, 1995; Ateshian and Wang, 1997; Ateshian *et al.*, 1998) helped in the understanding of the role of interstitial fluid pressurisation in reducing frictional coefficient.

The above models are excellent for simpler parametric studies but they cannot replicate the exact conditions in the joint. Whole joint models are thus needed. Mathematical models to predict contact stresses have been developed by several researchers (Ipavec *et al.*, 1999; Daniel *et al.*, 2001; Mavcic *et al.*, 2002; Daniel *et al.*, 2008). These models either use the measured hip resultant forces using instrumented prosthesis (Daniel *et al.*, 2008) or those calculated from mathematical models described before (Igljic *et al.*, 1993b).

A simple mathematical model was proposed by Brinckmann and colleagues to predict contact stresses in the simplified hip joint (Brinckmann *et al.*, 1981). Their model was created using anterior-posterior radiographs of 304 healthy persons. The average peak contact stress for normal hip was around 3.72 MPa for 5 times BW just before toe-off (**Table 1-5**). The corresponding value for a male subject was 3.64 MPa as compared to 3.80 MPa for females.

Ipavec and colleagues developed a model that was stated by non-linear algebraic equations, and used the calculated resultant hip joint force and known geometrical configuration to predict contact stresses (Ipavec *et al.*, 1999). They assumed the cartilage to be the part of the spherical surface and it was modelled as homogeneous, linearly elastic with uniform thickness. The frictional forces were assumed to be negligible. They found that the stress distribution over the

acetabulum cartilage surface and its maximum value varied with load direction. The highest contact stresses were observed in the superior-posterior region of the acetabulum and on the medial side of the femoral head, and contact stresses were distributed non-uniformly. A peak stress of 3.0 MPa was observed in the stance phase of the gait in the normal hip for a load of ~2000 N as against the measured value of around 4.0 MPa (Hodge *et al.*, 1989; Krebs *et al.*, 1991) after the gait had stabilised over 36 – 48 months.

Table 1-5 Peak hip contact stresses predicted by different analytical studies in normal joints

Reference	Peak Hip Contact Stress (MPa)		Load (N)	Activity
	Max	Average		
(Brinckmann <i>et al.</i> , 1981)	--	3.72	5 × BW	Walking
(Ipavec <i>et al.</i> , 1999)	3.0	--	2000	Walking
(Iglıc <i>et al.</i> , 2001)	4.0	2.1	--	One-legged stance
(Mavcic <i>et al.</i> , 2002)	4.27	2.45	1890	One-legged stance
(Recnik <i>et al.</i> , 2007)	--	1.6	2.58 × BW	One-legged stance
(Daniel <i>et al.</i> , 2008)	--	1.8	836 N BW	Walking (1.08 m/s)
	--	2.0	836 N BW	Ascending stairs (step height – 170 mm)
	--	2.1	847 N BW	Descending stairs (step height – 170 mm)

Iglic and colleagues compared the male and female population with respect to normalised peak contact pressures (Iglic *et al.*, 2001). They found mean peak contact pressure per BW was higher for females (4.045 kPa/N) compared to males (3.214 kPa/N). However, the female BW is generally lower than the male. Assuming female BW to be 500 N and that of the male to be 700 N, the absolute values of peak contact pressure works out to be 2.0 MPa for the female and 2.2 MPa for the male. The maximum peak contact pressure of 4.0 MPa was predicted in the female hip. Iglic and colleagues also found that moving the hip joint centre medially and proximal acetabulum over the femoral head laterally would reduce contact stresses (Iglic *et al.*, 1993b).

In another study, dysplastic hip contact stresses normalized with the body

weight were found to be 100% higher as compared to a normal hip in one legged stance (Mavcic *et al.*, 2002). They used the model previously investigated to determine hip muscle forces and contact forces (Igljic *et al.*, 1993c). According to this study, the contact stresses were dependent on the magnitude and direction of load, lateral femoral head coverage and the distance between the centres of two femoral heads. They found the average peak stress to be 3.5 kPa/N in normal hips in one-legged stance for the hip joint load of 2.7 times BW. Assuming BW to be approximately 700 N, the mean peak stress would be 2.45 MPa. The higher peak stresses were attributed to “smaller lateral coverage of the femoral head, the larger interhip distance, the wider pelvis and the medial position of the greater trochanter”.

The stresses are also dependent on acetabular anteversion angle for normal walking with 2.141 kPa/N (normalised to BW) for 7° versus 1.982 kPa/N for 42° (Daniel *et al.*, 2008). It was found that the stresses were higher going down the stairs compared to those in climbing stairs for normal hips. Higher stresses were observed in dysplastic hips. Hip contact stresses have found to be higher in obese subjects leading to faster progression of osteoarthritis (Recnik *et al.*, 2009). In this latter study, a significant correlation was found between obesity and hip arthroplasty carried out at younger age.

To simplify predictions, Daniel and colleagues presented nomograms to calculate maximum contact stresses in the hip in one legged stance (Daniel *et al.*, 2001). They used a model developed earlier (Igljic *et al.*, 1993c) to calculate resultant hip joint forces and then used Ipavec and colleagues' model to calculate contact stresses (Ipavec *et al.*, 1999). Both these models have been put together in the software HIPSTRESS (Igljic *et al.*, 2002). The femoral head and acetabulum were assumed to be spherical and the cartilage was assumed to be of uniform thickness. Once these nomograms were developed, they could be used to calculate maximum hip contact stresses for combinations of geometrical parameters (inter-hip distance, pelvic height, pelvic width, centre-edge angle, etc.) and body weight. The average difference between the maximum contact stresses predicted using HIPSTRESS and nomograms was 4.6%.

In another study, it was reported that the horseshoe shape of the cartilage helped to optimise the contact stresses (Daniel *et al.*, 2005). As seen, most of these models have been used mainly for parametric studies (Igljic *et al.*, 1993b; Igljic *et al.*, 2002).

1.8.2 Experimental and Clinical Studies

Many of the experimental studies performed in a laboratory setup are simplified in terms of specimens used. It has been found that the coefficient of friction decreases with increasing stress levels (Pickard *et al.*, 1998; Ateshian *et al.*, 2003; Katta *et al.*, 2007) and it may be due to flattening out of surface roughness as load/strain increases (Dowson and Jin, 1986; Ateshian *et al.*, 2003). However, recently it has been shown that for contact stresses higher than 0.5 MPa, the coefficient of friction actually increases (Katta *et al.*, 2009; McCann *et al.*, 2009). This was thought to be due to insufficient time available for the tissue to rehydrate itself in friction tests with 4mm stroke length (Katta *et al.*, 2009). This in turn would decrease the fluid load support thus increasing the coefficient of friction. The effect of joint conformity on contact stresses have been investigated in knee hemiarthroplasty (McCann *et al.*, 2009). It was found that the contact stresses increase with a decrease in the conformity resulting in a higher coefficient of friction. This in turn was found to induce more cartilage wear. The increasing contact stresses may also induce increased shear stresses (Katta *et al.*, 2009).

However, the experiments are becoming more and more sophisticated with many preferring to measure the *in vivo* contact forces and stresses. Many (Rydell, 1965; Bergmann *et al.*, 1984; Hodge *et al.*, 1986; Bergmann *et al.*, 1993; Catani *et al.*, 1995; Krebs *et al.*, 1998; Bergmann *et al.*, 2004) have conducted clinical studies on patients and animals using instrumented prosthesis to measure either contact forces or contact stresses. Similarly, a number of studies have been carried out under laboratory conditions (Afoke *et al.*, 1987; Ateshian *et al.*, 1994a; von Eisenhart *et al.*, 1999; von Eisenhart-Rothe *et al.*, 1999) for deriving not only forces and stresses but also the contact areas. Apart from contact parameters mentioned before, there are others such as sphericity of the acetabulum and femoral head, thickness of the cartilage, interstitial fluid pressurisation in the cartilage, etc which affect the contact mechanics of the synovial joints.

Rushfeldt and colleagues used instrumented endoprostheses (Rushfeldt *et al.*, 1981b) in their *in vitro* studies to investigate the pressure distribution in the acetabular cartilage. Loads of up to 2250 N were applied through the acetabulum in a hip joint simulator with prostheses of different sizes. A peak pressure as high as 14.3 MPa with a load of 1350 N (2.5 times BW) was observed for 2 mm undersized prostheses whereas for perfect fit the value was 6.78 MPa (**Table 1-6**). It was noticed that the peak and average pressure on the cartilage surface decreased, and contact area increased with time. The increase in clearance, however, decreased the contact area and increased both the peak and average contact pressure. The contact pressure was also found to vary non-linearly with load.

Table 1-6 Peak hip contact stresses measured in different experimental and clinical studies

Reference	Peak Hip Contact Stress (MPa)		Load (N)	Activity
	Max	Average		
(Day <i>et al.</i> , 1975)	5.3	--	1736	Static loading
(Rushfeld <i>et al.</i> , 1979)	6.8	--	1350	Static loading
(Rushfeldt <i>et al.</i> , 1981b)	6.78	--	1350	Static loading
(Brown and Shaw, 1982)	3.45	--	1557	Static loading
(Brown and Shaw, 1983)	--	8.80	2770	Walking
(Adams and Swanson, 1985)	8.57	--	2380	Walking
(Afoke <i>et al.</i> , 1987)	10.4	--	2936	Walking
(Hodge <i>et al.</i> , 1989)	5.5	--	667 N	Walking
	10.7	--	(BW);	Ascending stairs
	18.0	--	load not given	Rising from chair
(Krebs <i>et al.</i> , 1991)	3.69	--	667 N BW	Walking (1.2 m/s)
(Macirowski <i>et al.</i> , 1994)	5.0	--	900	Static loading
(von Eisenhart-Rothe <i>et al.</i> , 1997)	9.0	--	3 × BW	Static loading
(Hak <i>et al.</i> , 1998)	--	12.1	2013	Static loading
(McGibbon <i>et al.</i> , 1999)	6.5	--	--	Walking
(Park <i>et al.</i> , 1999)	5.2	--	530 N	Walking
	9.0	--	BW	Ascending stairs (step height – 180 mm)
	16.4	--		Descending stairs (step height – 180 mm)
	5.4	--		Rising from chair (100% knee height)
(von Eisenhart <i>et al.</i> , 1999)	9.75	7.7	3.45 × BW	Walking (1.08 m/s)
(Anderson <i>et al.</i> , 2008)	--	>10	1949	Walking (1.08 m/s)
	--	>10	2103	Ascending stairs (step height – 170 mm)
	--	>10	2207	Descending stairs (step height – 170 mm)

The pressure distribution, which was elongated in anteroposterior direction with steep medialateral pressure gradient, was neither uniform nor axisymmetric about the load vector and was attributed to the non-uniform cartilage thickness and irregular cartilage-bone interface (Rushfeld *et al.*, 1979; Rushfeldt *et al.*, 1981b). This was also shown by Brown and Shaw using miniature piezoresistive contact

stress transducers embedded in femoral head cartilage for their *in vitro* studies to investigate the contact stress distribution (Brown and Shaw, 1982). Their study found that the contact stress distribution was not axisymmetric and was also anteroposteriorly oriented as was found by Rushfeldt and colleagues. They found stresses of around 3.45 MPa for a load of 1557 N. In another study, they found a spatial mean pressure of 2.92 MPa and local mean peak pressure of 8.80 MPa for a load of 2700 N (Brown and Shaw, 1983). The maximum pressure was in the acetabular dome.

Adams and Swanson used piezoelectric pressure transducers and positioned them in the acetabulum through holes drilled in the cancellous bone (Adams and Swanson, 1985). The subchondral bone and the cartilage were kept intact. They noticed highest pressure ranged from 5.26 to 8.57 MPa during heel off when the load was 4.17 times BW (2380 N). In a study by Day and colleagues, using displacement transducers placed through the hole cut through the bone and the cartilage, the static load of 3 times BW was applied (Day *et al.*, 1975). In this study of seventeen cadaver hips, they found peak pressures of between 4.0 and 5.0 MPa. Average pressures were frequently observed in the lateral side of the acetabular cartilage. A peak pressure of 5.3 MPa was observed in one specimen near the acetabular notch with 3 times BW (1736 N).

Hodge and colleagues (Hodge *et al.*, 1986; Hodge *et al.*, 1989) used instrumented endoprosthesis to record the *in vivo* contact pressures in the hip joint during different activities. They kept the acetabular cartilage intact. During normal walking, maximum pressures of 5.5 MPa in the acetabular dome were recorded at twelve months post-operative. Stair climbing was another strenuous activity in which a contact pressure of 10.7 MPa was noted twelve months after the operation. Rising from the chair gave very high pressures in the acetabulum (9.2 – 15 MPa) and the pressure increased with the decrease in the chair height. Contact pressures as high as 18 MPa, have been reported (Hodge *et al.*, 1986; Hodge *et al.*, 1989; Morrell *et al.*, 2005) twelve months after joint replacement surgery while rising from the chair. The contact pressures were non-uniform and sudden change in their gradients with respect to time and location observed in this study agreed with those mentioned earlier. The pressure also depended upon different activities and it increased from walking to stair climbing to rising from the chair. However, peak pressures generally decreased with post-operative time and this was also observed by McGibbon and colleagues in their hemiarthroplasty study with instrumented prosthesis (McGibbon *et al.*, 1999). They observed peak pressures of 4.5 – 6.5 MPa in the acetabular dome during walking. The high pressures observed in these studies may be induced due to the muscle co-contraction (Park *et al.*, 1999) and

may result in cartilage degradation often observed in the dome (McGibbon *et al.*, 1999). In another hemiarthroplasty study with instrumented endoprosthesis, Park and colleagues observed peak pressure of more than 5.2 MPa for walking two years post-operative and the peak pressure for descending stairs (16.4 MPa) was higher than those for ascending stairs (9.0 MPa) (Park *et al.*, 1999). In a similarly instrumented study, *in vivo* a mean peak contact pressure of 3.69 MPa has been reported during walking with an average speed of 1.2 m/s (Krebs *et al.*, 1991) 48 months after operation.

The non-uniform pressure distribution was also observed by Macirowski and colleagues (Macirowski *et al.*, 1994) in static loading conditions. They conducted *in vitro* experiments on human acetabular cartilage using instrumented endoprosthesis. They also observed that the contact pressure distribution was mostly in the antero-posterior direction. Their experiments coupled with a numerical study confirmed the biphasic lubrication phenomenon. They observed pressures as high as 5.0 MPa for a load of 900 N which slowly decreased over time. They observed that when the cartilage was loaded the pressure difference within the surface distance of less than 10 mm was of the order of MPa. This they believed was due to an inter-articular sealing phenomenon. Though the acetabular and femoral cartilages are approximately spherical (Rushfeldt *et al.*, 1981a) or conchoidal (Menschik, 1997), their surfaces have ridges of around 150 μm height (root mean square distance). Thus when the cartilages are loaded, the peaks of these ridges will come in contact first thus trapping the fluid between them and forming a seal. Macirowski and colleagues believed that this caused the surface stresses to be non-uniform and contributed towards slower consolidation. They hypothesised that the breaking of these seals may lead to cartilage destruction.

Ferguson and colleagues, however, observed uniform hydrostatic pressure in the inter-articular fluid film in their *in vitro* studies of the hip joint (Ferguson *et al.*, 2002; Ferguson *et al.*, 2003) where the acetabular labrum was intact and inter-articular fluid was present. However, in the absence of any major short term contact between cartilages, how this would affect the contact stresses and what sort of stress distribution will be at the cartilage surfaces in the long run cannot be inferred from this study. Moreover, only one pressure transducer was used in this study and the pressure measurement could be local to the transducer placement.

Contact stresses have also been found using pressure sensitive films (Afoke *et al.*, 1987; Anderson *et al.*, 2008). In the *in vitro* study by Afoke and colleagues three distinct phases of gait; viz. heel strike, flat foot and just before toe off were simulated using loads of 3.3 times BW, 1.3 times BW and 4 times BW respectively. A peak pressure of 10 MPa was noted in this study during heel strike and the

pressure distribution was non-uniform with the antero-superior region of the acetabulum showing high pressure gradients. Anderson and colleagues used the film to find the contact stresses for comparison with FE results (Anderson *et al.*, 2007; Anderson *et al.*, 2008). Spatially averaged contact pressures in walking, climbing stairs and descending stairs were in the range of 4.4 – 5.0 MPa with the average pressures in stair climbing found to be higher than those during descending stairs. Antero-posterior and superior dome pressure distributions have also been observed by Bay and colleagues in their *in vitro* studies using pressure sensitive films (Bay *et al.*, 1997). Similarly Hak and colleagues observed a maximum peak pressure of 12.1 MPa with a load of 2013 N in the superior part of the acetabulum (Hak *et al.*, 1998).

In another *in vitro* study using pressure films, the antero-posterior distribution was clearly visible (von Eisenhart-Rothe *et al.*, 1997). However, the formation of the contact itself did not show any regular pattern. In some cases the contact was first formed at the anterior and posterior horns at lower loads merging with the dome at higher loads while in some other specimens it formed at the dome moving to the anterior and posterior regions. A maximum pressure of 8 – 9 MPa was observed at loads of 3 times BW. In their study for different phases of normal walking (1.08 m/s), von Eisenhart and colleagues found the mean peak pressure to be 7.7 MPa for a load of 3.45 times BW during mid-stance (von Eisenhart *et al.*, 1999). Maximum peak pressure was 9.75 MPa.

One of the important factors affecting contact stresses has been shown to be the contact areas. The spatially averaged contact stresses when climbing stairs were found to be more than when going down the stairs (5.0 MPa versus 4.4 MPa (Anderson *et al.*, 2008)) in spite of the peak contact forces being smaller in the former case (252% versus 260% BW (Bergmann *et al.*, 2001)). This was because the average contact area while ascending stairs (321.9 mm²) was smaller than descending stairs (~370 mm²)(Anderson *et al.*, 2008).

Contact areas have been measured *in vitro* using techniques such as dye staining, casting, pressure sensitive films, stereophotogrammetry (Ateshian *et al.*, 1994a). Newer techniques such as MRI have also been used (Yoshida *et al.*, 2009).

In the dye-staining method, either Safranin (Greenwald and O'Connor, 1971) or a combination of 0.01 M solutions of sodium ferrocyanide and ferric ammonium sulfate in normal saline (Black *et al.*, 1981; Ateshian *et al.*, 1994a) are used to dye non-contacting surfaces under load when injected into the joint capsule. The area can then be found by taking a photograph of the surface (Ateshian *et al.*, 1994a) or by using sheet of gauze with square holes and counting the holes within the non-dyed area (Greenwald and O'Connor, 1971).

In casting method, casting materials such as methylemethacrylate or silicone rubber are injected into the joint after loading and the cast will leave holes in the contact areas (Miyanaga *et al.*, 1984; Mow *et al.*, 1993; Wan *et al.*, 2006). In another technique called the 3S technique (silicone oil-carbon black powder suspension squeeze technique), the suspension is applied to one of the articulating surface (Yao and Seedhom, 1991). On being loaded, this suspension will be squeezed out of the contact area thus marking it. The areas are then photographed for further analysis. Polyether has also been used as a casting material with good reproducibility (Eckstein *et al.*, 1997; von Eisenhart-Rothe *et al.*, 1997).

Optical methods, such as stereophotogrammetry have also been used to find contact areas (Soslowky *et al.*, 1992; Ateshian *et al.*, 1994a). In this method, a stereogram was taken of the optical targets attached to the opposite bones of the articulating joint which was kept loaded in specially built calibration frame with 16 reference targets of known three-dimensional coordinates. Another stereogram of the optical targets as well the articular surface was then taken with the joint disarticulated. The optical grid was projected on the articular surfaces to get the distinct points. The two stereograms and the relative positions of optical targets and the surface grid points were then used to create geometric model of the joint which could be realigned to the desired position. The correction criterion was then applied for cartilage deformation and contact areas were found based on proximity of points on two surfaces.

Pressure sensitive films have been widely used to find out the contact areas (Ateshian *et al.*, 1994a; Anderson *et al.*, 2007). They are comprised of one or two sheets which when pressed burst the chemical containing micro-bubbles thus staining the same or the second sheet (Ateshian *et al.*, 1994a). The intensity of the colour will give the contact pressures and the stained area itself will be the contact area. In activities such as walking, ascending and descending stairs, average contact areas of 321.9 mm² – 425.1 mm² have been measured (Anderson *et al.*, 2008). Hak and colleagues measured increasing contact areas with increasing load (Hak *et al.*, 1998). They recorded the maximum contact area of 452.8 mm² for a load of 2835 N. The minimum contact area was 38.0 mm² for 141 N. A similar trend was also reported by Miyanaga and colleagues (Miyanaga *et al.*, 1984). They found contact areas as high as 78.6% of the total acetabular cartilage area or 1270 mm² for a load of 2000N. Corresponding values for 1000 N were 55.5% and 860 mm².

Radiography methods have also been employed in calculating actual or potential contact areas (Konishi and Mieno, 1993; Yoshida *et al.*, 2009). In radiography X-ray, CT or MRI is used to capture an image of the articulating surfaces which is then processed to calculate the contact area. Yoshida and

colleagues, in their MRI study of the tibiofemoral joint measured the contact length in each and every MR slice and built the contact area by combining these lengths.

The shape of the acetabular cup also plays an important role in the contact mechanics. Rushfeldt and colleagues (Rushfeldt *et al.*, 1981a) attempted to measure the *in vitro* acetabular cartilage geometry and thickness using an ultrasound technique. They noticed that the cartilage surface under unloaded conditions was more or less spherical with a deviation from sphericity of around 150 μm . The corresponding value for the cartilage-bone interface was found to be 500 μm . Menschik, based on his study of eight normal hips, concluded that both the acetabulum and femoral head approximate more closely to a conchoid shape rather than spherical one (Menschik, 1997). There are others who hypothesise the shape to be a rotational ellipsoid which has a better surface fitting error than conchoids (Gu *et al.*, 2008). The conchoid or rotational ellipsoid is more in line with the earlier findings that during the swing phase of gait, the contact developed at the anterior and posterior parts of the acetabulum with the dome slowly coming in contact as the load was increased (Greenwald and O'Connor, 1971; Greenwald and Haynes, 1972).

As can be seen from **Table 1-5** and **Table 1-6**, the contact stresses predicted by the analytical models were lower than those found in clinical studies. One of the reasons for that is the ideal geometry (usually spherical) that is being assumed for both the acetabular cup and femoral head. Secondly, the cartilage surfaces are very smooth in analytical studies as compared to those in subject-specific clinical studies. This causes the local contacts to be formed in the latter kind of studies as has been shown in this section. It should also be noted that the subjects in clinical studies have undergone hip replacement (either total or hemiarthroplasty) due to a medical condition and hence cannot be considered normal. In analytical studies, the parameters can be varied to study normal hips.

1.8.3 Finite Element/Numerical Studies

The simplest of these models represent a smaller cartilage specimen under a variety of configurations (Donzelli and Spilker, 1998; Warner *et al.*, 2001a; Federico *et al.*, 2004; Pawaskar *et al.*, 2007). Donzelli and colleagues developed a transversely isotropic linear biphasic model (Donzelli *et al.*, 1999). The surface principal stresses were found to increase with the decrease in the cartilage surface curvature which was not seen in isotropic models. The contact model with biphasic material properties by Warner and colleagues has shown that the compressive strains and the fluid pressure decreased with the increasing radius of a

hemispherical indenter (Warner *et al.*, 2001a). The values of the parameter were also lower when compared to a plane ended cylindrical indenter.

The axisymmetric poroelastic joint contact mechanics model presented by Federico and colleagues (Federico *et al.*, 2004) found that the fluid boundary conditions have a significant effect on the predictions. Open surface conditions were better suited than a sealed one for representing the actual cartilage. However, the contact dependent surface flow boundary conditions are ideal in investigating contact mechanics problems (Warner *et al.*, 2001b). Early OA cartilage was found to show decrease in peak fluid pressure by half and increase in contact area by 30% which agreed well with the experimental results on feline patello-femoral joints which showed 50% decrease in peak pore pressure and 22% increase in contact area (Herzog *et al.*, 1998).

The migrating contact problem has also been modelled (Pawaskar *et al.*, 2007). It was found that the fluid load support remained very high at around 80% over the entire duration of the simulation at a stroke length of 8 mm with sliding velocity of 4 mm/s. However, this decreased in the case of static loading and when the stroke length was such that most of the initial contact area always remained loaded.

Maciowski and colleagues used a simpler model (Maciowski *et al.*, 1994) to confirm very high (around 90%) fluid load support even after long time periods (20 min.), for loads of 450 N and 900 N. They also observed a reduction in normal fluid flow over time and that the maximum fluid velocities occurred at locations of high surface stress and gradients. The average contact stresses reported by them were around 1.9 MPa for the load of 900 N.

Ferguson and colleagues (Ferguson *et al.*, 2000a; Ferguson *et al.*, 2000b) have worked on poroelastic hip cartilage models with special emphasis on the acetabular labrum sealing effect. They proposed that the labrum trapped the fluid between the cartilage layers so that there was no cartilage to cartilage contact which helped in maintaining high interstitial fluid pressure over a long period of time thus providing excellent tribological properties. They also found that consolidation was 40% quicker in joints without the labrum. In one of their models (Ferguson *et al.*, 2000b) they modelled trapped incompressible fluid using poroelastic elements with very high permeability and water content, and very low stiffness. The inclusion of the labrum has also been found to decrease contact pressures in the acetabulum (Adams *et al.*, 2010). An increase in the labrum stiffness was found to change this pressure and increase labrum load support. Not everyone however, agrees with this observation (Konrath *et al.*, 1998).

The FE models of the hip joint are many times simplified (Brown and DiGioia, 1984; Cilingir *et al.*, 2007; Cilingir *et al.*, 2008). Brown and DiGioia analysed a two-dimensional plane strain non-linear model of hip joint (Brown and DiGioia, 1984). The cartilage was modelled as homogeneous, isotropic and linearly elastic. Only qualitative investigation of inter-articular contact stresses was carried out and they were found to increase almost linearly with the load. The coefficient of friction was found to have no effect on normal contact stresses. The increase in the cartilage modulus was found to increase the load taken up by the cartilage for the same amount of deformation with the corresponding increase in the stresses. The maximum stresses occurred at the “acetabular dome” region. Assuming the contact stress distribution to be axisymmetric about the load vector (which is not the case as seen in clinical studies in **Section 1.8.2**), the computational predictions of peak stresses were thought to be sufficiently close to the experimental results. However, if one compares the experimental and FE peak stresses at 2500N load, it could be seen that the difference was more than 25% (FE – 5.9 MPa v/s experimental – 8.0 MPa).

Cilingir and colleagues (Cilingir *et al.*, 2008) modelled the hip joint with biphasic acetabular cartilage interacting with a metallic hip resurfacing prosthesis. The model was simplified and axisymmetric and surface flow conditions were manually imposed. They found an increase in both the contact and fluid pressures (at the centre of the contact) with increasing radial clearance. Moreover, an increase in the load and a decrease in the cartilage thickness were accompanied by an increase in these pressures (both contact and fluid). For a load of 2500 N, radial clearance of 0.5 mm and cartilage thickness of 2mm; the contact pressure at the centre of the contact was found to be around 3.75 MPa whereas the corresponding fluid pressure was 3.5 MPa.

The computational models are becoming more and more complex and realistic (Genda *et al.*, 1995; Bachtar *et al.*, 2006; Yoshida *et al.*, 2006; Anderson *et al.*, 2008) as higher computational speeds and larger processing space are available at a cheaper price. In these models, usually loads are applied to the hip joint and the contact pressures and areas are predicted.

Cilingir and colleagues analysed a three-dimensional hip model with homogeneous, isotropic and linearly elastic acetabular cartilage (Cilingir *et al.*, 2007) and a metallic femoral resurfacing prosthesis. They reported peak contact stresses of 2.29 MPa for a load of 3200 N, radial clearance of 0.5 mm and cartilage thickness of 2 mm. The corresponding contact area was 958 mm².

Table 1-7 Peak hip contact stresses predicted by different finite element/numerical studies

Reference	Peak Hip Contact Stress (MPa)		Load (N)	Activity	Type of Study
	Max	Average			
(Brown and DiGioia, 1984)	--	5.9	2500	Static loading	FE
(Genda <i>et al.</i> , 1995)	--	2.55	2482	Walking	RBSM
(Hipp <i>et al.</i> , 1999)	2.2		2113	Walking	SDM
	4.75		4635	Ascending stairs	
(Kumagai <i>et al.</i> , 2003)	22.4	--		Normal walking	RBSM
	25.4	--		Ascending stairs	
	13.2	--		Rising from chair	
(Bachtar <i>et al.</i> , 2006)	5.5	--		Walking (1.08 m/s)	FE
	5.34	--		Rising from chair (chair height – 500 mm)	
	4.99	--		Knee bending	
(Yoshida <i>et al.</i> , 2006)	2.87	--		Slow walking	DEA
	3.26	--		Normal walking	
	3.28	--		Fast walking	
	5.71	--		Ascending stairs	
	3.77	--		Descending stairs	
	8.97	--		Rising from chair	
	9.36	--		Sitting on chair	
3.65	--		Knee bending		
(Cilingir <i>et al.</i> , 2007)	2.29	--	3200	Static loading	FE
(Cilingir <i>et al.</i> , 2008)	3.75	--	2500	Static loading	FE
(Anderson <i>et al.</i> , 2008)	10.78	--	1949	Normal walking (1.08 m/s)	FE
	11.61	--	2103	Ascending stairs (step height – 170 mm)	
	12.73	--	2207	Descending stairs (step height – 170 mm)	
(Harris <i>et al.</i> , 2009)	--	9.1	1949	Normal walking	FE
	--	12.0	2103	Ascending stairs	
	--	13.1	2207	Descending stairs	

Anderson and colleagues investigated patient specific finite element models of the hip joint (Anderson *et al.*, 2007). The cartilage was again modelled as a “homogeneous, isotropic, incompressible, neo-Hookean hyperelastic material.” They demonstrated the insensitivity of the FE predictions such as contact stresses and contact areas with respect to cartilage shear modulus. They were, however,

sensitive to bone being modelled as rigid or elastic and were dependent on load and boundary conditions (Anderson *et al.*, 2008). However, Donahue and colleagues (Donahue *et al.*, 2002) found less than 2% difference in FE predictions between knee models with rigid and elastic bones. This may be due to the differences in geometry, boundary and loading conditions of the two joints involved as well as due to the different methodologies adopted in two studies. The cartilage was modelled as elastic, isotropic and homogeneous in Donahue and colleagues' models. However, their predictions were also influenced by boundary conditions.

Anderson and colleagues also concluded that the incompressibility of the cartilage needed to be taken into account for rapid loading cycles. They then experimentally validated FE models for normal walking and, ascending and descending stairs (Anderson *et al.*, 2008). They reported peak contact pressures of 10.78 MPa, 11.61 MPa and 12.73 MPa respectively for the three activities they modelled (**Table 1-7**). Spatially averaged contact pressure for ascending stairs was 5.1 MPa. The corresponding value for descending stairs was 6.2 MPa. The respective contact areas were 366.1 mm² and around 330 mm². This was opposite to what they reported for corresponding experiments as seen in **Section 1.8.2**.

Bachtar and colleagues investigated the contact mechanics of the hip joint with actual anatomical geometry of the whole joint (Bachtar *et al.*, 2006). The cartilage was modelled as isotropic, homogeneous and linearly elastic. They investigated three daily activities; walking, rising from the chair and knee bending. It was found that the location of high stresses on the femoral head changed with different activities, however, the maximum stress variation with time was found to be similar to hip force variations. A maximum stress of 5.5 MPa was observed at heel strike for normal walking (1.08 m/s). In all three activities, the peak stresses were in the anterior-superior regions of the femoral head.

Yoshida and colleagues observed a maximum contact pressure of 3.26 MPa in the superior-posterior region of the acetabulum for normal walking in their discrete element analysis study (Yoshida *et al.*, 2006). The cartilage was modelled as a combination of compressive and shear springs. They observed that the contact pressure was dependent on body weight, direction of the applied load, relative positions of the bones, contact area and the activity performed. The cartilage thickness distribution was found to be directly proportional to the peak contact pressure in that area. They found peak pressure with the maximum contact area to be in the anterior-superior region of the lateral roof. The cartilage is thickest in this area (von Eisenhart *et al.*, 1999). The peak contact pressure while ascending stairs was 5.71 MPa in the superior-posterior region of the lateral side of the acetabular cartilage at 11% of the activity. While descending stairs a corresponding value of

3.77 MPa was observed in the same region at 55% of the activity. However, they used the data from Bergmann (Bergmann, 2001) wherein the loads during ascending stairs were smaller than those during descending stairs as seen in **Section 1.8.2**. This was because while ascending stairs only 52.1% of the total possible contact area was in contact. For descending stairs the corresponding value was 80.6%. However, an opposing observation was made in a subject-specific FE study with hyperelastic cartilage in which the average peak pressure during climbing stairs was 12.0 MPa which was lower than that during descending stairs (13.1 MPa) (Harris *et al.*, 2009). The average contact area for walking, ascending stairs and descending stairs were 732 mm², 735 mm² and 582 mm² respectively. They showed that the magnitude and location of contact pressure can vary substantially from subject to subject for the same kind of loading depending upon the geometry of the cartilage and the bone. Anderson and colleagues also predicted a lower peak contact pressure while ascending stairs compared to descending stairs (Anderson *et al.*, 2008) as seen previously.

Numerical studies are widely used for parametric studies as it is more convenient to vary different variables compared to experimental studies. In a rigid body spring model (RBSM), Genda and colleagues carried out such a study on normal and dysplastic hips by varying the Wiberg CE angle (Genda *et al.*, 1995). This angle represents the acetabular coverage of the femoral head (Wiberg, 1939). Normal hips had a CE angle of $> 20^\circ$. The average peak contact pressure for the normal hip was 2.55 MPa for 4.3 times BW at heel strike. However, it increased with decreasing CE angle in the dysplastic range.

Another interesting numerical technique was used by Hipp and colleagues (Hipp *et al.*, 1999). For want of better terminology, the author of the present study has named it "Surface Discretization Method (SDM)". In this method, CT scans were used to reconstruct the acetabulum and femur. A lunate surface was then created by digitising the acetabular rim and notch, and then creating a best-fitting sphere. The lunate surface was divided into 0.5 mm² patches. A force vector was then projected onto each patch by using normal to that patch. The pressure thus calculated was considered only if it was greater than the threshold of 0.5 MPa. The hips were divided into normal, intermediate and dysplastic based on the CE angle of Wiberg. Those with a CE angle $> 25^\circ$ were normal whereas those with a CE angle $< 15^\circ$ were dysplastic. The loads applied were taken from a study by Cheal and colleagues (Cheal *et al.*, 1992). The peak contact pressure in normal hip was found to be 2.25 MPa during mid stance when the load was 2113 N. However, 2793 N was applied to simulate heel strike. It is not clear what the contact pressure was during this phase. A 23% increase in the peak contact pressure was observed in

dysplastic hips in loading conditions corresponding to mid stance. The decrease in contact area was 26% for the same loading conditions.

The shape of the cartilage in FE simulations plays an important role. As discussed earlier, most of the studies assume it to be spherical. It has been also hypothesised that conchoids and rotational ellipsoids are better approximations than a spherical shape which supports the clinical findings as discussed in **Section 1.8.2**. Anderson and colleagues studied the suitability of using simplified geometry to model cartilage (Anderson *et al.*, 2010). They showed that both conchoid and spherical shapes underestimated peak contact stresses by nearly 50% and overestimated contact areas by around 25% when compared to subject-specific models. Average elemental pressures were underestimated by around 30%. Kumagai and colleagues, on the other hand, using their rigid body spring model (RBSM) predicted very high stresses during walking of around 22.4 MPa in spite of assuming spherical geometry (Kumagai *et al.*, 2003). The higher estimates in Yoshida and colleagues' study were also observed in spite of using a spherical acetabulum and femoral head (Yoshida *et al.*, 2006).

Boundary conditions also play important role in any FE modelling. Care must be taken while imposing these boundary conditions (Rapperport *et al.*, 1985). It was shown using a two-dimensional model that the contact pressures are highly sensitive to the applied boundary conditions and may dictate the outcome of any theoretical and experimental studies. By choosing the conditions close to those existing anatomically will give more realistic predictions of the stresses. This was also shown by Anderson and colleagues by modelling bones as rigid (Anderson *et al.*, 2008). Any simplification will influence the FE predictions and the outcomes need to be carefully evaluated and validated against experiments before such models can be safely used in the clinical, design or parametric setup.

Finding the contact area in 3-D FE studies is obviously easier when compared to clinical studies. The contact stress distribution contours on the cartilage will show the contact areas as well (Russell *et al.*, 2006; Anderson *et al.*, 2007; Anderson *et al.*, 2008) which can be calculated using element information.

The differences observed by researchers in these three kinds of investigations are due to a variety of reasons. The protocols and methodologies used in experiments are invariably different. The mathematical objective functions chosen vary among different groups of researchers. Different kinematic and kinetic data will obviously generate varying outcomes. In FE models, geometry, material properties and boundary conditions may affect the predictions substantially.

As can be seen from **Table 1-5**, **Table 1-6** and **Table 1-7**, the contact

pressure varies depending upon type of study and activities performed. Some activities are more strenuous such as going down the stairs or rising from the chair. Contact pressures as high as 18 MPa were observed 12 months after surgery while getting up from the chair. The analytical studies and most of the numerical studies tend to predict lower stresses mainly due to idealized geometry. In RBSM, sometimes the predicted pressures are too high and this may be due to the assumption of the cartilage material properties which is modelled as compressive and shear springs or due to assumptions such as rigid pelvis and femoral head, uniform shear and compressive spring stiffness throughout the joint surface or due to the way the springs carrying tensile forces are eliminated from equilibrium equations (Kumagai *et al.*, 2003). The subject-specific FE models tend to reproduce results seen in experiments or clinical findings (Anderson *et al.*, 2008).

However, most of the models tend to assume cartilage to be a single-phased homogeneous, isotropic, linearly elastic (Bachtar *et al.*, 2006; Kim *et al.*, 2007) or hyperelastic (Anderson *et al.*, 2007; Anderson *et al.*, 2008) material. Moreover, these models were either two-dimensional (Brown and DiGioia, 1984; Rapperport *et al.*, 1985) or three dimensional with non-biphasic cartilage. Simplified models with biphasic cartilage (Macirowski *et al.*, 1994; Cilingir *et al.*, 2008) are good for parametric studies but cannot give clinically relevant information. Moreover, surface fluid flow boundary conditions based on a developing contact needs to be implemented in order to make the models more realistic. To capture the realistic tribological phenomenon inside the joint, an actual anatomical joint must be modelled with physiological loading and kinematic conditions. It is also required to investigate the influence of interstitial fluid pressurisation on the contact mechanics of the joint as it contributes towards biphasic lubrication by sustaining most of the load. The current study is thus centred on modelling an anatomical hip joint; both natural and with a hemiarthroplasty. For the simplification of the study, a basic unipolar hemiarthroplasty has been considered in this study. It is the endeavour of this study to model articular cartilage as a biphasic material with its implications to contact mechanics and tribology.

1.9 Aims and Objectives

1.9.1 Aims

This study is aimed to develop a general robust methodology for modelling the human hip joint; both natural and with a hemiarthroplasty, investigate the role of fluid in contact mechanics and tribology of the joint using biphasic poro-hyperelastic articular cartilage, validate the hemiarthroplasty model using a porcine hip joint and apply the methodology to investigate the effect of clearance and activities of daily living.

1.9.2 Objectives

Objectives of this study are:

- 1) To refine, apply and validate contact dependent algorithm to impose surface fluid flow boundary conditions for 3-dimensional models.
- 2) To develop a physiologically and anatomically relevant human hip joint model with biphasic poro-hyperelastic spherical articular cartilages.
- 3) To obtain CT scans of porcine acetabular cups to create subject-specific FE models.
- 4) To perform indentation tests on porcine articular cartilage (metal spherical indenter on cartilage) to determine mechanical properties.
- 5) To develop a biphasic poro-hyperelastic FE model of the porcine acetabular cup with articular cartilage from scanned images to create, validate and refine the FE methodology in hemiarthroplasty.
- 6) To apply the developed model to hemiarthroplasty in order to investigate joint contact mechanics with different clearances.
- 7) To apply physiological loads with spatial and temporal variations and physiological kinematics to the model in order to analyse joint contact mechanics and tribological phenomenon in activities of daily living.

Chapter 2 Contact Mechanics of Articular Cartilage

2.1 Introduction

The load partitioning between fluid and solid phases in articular cartilage depends, among other factors, upon the surface flow conditions existing at the cartilage surfaces, which in turn are affected by the extension of the contacting area. Analytical and finite element studies have stressed the importance of detecting the contact as two cartilage surfaces or as a rigid surface and a cartilage surface approach each other. This is not a problem in case of a plane ended cylindrical indenter against a plane cartilage surface, where the contact is developed immediately and the contact area remains unchanged under static loading (Cao *et al.*, 2006; Chiravarambath *et al.*, 2009). However, in natural synovial joints, cartilage surfaces are curved and so is the spherical prosthesis surface in the case of the hemiarthroplasty. In both cases, the contact develops over a period of time, is non-linear and is generally part of the solution. A similar incremental contact develops when two cartilages or the rigid indenter and the cartilage slide relative to each other. Accordingly, the surface flow boundary conditions will change continuously. Free flow conditions will apply on all regions on the cartilage surface which are not in contact with the indenter/cartilage whereas on the regions closed by the impermeable indenter there will not be any flow. When the contact is between two cartilages, the flow will depend on the fluid pressure difference across the interface and the fluid will flow in the direction of decreasing fluid pressure. Therefore, at every increment in a finite element simulation, it is important to know which nodes are in contact and which are not, so that the correct boundary conditions can be applied at each node.

The techniques proposed earlier for deciding a point/node in contact included; measuring the vertical displacements of the points on both the indenter and cartilage with respect to the cartilage surface (Hale *et al.*, 1993) or using a minimization function to determine the points in contact. (Donzelli and Spilker, 1998; Yang and Spilker, 2007). One potential problem with this method is that the points may have just come in contact and no load transfer will have actually started.

Another methodology, applicable only to the two-dimensional or axisymmetric elements with mid-side nodes, was developed by Warner (Warner, 2000; Warner *et al.*, 2001b). The contact stress at the mid-side node of an element was used to apply fluid flow boundary conditions on the entire surface of that element. This had

a drawback of the neighbouring corner node being closed even when it was not. Although, the method developed by Warner has wide applicability, it cannot be used for the models with linear elements which do not have mid-side nodes. Moreover, this method is applicable only when a rigid indenter is interacting with the cartilage and cannot be used in three-dimensional models and when two cartilage surfaces are in contact.

The aforementioned techniques are too specific, in the sense that they could only be used for certain configurations, needed minimization function or they could only be used for specific kinds of elements. Therefore, the aim of this study was to develop a new, robust and general method for determining surface nodes in contact by making use of contact stresses as a major deciding factor, and applying fluid flow boundary conditions accordingly, for the study of cartilage contact mechanics.

This algorithm was developed earlier (Pawaskar, 2006) for two-dimensional and axisymmetric models. Here, the algorithm is refined, adapted and extended to three-dimensional models.

2.2 Models and Methods

In order to investigate the proposed contact detection algorithm, two basic models were implemented in the commercial package ABAQUS (Dassault Systemes, Suresnes Cedex, France). The first model was of the indentation of the cartilage with a rigid impermeable spherical indenter, and the second was of the contact mechanics between two cartilages (Pawaskar, 2006). In both these models, a small strain was applied to the cartilage layers and the cartilage was then allowed to relax for a fixed time duration.

2.2.1 Contact formulation, detection and imposition of fluid flow boundary conditions

When two cartilage surfaces are in contact, the biphasic jump condition (i.e. maintaining continuity of the normal component of the pore fluid velocity w_n) reads, (Hou *et al.*, 1989),

$$\llbracket \varphi^f (v^f - v^s) \rrbracket \cdot n = \llbracket w \rrbracket \cdot n = 0 \Rightarrow \llbracket w_n \rrbracket = 0 \quad (2.1)$$

where,

$w = \phi^f (v^f - v^s)$ is the filtration velocity

ϕ^f – Fluid phase volume fraction

v^f – Velocity field in fluid phase

v^s – Velocity field in solid phase

n – is the outward normal to the surface

w_n – The pore fluid velocity component in the outward normal direction

If the two surfaces are indicated by 1 and 2, the jump condition for surface 1 can then be written as (Federico *et al.*, 2004),

$$w_n^1 = k_s (p^1 - p^2), \text{ in the contact region,} \quad (2.2)$$

$$\left. \begin{array}{l} w_n^1 = k_s p^1 \quad \forall p^1 \geq 0 \\ w_n^1 = 0 \quad \forall p^1 < 0 \end{array} \right\}, \text{ in the free-draining area} \quad (2.3)$$

where,

p^1 – pore pressure on surface 1

p^2 – pore pressure on surface 2

k_s – seepage co-efficient

Similar equations may be written for surface 2 by interchanging superscripts '1' and '2'.

When one of the surfaces is replaced by a permeable indenter, **Equation (2.3)** applies to the entire cartilage surface as it is freely draining everywhere. However, when a rigid impermeable indenter or prosthesis articulates against the cartilage surface, the right hand side of **Equation (2.2)** reduces to zero, whereas **Equation (2.3)** still holds true in non-contact regions.

FORTRAN was used as the programming language of choice to code both

algorithms since it was not possible to directly implement the jump conditions in **Equations (2.1) to (2.3)** in ABAQUS. Fluid pressure, contact stress and geometrical co-ordinates of the nodes on the surfaces were recorded in a file as the contact developed incrementally. Two different ABAQUS subroutines were used; one to read the file (URDFIL) and the other to impose the fluid flow boundary conditions (FLOW). A COMMON block, populated by URDFIL, was used so that the information could be shared across these two subroutines.

The algorithm used for a rigid indenter interacting with the cartilage was as follows (Pawaskar, 2006):

- 1) The result file was read after each increment.
- 2) The elements used in defining the cartilage surface, along with the nodes on the surface, were found and stored in the COMMON block.
- 3) The pore pressure and co-ordinates of each of these surface nodes were found and stored.
- 4) The contact stress at each of these nodes was recorded and if this contact stress was above some threshold (0.0 MPa was used in this study), the node was assumed to be in contact or otherwise to be open. This information was also stored.
- 5) Sealed (or no-flow) condition was applied if the node was in contact; otherwise free flow condition was applied.
- 6) Step 5 was repeated for each node until the increment converged.
- 7) Data was written to the results file on increment convergence.
- 8) The steps 1 – 7 were repeated until the end of simulation.

The algorithm is also explained by the flowchart in **Figure 2.1** consolidated from an earlier study (Pawaskar, 2006).

Step **(3)** was possible as the pore pressure in poroelastic elements was treated in ABAQUS as an additional nodal degree of freedom along with the three translational ones.

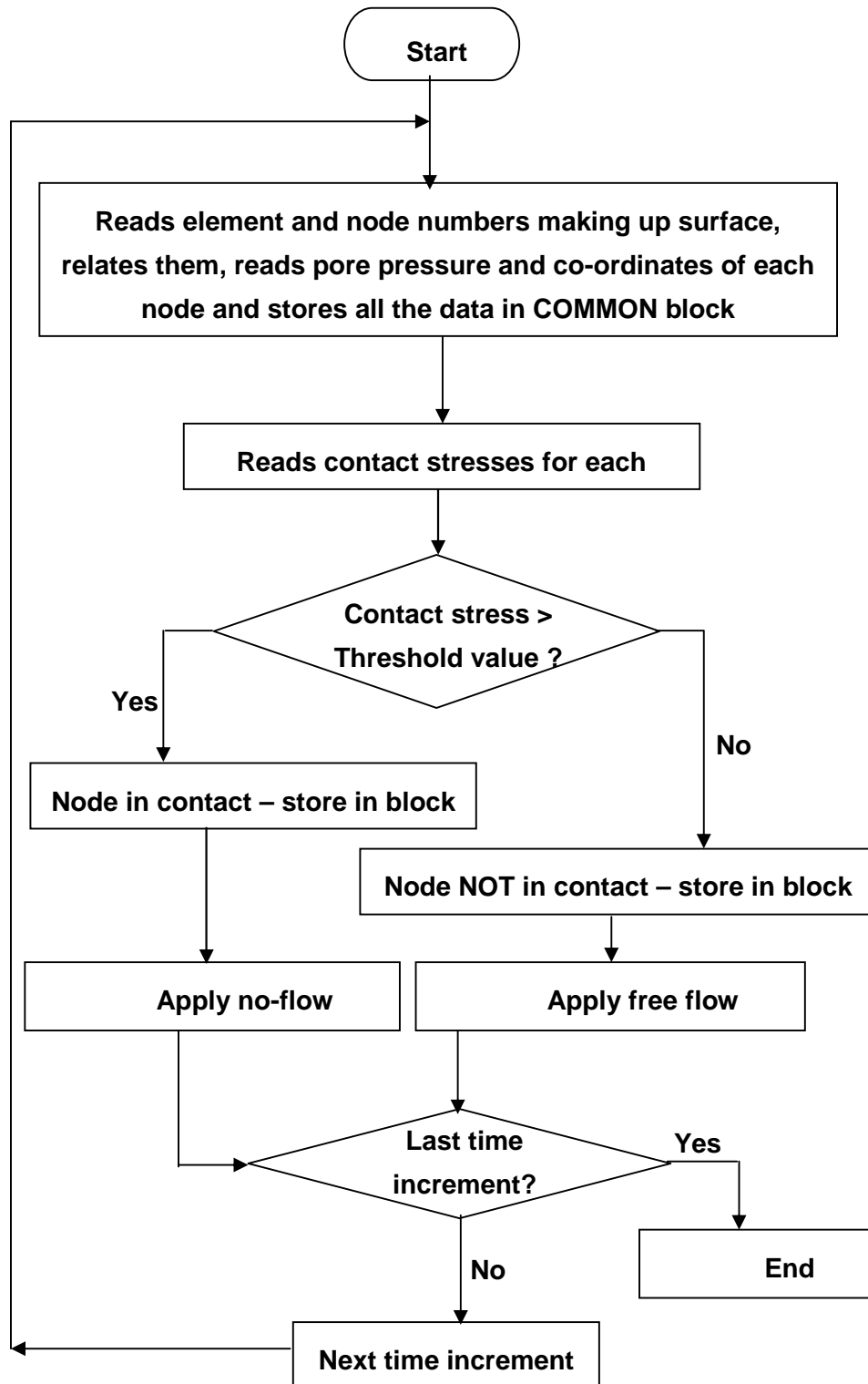


Figure 2.1 Flowchart of the proposed algorithm

The algorithm was then extended to include two cartilage surfaces in contact. In steps **(2)** – **(3)**, the data was stored for both the cartilage surfaces instead of just one surface. An additional step was performed for the second surface. This was carried out since ABAQUS required one surface to be defined as slave and the other as master, and wrote contact data, such as contact stress, to a file only for the slave surface. The second surface was the master and hence the proximity of each and every node on this surface to the first surface was calculated. If this distance was less than the predefined threshold (this study used 0.0 mm) then the node was assumed to be in contact. This was slightly different to the version included in earlier study (Pawaskar, 2006). In that earlier version, the master surface node closest to the slave surface node was identified and assumed to be closed or open depending upon the slave node condition. This would not make a difference when the cartilages in contact are symmetrical and have similar meshes but when the geometry becomes more complex and/or when the interacting cartilages are meshed differently the discrepancies will be increased.

This information was stored along with the other surface information. The COMMON block now contained element and node numbers making up the first cartilage surface along with pore pressures, co-ordinates, and contact information of those nodes. Similar information of the corresponding nodes on the second surface was also stored in the COMMON block. This information was related based upon the proximity of the master surface nodes to the slave surface nodes. The surface flow conditions were then applied based on whether the node was closed or open (Pawaskar, 2006).

If a node on the surface was not in contact, free flow conditions were applied as shown in **Equation (2.3)**. If the node was in contact then the jump condition mentioned in **Equation (2.2)** was imposed. If the pore pressures on the two opposing surfaces were to be equal there would not be any flow, otherwise it would be proportional to the difference in these pore pressure values. This was repeated for each and every node on both the surfaces. These steps were repeated and the information was written to the file upon convergence and the entire procedure was repeated until the end of simulation.

The seepage co-efficient, k_s , was used to either allow the fluid flow (value of 1 mm³/N.s) or stop the fluid flow (value of 0 mm³/N.s). This seepage co-efficient should be such that (Federico *et al.*, 2004; ABAQUS., 2007):

$$k_s \gg \frac{k}{c} \quad (2.4)$$

where,

k – Permeability

c – characteristic length of the underlying element

By choosing the value of $1 \text{ mm}^3/\text{N.s}$ for k_s and keeping the characteristic element length lower than 0.6 mm in all the models, it was ensured that k_s was greater than 10^3 times the expression on the right hand side of **Equation (2.4)**. This would approximately ensure zero pore pressure on the free draining saturated cartilage surface (ABAQUS., 2007).

The “sink pore pressure” was assigned a value of zero in the indenter-cartilage model and in the non-contacting region of cartilage-cartilage model whereas in the contacting region of the cartilage-cartilage model, it was assigned a fluid pressure value of the nearest point on the opposite surface, thus satisfying the biphasic jump conditions given in **Equations (2.1)** and **(2.2)**.

2.2.2 A Rigid Impervious Surface against Cartilage Surface

The objective of this part of the study was to verify the model and the proposed algorithm against the study carried out by Warner (Warner, 2000; Warner *et al.*, 2001b). The cartilage was modelled as a flat circular disc, 3 mm in thickness and 20 mm in radius, whereas the spherical indenter was 5 mm in radius. The cartilage was poroelastic and biphasic. Material properties as shown in **Table 2-1** were taken from previous studies (Spilker *et al.*, 1992; Goldsmith *et al.*, 1995; Warner, 2000).

There were five separate sub-models in this configuration, one each with:

- no-flow (sealed) surface condition,
 - free flow surface condition, and
 - contact dependent surface flow boundary conditions
- all three with 4-noded axisymmetric elements.
- contact dependent surface flow boundary conditions with 8-noded axisymmetric elements
 - contact dependent surface flow boundary conditions with 8-noded three-dimensional elements.

Of these, only the first four were investigated previously (Pawaskar, 2006). In that study, the predictions for the 8-noded axisymmetric model had discrepancies at the node on the axisymmetric axis. This has been addressed in the current study. Moreover, all these models have been improved using full integration elements in this study. However, the investigation into the three-dimensional model and its comparison with contact dependent 4-noded and 8-noded axisymmetric models was new to the current study.

Table 2-1 Material properties used in the model of cartilage indentation with spherical indenter (Spilker *et al.*, 1992; Goldsmith *et al.*, 1995; Warner, 2000)

Parameter	Value
Young's modulus of cartilage, $E_{\text{cartilage}}$	0.54 MPa
Poisson's ratio, $\nu_{\text{cartilage}}$	0.08
Permeability, k	$4.0 \times 10^{-15} \text{ m}^4/\text{N.s}$
Void ratio, e	4.0 (80 % interstitial fluid)
Coefficient of friction, μ	0.02
Seepage coefficient, k_s	1 $\text{mm}^3/\text{N.s}$ – Flow 0 $\text{mm}^3/\text{N.s}$ – No flow

The cartilage in the first three axisymmetric models was meshed with 896 CAX4P (4-node bilinear displacement and pore pressure) elements (**Figure 2.2**). A total of 224 CAX8P (8-node biquadratic displacement, bilinear pore pressure) elements were used for the axisymmetric model with 8-noded elements. The cartilage in the three-dimensional model had 24480 C3D8RP (8-node trilinear displacement and pore pressure, reduced integration) elements. The spherical indenter was modelled as an analytical rigid body with a reference point at its centre. Mesh sensitivity analysis was carried out individually for the 4-noded, 8-noded and three-dimensional models.

Boundary and interface conditions similar to those used by Spilker and colleagues were imposed on the cartilage and indenter (Spilker *et al.*, 1992; Warner, 2000). Most of these conditions were also applied to the three-dimensional model except those on the vertical axis of symmetry. As the incremental surface contact conditions were detected, the proposed algorithm was used to impose fluid flow conditions accordingly. The rotation of the reference node/point of the spherical indenter was constrained about all three axes.

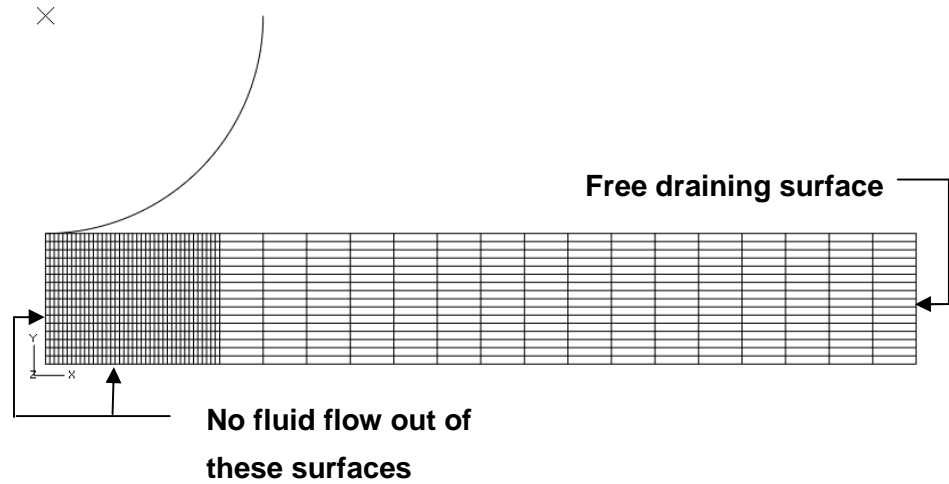


Figure 2.2 Finite element mesh of axisymmetric model of articular cartilage with a rigid spherical indenter

The indenter was moved vertically to impose a 10% nominal compressive strain in the cartilage over a ramp time of 2 seconds and maintained in that position for further 1000 seconds. The coefficient of friction was assumed to be 0.02 (Warner, 2000).

2.2.3 Cartilage Surface against Cartilage Surface

The objective of this analysis was to verify the model and the extended algorithm against the results presented by Federico *et al.* (Federico *et al.*, 2004) by using the algorithm verified in the model of a rigid spherical indenter articulating with the cartilage. Two identical, spherical and axisymmetric cartilages, 1 mm thick, still attached to the bone were modelled (Federico *et al.*, 2004). The radius of curvature was 400 mm. Both the cartilages were poroelastic and biphasic and material properties given in **Table 2-2** were taken from the previous study (Federico *et al.*, 2004).

Non-linear void dependent permeability was used in this model and was calculated using **Equation (2.5)** (Holmes, 1986; Wu and Herzog, 2000).

$$k = k_0 \left(\frac{e}{e_0} \right)^\kappa \exp \left(\frac{M}{2} \left[\left(\frac{1+e}{1+e_0} \right)^2 - 1 \right] \right) \quad (2.5)$$

where,

k – Permeability

e – Void ratio

k_0 – Initial permeability

e_0 – Initial void ratio

M - Material parameter for k - e

κ – Material parameter for k - e

Each cartilage was meshed with 2000 CAX4P elements whereas each bone component was meshed with 1000 CAX4 (4-node bilinear) elements as shown in **Figure 2.3**. A node N1, located 0.2 mm below the cartilage surface, was monitored throughout the simulation for the variation of fluid pressure and solid stresses.

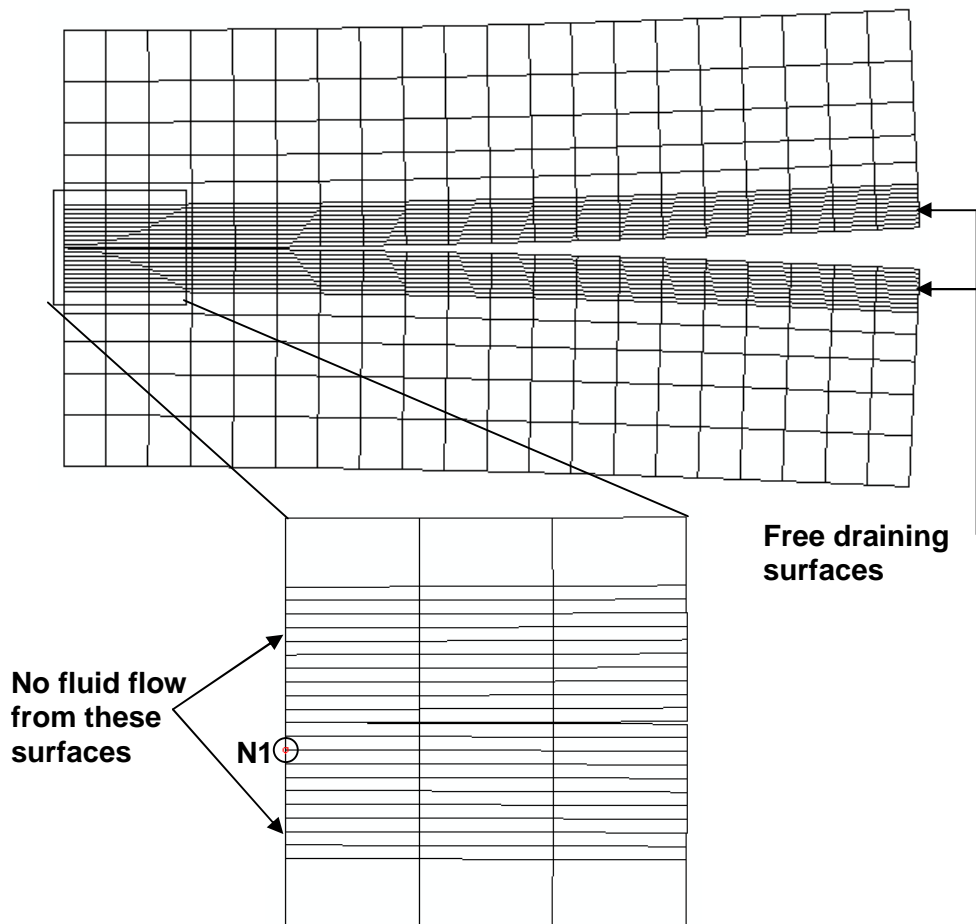


Figure 2.3 Finite element mesh of axisymmetric model of joint contact mechanics of identical articular cartilages with node N1 0.2 mm below lower cartilage surface

The bottom nodes of the lower bone were constrained in both horizontal and vertical directions. The nodes on the axis on the lower as well as the upper cartilage and bone, and those on the base of the upper bone were held in the horizontal

direction only. No fluid flow was allowed from the nodes on the vertical axis of symmetry as shown in **Figure 2.3**. The pore pressure on the nodes of the outer edge of each cartilage was maintained at zero to have unrestricted fluid flow. The flow conditions on the interacting cartilage surfaces were imposed using the proposed algorithm.

A vertical displacement of 0.3 mm was applied to the base of the upper bone which was equivalent to a maximum 15% deformation in each cartilage. This deformation was ramped up in 10 seconds and was maintained for further 300 seconds (Federico *et al.*, 2004).

Table 2-2 Material properties used in the model of joint contact mechanics of articular cartilages (Federico *et al.*, 2004)

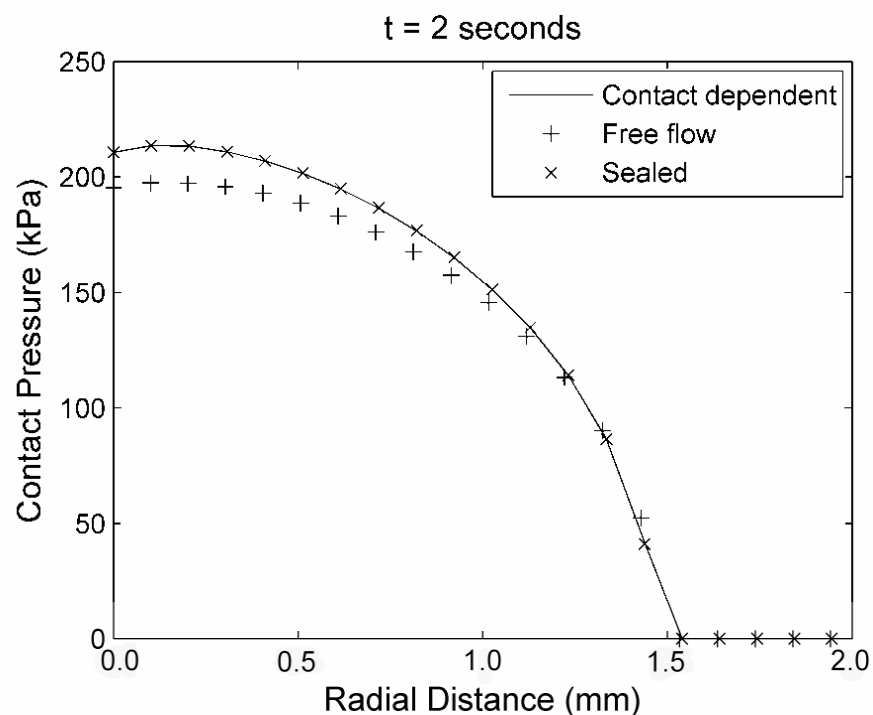
Parameter		Value
Young's modulus of cartilage, $E_{\text{cartilage}}$		0.450 MPa
Poisson's ratio of cartilage, $\nu_{\text{cartilage}}$		0.106
Initial permeability, k_0		$1.16 \times 10^{-3} \text{ mm}^4/\text{N.s}$
Initial void ratio, e_0		4.2 (approx. 80.75 % interstitial fluid)
Material parameter for k - e relationship – Equation (2.5)	M	4.638
	κ	0.0848
Seepage coefficient, k_s		1 $\text{mm}^3/\text{N.s}$ – Flow 0 $\text{mm}^3/\text{N.s}$ – No flow
Young's modulus of bone, E_{bone}		2 GPa
Poisson's ratio of bone, ν_{bone}		0.20

If the two interacting cartilages have identical geometry and material properties, then one of them can be replaced by a rigid impermeable plane (Ateshian *et al.*, 1994b) at the plane of symmetry. Hence, an equivalent model was created by replacing the upper cartilage-bone by a steel block modeled using 300 CAX4 (4-node bilinear) elements. A maximum 15% strain was applied in a ramp step in 10 seconds using a 0.15 mm displacement on the base of the steel block. The same boundary and interface conditions were maintained for lower cartilage-bone component as in the earlier case. The nodes on the axis and the base of the steel block were not allowed to move in the horizontal direction. The contact was assumed frictionless in both models. Two variations of both these models were

investigated; with and without non-linear geometry (i.e. using or not using NLGEOM flag, respectively). The former was not considered in the study of Federico and colleagues and an analytically rigid plane was used in this study instead of a steel block. The cartilage/cartilage and cartilage/steel block or plate models were equivalent and the latter was mostly preferred due the reduction in computational time and the modeling complexities. The algorithm already verified for a rigid indenter and cartilage was used in this equivalent model in order to verify the algorithm for cartilage-cartilage contact mechanics.

2.3 Results

The variation of contact pressure and pore pressure over the cartilage surface soon after applying the total strain and after 1000 seconds of maintaining that strain for the three cases of contact dependent, free and no-flow surface flow conditions were similar to those predicted in the previous study (Pawaskar, 2006) as shown in **Figure 2.4** and **Figure 2.5**.



(a)

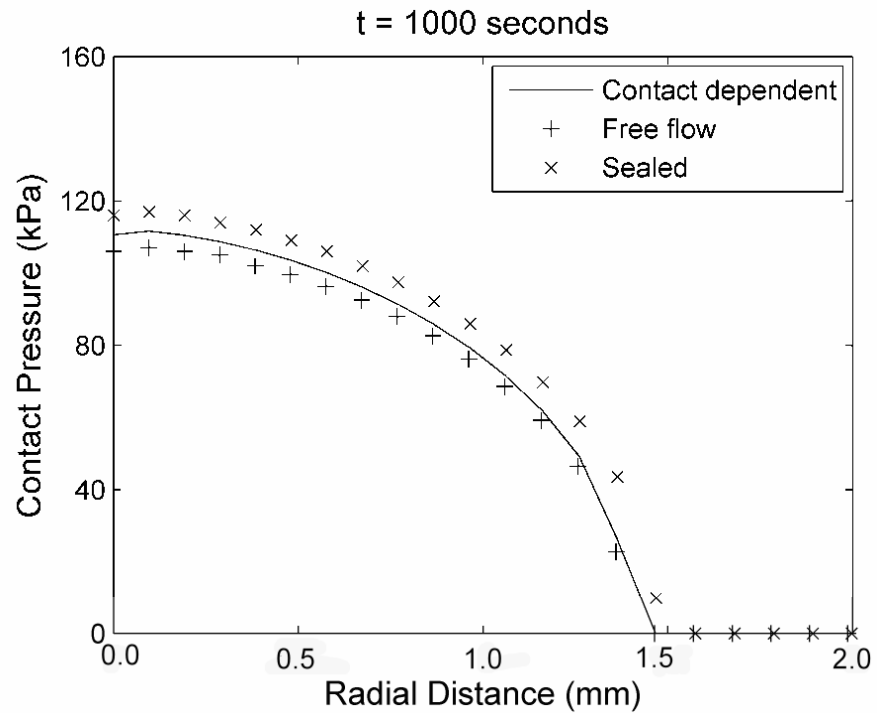
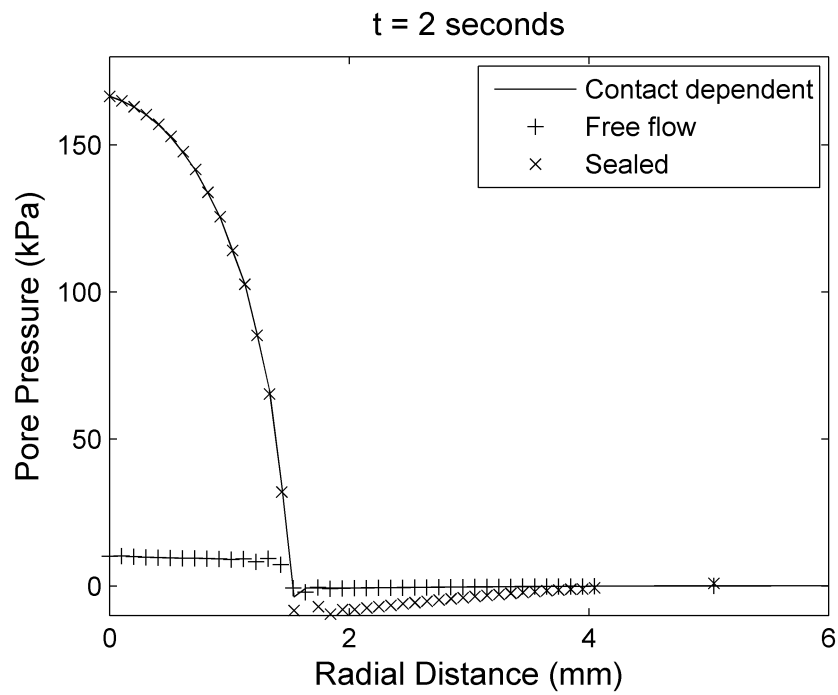
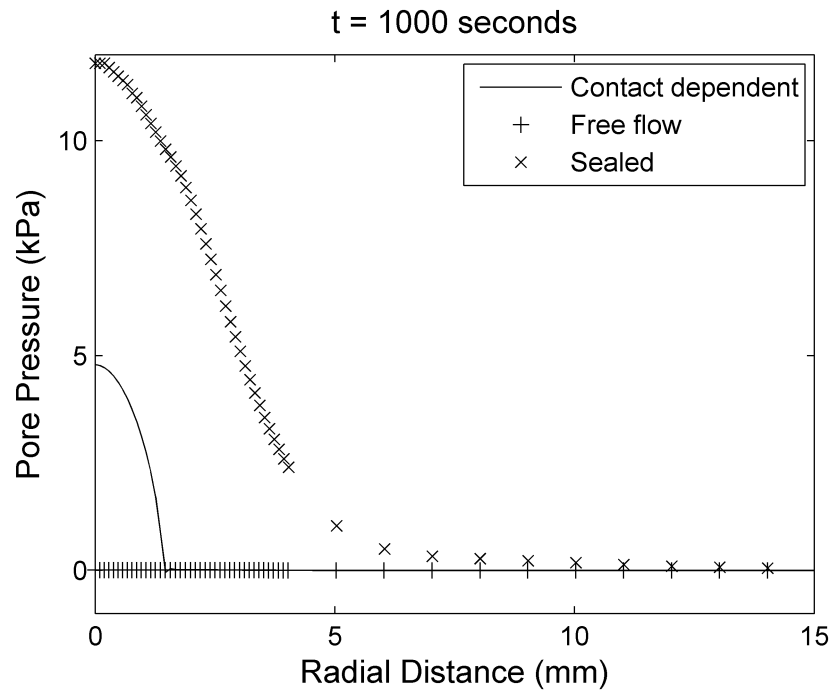


Figure 2.4 Distribution of contact pressure at the cartilage surface after (a) 2 seconds and (b) 1000 seconds for different surface flow conditions



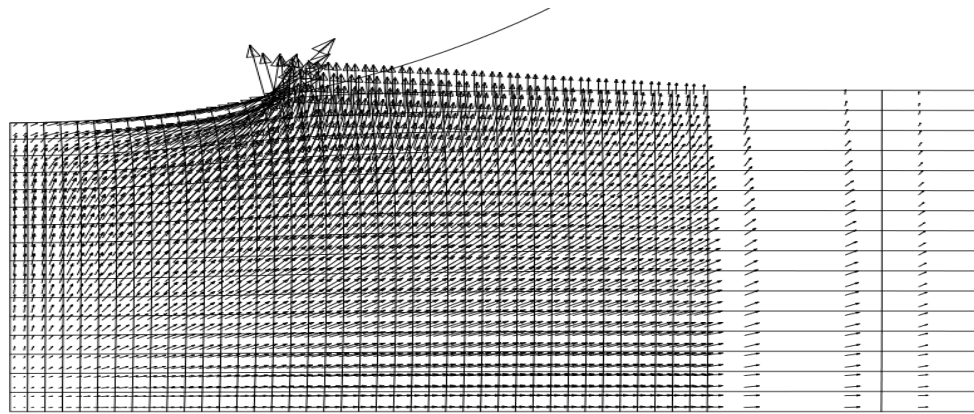


(b)

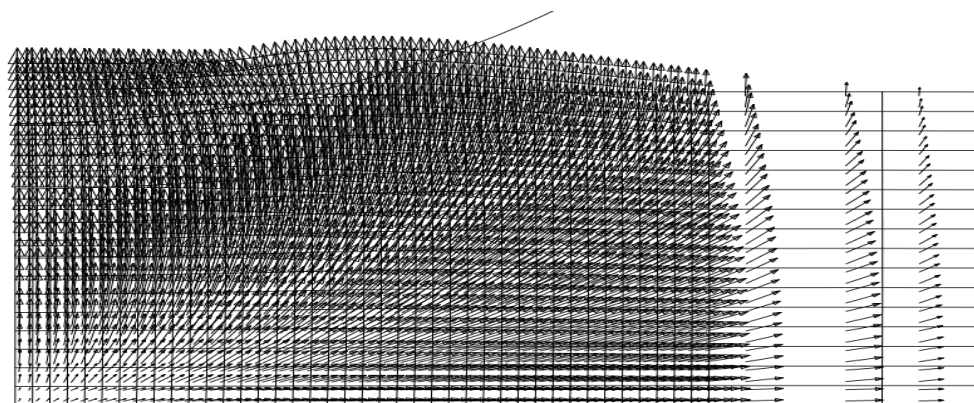
Figure 2.5 Distribution of pore pressure at the cartilage surface after (a) 2 seconds and (b) 1000 seconds for different surface flow conditions

The reduction in contact pressure after 1000 seconds was not markedly different in all three cases (maximum contact pressure reduced from approximately 211 kPa to 111 kPa). However, the reduction in pore pressure (**Figure 2.5**) depended on surface flow conditions (maximum pore pressure reduced from approximately 167 kPa to 5 kPa for contact dependent surface flow conditions). The corresponding values in the study by Warner (Warner, 2000) were approximately 168 kPa and 7 kPa.

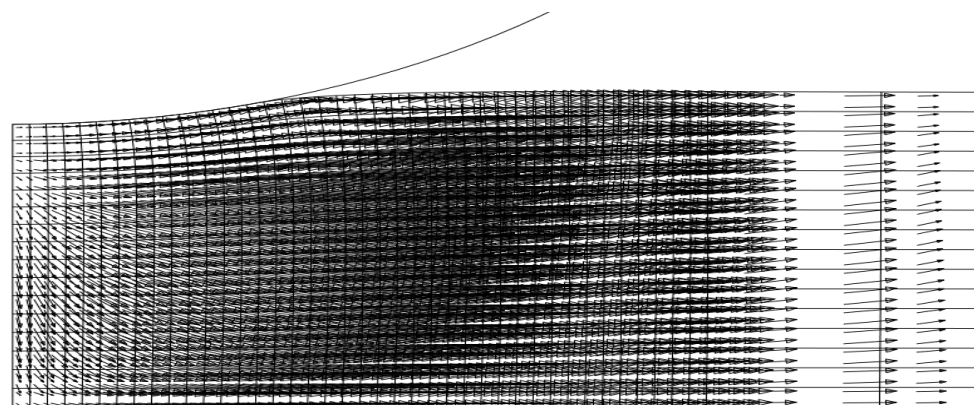
The fluid flow direction in the cartilage for different fluid flow conditions after 1000 seconds of maintaining the constant strain is shown in **Figure 2.6**. The maximum fluid exudation for contact dependent flow was observed near the contact edge (**Figure 2.6a**).



(a)



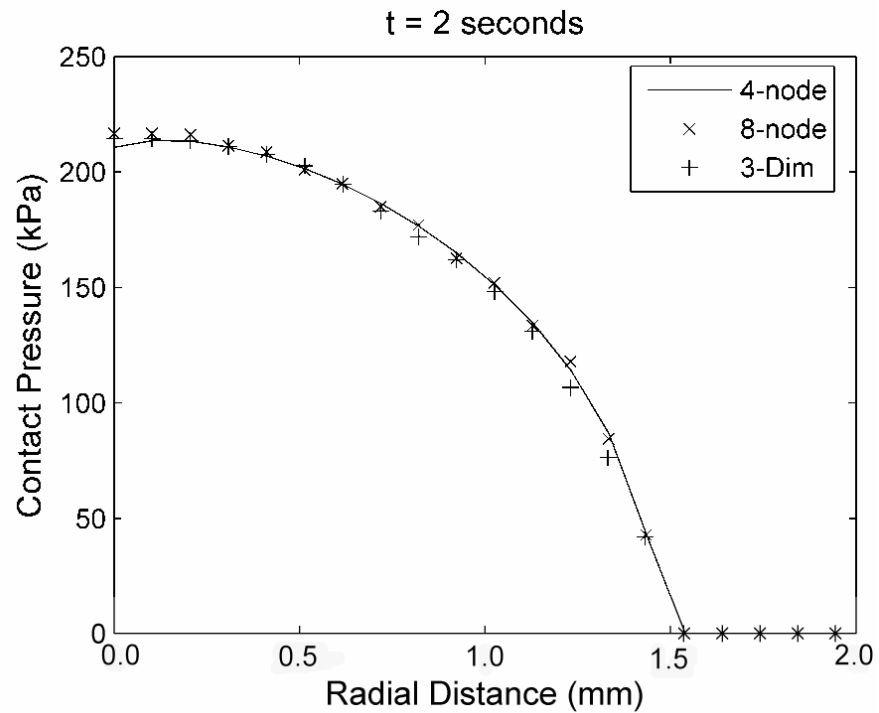
(b)



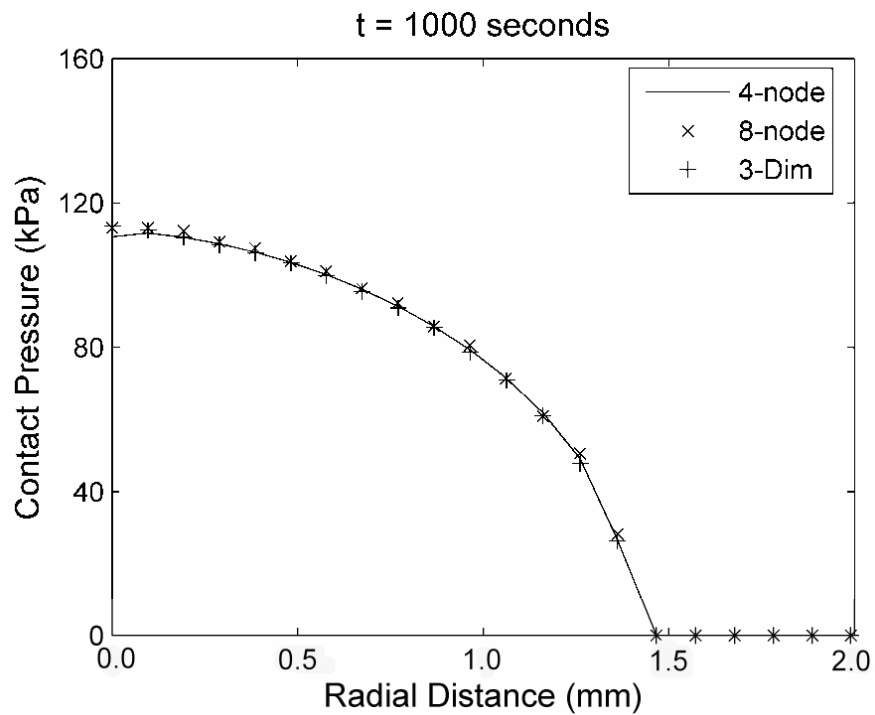
(c)

Figure 2.6 Fluid velocity directions after 1000 seconds for (a) contact dependent, (b) free flow and (c) sealed surface flow conditions

The variation in contact pressure for 4-noded axisymmetric, 8-noded axisymmetric and three-dimensional models using contact dependent surface flow conditions is shown in **Figure 2.7**.



(a)



(b)

Figure 2.7 Distribution of contact pressure at the cartilage surface after (a) 2 seconds and (b) 1000 seconds with contact dependent surface flow conditions for different element types

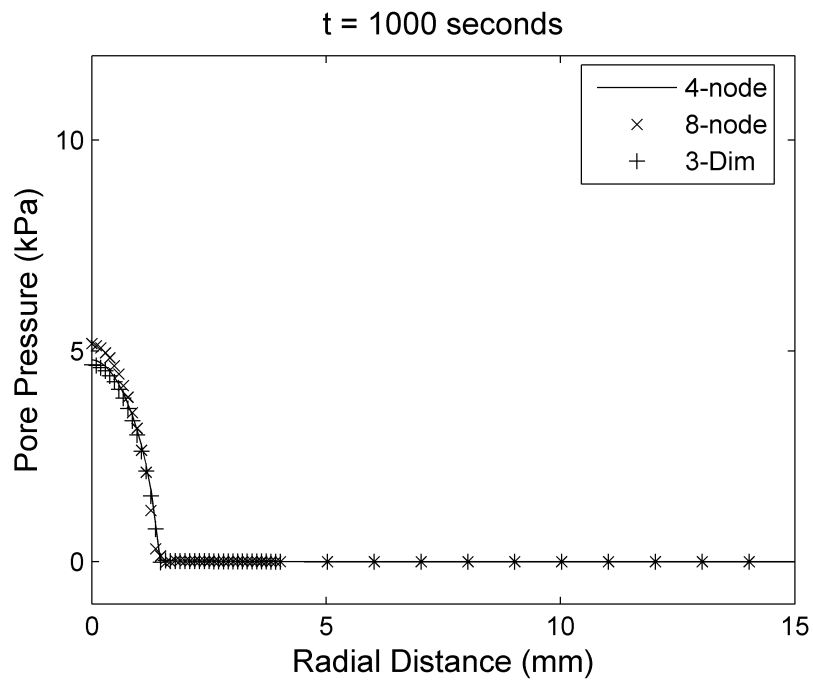
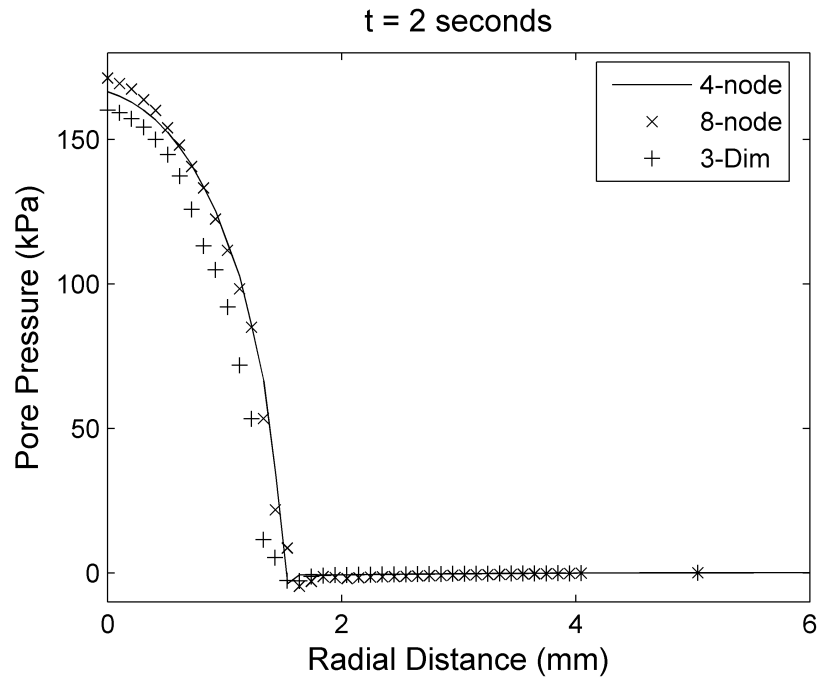


Figure 2.8 Distribution of pore pressure at the cartilage surface after (a) 2 seconds and (b) 1000 seconds with contact dependent surface flow conditions for different element types

The corresponding pore pressure distribution is shown in **Figure 2.8**. The variation and reduction in both the contact pressure and pore pressure were similar in all three cases. The maximum contact pressure reduced from approximately

211 kPa to 110 kPa whereas the maximum pore pressure reduced from approximately 170 kPa to 5 kPa. The difference of 3.84% was found in the pore pressure at the point of maximum deformation between 4-noded and three-dimensional models after 2 seconds of loading (**Figure 2.8a**). The corresponding value was 2.82% between 4-noded and 8-noded models. The differences in contact pressure were 1.78% and 2.81% respectively.

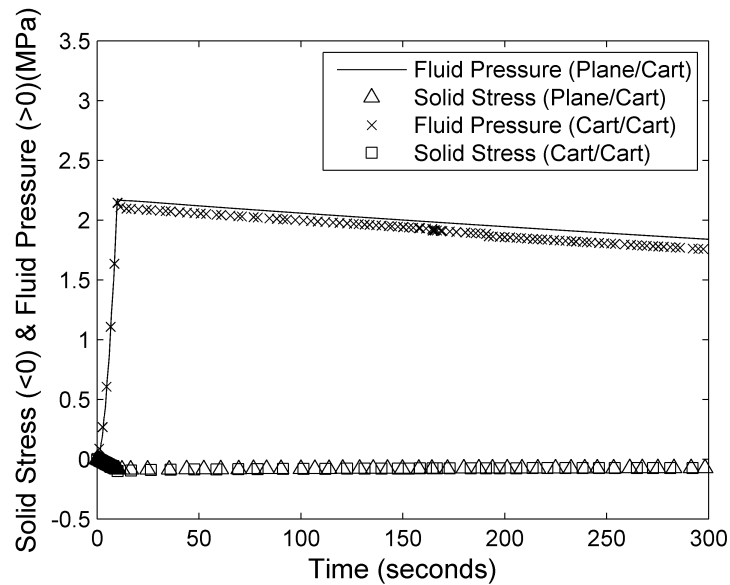


Figure 2.9 Fluid pore pressure and solid compressive axial stress over time at node N1 cartilage-cartilage and equivalent models when non-linear geometry was not considered

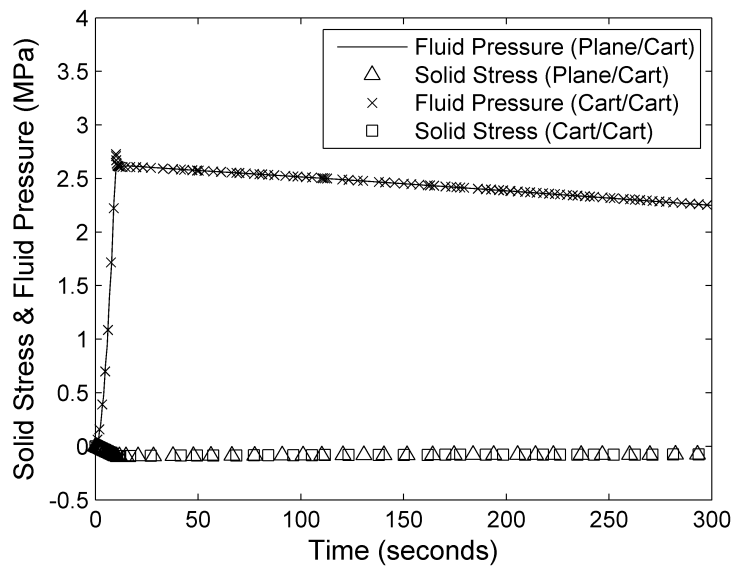


Figure 2.10 Fluid pore pressure and solid compressive axial stress over time at node N1 cartilage-cartilage and equivalent models when non-linear geometry was considered

In the case of the cartilage-cartilage joint contact mechanics problem, the variation in pore pressure and solid stresses were similar in both the cartilage over cartilage as well as the corresponding plane (steel block or analytically rigid plane) over cartilage models. The maximum pore pressure at node N1 was 2.15 MPa after 10 seconds of deformation when NLGEOM (parameter to take finite deformation into account) was not used. This was 1.65% lower than the pore pressure attained in plane over cartilage model after 10 seconds of deformation.

When non-linear geometry was accounted for, the maximum pore pressure increased to 2.73 MPa (**Figure 2.10**) which was 5.64% higher than the pore pressure predicted in plane over cartilage model. The corresponding maximum strain was 15% in each cartilage in both the cases. There was no difference in pore pressure during relaxation as shown in **Figure 2.10**. The fluid flow within the contact zone was parallel to the surface (**Figure 2.11a**) and the maximum fluid exudation was observed at the edge of the contact area (**Figure 2.11b**).

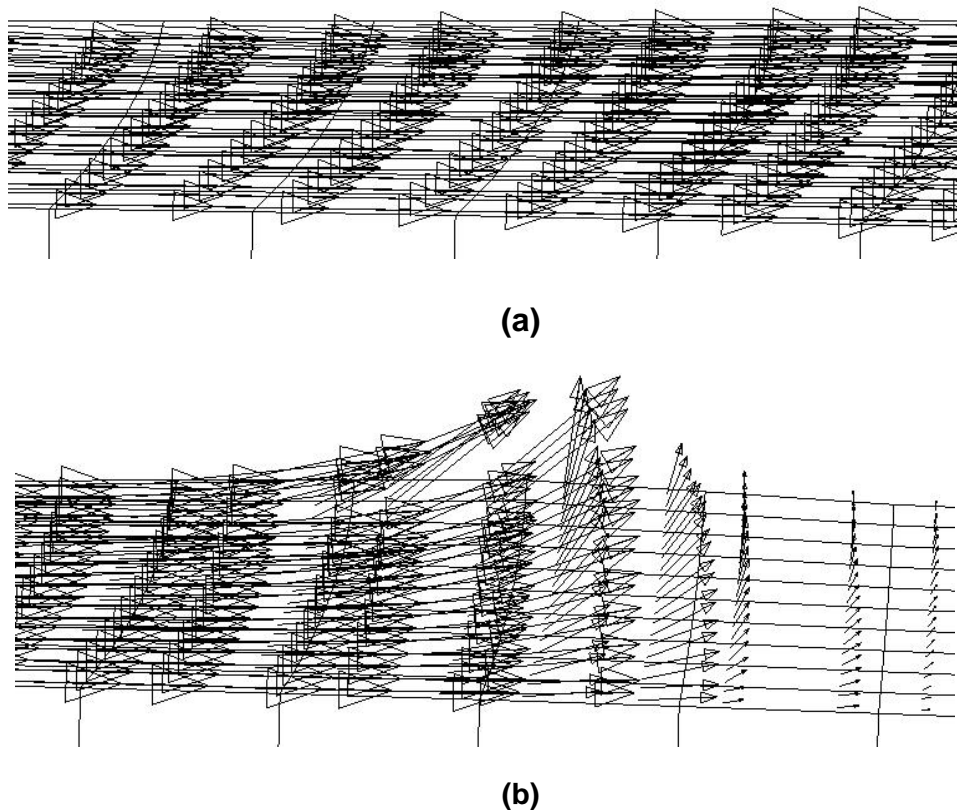


Figure 2.11 Fluid velocity directions after 300 seconds (a) in the contact zone (b) at the end of the contact zone; of the lower cartilage

2.4 Discussion

The fluid flow boundary conditions are important in cartilage contact mechanics problems as they influence the interstitial fluid pressurisation affecting

the frictional coefficient and wear of the cartilage. In the previous study by the author (Pawaskar, 2006), an algorithm to impose such surface fluid low boundary conditions with the evolving contact was proposed. In the current study, the algorithm has been refined and adapted for the three-dimensional model apart from investigating the previous models with a few changes. Displacement control was used in this study. However, the algorithm was equally effective in case of tests made in force control. Two basic models were investigated. The first one was with a rigid impermeable spherical indenter applying deformation to the cartilage. This not only represented the indentation experiment, but also the hemiarthroplasty of the joint in which the metallic prosthesis articulates with the natural cartilage. In the second model the cartilage was interacting with another cartilage, and was representative of the natural joint.

The importance of evolving contact on FE predictions is very clear from **Figure 2.5b** showing the pore pressure variation on the cartilage surface after 1000 seconds of relaxation. The no-flow or sealed conditions gave higher pore pressure as the fluid could not escape from the surface whereas the free flow surface conditions gave zero pore pressure as the fluid exuded from the surface without any resistance. However, the contact dependent flow predictions were more realistic with the pore pressure value between those of no-flow and free flow conditions, as the fluid was allowed to flow from the non-contacting surface only. The flow in the contact area was completely prevented due to the impermeable indenter. The reduction in contact stresses after 1000 seconds as seen in **Figure 2.4b** was due to the reduction in load as the 10% deformation was being maintained. The effectiveness of the proposed contact detection algorithm is also evident from **Figure 2.6** showing the fluid flow after 1000 seconds.

The algorithm was then tested on 8-noded axisymmetric elements and 8-noded 3D elements. The fit of different curves was deemed acceptable only when the contact/pore pressure at the point of maximum deformation differed by less than 5% of corresponding contact/pore pressure in 4-noded model. There were no marked differences in the predictions from all the 3 models after the application of deformation as well as after 1000 seconds of relaxation (**Figure 2.7** and **Figure 2.8**). This was possible due to the imposition of the surface fluid flow boundary condition at each node rather than all the nodes making up the individual elemental surface. This micro management at the node level was more realistic as the contact evolved very gradually and one node at a time. This was obvious from the pore pressure values after 1000 seconds which was around 5 kPa in the current study, compared to the 7 kPa value predicted in an earlier study (Warner, 2000). The higher value in the latter case was due to the fact that all the nodes on the element

surface were assumed to be closed once the mid-side node exceeded the threshold contact pressure, even when they were not in contact which restricted the fluid exudation from those nodes.

The algorithm was then extended to take into account two interacting cartilage surfaces. The algorithm without this extension was also used to show the robustness of the algorithm by analyzing an equivalent model with the upper cartilage replaced by a plane (steel block or analytically rigid plane) and with half the displacement. In this case, plane over cartilage model was considered as the base model and the allowable difference in pore pressure at the node N1 was 10% for acceptable fit of the curves. The relaxed criterion was to take into account numerical difficulties encountered during contact modelling of soft poroelastic material. The results as shown in **Figure 2.9** were very encouraging as they agreed quantitatively and qualitatively not only with an earlier study (Federico *et al.*, 2004) but also with the equivalent model. However, no difference was found when compared with the previous similar study by the author (Pawaskar, 2006) where the master surface contacting nodes were decided differently as highlighted in **section 2.2.1**. This was due to the fact that the cartilages considered were symmetrical and had similar meshes which caused the same nodes to be identified no matter which approach was taken.

However, the difference in the predictions between this study and the study to which it is being compared (Federico *et al.*, 2004) was large when non-linear geometry was accounted for (**Figure 2.10**). In this case, there was no difference between cartilage on cartilage and equivalent model predictions as far as the current study was concerned. A small difference seen after 10 seconds of deformation was due to numerical errors. The fluid flow direction as shown in **Figure 2.11** is a clear indication of the effectiveness of the algorithm.

The differences observed in the predictions when compared to the earlier studies were mainly due to the difference in FE formulations, methodologies and algorithms used to impose fluid flow boundary conditions. It should also be noted that ABAQUS treats two surfaces in contact differently (i.e. one surface as master and the other as slave). Contact information is not printed for the master and hence it was necessary to use a slightly different approach in deciding nodes in contact for different surfaces; nodal contact stresses for slave and nodal proximity for master. This gave the advantage of implementing fluid boundary conditions at individual nodes. The current algorithm is more general in that sense, since it could be used not only for quadratic elements but also for linear elements. In fact, it does not impose any conditions on the number of nodes making up the elemental surface. Moreover, it could be used both in 2D (including axisymmetric) and 3D problems. It

could be used in simulations involving contact of a rigid indenter with the cartilage and, with a slight modification, for contact between two cartilage surfaces.

It should be noted that the study by Federico *et al.* (Federico *et al.*, 2004) was focussed mainly on the effect of fluid boundary conditions on the contact mechanics of a joint and, for the sake of simplicity, used such a geometry so that there was no fluid exchange in the contacting region, because of symmetry. Hence the biphasic jump condition in **Equation (2.2)** was easier to implement as the right hand side of that equation was always zero. However, the current study was more exhaustive in the sense that, all the geometrical limitations that were present in the work of Federico *et al.* were completely removed. It focussed on providing a general methodology to read the contact information and apply fluid flow boundary conditions based on that information. The proposed method allowed the fluid exchange between the contacting cartilages by implementing **Equation (2.2)** and as such the method could be used in the modelling of actual natural joints irrespective of their geometries.

Apart from being general, the proposed algorithm is also robust. In the worst case, its time complexity will be $O(m^2)$, m being the number of surface elements. This is due to the two FORTRAN programme loops running one inside the other. The outer loop runs through the elements till a required node is found. The inner loop, with respect to the first loop, then loops through all the elements to find any additional occurrences of the same node. It means that the effect of using this algorithm will be such that the time required to complete the simulation will be proportional to the square of number of elements in addition to that required to execute core ABAQUS code. Thus, the proposed algorithm is highly scalable and will be able to take care of increasing number of elements in a fairly realistic way. Moreover, as discussed before, the contact stress or proximity at nodal points was used to implement fluid flow boundary conditions at that node rather than at all the nodes making up that element surface. This makes the proposed algorithm more accurate in terms of predictions. The predictions using this algorithm were very encouraging. The use of the algorithm in the FE modelling of whole natural joints and those with hemiarthroplasty will be considered in future studies.

One major limitation of this algorithm was the fact that the condition of proximity of nodes on the master surface to the slave had to be used. This approach was used as the contact stress information for the master is not written to the results file in ABAQUS. It would have been ideal to use that information in deciding the master surface nodes in contact as was done for slave surface nodes. The possibility of using other software packages to address this issue needs to be investigated.

Chapter 3 Natural Human Hip Joint: Contact Mechanics and Fluid Load Support

3.1 Introduction

The clinical and laboratory studies on hip joints involve a metallic instrumented femoral prosthesis interacting with the natural acetabular cartilage (Brown and Shaw, 1983; Hodge *et al.*, 1989; Bergmann *et al.*, 2001). These instrumented prostheses can measure contact forces as well as stresses as the subject undergoes routine activities. However, these studies are not only intrusive but also the measured parameters obviously cannot be compared with those existing in natural joints. The current technology also does not allow the study of contact mechanics and tribology of the natural joint non-intrusively (Anderson *et al.*, 2008). Thus the only method is to utilise analytical or numerical models. The human hip joint is a ball and socket joint and as such easier to investigate in terms of these models. Analytical or numerical models have been quite successful in reproducing clinical outcomes (Brand *et al.*, 1994; Stansfield *et al.*, 2003; Bachtar *et al.*, 2006).

There are many FE models which have attempted to address the contact mechanics problem in the hip joint. They range from simpler two-dimensional (Brown and DiGioia, 1984) to complex three-dimensional (Bachtar *et al.*, 2006) models. They, however, cannot be used to study the role played by interstitial fluid in the tribology and contact mechanics of the joint since the cartilage in these models was mostly modelled as either elastic or hyperelastic material.

The current study thus aimed to develop a FE model of the natural hip joint with biphasic articular cartilage.

3.2 Model and Methods

The solid model of a male left pelvis created from CT scans (Visible Human Project, 2005) (**Figure 3.1**) was obtained and converted into FE model by using I-DEAS (ver. 11, Siemens PLM Software, Plano, TX, USA) and ABAQUS (ver. 6.7-1, Dassault Systemes, Suresnes Cedex, France). ABAQUS was also used for the analysis of the model and post-processing the predictions.

The Boolean operation was performed in I-DEAS to create the acetabular bony cavity of 30 mm radius. Horseshoe shaped acetabular cartilage was then created from the contour of the lunate surface in the acetabular cavity. The cartilage

was of uniform thickness (Yoshida *et al.*, 2006) and was 2 mm thick which was the highest mean reported previously for acetabular cartilage (Shepherd and Seedhom, 1999). It was spherical with inner radius of 28 mm which was the maximum radius reported in earlier studies (Xi *et al.*, 2003; Quiñonez *et al.*, 2008). The hip joint contact force data adopted for the present model already accounted for muscle forces (Bergmann, 2001; Bergmann *et al.*, 2001) and hence they were not modelled. The cancellous, cortical and sub-chondral bones were created in the model with pelvic cortical bone of 1.41 mm thickness (Anderson *et al.*, 2005).

A spherical ball was used to create femoral head cartilage of 28 mm outer radius with the help of Boolean operations in I-DEAS. It was also 2 mm uniformly thick. Another spherical ball was used to represent the femoral head which was assumed to be made up of only cortical bone.

The centres of the acetabular and femoral cartilages, and spherical femoral head bone were coincident at the origin of the coordinate system. The clearance between the two was 0.0 mm. This was more or less anatomical as MR images have shown that both the acetabular and femoral head cartilages appear as one with a little or no inter-articular gap (Naish *et al.*, 2006; Li *et al.*, 2008).

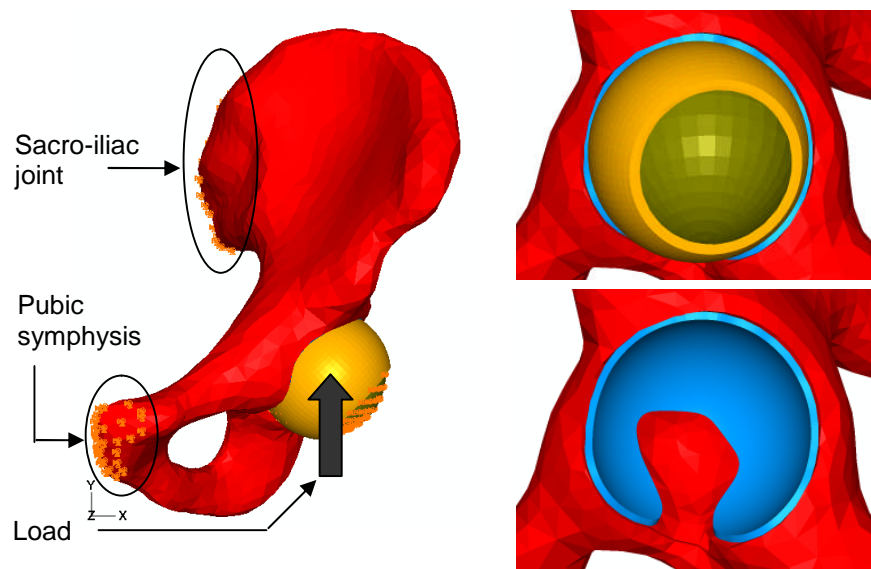


Figure 3.1 FE model of natural hip joint

The acetabular cartilage in the current study was modelled with poroelastic elements whereas bones had elastic elements. The pelvis was meshed using 12165 four-node linear tetrahedral elements (C3D4) representing cancellous bone

and 3468 six-node linear triangular prism elements (C3D6) for the cortical layer. Sub-chondral bone was meshed with 247 elements of C3D4 type. The acetabular cartilage had 23976 eight-node trilinear displacement and pore pressure, reduced integration elements (C3D8RP). The femoral head bone had 432 six-node linear triangular prism elements (C3D6) and 1872 eight-node linear brick elements (C3D8). Femoral cartilage was made up of 5322 eight-node trilinear displacement and pore pressure, reduced integration elements (C3D8RP). A care was taken that there were at least three elements through the thickness of both the cartilages (Anderson *et al.*, 2008). The femoral head cartilage was made the master surface, while the acetabular surface was the slave. The mesh could thus be coarser in the case of the femoral cartilage due to strict master-slave algorithm which prevents slave node penetration into the master (ABAQUS., 2007). Mesh sensitivity analysis was carried out to ensure that the difference in the predictions between consecutive meshes was less than 5%.

The elastic modulus of cancellous bone of pelvis was 70 MPa with Poisson's ratio of 0.2 (Dalstra *et al.*, 1995). The corresponding properties for pelvic cortical bone were 17 GPa and 0.3 and for subchondral bone they were 2 GPa and 0.3 (Dalstra *et al.*, 1995). The femoral head bone was assumed to be only cortical with the same material properties as those used for pelvic cortical bone. The material properties for the acetabular and femoral cartilages were: equilibrium elastic modulus, $E=1.072$ MPa, Poisson's ratio, $\nu=0.011$ and permeability, $k=9.83 \times 10^{-16}$ m⁴/N.s (Athanasίου *et al.*, 1994) and water content of 80% (Armstrong and Mow, 1982).

The cartilage solid phase was modelled as neo-Hookean, with elastic strain energy potential given in **Equation (3.1)** (ABAQUS., 2007).

$$W(C) = \frac{G}{2} (\bar{I}_1 - 3) + \frac{K}{2} (J - 1)^2 \quad (3.1)$$

where,

C – Right Cauchy-Green deformation tensor

G – Shear modulus

\bar{I}_1 – First deviatoric strain invariant

K – Bulk modulus

J – Total volume ratio when linear thermal expansion strain is not considered

Bulk modulus, K and shear modulus, G are related to Young's modulus, E and Poisson's ratio, ν by **Equations (3.2)** and **(3.3)**.

$$E = 3K(1 - 2\nu) \quad (3.2)$$

$$E = 2G(1 + \nu) \quad (3.3)$$

The sacro-iliac joint nodes and those on the pubic symphysis contralateral side were fixed in three directions. Unrestricted free fluid flow was imposed on the side surfaces through the thickness of the cartilage as they always remained open. No fluid flow was allowed from the cartilage surface towards the impermeable lunate surface of the acetabulum as it was tied to this lunate surface throughout the analysis. The femoral head was allowed to move only in the vertical direction and was constrained in the other two directions. The inside surface of the femoral cartilage was tied to the femoral head and no fluid flow was allowed through this surface. Free fluid flow was allowed at the nodes through the cartilage thickness. The fluid flow on the acetabular and femoral cartilage surfaces which interacted with each other was based on the developing contact and was imposed using contact dependent fluid flow algorithm described in **Chapter 2**. The contact was assumed frictionless and soft contact formulation was used (ABAQUS., 2007).

A vertical load of 2000 N was applied at the centre of the head, as shown in **Figure 3.1**, in one second. Total fluid load support, peak contact stress, peak fluid pressure and contact area were recorded throughout the simulation.

This model was not validated in a conventional way using experiments and was beyond the scope of the present study. So another simpler three-dimensional poro-hyperelastic model of the cup and ball was created and its results compared with an already verified axisymmetric cartilage on cartilage model methodology (**Chapter 2**). The models are shown in **Figure 3.2**.

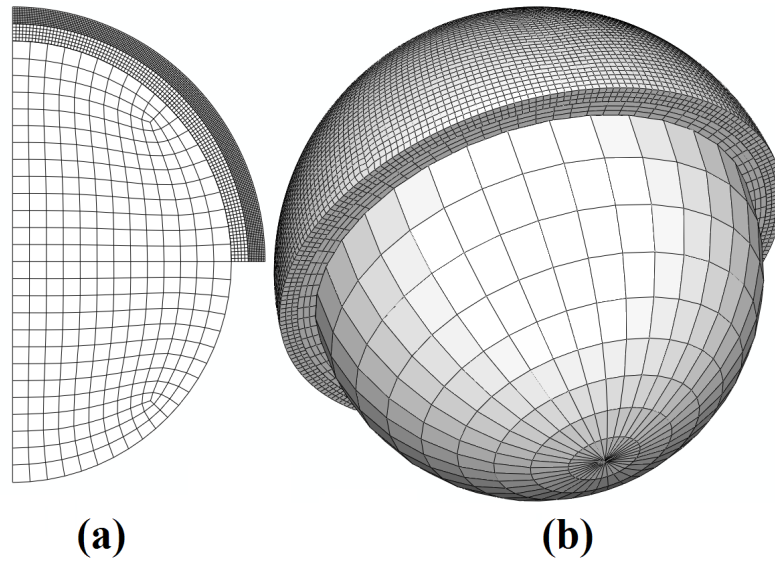


Figure 3.2 Axisymmetric and three-dimensional model of ball and cup

The elements used in the axisymmetric and three-dimensional cup and ball model are given in **Table 3-1**. The thickness of the cups representing acetabular and femoral head cartilages was similar to that in the natural joint model. Individual cartilage surfaces were also formulated similarly. The material properties used were also similar to those used in the natural hip joint model.

Table 3-1 Elements used for the cup and ball model

Component	Element (Axisymmetric)		Element (3D)	
	Type	Number	Type	Number
Cup Cartilage	CAX4P	2280	C3D8RP	33852
Ball Cartilage	CAX4P	530	C3D8RP	4356
Femoral head ball (bone)	CAX4	320	C3D6	432
			C3D8	1872

The back of the acetabular cartilage was constrained in the vertical and horizontal directions in the axisymmetric model whereas in the three-dimensional model it was constrained in the third direction as well. The fluid was not allowed to flow from this surface in both the models. These two conditions represented the cartilage attached to the lunate surface of the acetabular cavity. In the axisymmetric model, the nodes on the vertical axis of symmetry of the acetabular cartilage, femoral head and femoral head cartilage were not allowed to move in the horizontal direction. In the three-dimensional version, the movement of the femoral head was allowed only in the vertical direction and the femoral head cartilage was tied to the

head. The flow of fluid was prevented from both the cartilage surfaces on the vertical axis of symmetry in the axisymmetric model. Free fluid flow was allowed from the exposed cartilage surfaces through the thickness in both the models. The contact dependent algorithm proposed in **Chapter 2** was used to impose fluid flow boundary conditions on contacting surfaces. The soft contact formulation was used in both the models with contact being frictionless.

In the axisymmetric model UTOL which is the maximum fluid pressure change allowed in a single increment, was kept at approximately 6% of the maximum fluid pressure predicted by the model (Goldsmith *et al.*, 1995). However, some of the constraints were relaxed in three-dimensional models. UTOL was assigned a value of 100 MPa which was very high. Controls for the largest residual force and volume flux were set to a large value of 1000000% of average flux norm over time. Controls for the largest displacement and fluid pressure correction were set to 100% of the largest corresponding increment. Moreover, soft contact constraint compatibility tolerances for non-zero and zero contact pressures were both set to 1.

A vertical load of 2000 N was applied in both the models in one second. Peak contact and fluid pressures, contact area and total fluid load support were monitored throughout the simulation.

3.3 Results

The peak contact stresses in the cup and ball configuration were 1.242 MPa and 1.256 MPa for the axisymmetric and three-dimensional models respectively (**Table 3-2**). The corresponding values for peak fluid pressure were 1.224 MPa and 1.246 MPa. The percentage difference in peak contact stresses was 1.13% whereas peak fluid pressure differed by 1.80%.

Table 3-2 Comparison of two- and three-dimensional cup and ball model for validation

	Peak Contact Pressure (MPa)	Contact Area (mm²)	Peak Fluid Pressure (MPa)	Total Fluid Load Support (%)
Axisymmetric model	1.242	4807.22	1.224	98.25
3D model	1.256	4866.24	1.246	98.75
Difference (%)	1.13	1.23	1.80	0.51

The contact area difference in the two models was 1.23% with the axisymmetric model predicting 4807.22 mm² and the three-dimensional model giving 4866.24 mm². The difference in total fluid load support was very small (0.51%). The large load was supported by the fluid in both the models (~98%).

The contours of fluid pressure after 1 seconds of loading were similar in both the cases with a central contact zone of maximum pressure which gradually reduced towards the edges (**Figure 3.3**).

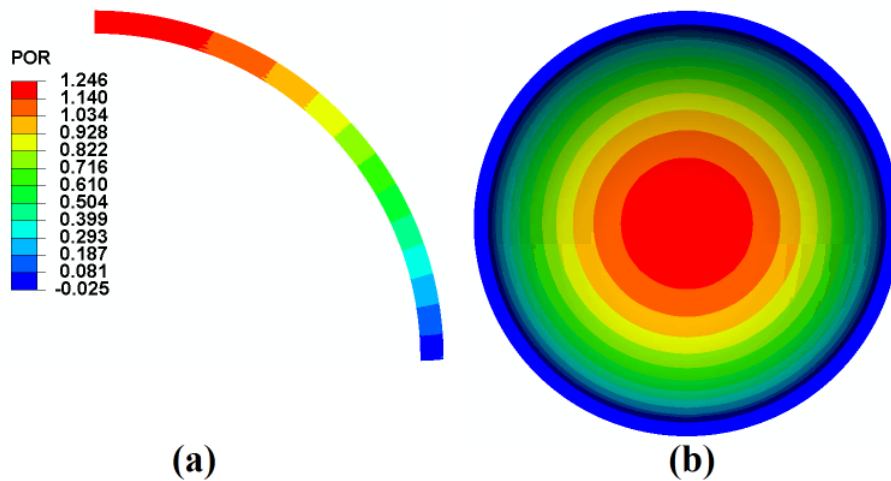


Figure 3.3 Contour plots of fluid pressure (MPa) after 1 second of loading in a) axisymmetric and b) 3D models

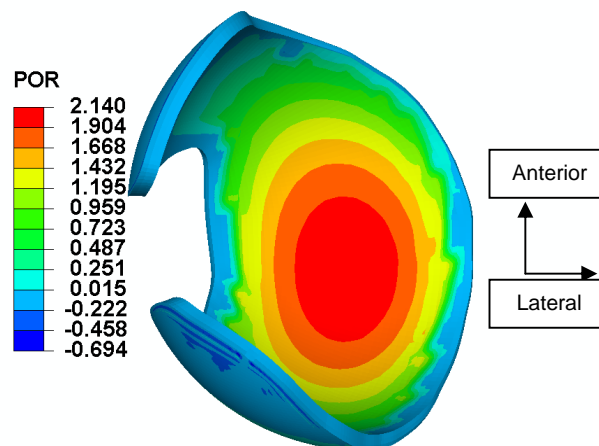


Figure 3.4 The contour of fluid pressure (MPa) on acetabular cartilage contact surface after 1 second of loading

This methodology was then applied to the natural hip joint. Peak fluid pressure, in the natural joint, soon after loading was 2.140 MPa whereas peak

contact stress was 2.152 MPa. These pressure distributions were in the antero-posterior direction. The area of contact was approximately 2787.08 mm² which was around 83.02 % of the total potential area available for contact. The total fluid load support was high around 94.40 %. The contours of fluid pressure after 1 second of loading are shown in **Figure 3.4**.

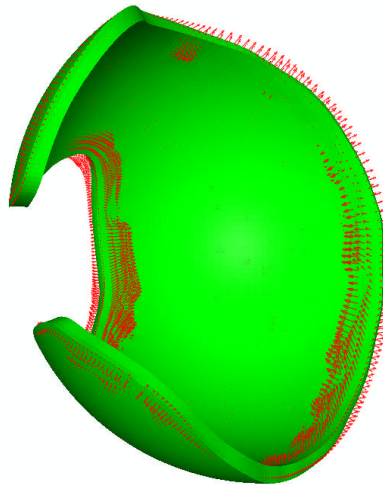


Figure 3.5 Fluid velocity vectors after 1 second of loading

The fluid velocity vectors with magnitudes in the range of $10^{-3} - 10^{-6}$ mm/s, after 1 second of loading are shown in **Figure 3.5**. It was observed that the fluid exudation was from non-contacting regions.

3.4 Discussion

Natural joint tribology and contact mechanics is difficult to investigate *in vivo* due to limitations of the technologies. Most of these are invasive such as the use of instrumented prosthesis. However, the invasive interventions affect the structural integrity of the joint and cannot be used as a representative of a natural joint. Moreover, the prostheses are implanted whenever there is a medical condition to rectify and hence the joints are not normal to begin with. The obvious choice is to use mathematical/numerical models which can predict the required parameters. The current study aimed to create methodology which could be used to model the natural joint. The acetabular and femoral head cartilages were modelled as biphasic in order to understand the extent to which interstitial fluid pressurisation affects the contact mechanics and tribology of the joint.

Moreover, cartilages were modelled as neo-Hookean poro-hyperelastic

material to take into account the large deformations (maximum of around 23% was observed in the natural joint model) that might typically exist in the joint. It also represented the simplest form of non-linear elasticity and allowed for easy conversion of elastic modulus into shear and bulk modulus. Though Mooney-Rivlin and Yeoh models are best suited for simulating compressive behaviour of the articular cartilage, neo-Hookean material model has been recommended to reduce the processing time (Brown *et al.*, 2009).

Since the model could not be validated using experimental or clinical studies, an idealised three-dimensional model of the cup and ball was created and compared with an axisymmetric model; the methodology for which was already established in **Chapter 2**. An excellent agreement was found between the two models with respect to all the variables of interest. The maximum difference between the two models was 1.80% in the predictions of peak fluid pressure.

Relaxation of some of the controls and UTOL in three-dimensional model of the cup and ball had a negligible effect on the predictions of peak contact stress, peak fluid pressure, contact area as well as total fluid load support. It should be noted that these parameters were very stringent in axisymmetric model. This change in parameters was done by trial and error and was needed to avoid the convergence difficulties encountered while using default criteria in three-dimensional models as well as to reduce the computational time. The three dimensional methodology adopted was thus deemed fit for the more complex natural hip joint.

The peak contact and fluid pressures were low despite a very high load applied in the model. Though this was mostly due to the spherical geometry and zero clearance being used, it was still low for such configurations. The larger contact areas suggested that there was a high degree of conformity between two soft cartilages contacting each other. This helped in spreading the load over a larger part of the acetabulum thus reducing contact stresses and fluid pressures. The load carried by the fluid was large thus reducing the coefficient of friction due to the decrease in solid-to-solid contact. Both the reduced contact stresses and lower coefficient of friction would help in reducing the frictional shear stresses. This would protect the cartilage from fibrillation in the long term and might explain the survival potential of natural cartilage for almost the life time of a person.

It should be noted that the contact stresses were “effective stresses” in this kind of formulation (ABAQUS., 2007). They did not include fluid pressure. The total fluid load support was so high in this case that the solid stress contribution was almost two orders of magnitude smaller (**Table 3-2**) and hence only fluid pressure contours are shown in **Figure 3.4**.

Fluid exudation from the non-contacting region could be clearly seen in the model. The contacting region prevented any fluid flowing from one cartilage into another. This was due to approximately equal fluid pressure on the opposite sides of the contact which was also influenced by the same permeability being used for both the cartilages.

One limitation of this study was that it could not be extended to observe the creep-deformation. The main reason for this was an inability to get the solution to converge even for a few minutes immediately after ramp loading. High levels of element distortions were observed along with excessive overclosure. It may be seen in **Chapter 5**, which dealt with hemiarthroplasty, that for similar levels of loads the deformation of the elements was not severe to influence the predictions. The difference was due to the way the contact was treated in these studies. In the hemiarthroplasty model, a hard contact was used whereas in the natural joint model the contact was formulated as soft. An attempt was made at using a hard contact for the natural hip joint model but this resulted in large residual forces/volume fluxes or large displacement/fluid pressure corrections which could not be taken care of even after relaxing the default contact criteria (ABAQUS., 2007). These numerical difficulties led the time increment to reduce to a very small value (1.0×10^{-15} sec) during the iteration process. Even after such a small time increment the solution could not converge. A further thorough investigation is required into this in order to increase the utility value of the proposed model. Moreover, the acetabulum and femur are not perfectly spherical (Menschik, 1997; Gu *et al.*, 2008) and need to be modelled using subject-specific CT or MRI scans which would give the local variable clearances and more realistic localised contact areas (Anderson *et al.*, 2010) both affecting the load carried by the fluid phase. This would in turn affect the contact stresses and shear stresses which have the potential of inducing cartilage fibrillation. It would be interesting to know under such circumstances whether the contact areas remain localised or if the load gets more evenly distributed as the joint undergoes repeated motion during activities of daily living. It has been seen previously, in experimental studies that the contact develops at the posterior and anterior ends of the acetabulum during the swing phase of walking leaving the acetabular dome in non-contacting state (Greenwald and O'Connor, 1971; Greenwald and Haynes, 1972). However, during the stance phase the contact slowly covers that area as well (Greenwald and O'Connor, 1971). Acetabular labrum also needs to be included in the model to investigate not only its sealing effect (Ferguson *et al.*, 2000b; Ferguson *et al.*, 2003) but also its influence on contact mechanics in general and, load distribution and fluid load support in particular.

In conclusion, despite the limitations mentioned above, the proposed model was useful. Very high fluid load support was indicative of the effectiveness of biphasic lubrication. Moreover, lower contact stresses would perhaps aid in protecting the cartilage in the long term. This model can be seen as an interesting potential tool to aid clinicians, biologists and engineers to understand the joint in its natural form which can have long-term implications on the treatment of musculoskeletal diseases of the hip joint.

Chapter 4 Porcine Hip Joint: Hemiarthroplasty Validation

4.1 Introduction

Theoretical and finite element (FE) or numerical predictions are becoming more and more successful in reproducing experimental/clinical outcomes (Brand *et al.*, 1994; Stansfield *et al.*, 2003; Bachtar *et al.*, 2006; Yoshida *et al.*, 2006; Anderson *et al.*, 2008). These models have become complex over a period of time and have been an excellent non-invasive tool for understanding the mechanical and functional aspects of the joints. However, the analytical/numerical results have always been viewed with scepticism whenever they are not backed up by experimental/clinical observations.

Validation thus plays an important role in these types of studies. The confidence placed in the FE predictions will increase if they can be compared favourably with clinical observations or those in experimental setups. Only then, will these models be deemed safe to use as an indispensable tool for preoperative planning, postoperative rehabilitation or designing of new prosthesis.

Several studies, both mathematical and FE, have used validation to corroborate their findings (Brand *et al.*, 1994; Stansfield *et al.*, 2003; Anderson *et al.*, 2008) but none have involved articular cartilage modelled as a biphasic material in a whole joint model. Therefore, in the present study, an attempt was made to validate the methodology used in hemiarthroplasty models using porcine acetabular cups and a rigid metallic femoral head.

4.2 Model and Methods

The validation was a long process which started with deriving the material properties of the porcine acetabular cartilage which were then used in the FE model of the whole porcine hip joint. The material properties such as equilibrium elastic modulus and the permeability were derived. The entire process is shown in the flowchart in **Figure 4.1**. Different instruments/machines were used in this process and **Table 4-1** lists them all with their specifications and, resolution and accuracy.

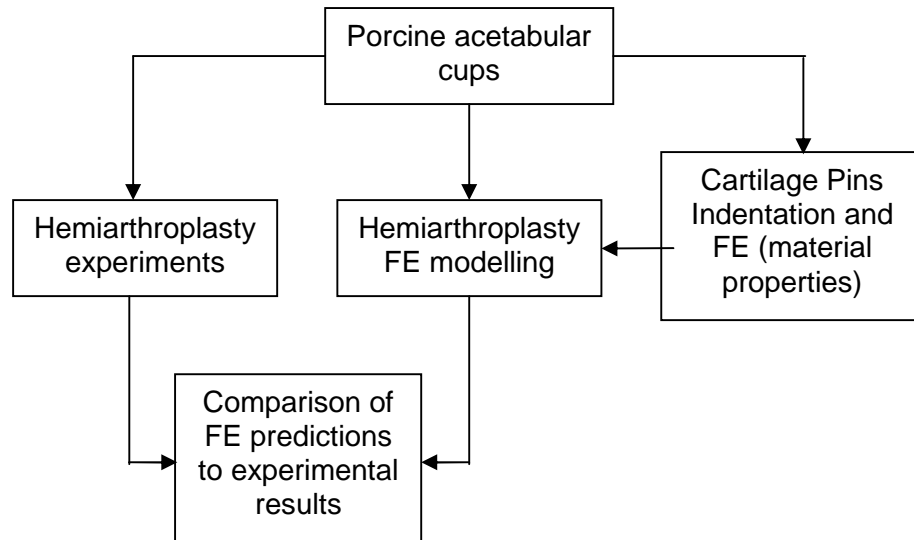


Figure 4.1 Flowchart for experimental validation of hemiarthroplasty

4.2.1 Material properties derivation

Acetabular cups were extracted from healthy pigs of around 6 months old within 36 hours of slaughter. The cartilage pins/plugs of 9 mm diameter together with subchondral and cancellous bones were then extracted from three different locations of these cups using a surgical plug extractor (see **Figure 4.2** and **Figure 4.3**). The cartilage surface was kept hydrated throughout this process by using phosphate buffered saline (PBS) solution. There were at least 6 plugs taken from each site; one each from corresponding site of a single cup. However, all the pins were considered together for the final calculations as the aim was to derive homogeneous and isotropic material properties. The sample size thus arrived at was quite large ($n = 21$). The plugs were then stored at $-20\text{ }^{\circ}\text{C}$ in PBS. Prior to their use, the pins were defrosted in a warm water bath for at least an hour.

The pins were not completely flat as they were extracted from the highly curved porcine acetabular cup. It was thus felt necessary to measure the radius of curvature of these pins in order to accurately reproduce them in FE models. The Talysurf (**Table 4-1**) was used to measure this radius (see **Figure 4.4**). Two perpendicular readings were taken. The average of two readings was then used as the final radius of curvature.

Table 4-1 Accuracy and Resolution of the instrumentation/machines used for experimental validation

Sr. No.	Instrument/Machine	Resolution	Accuracy
1	Form Talysurf – 120L, Taylor-Hobson Precision, A Division of Ametek, Leicester, UK Stylus – 2 μm radius conical shaped diamond tip 1) Transverse unit 2) Contour pickup	1) 10 nm @ 4 mm range 2) 12 nm @ 0.4 mm range	1) 0.5 μm over 120 mm 0.1 μm over 20 mm
2	Nikon Profile Projector (Model V-16D), Nippon Kogaku K. K., Japan. 1) Stage 2) Viewing Screen (360°) 3) Magnification illumination	1) 1 μm 2) 1'	1) 3 μm (incl. quantum error) 2) 2' 3) $\pm 0.1\%$ - contour (error) $\pm 0.15\%$ - surface (error)
3	Indentation Rig 1) Load Cell (Model D; part# - 060-1896-02) 2) Linear Variable Differential Transformer (D5-200H) Both - RDP Electrosense, Pottstown, PA, USA	1) 0.04 N @10 gms range 2) 0.4 μm @ 10 mm range	1) $\pm 0.5\%$ F.S. (linearity error) 2) $\pm 0.5\%$ F.S. (linearity error)
4	μCT 80, SCANCO Medical AG, Brüttisellen, Switzerland	5 - 144 μm	
5	Instron (3365), Instron Corporation, Norwood, MA, USA. ± 500 N Static Load Cell	0.02 N	$\pm 0.25\%$
6	Spectrodensitometer (500 Series), Sensor Products Inc., Madison, NJ, USA	--	$\pm 1\%$
7	Coordinate Measuring Machine (Kemco 400, CNC), Keeling Metrology, Keeling, Derby, UK	1 μm	$\pm 3 \mu\text{m}$ (error)

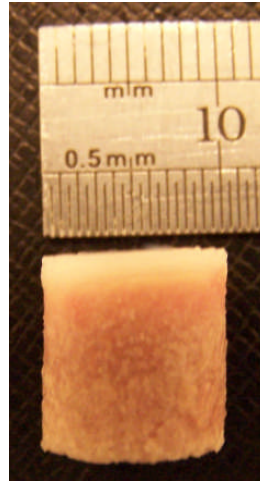


Figure 4.2 Porcine acetabular cartilage pin of 9 mm diameter

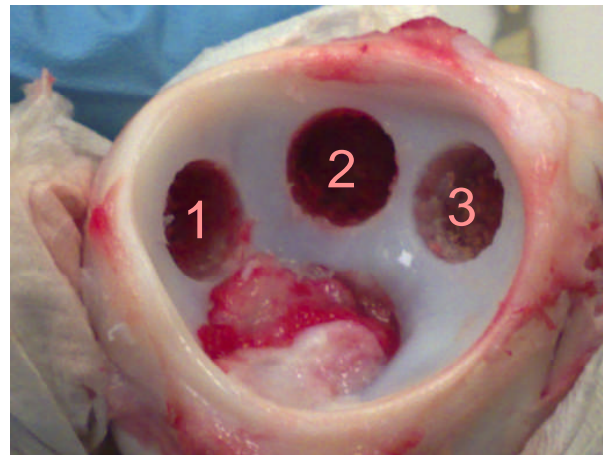


Figure 4.3 Location of porcine acetabular cup pins

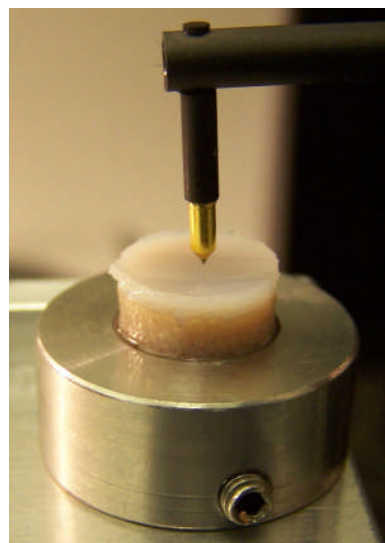


Figure 4.4 Radius of curvature measurement using Talysurf

The thickness of a pin was measured using a Nikon profile projector (**Table 4-1**) as shown in **Figure 4.5**. The readings were taken at positions '1' and '2' and the difference then gave the thickness. A set of twelve readings were taken for each pin around its circumference and the average was then calculated.

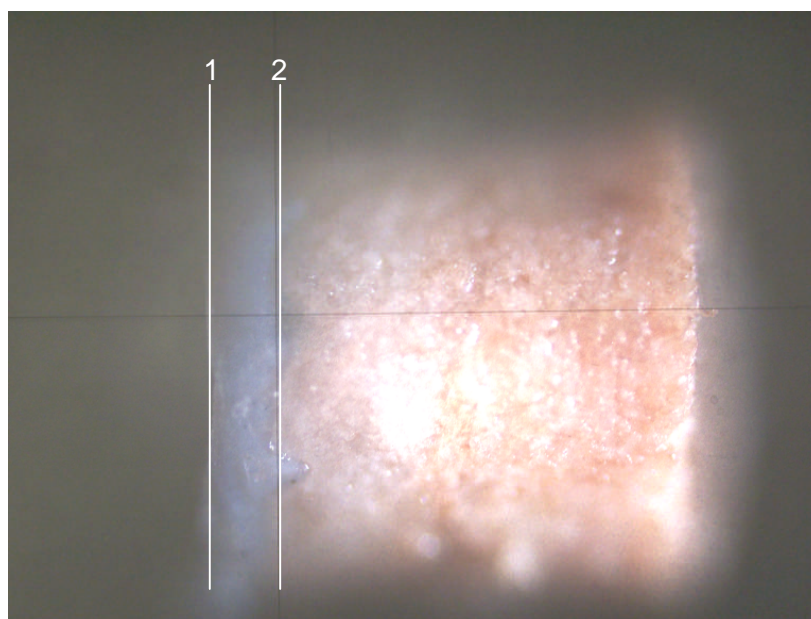


Figure 4.5 Thickness measurement of cartilage using Nikon profile projector

The radii of curvature and the thickness measurements of all the pins ($n = 21$) were then averaged to give the values of 16.347 ± 2.719 mm and 1.494 ± 0.238 mm respectively.

Each cartilage pin was then subjected to creep-deformation using indentation as shown in **Figure 4.6** (Swann and Seedhom, 1989; Katta, 2008). A linear variable differential transformer (LVDT) was mounted on the top to measure the displacement of the main shaft. The load cell was mounted on the bottom of this shaft and the indenter was screwed on to the purpose-built fixture attached to this load cell. The bearing guided the loaded shaft and its speed was controlled by oil dashpot. The LVDT and load cell voltages were converted into digital format (BNC – 2090, National Instruments Corporation, Austin, TX, USA) and this data was then acquired at a sampling frequency of 5 Hz using LabVIEW 8.0 (National Instruments Corporation, Austin, TX, USA). The test specimen holder was screwed onto the base of the indentation rig. The collet was used to hold the cartilage pin such that cartilage sides were exposed (**Figure 4.6**). This collet was then mounted in the specimen holder which kept the pin in position throughout the test.

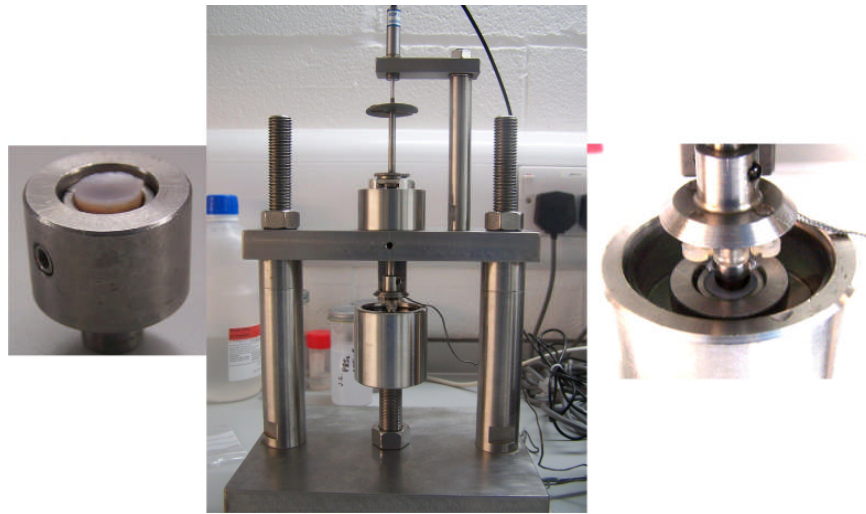


Figure 4.6 Indentation of porcine acetabular cartilage pin

A rigid spherical indenter of 6.33 mm diameter was used to apply a load of 10 gms. In addition to this, the individual components of the indenter loading assembly applied their own weights and are shown in **Table 4-2**. This load is applied almost instantaneously (within 40 ms).

Table 4-2 Weights of the individual components of indenter loading assembly

Sr. No.	Component	Weight (gms)
1	Main Shaft with oil dashpot	52
2	Load Cell	15
3	Small shaft from LVDT (connected to main shaft)	3
4	Spherical Indenter (diameter – 6.33 mm)	2

Therefore a total load of 82 gms or 0.8 N was applied to the cartilage for one hour. The deformation during this period was recorded. The instance at which the full load was recorded was assumed to be the start time (zero seconds). The cartilage pin was kept submerged in the PBS solution for the duration of the test.

The average of the deformations for all the samples (n=21) was then calculated and is shown in **Figure 4.7**. This was used to derive the equilibrium elastic modulus and permeability of the articular cartilage.

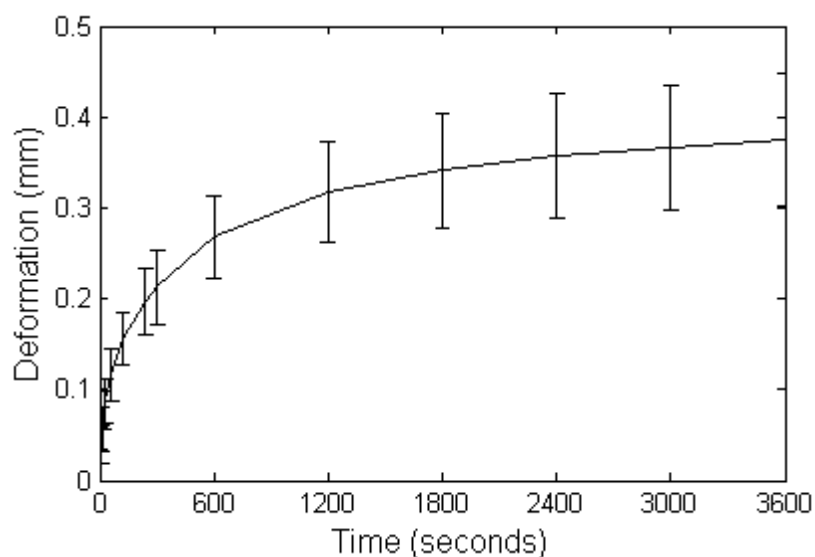


Figure 4.7 Mean deformation curve for cartilage pins (n=21, Mean \pm SD)

The FE model was then created and analysed in ABAQUS (ver. 6.7-1, Dassault Systemes, Suresnes Cedex, France) based on the radius of curvature and cartilage thickness measured, as explained previously. The geometry and the mesh used are shown in **Figure 4.8**. All the dimensions are in mm.

The model consisted of 1125 four-node bilinear displacement and pore pressure axisymmetric elements (CAX4P) representing cartilage whereas bone was meshed using 525 four-node bilinear elastic axisymmetric elements (CAX4). The indenter was analytically rigid with the reference point at its centre.

The bottom nodes of the bone were constrained both in the vertical and horizontal directions representing the pin held in the collet in experimental setup. The bone and the cartilage nodes on the axisymmetric vertical axis and the indenter reference point were constrained in the horizontal direction due to symmetry to represent the specimen and indenter integrity in the indentation test. Free fluid flow was allowed at the outer edge of the cartilage whereas no fluid flowed from the cartilage surface on the axis of symmetry. The fluid flow boundary conditions on the upper cartilage surface depended on the developing contact over time and were applied using the algorithm discussed in **Chapter 2**.

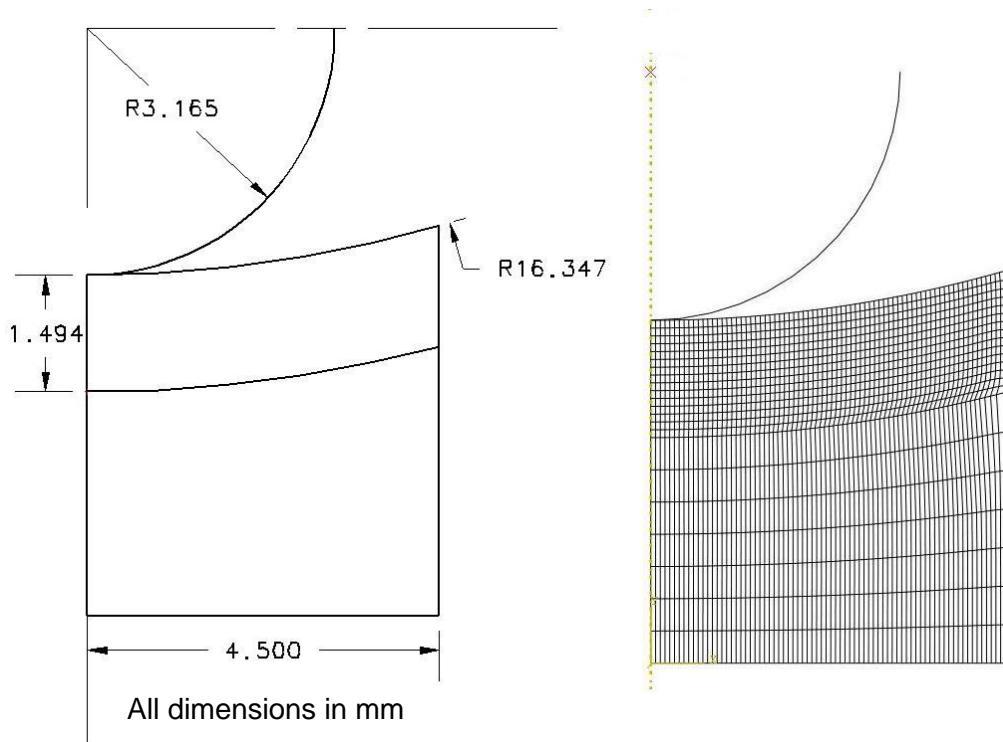


Figure 4.8 Geometry and FE Model of average cartilage pin

Cartilage Poisson's ratio was assumed to be 0.0 (Jin *et al.*, 2000). Its water content was 70.1 % (Simunek and Muir, 1972; Nakano and Aherne, 1992). The elastic modulus and Poisson's ratio of the bone were 17 GPa and 0.3 respectively (Dalstra and Huiskes, 1995). The contact was assumed to be frictionless.

The load of 0.8 N was applied vertically downwards at the reference point of the indenter in 2 seconds and then held constant for further 3600 seconds similar to experiments. The equilibrium elastic modulus and permeability were estimated using the final 30% of experimental deformation curve and FE curve, and by minimizing squared error between the two (Lei and Szeri, 2007). A function 'lsqnonlin' in MATLAB (The MathWorks, Inc., Natick, MA, USA) was used to optimise the solution of this non-linear problem (Lei and Szeri, 2007). The function needed initial values of equilibrium elastic modulus and permeability to begin the iteration. Five different initial pairs of values were used to ensure that the solution did not get stuck in the local optima. ABAQUS command was then repeatedly called from within MATLAB function and these function calls continued comparing the squared error until the solution converged or a certain number of threshold iterations were performed (100 was used in this study which was never exceeded). The final solution gave the optimum values of equilibrium elastic modulus and permeability of the cartilage for the corresponding experimental deformation curve.

The model with final material properties was then allowed to run for 4 hours in order

to compare it to the short term experimental response as this was the typical time duration required for creep equilibrium of 2 mm thick articular cartilage (Mow *et al.*, 1980; Mow and Hung, 2001).

4.2.2 Porcine acetabular cup – validation process

Porcine acetabular cups were extracted as before. However, most of the unwanted tissue still attached to the bone was removed using scalpel. The acetabular labrum was kept intact to avoid any structural damage to the tissue structure of the acetabular cartilage. The cartilage was kept hydrated all the time using PBS. The cups were always stored at -20 °C in PBS and before use they were defrosted for at least an hour in a warm water bath.

4.2.2.1 Experimental Measurement of Contact Stress and Area

Each acetabular cup was fixed in polymethylmethacrylate (PMMA) cement at approximately 45° in order to carry out compression tests. The cemented acetabular cup was kept in a holder which was then mounted on a platform of the Instron (**Table 4-1**). The cup was always kept hydrated using PBS. The remaining part of the ligamentum teres was carefully removed from the acetabular fossa before testing.

The spherical prosthetic femoral head (CoCr - DePuy) of 34 mm diameter was screwed in the attachment mounted on the underside of the load cell. The load cell was fixed to the frame of the Instron which could be moved vertically to apply the compressive load.

Fuji pressure sensitive film (Sensor Products, LLC, USA) was used to measure the contact pressures developed on the articular surface as well as contact area when loaded with the prosthetic femoral head. These films are either “two-sheet” type or “mono-sheet” type. The thickness of each sheet in two-sheet type is $90 \pm 5 \mu\text{m}$ and that of single-sheet type film is $110 \pm 5 \mu\text{m}$ (FUJIFILM Recording Media GmbH., 2007). The donor sheet in two-sheet type film is coated with microcapsules of colour forming material on a polyester base whereas the receiver sheet is also polyester base coated with colour developing material. The two films are kept with coated sides facing each other in between two contacting surfaces to measure the contact pressure. When the pressure is applied microcapsules break and the colour forming and colour developing materials react with each other forming red patches. The density of the colour patches, which can be measured using a Spectrodensitometer (**Table 4-1**), corresponds to the contact pressure values. In single-sheet pressure film a polyester base is first coated with

colour developing material and then micro-encapsulated colour forming material is coated on top. The accuracy of these films is $\pm 10\%$ or less at 23°C when measured with a densitometer (FUJIFILM Recording Media GmbH., 2007).

Different sensitivity films from superlow to medium were used to measure either the contact stresses or contact area. Contact areas were measured using film that was one grade lower than that used for measuring contact stresses. Low sensitivity (2.5 – 10 MPa) Fuji pressure sensitive film was used to measure the contact stresses for all the acetabular cup specimens except '*pc140509_74_7kg*' where medium sensitivity (10 – 49 MPa) film was used. The film was cut in the rosette pattern to avoid wrinkling when it wrapped around the spherical prosthetic head. It was then covered with two polyethylene sheets of approximately 0.004 mm thickness to avoid contact with the PBS which was still in the acetabular cup. The room temperature and relative humidity were recorded throughout the tests. The experimental set up is shown in **Figure 4.9**.

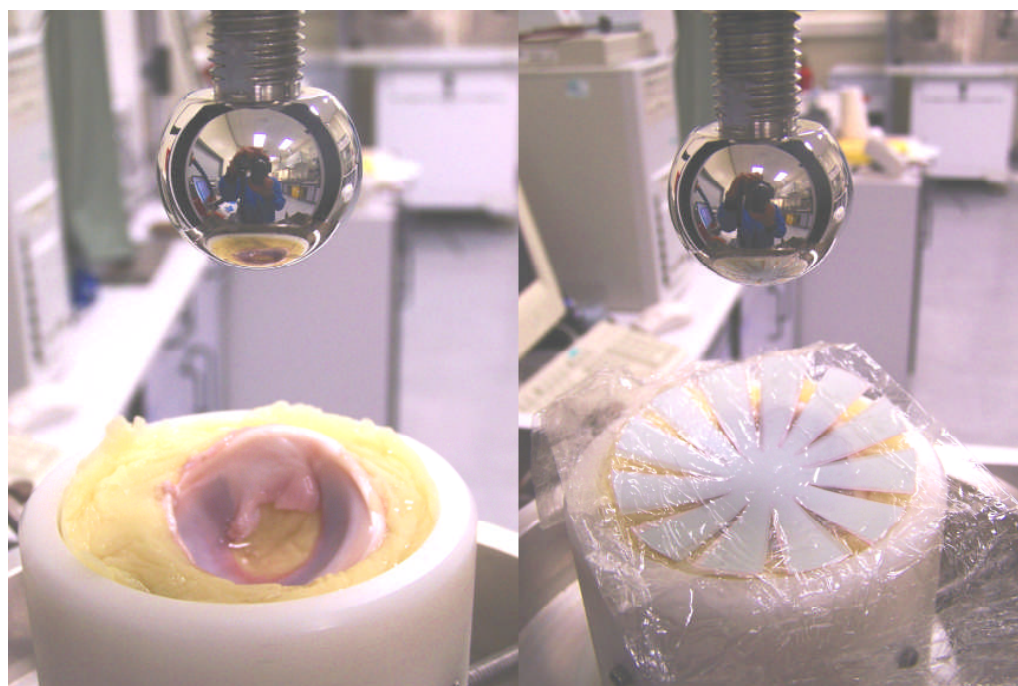


Figure 4.9 Vertical loading of acetabular cup using Instron and the use of Fuji film to measure contact stress and contact area

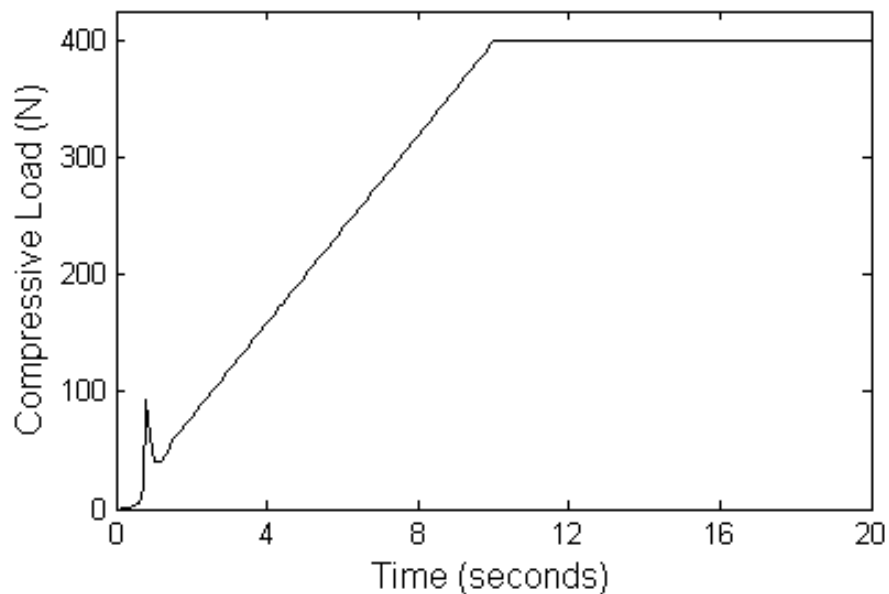
The superlow and low sensitivity films were two-sheet type whereas the medium sensitivity film was mono-sheet type. The colour density of the pattern was measured using a Spectrodensitometer. PointScan (Version 2.15, Sensor Products Inc.) software was then used to convert these density values into contact pressure values. Temperature, relative humidity and exposure time were also needed as inputs to PointScan (**Table 4-3**).

Table 4-3 Parameters used to convert colour intensity into contact stresses

Parameter	Value
Length of Exposure (seconds)	20
Relative Humidity (%)	20.04
Temperature (°C)	20.8

Low sensitivity film was used for specimen '*pc140509_74_7kg*' to measure the contact area whereas for the specimens '*pc120509_95_3kg*' and '*pc140509_71_5kg*', superlow sensitivity (0.5 – 2.5 MPa) film was used. While measuring contact area, since the area where the contact stresses were lower than 0.5 MPa did not produce any distinct red pattern, a larger area than that which appeared on the film was considered for measurements. This larger area was taken into account only when there was a presence of scarcely dispersed red dots. Completely white areas were not taken into account.

The Fuji film was kept in between the head and the cup as shown in **Figure 4.9**. The compressive load of 400N was then ramped up in 10 seconds and maintained for another 10 seconds to allow for the Fuji film pattern to stabilize. A typical loading curve is shown in **Figure 4.10**.

**Figure 4.10 Typical loading curve on Instron**

The load of 400N was chosen based on the findings in quadrupeds (Bergmann *et al.*, 1984; Bergmann *et al.*, 1999). For sheep, the median hip joint forces during walking (at 3.5 km/h) have been shown to range between approximately 20 – 140% BW and were generally found to increase with the walking speed and postoperative period during first five to nine months. (Bergmann *et al.*, 1984; Bergmann *et al.*, 1999). The forces then either remain constant or decrease with postoperative time. In a short term study (2 months postoperative) of canines, loads as low as approximately 5% of BW and as high as 80% of BW were found during walking at 1.25 m/s (Bergmann *et al.*, 1984). The hip joint loads are generally lower in quadrupeds when compared to humans (Bergmann *et al.*, 2001). A standard compressive load of 400N was thus used in tests and FE models. This lay within the physiological load limits of quadrupeds though nearer lower range (**Table 4-4**). The load was increased from 0 to 400 N in 10 seconds.

Table 4-4 Percentage of body Weight (with reference to 400 N) used in the validation process of FE models

Sr. No.	Specimen	Porcine Weight (Kg)	Porcine Weight (N)	%BW for 400N
1	pc120509_80_8kg	80.8	792.648	50.46
2	pc120509_86_4kg	86.4	847.584	47.19
3	pc120509_95_3kg	95.3	934.893	42.79
4	pc130509_78_0kg	78.0	765.18	52.28
5	pc140509_71_5kg	71.5	701.415	57.03
6	pc140509_74_7kg	74.7	732.807	54.58

It was necessary to reproduce the exact spatial orientation of the cup in this test, in the FE model so that both the test and FE results could be compared with as little variation as possible. In order to do this, a coordinate measuring machine (CMM - **Table 4-1**) was used. Three distinct non-linear landmarks such as peaks (**Figure 4.11**) or the lowest points on the edge were chosen for each acetabular cup and their spatial coordinates were measured. Three readings were recorded for each point and then their average was calculated.

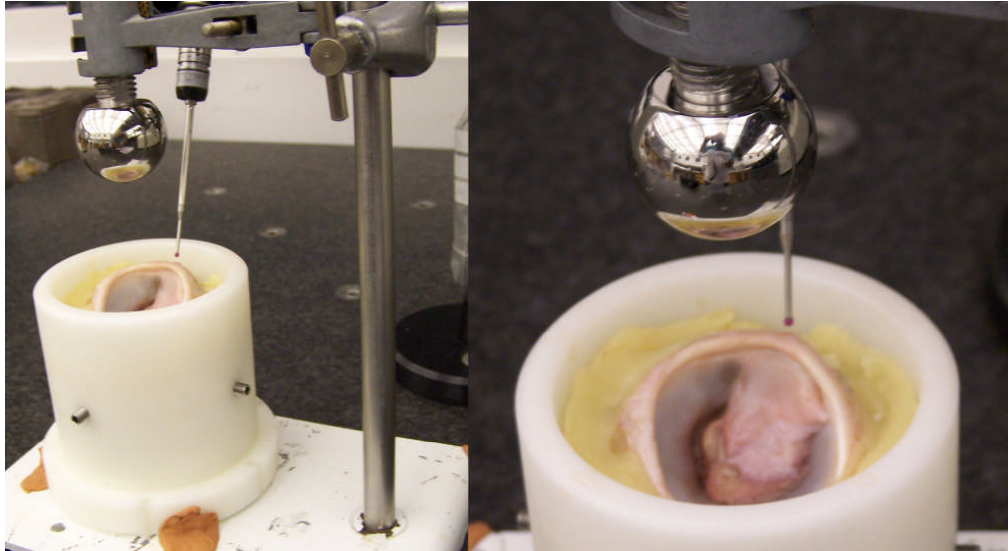


Figure 4.11 Measuring acetabular cup orientation using CMM

4.2.2.2 μ CT Scanning and Segmentation

Various steps were involved in converting μ CT scans into the FE model. These steps are listed in the flowchart in **Figure 4.12**.

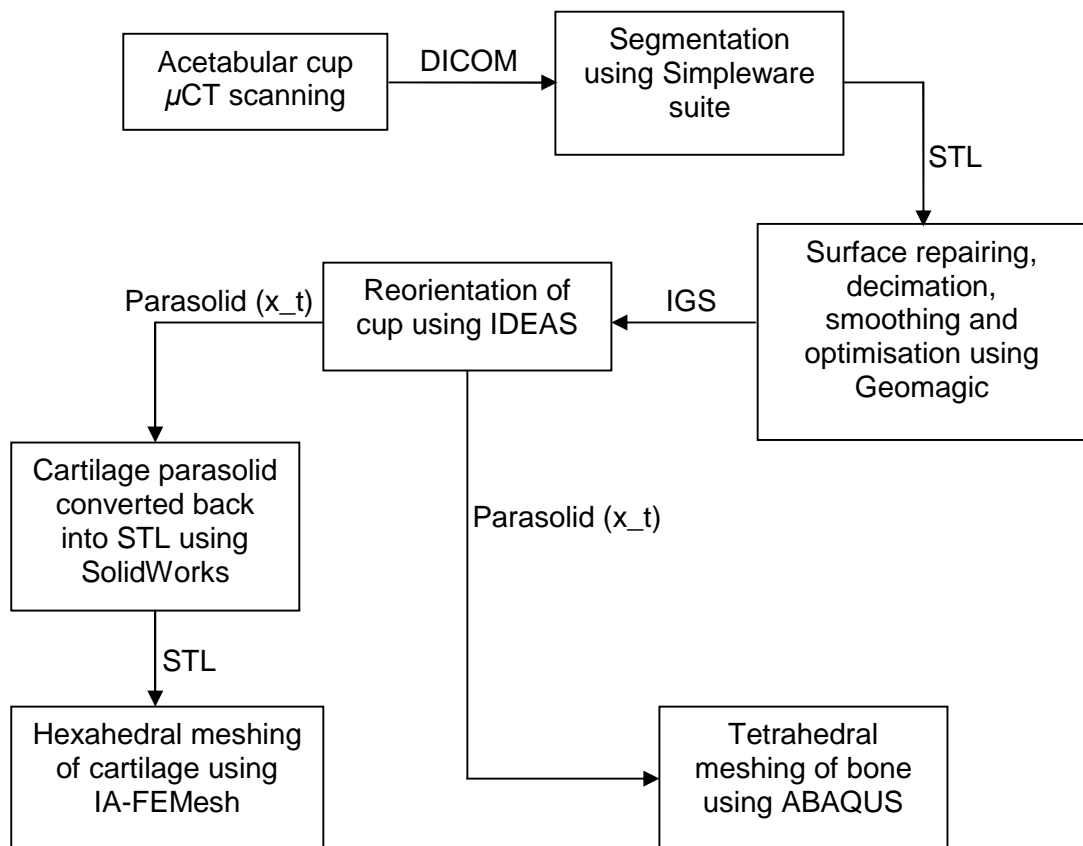


Figure 4.12 Flowchart for converting μ CT data into FE model

Individual acetabular cups were placed in a container of 61.4 mm diameter with the lunate area facing upwards. The cup was firmly held in position using pieces of foam so that it would not move during scanning. The cartilage was kept hydrated using PBS and then covering the opening of the container using polyethylene sheet. The cup was then imaged using the μ CT scanner (**Table 4-1**) at 60 μ m resolution, 70 kV and 114 μ A. The number of slices varied depending on the size of the acetabular cup. The high resolution images were then converted to stack of images in the DICOM file format. A typical DICOM slice is shown in **Figure 4.13** which shows both the bone and tissue very vividly.

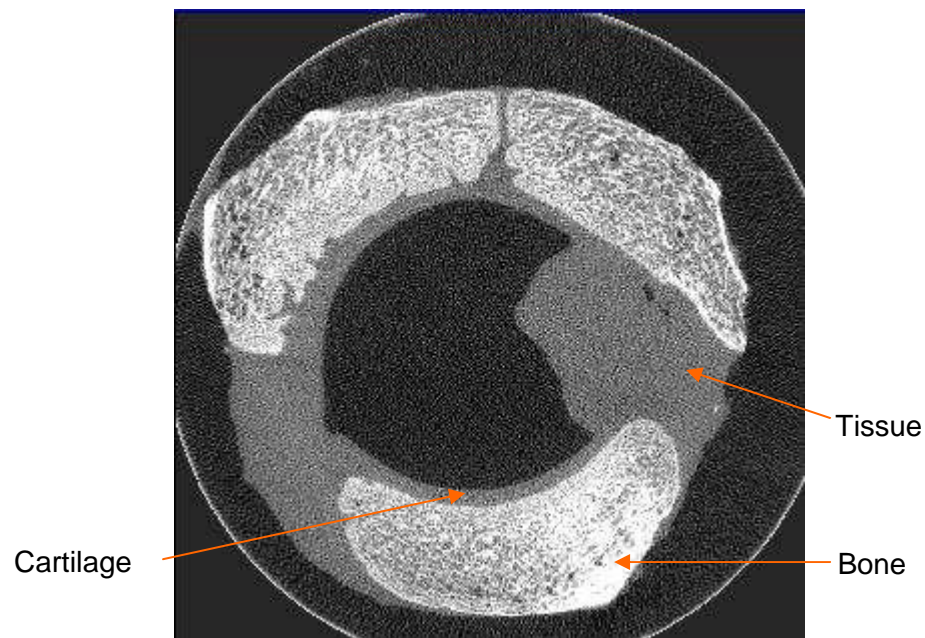


Figure 4.13 A typical μ CT slice

The images were then segmented using ScanIP from the Simpleware suite (Simpleware Ltd., Exeter, UK) of image processing software. The stacks of DICOM images were imported into ScanIP. After choosing the brightness level to clearly see both the bone and tissue, the images were down sampled without losing any required details. Two masks were then created, one for tissue and the other for the bone based on respective threshold values. One disadvantage of μ CT is that, it cannot differentiate between different tissues. So the cartilage could not be differentiated from the fibrous tissues or ligaments. The part of the ligamentum teres that was still attached to the acetabular fossa and the other tissue still attached to the outside of the bone had to be manually removed. This was carried out at software level using manual erasing in ScanIP. The segmented cartilage and

bone were then smoothed (**Figure 4.14**). Both the cartilage and bone were then separately exported as individual meshes (.sfh format). The meshes were then imported in the ScanFE part of Simpleware suite where they were refined. The native meshes created by ScanFE contained around a million elements each representing cartilage and bone. This high number of elements would increase the computational time without improving the accuracy of the solution. Hence they were exported as STL surfaces for further processing.

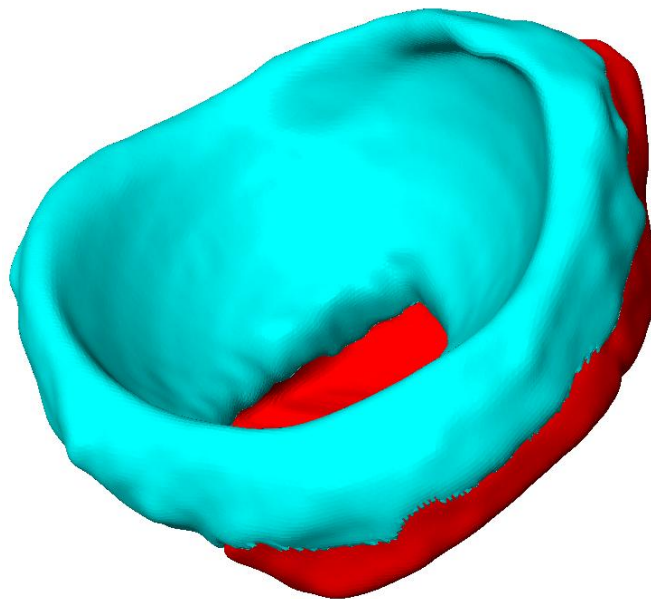


Figure 4.14 Segmented acetabular cup from μ CT

4.2.2.3 FE model

The STL files were imported in Geomagic Studio 11 (Geomagic Inc., Research Triangle Park, NC, USA) where the surfaces were repaired, decimated, smoothed and optimised. The decimation was required to reduce the number of triangular elements making up the STL surfaces in order to reduce the computational cost of time and space. The surfaces were then exported as IGES files which were imported in IDEAS (ver. 11, Siemens PLM Software, Plano, TX, USA).

The coordinates of three non-linear points on the cup edges that were measured using CMM were then transferred to the corresponding acetabular cup in IDEAS thus reorienting it in the position which would be used during tests.

Once the acetabular cup was oriented in its final position, both the cartilage and the bone were exported as parasolids. Bone was then imported as a solid in ABAQUS and was meshed using four-node linear tetrahedron elements (C3D4 - **Figure 4.15**).

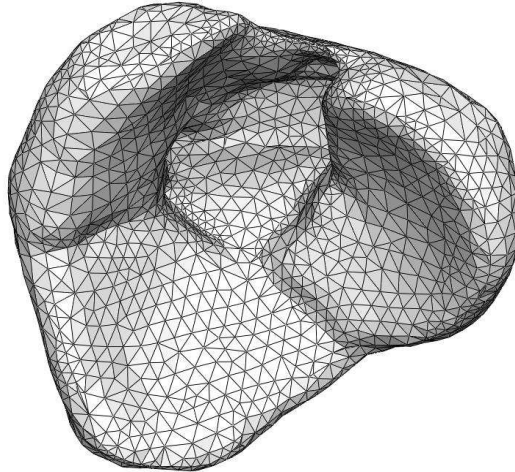


Figure 4.15 A typical FE model of acetabular bone

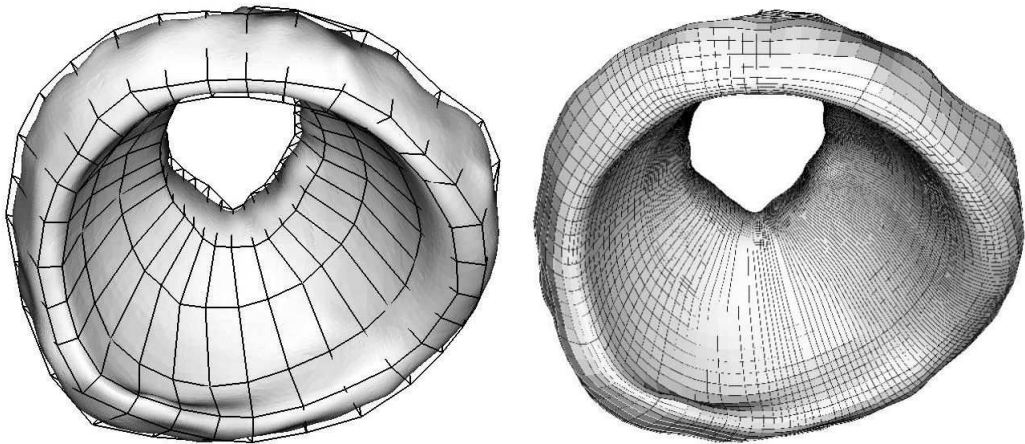


Figure 4.16 Acetabular cartilage mesh generation using blocks in IA-FEMesh (Grosland *et al.*, 2009)

However, meshing the cartilage was not straight forward as hexahedral elements were needed for contact mechanics simulations. The shape of the cartilage was not only highly irregular but also had finer details which posed difficulty in meshing it using ABAQUS. Alternative software called IA-FEMesh (Grosland *et al.*, 2009) was therefore employed. However, IA-FEMesh needs STL files to build mesh. Hence, the cartilage in parasolids format was converted back to

STL using SolidWorks (Dassault Systèmes SolidWorks Corp., Concord, MA, USA). Rectangular blocks were created around the cartilage as required by IA-FEMesh (**Figure 4.16**). The dimensions of the blocks were varied in order to cover the finer details of the cartilage. Seeds were then created on these blocks which were used to create the mesh by projecting them onto the cartilage surface. The mesh was then smoothed. Dr N M Grosland's group from the University of Iowa assisted in creating the correct meshes.

Eight-node trilinear displacement and pore pressure, reduced integration elements (C3D8RP) were used in the cartilage mesh. The prosthetic femoral head was modelled as an analytically rigid solid with a reference point at its centre. A typical final FE model of the porcine acetabular cup with prosthetic femoral head, representing the compressive test setup is shown in **Figure 4.17**. The number of elements used in FE models of each specimen has been given in **Table 4-5**.

The cartilage surface was tied to the bone and the contact between the cartilage and the prosthetic head was assumed to be frictionless. A part of the bottom of the bone was pinned to represent the cemented cup in the test setup. This would prevent any movement of the acetabular cup when the load was applied. The head was constrained in such a way that only its vertical movement was possible. It was also prevented from rotating in all three directions. At the contacting articular surface, fluid flow boundary conditions were applied depending upon the developing contact using a contact dependent algorithm (see **Chapter 2**).

The equilibrium elastic modulus and permeability derived earlier for the porcine cartilage were used in the model. Its Poisson's ratio and water content were assumed to be 0.0 (Jin *et al.*, 2000) and 70.1% (Simunek and Muir, 1972; Nakano and Aherne, 1992) respectively. Bone was assumed to be cortical only with elastic modulus of 17 GPa whereas its Poisson's ratio was 0.3 (Dalstra *et al.*, 1995).

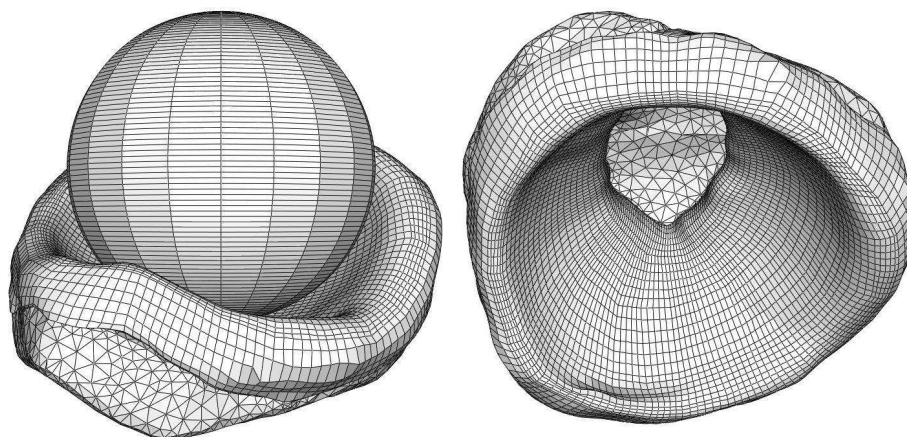


Figure 4.17 A typical final porcine acetabular cup FE model

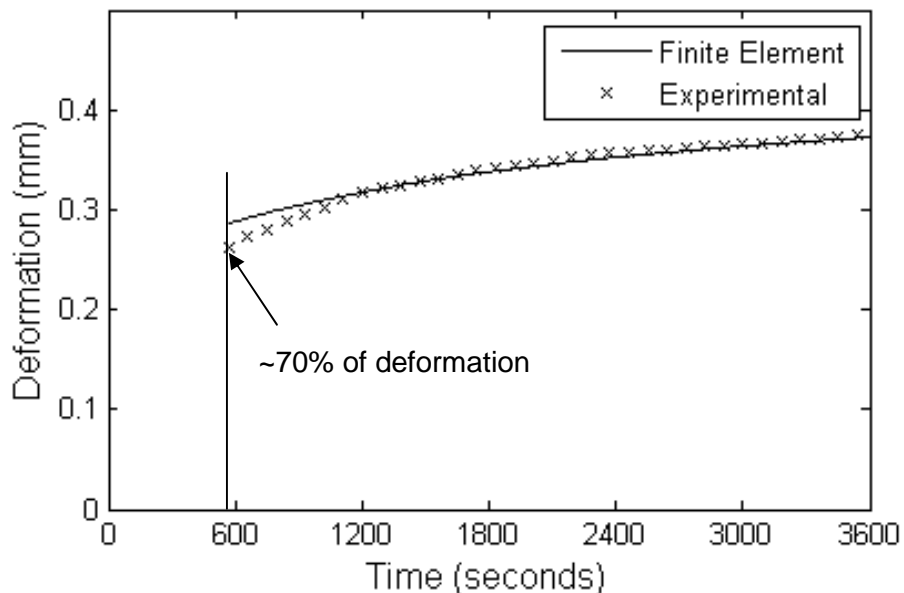
Table 4-5 Number of elements used in FE models of each specimen

Sr. No.	Specimen	Number of Elements	
		Bone (C3D4)	Cartilage (C3D8RP)
1	pc120509_80_8kg	14768	27097
2	pc120509_86_4kg	15558	39144
3	pc120509_95_3kg	15080	25926
4	pc130509_78_0kg	14137	26064
5	pc140509_71_5kg	19124	27456
6	pc140509_74_7kg	16595	28360

The solid phase of the cartilage was modelled as neo-Hookean poro-hyperelastic material and bulk modulus, K and shear modulus, G were obtained using **Equations (3.2)** and **(3.3)**. Elastic strain energy potential given in **Equation (3.1)** was then used in the FE model.

UTOL was kept very high with a value of 100 MPa. Ratio of the largest residual force to average flux norm over time was set to 1000000% whereas ratio of largest displacement correction to largest corresponding increment was set to 10%. Other controls were kept unchanged.

4.3 Results

**Figure 4.18 FE Curve fitting to experimental deformation plot**

The FE curve fitted to the final 30% of experimental deformation data is shown in **Figure 4.18**. The curve had a squared error of 1.28×10^{-1} and the final

values of equilibrium elastic modulus and permeability were 0.455 MPa and $1.07 \times 10^{-15} \text{ m}^4/\text{N}\cdot\text{s}$ respectively. The corresponding properties were 0.562 MPa and $1.57 \times 10^{-15} \text{ m}^4/\text{N}\cdot\text{s}$ when the entire deformation curve was considered. The squared error in this latter case was 3.34.

It should be also noted that the cartilage pin did not reach equilibrium during the indentation test time of 3600 seconds and the deformation was still in the biphasic region of the deformation curve (**Figure 4.19**).

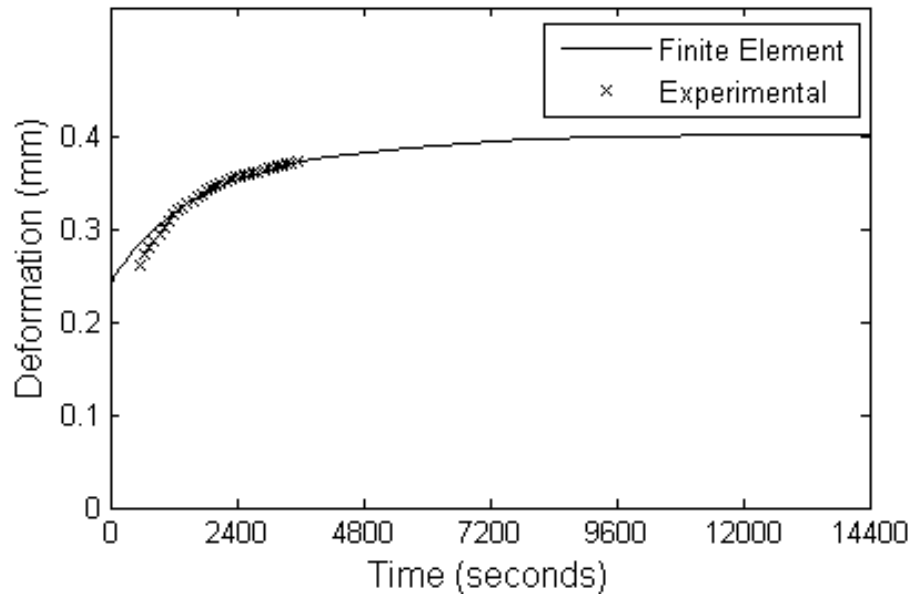


Figure 4.19 FE deformation curve for a longer duration corresponding to the one in Figure 4.18

The contact area patterns in experiments (**Figure 4.20**) and in FE models (**Figure 4.21**) were similar. **Table 4-6** gives the measured and calculated contact areas with the percentage difference. Three specimens had to be omitted from the tests for a variety of reasons as given in **Table 4-6**.

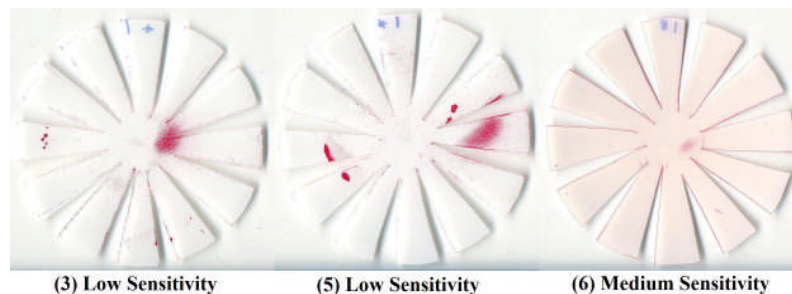


Figure 4.20 Rosette pattern of Fuji film after the removal of load

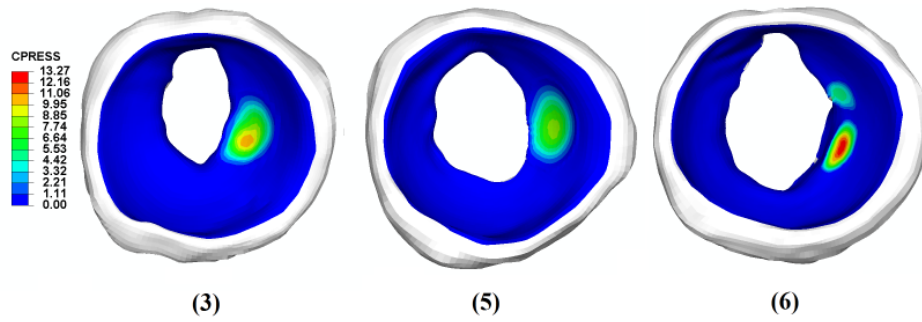


Figure 4.21 FE model prediction of the contact stresses in MPa (Refer Table 4-6 for specimen numbers)

Table 4-6 Experimental results and FE predictions of contact area

Sr. No.	Specimen	Contact Area (mm ²)		Difference (%)	Remarks
		Experimental	FE		
1	pc120509_80_8kg	--	--	--	PMMA obstruction
2	pc120509_86_4kg	--	--	--	Distorted elements
3	pc120509_95_3kg	117.76	148.48	20.69	
4	pc130509_78_0kg	--	--	--	Cartilage cut by scalpel
5	pc140509_71_5kg	147.19	175.11	15.94	
6	pc140509_74_7kg	90.10	92.88	2.99	

The experimental contact area was within 2.99% of FE prediction for specimen '*pc140509_74_7kg*' and was the lowest amongst all the three specimens. The contact pattern however, was bi-centric in FE prediction of this specimen which was not observed in experiment. The maximum difference of 20.69 % was observed in specimen '*pc120509_95_3kg*'.

Table 4-7 Experimental results and corresponding FE predictions of peak contact stresses

Sr. No.	Specimen	Peak Contact Stress (MPa)		Difference (%)
		Experimental	FE	
1	pc120509_80_8kg	--	--	--
2	pc120509_86_4kg	--	--	--
3	pc120509_95_3kg	9.72	11.10	12.42
4	pc130509_78_0kg	--	--	--
5	pc140509_71_5kg	8.54	8.30	2.89
6	pc140509_74_7kg	14.09	13.27	6.21

The contact stress values are given in **Table 4-7**. The maximum difference of experimental peak contact stresses measured using Fuji film and those predicted by FE models was 12.42% of FE results, for specimen 'pc120509_95_3kg'. The lowest difference was 2.89% for 'pc140509_71_5kg'.

Maximum total fluid load support predicted by FE models was 82.46% for specimen 'pc140509_74_7kg' whereas the minimum of 75.53% was predicted for specimen 'pc140509_71_5kg' (**Table 4-8**).

Table 4-8 FE predictions of total fluid load support (TFLS)

Sr. No.	Specimen	TFLS (%)
1	pc120509_80_8kg	--
2	pc120509_86_4kg	--
3	pc120509_95_3kg	80.70
4	pc130509_78_0kg	--
5	pc140509_71_5kg	75.53
6	pc140509_74_7kg	82.46

Clearance in each cup was variable due to the non-spherical nature of the acetabulum. From the FE studies, radial clearance as calculated on the labrum edge ranged between approximately 1 and 4 mm.

4.4 Discussion

Experimental/clinical validation of analytical or numerical models is important in order to improve confidence in their predictions, increase their usability and to be widely accepted in clinical community. Though, there are several studies which have compared the analytical/numerical outcomes with already published clinical/experimental results, there is perhaps just one study, to the best of author's knowledge, which validated a human hip joint contact mechanics FE model using experimental results from the same human cadaver (Anderson *et al.*, 2008). However, that study used bovine material properties for articular cartilage and the cartilage itself was modelled as hyperelastic. The current study was thus carried out to validate the hemiarthroplasty model with biphasic articular cartilage that could then be used for a variety of different applications.

It should be noted that some of the controls and UTOL had to be relaxed in

order to avoid the convergence problems during analysis. In spite of this, FE predicted contact stresses and contact areas showed good agreement with those measured in experiments not only in magnitude but also in their locations.

A porcine acetabular cup and metallic prosthetic femoral head were used in this study. Porcine acetabular cartilage material properties such as equilibrium elastic modulus and permeability were first derived using indentation and curve-fitting of FE creep-deformation to that observed in experiment using the least squared error method. The first 70% of the deformation curve is usually omitted in such analysis (Mow *et al.*, 1989; Roemhildt *et al.*, 2006; Keenan *et al.*, 2008). The initial time response of the experimental and theoretical creep differ and has been observed previously (Mow *et al.*, 1989; Setton *et al.*, 1994; Roemhildt *et al.*, 2006). This difference is usually attributed to the assumption of frictionless contact between the indenter tip and cartilage surface in theoretical models (Mow *et al.*, 1989; Setton *et al.*, 1994). This perfect frictionless contact is difficult to achieve in an experimental setup. Moreover, the initial loading conditions are also difficult to match precisely (Roemhildt *et al.*, 2006). The inhomogeneous and anisotropic nature of the cartilage as well as strain-dependent permeability (none of which was implemented in the FE models in the current study) may also cause this difference (Mow *et al.*, 1989). Thus only the final 30% of the deformation curve was used to derive material properties.

It should be noted that the human cortical bone properties for the pelvis were used throughout this validation as they have been reported to be similar to porcine bone properties (Mulder *et al.*, 2008). The bone was assumed to be made up of only cortical bone. The reason for this assumption was that the focus here was on the articular cartilage surface. The bone is rigid compared to softer cartilage and it has been modelled as such in previous studies due to very small strains induced in the bones (Macirowski *et al.*, 1994; Dalstra *et al.*, 1995; Ferguson *et al.*, 2000a).

Derived cartilage material properties were then used in the models of porcine acetabular cups created by using μ CT scanning and a series of processes involving different software. The acetabular labrum was kept intact in both experiments and FE models. It was given the same material properties as those of cartilage. Its permeability had been assumed to be lower than that of the cartilage in an earlier study (Ferguson *et al.*, 2000a) thus offering more resistance to the fluid flow away from the cartilage. However, this would have had a little impact on the predictions of the current study as the contact areas in all the cases were located away from the labrum.

The measured contact areas using Fuji film were close to FE predictions with maximum difference of 20.69%. In an exhaustive validation study of subject-specific

human hip joint by Anderson and colleagues, the corresponding maximum percentage difference was ~40% for walking (Anderson *et al.*, 2008). The contact areas tended to be overestimated by FE models, which was exactly opposite to the predictions of the study by Anderson and colleagues. In the current study, the bi-centric contact pattern seen in FE prediction of specimen 'pc140509_74_7kg' was not seen in the experimental measurement.

Peak contact stresses predicted by FE models were close to those measured experimentally. The maximum difference between experimentally measured peak contact stresses and those predicted by the FE model was 12.42%. In the study by Anderson and colleagues, the maximum difference in average experimental and FE predicted contact stresses was ~29% for descending stairs (Anderson *et al.*, 2008). Their study could not measure absolute peak pressure as the pressure films used in their study could register contact pressures of up to only 10 MPa. In the present study, however, the contact stresses as high as 14.09 MPa were measured. Contact stresses were mostly underestimated in the current study and were concentrated in one area as the cartilage was non-spherical with localised undulations in contact with a perfectly spherical prosthetic femoral head. This caused only a small area to be in contact.

The relative humidity made a huge difference in the experimental contact stress values. The values reported in the **Table 4-7** were derived using a relative humidity of 20.04% which was averaged over the duration of all the tests. For example, at this value of relative humidity the peak contact stresses were measured to be 8.54 MPa for specimen 'pc140509_71_5kg' for a colour intensity value read using the Spectrodensitometer. For the same colour intensity value, the stress values would have been 6.49 MPa and 4.58 MPa for relative humidity of 50% and 90% respectively. Thus, it is important to keep a record of relative humidity in all the experiments involving Fuji film.

Total fluid load support was high in all the three cases but did not reach the 90% level. The major reason for this was that the acetabular cartilage not being spherical and articulating with the spherical prosthetic head resulted in variable clearance. This caused the contact area to be localised to a small area. The larger non-contacting area thus offered unrestricted fluid exudation as the acetabular cup was loaded. This reduced the total fluid load support. In spherical contacting surfaces the fluid load support would rise to around 90% due to increasing congruence as has been previously showed (Ateshian and Wang, 1995; Kelkar and Ateshian, 1995; Ateshian, 1997). The current study also supported this observation and will be dealt with in **Chapter 5** of this thesis. It will also be highlighted that the decrease in clearance between contacting surfaces will increase the fluid load

support as well as decrease the contact stresses. The reduction in contact stresses with the increasing conformity was also observed in experiments carried out *in vitro* (McCann *et al.*, 2009).

Studies of this nature are not without limitations and the errors from several sources may affect the final predictions. Though the results of the current study showed good agreement between the experimental and FE models, these should be treated with caution. Several flaws (apart from those mentioned earlier) have been identified which could adversely dictate the outcomes of such studies. They include but are not limited to the following:

- 1) Only one experiment per acetabular cup was performed. It would have been ideal to conduct a series of experiments on each cup and then use the average of parameters.
- 2) After μ CT, tissue characteristics might change (the bone colour changed from pinkish white to blackish). Though the cartilage was kept hydrated during scanning, this needs to be further analysed as CT generates a lot of heat.
- 3) Cementing (using PMMA) is an exothermic process and it also has the potential to damage the tissue.
- 4) No distinct points were physically marked on the acetabular cup for fixing the cup coordinate system. The points, whose coordinates were measured using CMM, were arbitrarily chosen by visual inspection. These measurements were then used to spatially orient the cup. This method was very subjective and likely introduced error. Methods such as using registration blocks (Fischer *et al.*, 2001)) can be used in the future to positively define a fixed coordinate system for the cup at the beginning of the process.
- 5) Segmentation is inherently an approximate method. Moreover, with μ CT it was not possible to differentiate between cartilage and other tissues (e.g. part of ligamentum teres still attached to the fossa). Hence, separating or removing them had to be done manually. Smoothing would also lose some surface details. Moreover, the tidemark was not very clear in porcine acetabular cups (unlike in bovine) and had to be approximated based on visual inspection. Alternative imaging techniques such as MRI needs to be evaluated to improve segmentation process.

- 6) Objective protocol needs to be developed for the measurement of contact areas on Fuji film as the areas with pressures smaller than the lower film specification values cannot be properly demarcated.
- 7) Bone was modelled as cortical only with human material properties. It has been shown recently that modelling the bone as rigid and altering its properties affects the FE predictions of contact stress and area but is dependent on loading conditions (Anderson *et al.*, 2008). This also needs to be investigated further.
- 8) Material properties were derived using indentation and using least-squared error curve fitting. The equilibrium elastic modulus derived using different methods will give different results. The indentation method usually gives higher value when compared with confined and unconfined compression (Korhonen *et al.*, 2002). Thus the cartilage will be stiffer giving lower deformation.

In spite of the several limitations listed here, good agreement in the experimental measurements and FE predictions of contact stresses and contact areas, as well as their location was found in the current study. The exceptionally positive outcome from this study was an encouraging indication about the correctness and usefulness of the FE methodology of hemiarthroplasty of the hip joint developed here. The new methodology of modelling acetabular cartilage as a biphasic material can thus be used for further studies involving hemiarthroplasty. This method will not only help in understanding the load distribution in the acetabular cup by means of contact stress distribution and contact area locations but also in comprehending the biphasic lubrication phenomenon by predicting total fluid load support. This in turn will help in understanding the frictional characteristics of the cartilage. This may also aid in uncovering the mysteries of OA, in developing new biomaterials for substitution and new designs for implants.

Chapter 5 Human Hip Joint with Hemiarthroplasty: Effect of Clearance on Fluid Load Support

5.1 Introduction

Hemiarthroplasty is a conservative alternative to total hip replacement to alleviate joint complications as seen in **Section 1.7.3**. Increasing numbers of patients are receiving hip joint hemiarthroplasty compared to total hip arthroplasty (Jain *et al.*, 2008). However, complications such as cartilage erosion (D'Arcy and Devas, 1976; Devas and Hinves, 1983; Dalldorf *et al.*, 1995) and protrusion (Whittaker *et al.*, 1972; Soreide *et al.*, 1982; Kofoed and Kofod, 1983) may develop. The additional risks of modular component dislocation (Georgiou *et al.*, 2006; Guo *et al.*, 2008; Lee *et al.*, 2008), osteolysis due to polyethylene wear debris (Bose *et al.*, 1995; Coleman *et al.*, 2001; Rizzo and Pace, 2003) and metallosis as seen in total hip arthroplasty (Matsuda and Yamamuro, 1994) can also adversely affect bipolar hemiarthroplasties.

Erosion due to the metallic femoral head bearing surface interacting with the natural cartilage and due to repetitive stresses (McGibbon *et al.*, 1999), leads to severe pain (Dalldorf *et al.*, 1995) as it results in the prosthesis contacting with the bone. The importance of acetabular fit, to maintain the structural integrity and functionality of the cartilage, has long been recognised in the clinical performance of hemiarthroplasty (Yamagata *et al.*, 1987). A smaller prosthetic head size leads to reduced conformity and contact area resulting in increased stresses leading to cartilage erosion and pain, and potentially, migration of the implant (Harris *et al.*, 1975; Kosashvili *et al.*, 2008). Oversized heads, however, also tend to increase the periacetabular stresses and stresses towards the medial side (Finlay *et al.*, 1986). Thus the selection of the correct femoral head size for congruent acetabular fit is an important parameter to be considered when hemiarthroplasty is the chosen intervention (Yamagata *et al.*, 1987; Jeffery and Ong, 2000). The importance of conformity in minimising contact stresses and degradation of the cartilage has also been shown in *in vitro* studies (McCann *et al.*, 2008).

The biphasic nature of the cartilage also affects contact mechanics of the hip joint. Friction is reduced due to load partitioning (Mow and Lai, 1980) with the fluid phase taking a larger percentage of the load, thus protecting the cartilage. Macirowski and colleagues carried out hemiarthroplasty experiment using instrumented endoprosthesis and applied experimentally measured surface

stresses to biphasic acetabular cartilage surface in their three-dimensional biphasic FE model of acetabular cartilage (Macirowski *et al.*, 1994). They found high fluid load support of more than 90%. However, there have been no three-dimensional FE studies of the whole joint investigating the relationship between fluid load support in cartilage and contact mechanics in hemiarthroplasty. This has not been possible, since there are few three-dimensional finite element (FE) models of the hip joint and the cartilage in these models has largely been modelled either as an elastic or hyperelastic material (Bachtar *et al.*, 2006; Cilingir *et al.*, 2007; Kim *et al.*, 2007; Anderson *et al.*, 2008; Anderson *et al.*, 2010). Moreover, biphasic cartilage requires contact dependent surface fluid flow boundary conditions to be implemented as discussed in **Chapter 2**.

The aim of this study was to model hemiarthroplasty in the hip joint with poro-hyperelastic acetabular cartilage in order to understand the role of fluid load support in the contact mechanics of the joint and the degree to which clearance influences these parameters.

5.2 Model and Methods

The pelvis and acetabular cartilage models were similar to that described in **Chapter 3 (Figure 5.1)**. Radial clearances of 0.0 mm, 0.5 mm, 1.0 mm and 2.0 mm with acetabular cup were simulated using a spherical metallic prosthetic femoral head of radius 28.0 mm, 27.5 mm, 27 mm and 26 mm respectively. The centre of the spherical ball and that of the acetabular cartilage were at the centre of the coordinate system.

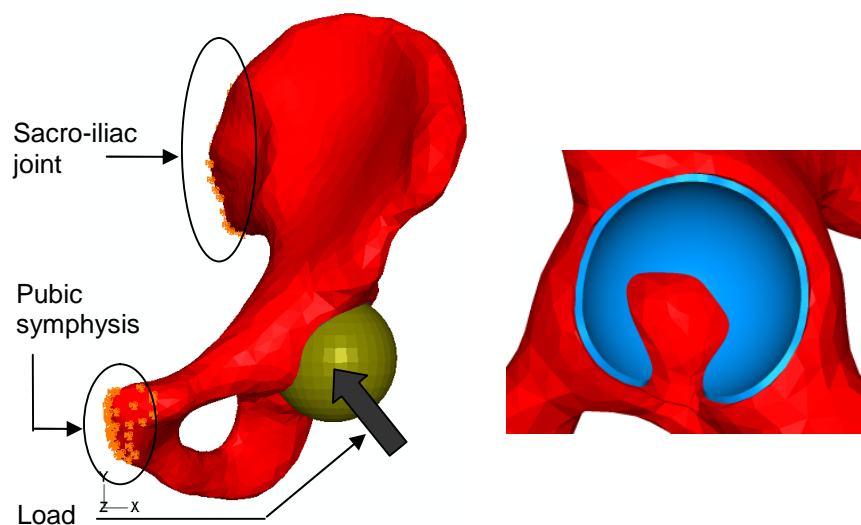


Figure 5.1 FE model of hip hemiarthroplasty

The type and number of elements used for the pelvis were similar to those used for the natural hip model (**Section 3.2**). However, the number of elements used for acetabular cartilage was different and is given in **Table 5-1** along with their types. There were a minimum of three elements through the cartilage thickness (Anderson *et al.*, 2008). The number of eight-node linear brick elements (C3D8) used for the prosthetic head was 2304 for the first three clearances. The corresponding number of elements was 1872 for 2.0 mm radial clearance.

Table 5-1 Elements used in Hemiarthroplasty Model

Component	Element	
	Type	Number
Acetabular Cartilage	C3D8RP	14772
Prosthetic Head	C3D6	432
	C3D8	2304/1872

The metallic prosthetic head, being stiffer than the acetabular cartilage, was made the master surface, while the acetabular surface was the slave. The mesh could be coarser for the metallic prosthetic femoral head due to strict master-slave algorithm which prevents slave node penetration into the master (ABAQUS., 2007). Mesh sensitivity analysis was carried out independently for all the four clearances to ensure that the difference in the predictions between consecutive meshes was less than 5%.

The material properties used for the pelvis and acetabular cartilage were similar to those mentioned in **Section 3.2**. The prosthetic head was assumed to be made of CoCr with an elastic modulus of 220 GPa and Poisson's ratio of 0.3 (Liu *et al.*, 2005).

The boundary conditions on pelvis and acetabular cartilage were exactly the same as those imposed in natural hip joint (**Section 3.2**). The fluid flow on the cartilage surface which interacted with the prosthetic head was based on the developing contact and was imposed using a contact dependent fluid flow algorithm described in **Chapter 2**. The contact was frictionless. UTOL and other controls were relaxed as described in **Section 4.2.2.3**.

In the first two steps, the femoral prosthetic head was brought in contact with the acetabular cartilage for all the non-zero clearance models. For 0.5 mm radial clearance, the head was moved in the x-direction (**Figure 5.1**) by -0.36 mm and was constrained in other two directions. It was then moved in the y-direction by

0.36 mm while constraining it in the x- and z-directions. The corresponding displacements for 1.0 mm radial clearance were -0.71 mm and 0.71 mm whereas in case of 2.0 mm radial clearance, the head was moved by -1.42 mm in the x-direction and 1.42 mm in the y-direction.

A physiological resultant load of approximately 1935 N (Bergmann *et al.*, 2001) was then applied at the centre of the head, as shown in **Figure 5.1**, in 3 seconds which was approximately half the typical time taken by subjects during standing on 2-1-2 legs (Bergmann, 2001). The load was applied in three steps of 1 second each for every direction. In the first step, a load of approximately 241 N was applied in the negative x-direction by constraining it in the other two directions. This load was maintained in the second step. In this step, the constraint in the y-direction was removed and simultaneously a load of approximately 1916 N was applied in that direction. In the third step, the remaining constraint was removed and the two loads already applied were maintained. The third load of approximately 117 N was then applied in the z-direction.

The loads were held constant for another 600 seconds to allow for consolidation to take place. The load vector was rotated in such a way that it accounted for pelvic orientation for that load (Bergmann, 2001). Total fluid load support, peak contact stresses, peak fluid pressure and contact area were recorded throughout the simulation.

5.3 Results

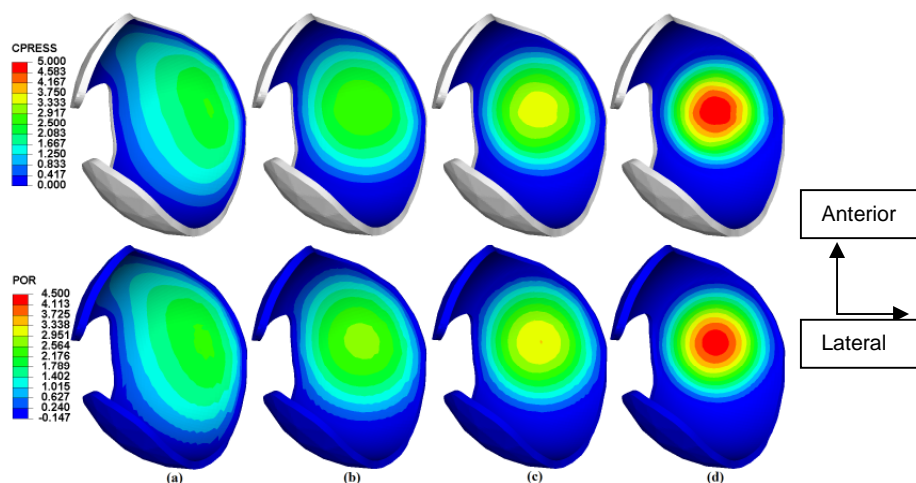


Figure 5.2 Contour plots of contact stresses and fluid pressure (MPa) after 3 seconds of loading for radial clearance of (a) 0.0 (b) 0.5, (c) 1.0 and (d) 2.0 mm

There was an increase in the peak contact stresses on the surface and fluid pressure with an increase in clearance (**Figure 5.2**). Peak contact stresses were 2.52 MPa, 2.88 MPa, 3.62 MPa and 4.95 MPa for the four clearances with the corresponding peak fluid pressure of 2.23MPa, 2.69 MPa, 3.32 MPa and 4.35 MPa. These contact stresses and fluid pressure were located in the superior dome of the acetabulum with antero-posterior distribution corresponding to the direction of loading.

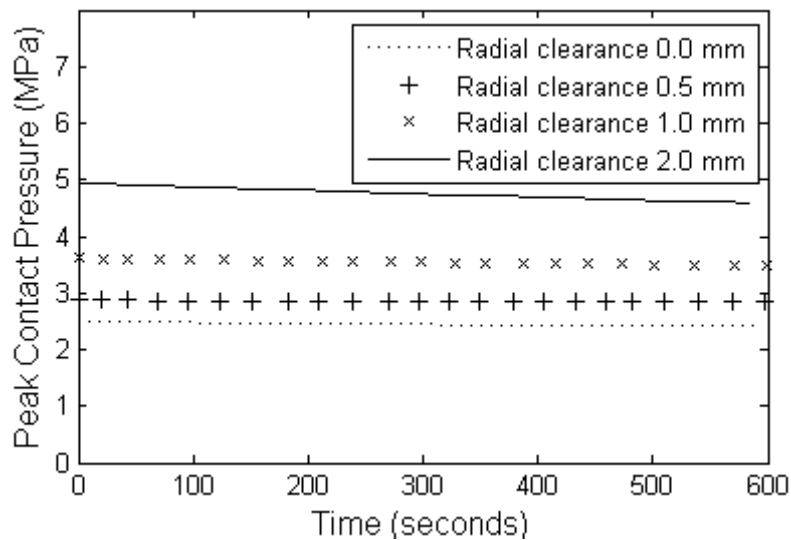


Figure 5.3 Variation of peak contact pressure with time for different radial clearances

Reductions in maximum contact stress (**Figure 5.3**) and maximum fluid pressure (**Figure 5.4**), were small even after 600 seconds. For example, reductions of 7.39% and 6.55% were observed in contact and fluid pressures respectively for 2.0 mm radial clearance. However, recently, in two-dimensional plane strain hemiarthroplasty model of human glenohumeral joint, fluid load support was shown to decrease to zero within 2000 seconds whereas there was no decrease in case of natural joint (Rajan *et al.*, 2010). No such observation was made in the current hemiarthroplasty study which was probably due to highly congruent nature of hip joint and different FE formulations in these studies (Ateshian, 2010; Rajan *et al.*, 2010).

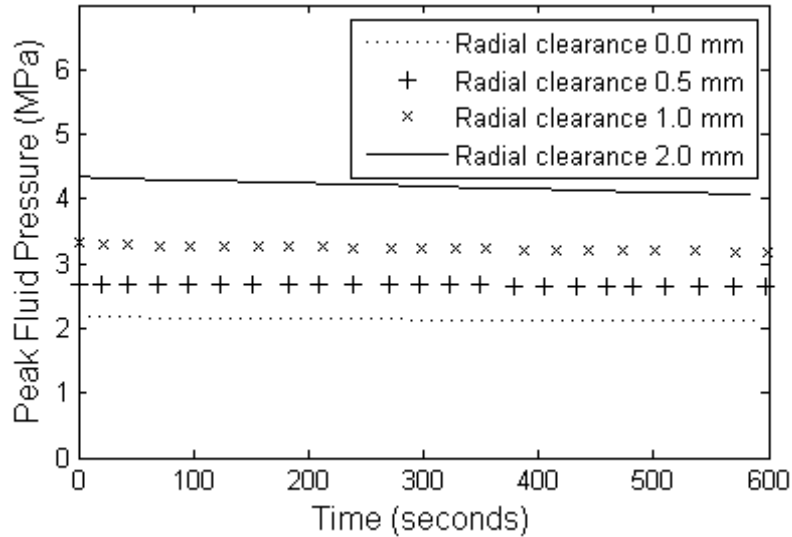


Figure 5.4 Variation of peak fluid pressure with time for different radial clearances

The contact area decreased as the clearance increased as shown in **Figure 5.2**. The change in contact area with the consolidation was not considerable over a period of 600 seconds. For 2.0 mm radial clearance, the contact area increased by merely 1.42%.

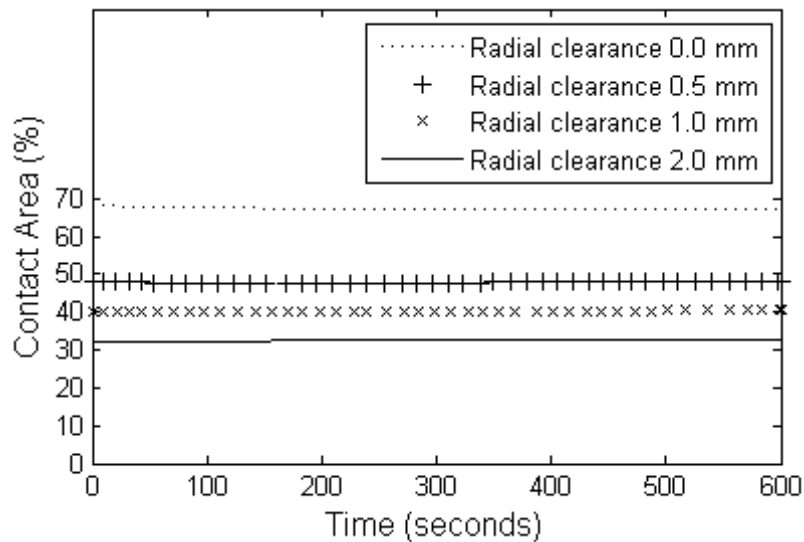


Figure 5.5 Variation of percentage contact area with time for different radial clearances

The percentage contact area was calculated based on the total surface area of cartilage available for articulating with the prosthetic head. As shown in

Figure 5.5, the percentage contact area remained almost unchanged with respect to time but decreased with increasing clearance. The percentage contact area after the load was applied, was found to be 68.17%, 47.89%, 40.20% and 32.37% for the four increasing clearances that were investigated.

The total fluid load support soon after load application was found to be 90.99%, 90.36% and 88.76% with 0.5 mm, 1.0 mm and 2.0 mm clearances respectively. The reduction in fluid load support after 600 seconds was minimal (**Figure 5.6**). In the case of the largest radial clearance of 2.0 mm, it reduced by only 0.72%. The total fluid load support was 89.94% in case of radial clearance of 0.0 mm, which was lower than fluid load support for 0.5 and 1.0 mm clearance.

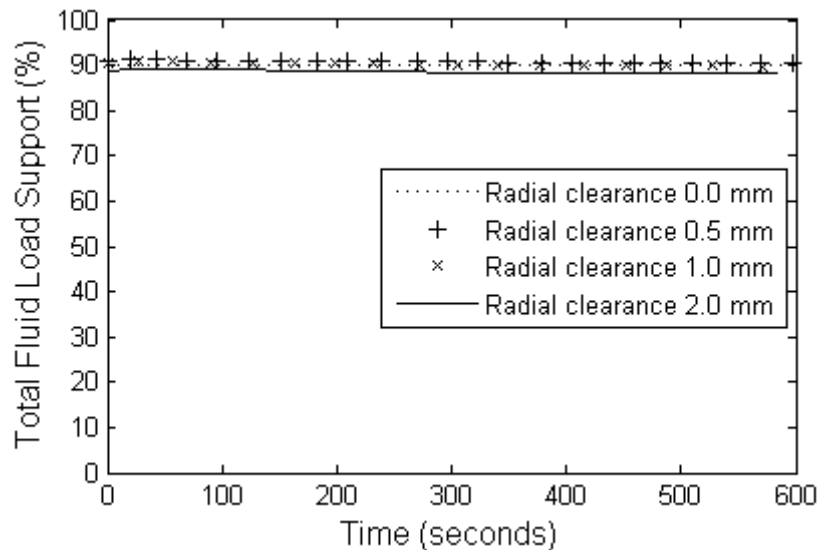


Figure 5.6 Variation of total fluid load support with time for different radial clearances

5.4 Discussion

It was observed that with an increase in clearance, the maximum contact stresses increased. This was due to the decrease in the conformity and the decrease in contact area as the clearance increased and has been shown in *in vitro* studies (Rushfeldt *et al.*, 1981b; McCann *et al.*, 2009). Shear stresses increase as a result of either an increase in contact stresses or coefficient of friction. Thus the shear stresses would increase with increasing clearance. The contact stresses observed here were physiological in nature and were comparable to those reported in numerical studies (2.87 – 9.36 MPa for different activities) (Yoshida *et al.*, 2006) as well as in *in vitro* (3.45 MPa for static loading) (Brown and Shaw, 1982) and *in vivo* (≤ 6.5 MPa for walking) (McGibbon *et al.*, 1999) experimental studies. The

predictions of the current study were also comparable to those reported in axisymmetric resurfacing hemiarthroplasty model (Cilingir *et al.*, 2008). They observed the peak contact stress of 3.75 MPa and the peak fluid pressure of 3.5 MPa for the load of 2500 N, radial clearance of 0.5 mm and acetabular cartilage thickness of 2 mm.

The total fluid load support observed with three clearances of 0.5 mm, 1.0 mm and 2.0 mm was high with decreasing values as the clearance increased. The decreasing percentage load supported by the fluid would proportionately increase the frictional coefficient leading to an increase in frictional shear stresses. The linear correlation between the total fluid load support and coefficient of friction has been shown experimentally by Krishnan and colleagues (Krishnan *et al.*, 2004).

The decrease in total fluid load support with increasing clearance was, however, too small to have an effect on the contact mechanics of the joint in the current study. Nevertheless, it should be noted that the radial clearances investigated in the current study were small (≤ 2 mm). Moreover, if the effects of variable clearance were to be considered using subject-specific models which are generally non-spherical, the larger local clearances would cause more fluid exudation as the non-contacting area available for outward flow of fluid would be increased. This was seen in experimental validation of hemiarthroplasty using an anatomical porcine acetabular cup (**Chapter 4**). As seen in **Table 4-7**, the total fluid load support was around 80% in that case. It should be noted, however, that a fixed load was applied in the current study and was representative of standing. The loads in other routine activities such as walking are much more complex and dynamic in nature. This may in turn allow fluid to be imbibed back into the cartilage due to migrating contact, resulting in sustained fluid load support (Katta *et al.*, 2009). Diffusive velocity of the interstitial fluid is very low ($\sim 10^{-4} - 10^{-6}$ mm/s). If the migrating contact moves faster than this velocity, it may be possible to maintain higher fluid pressurisation over longer time duration (Caligaris and Ateshian, 2008; Ateshian, 2009). It should also be noted that the application of the load in three steps did not make a difference to the predictions when compared to the formulation in which the load was applied in a single step.

The increase in frictional shear stresses due to the increase in frictional coefficient, coupled with the increase in the contact stresses has the potential of inducing cartilage fibrillation leading to its erosion as has been observed in different studies (Harris *et al.*, 1975; Yamagata *et al.*, 1987; Kosashvili *et al.*, 2008). The increased local loading due to decreased contact areas at larger clearances may also induce acetabular protrusion (Binns, 1989; van der Meulen *et al.*, 2002). In diseased cartilage such as osteoarthritis this is even more crucial as the increased

local contact and shear stresses will further aid in breaking down the structural integrity of the cartilage. As in the case of dysplasia of the natural joint (Mavcic *et al.*, 2002), the misalignment of the hemiarthroplasty joint may also lead to the degeneration of the cartilage due to increased level of stresses. The outcomes of the current study indicated that this could be especially severe in the case of higher clearances. This confirmed the previous findings of the importance of choosing the correct size of head for hemiarthroplasty (Harris *et al.*, 1975; Finlay *et al.*, 1986; Yamagata *et al.*, 1987; Jeffery and Ong, 2000; Kosashvili *et al.*, 2008). The undersizing of the head increases the stresses (Harris *et al.*, 1975; Rushfeldt *et al.*, 1981b).

It should be noted that the total fluid load support for 0.00 mm clearance was lower than those of 0.5 mm and 1.0 mm clearance as the contact area moved towards the lateral edge of the cartilage. The absence of the acetabular labrum which has lower permeability than the cartilage (Ferguson *et al.*, 2000a) coupled with the free fluid flow boundary conditions at the outer edge caused more fluid to flow out, thus decreasing the fluid load support. Thus the location of load bearing area is an important factor that needs to be considered in investigating fluid load support along with the acetabular fit, particularly when different activities are considered.

The acetabulum is usually thought to be spherical (Rushfeldt *et al.*, 1981a), however, it has been shown in recent years that it can be better approximated by conchoid (Menschik, 1997) or rotational ellipsoid (Gu *et al.*, 2008). These latter shapes will introduce variable clearances with a spherical prosthetic head used in hemiarthroplasty. However, the actual subject-specific acetabulum is much more complex in shape and can hardly be confined to regular shapes in order to conduct realistic studies of contact mechanics. The contact stresses are generally higher in subject-specific models (Anderson *et al.*, 2008) and this has been observed in some *in vivo* studies (Hodge *et al.*, 1986; Hodge *et al.*, 1989). Nevertheless, the approximation of the acetabulum by regular shapes is helpful in reducing the complexity of the problem and hence, in the current study, the acetabulum was assumed to be spherical. In future studies, more relevant non-spherical cartilage surfaces and non-uniform thickness should be modelled. This would provide better predictions since non-sphericity is likely to increase the local clearance and potentially increase both frictional shear and contact stresses. Daily activities such as walking, climbing stairs, etc. also need to be simulated in order to better understand *in vivo* joint contact mechanics vis-à-vis fluid load support.

The non-inclusion of strain-dependent permeability may seem like a limitation of this study. However, as discussed in **Section 6.4**, this does not change the

predictions substantially and therefore not included in this investigation.

In conclusion, the current study indicated increasing contact stresses and a slight decrease in total fluid load support with increasing clearance. This was due to the decreasing conformity and contact area. The consequential increase in shear stresses together with contact stresses has the potential to induce cartilage surface fibrillation. The local cartilage loading may also cause acetabular protrusion.

Chapter 6 Applications of Hemiarthroplasty Model - Gait Analysis

6.1 Introduction

A person undergoes a series of activities including walking, climbing stairs, rising from a chair in the course of a day. The joints of the lower extremities have to bear not only the weight of the body but also the forces that are generated due to muscles and their moments. Though the articular cartilage can withstand extreme loads and motions, mechanical factors such as excessive contact stresses may cause structural as well as biochemical changes in articular cartilage (Radin *et al.*, 1978; Muehleman and Arsenis, 1995; Aigner and McKenna, 2002).

Loss of cartilage in the hip joint may lead to total hip joint replacement to alleviate pain and improve quality of life. When only the femoral head is affected, hemiarthroplasty is an option. To understand the potential effect of hemiarthroplasty on the acetabular cartilage and improve prosthetic design, it is important to investigate the conditions under which the joint operates during different activities of daily living.

None of the three-dimensional FE/numerical studies, to the best of author's knowledge, have considered the biphasic nature of the cartilage and hence, those studies are not able to account for interstitial fluid pressurization and its influence on tribology and the contact mechanics of the articular cartilage within the joint. Hemiarthroplasty may alter the biphasic fluid load support. The aims of this study were to investigate the hip joint with a hemiarthroplasty during several activities of daily living in order to understand the tribology and contact mechanics of the biphasic cartilage under varying and complex conditions.

6.2 Models and Methods

The model used in this study was similar to the one described in **Section 5.2**. The acetabular cartilage was of uniform thickness of 2 mm. The acetabular cartilage was approximately divided into four regions as shown in **Figure 6.1**. Superior dome was made of middle region comprising a part of lateral roof and a part of medial roof. Cortical, cancellous and subchondral bones in the pelvis were all modelled. The femoral prosthetic head was assumed to be made of CoCr. The material properties of the pelvis and acetabular cartilage were as mentioned in

Section 3.2. The acetabular cartilage was tied to the acetabular cavity. The boundary conditions on the pelvis and acetabular cartilage were similar to those described in **Section 3.2**. The radial clearance between acetabular cartilage and prosthetic head was 0.5 mm.

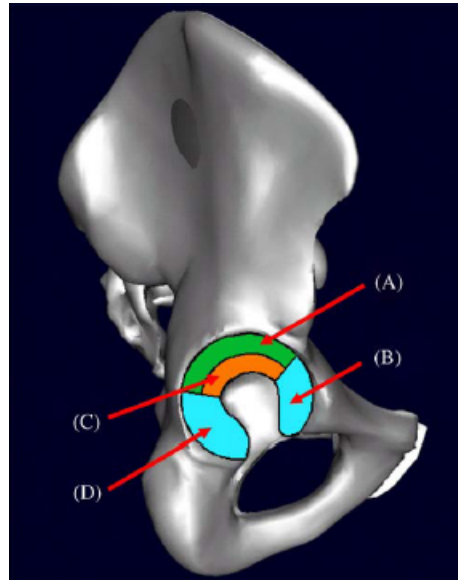


Figure 6.1 Anatomic regions of acetabular cartilage (A) Lateral roof, (B) anterior horn, (C) medial roof, (D) posterior horn (Yoshida *et al.*, 2006)

Table 6-1 List of activities with their start and end (Bergmann *et al.*, 2001)

Activity	Start At	End At	Cycle Time (Sec)
Slow walk (0.98 m/s)	Heel strike	Ipsilateral heel strike	1.248
Normal walk (1.09 m/s)	Heel strike	Ipsilateral heel strike	1.103
Fast Walk (1.46 m/s)	Heel strike	Ipsilateral heel strike	0.953
Stand Up (chair height – 500 mm)	Beginning of getting up	Standing position	2.489
Sit Down (chair height – 500 mm)	Standing position	Sitting in a relaxed position	3.719
Down Stairs (stair height – 170 mm)	Toe off	Ipsilateral toe off	1.439
Up Stairs (stair height – 170 mm)	Heel strike	Ipsilateral heel strike	1.593
Knee Bend	Standing position	Standing position	4.665
Stand 2-1-2 Leg	Two legged stance	Two legged stance	6.703

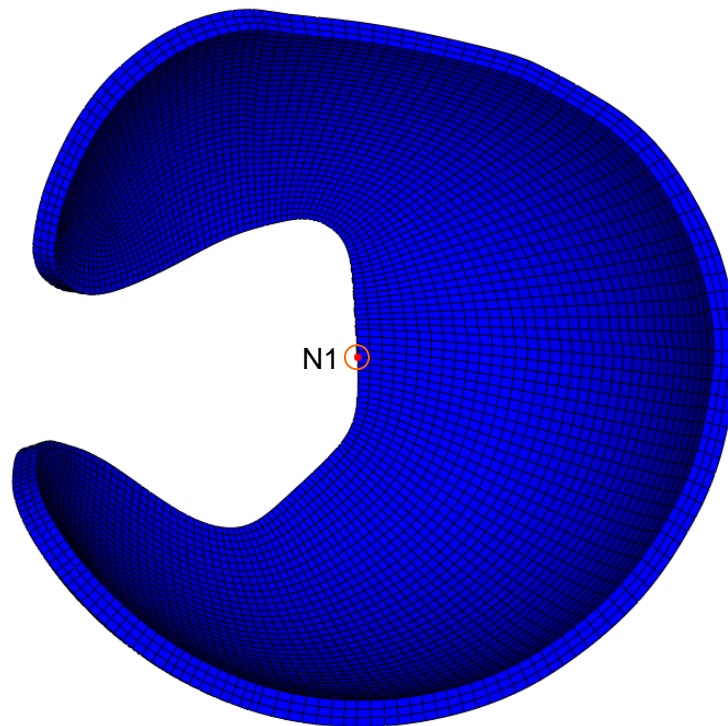


Figure 6.2 Node N1 at which fluid velocity was monitored during first cycle of slow, normal and fast walking

As was done in the clearance model described in **Section 5.2**, in the first two steps, the femoral prosthetic head was brought in contact with the acetabular cartilage. The head was first moved in the x-direction (**Figure 5.1**) by -0.36 mm while constraining it in the other two directions. In the second step, displacement of 0.36 mm was prescribed on the head in the y-direction and was constrained in the x- and z-directions.

One cycle each of the nine activities of daily living as shown in **Table 6-1** and **Figure 6.3** was simulated with their respective load vectors (Bergmann *et al.*, 2001). A longer time duration of five cycles was analysed only for normal walking. Femoral rotation was already accounted for in these load vectors. The hip joint contact force data used in this study also accounted for muscle forces (Bergmann, 2001; Bergmann *et al.*, 2001). The pelvis rotates about both the transverse axes during activities (Bergmann *et al.*, 2001). However, in the FE model, the pelvis was fixed. The load vectors were rotated to take into account this pelvic orientation. The loads were applied at the centre of the head, as shown in **Figure 5.1**. Each cycle of an activity was divided into 201 steps (Bergmann, 2001). A load vector corresponding to each step was applied in a single ABAQUS step. The load vector in the first step was applied in 1 second whereas remaining vectors were applied

within time durations specified in the gait analysis data (Bergmann, 2001). The head was not constrained in any direction when the load was applied and the initial contact between the acetabular cartilage and femoral head prevented any rigid motion of the head. The entire analysis was quasi-static with different load vectors being applied one after the other in each step without changing any of the boundary conditions. The predictions of total fluid load support, peak contact stresses, peak fluid pressure and contact area were monitored throughout the simulation. The fluid velocity at node N1 (**Figure 6.2**) on the edge of the acetabular cartilage was monitored for slow, normal and fast walking.

Another set of models, representing all the activities were analysed using non-linear void dependent permeability. This was calculated using **Equation (2.5)** (Holmes, 1986; Wu and Herzog, 2000). Material parameters, M and κ used in this equation are given in **Table 2-2**. Initial permeability and initial void ratio (water content) were constant permeability and void ratio values respectively, that were used in the models without void-dependent permeability.

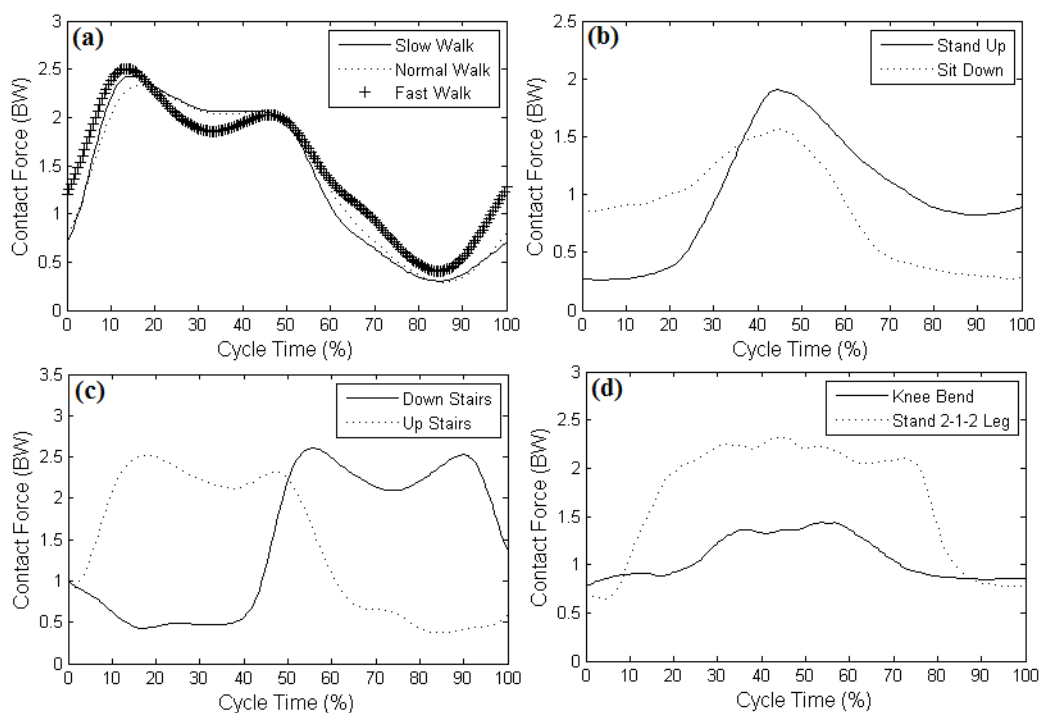


Figure 6.3 Hip joint contact forces during different activities of daily living (Bergmann, 2001)

6.3 Results

The variation of peak contact pressure on the acetabular cartilage surface for one cycle of slow, normal and fast walking is depicted in **Figure 6.4a**. In the case of normal walking, the maximum peak contact pressure of 2.78 MPa was found in the superior dome of the acetabulum at 15.5% of the cycle (**Figure 6.4a** and **Table 6-2**). The pressure distribution was in the antero-posterior direction but slightly towards the posterior side similar to that observed at 15% and 20% cycle time (**Figure 6.6**). The corresponding contact area was 52.00% of the total potential contact area and total fluid load support was 91.21%. The maximum fluid pressure at this instant was 2.59 MPa.

Table 6-2 Maximum peak contact pressure with corresponding peak fluid pressure, contact area and total fluid load support (TFLS) for different activities and where and when they occurred

Activity	Peak Contact Pressure (MPa)	Peak Fluid Pressure (MPa)	Where	Contact Area (%)	TFLS (%)	Cycle time (%)
Slow walk	2.97	2.77	Superior dome	49.64	90.11	16.5
Normal walk	2.78	2.59	Superior dome	52.00	91.21	15.5
Fast Walk	2.99	2.77	Superior dome	53.10	90.95	12.5
Stand Up	2.98	2.53	Posterior horn	55.13	84.10	44.5
Sit Down	2.57	2.19	Posterior horn	49.88	85.39	45.0
Down Stairs	4.63	3.85	Lateral roof	38.88	81.80	88.0
Up Stairs	3.00	2.77	Superior dome	53.79	91.07	16.0
Knee Bend	2.42	2.10	Medial roof nearer posterior side	46.77	86.99	53.5
Stand 2-1-2 Leg	4.40	3.71	Lateral roof	40.43	83.42	46.0

Table 6-3 Average total fluid load support (TFLS) for different activities

Activity	Average TFLS (%)
Slow walk	89.28
Normal walk	90.96
Fast Walk	90.08
Stand Up	87.74
Sit Down	87.18
Down Stairs	88.45
Up Stairs	89.82
Knee Bend	88.97
Stand 2-1-2 Leg	88.23

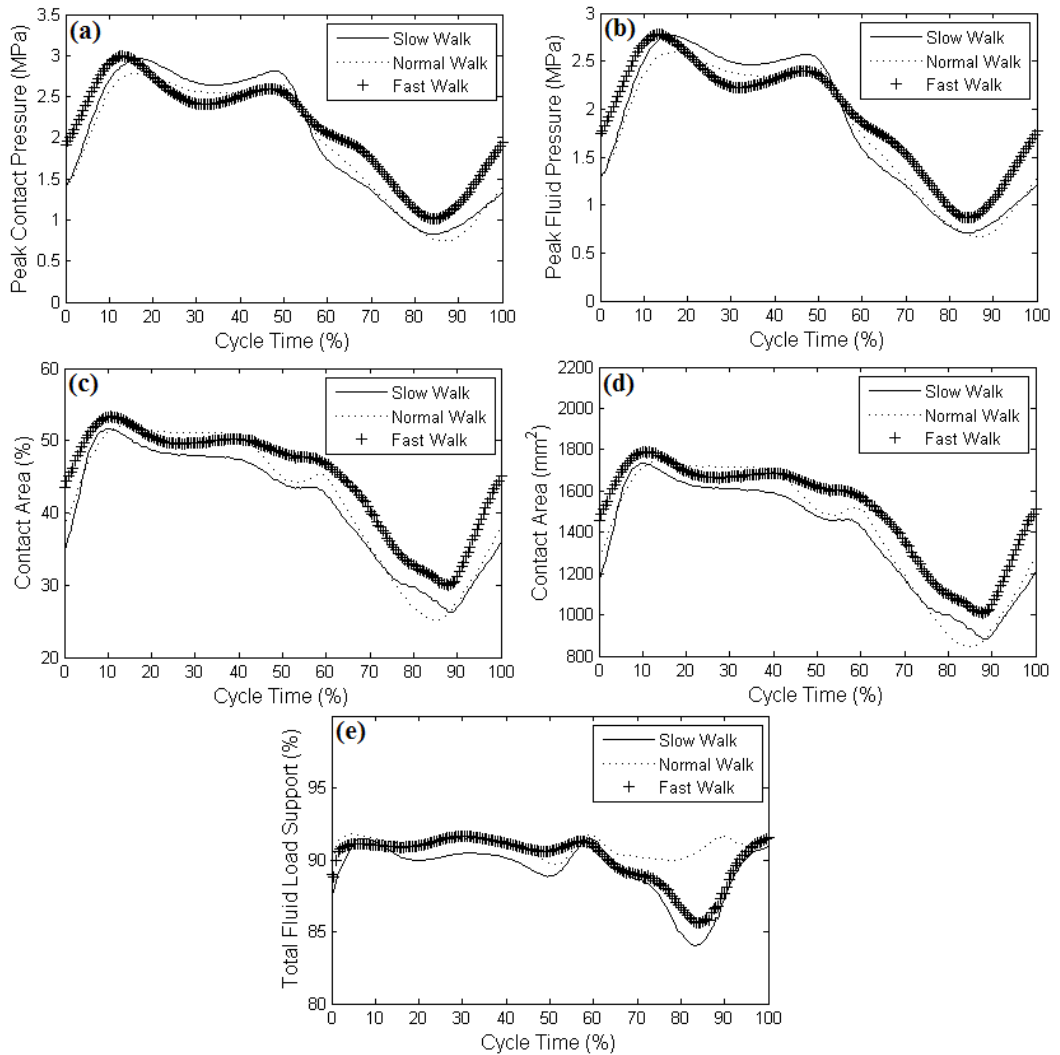


Figure 6.4 (a) Peak contact pressure, (b) peak fluid pressure, (c), (d) acetabular contact area and (e) total fluid load support during first cycle of slow, normal and fast walking

The variation of peak contact pressure, peak fluid pressure and the contact area with respect to time was similar to that of contact force for all three walking speeds (**Figure 6.4a**, **Figure 6.4b**, **Figure 6.4c** and **Figure 6.4d**). The variation of total fluid load support in general seemed to follow contact force variation for slow and fast walking whereas it deviated towards the last 35% of the cycle in the case of normal walking (**Figure 6.4e**). However, it always remained high and on an average it was found to be 89.28%, 90.96% and 90.08% for slow, normal and fast walking respectively (**Table 6-3**). The total fluid load support decreased only slightly (0.17%) over five cycles of normal walking (**Figure 6.5**).

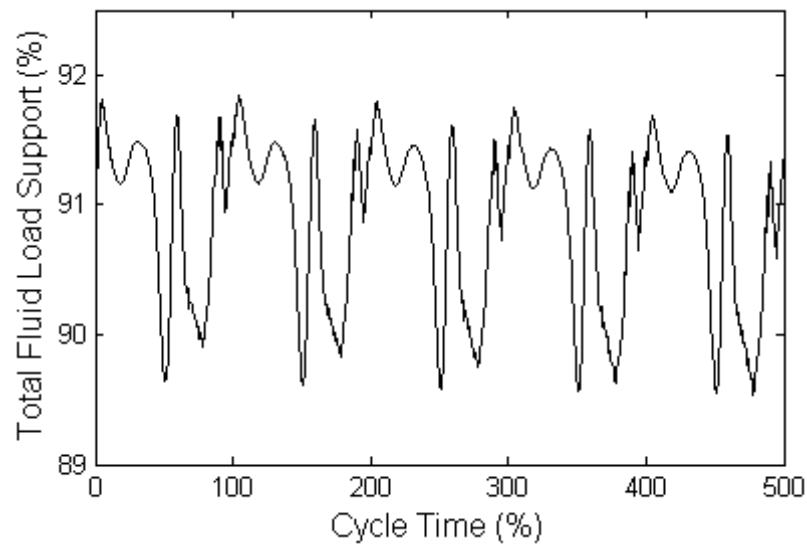


Figure 6.5 Total fluid load support for five normal walking cycles

The contours of the contact pressure at different stages of one normal walking cycle for the first cycle are shown in **Figure 6.6**. It can be seen that throughout the stance phase when the load was high the contact was mostly maintained in the superior dome of the acetabulum. It then started moving towards the medial roof during the swing phase. It moved more medially in cases of slow and fast walking compared to normal walking (**Figure 6.7**). The fluid velocity at node N1 for normal walking was lower than those for slow and fast walking after around 70% of walking cycle (**Figure 6.8**).

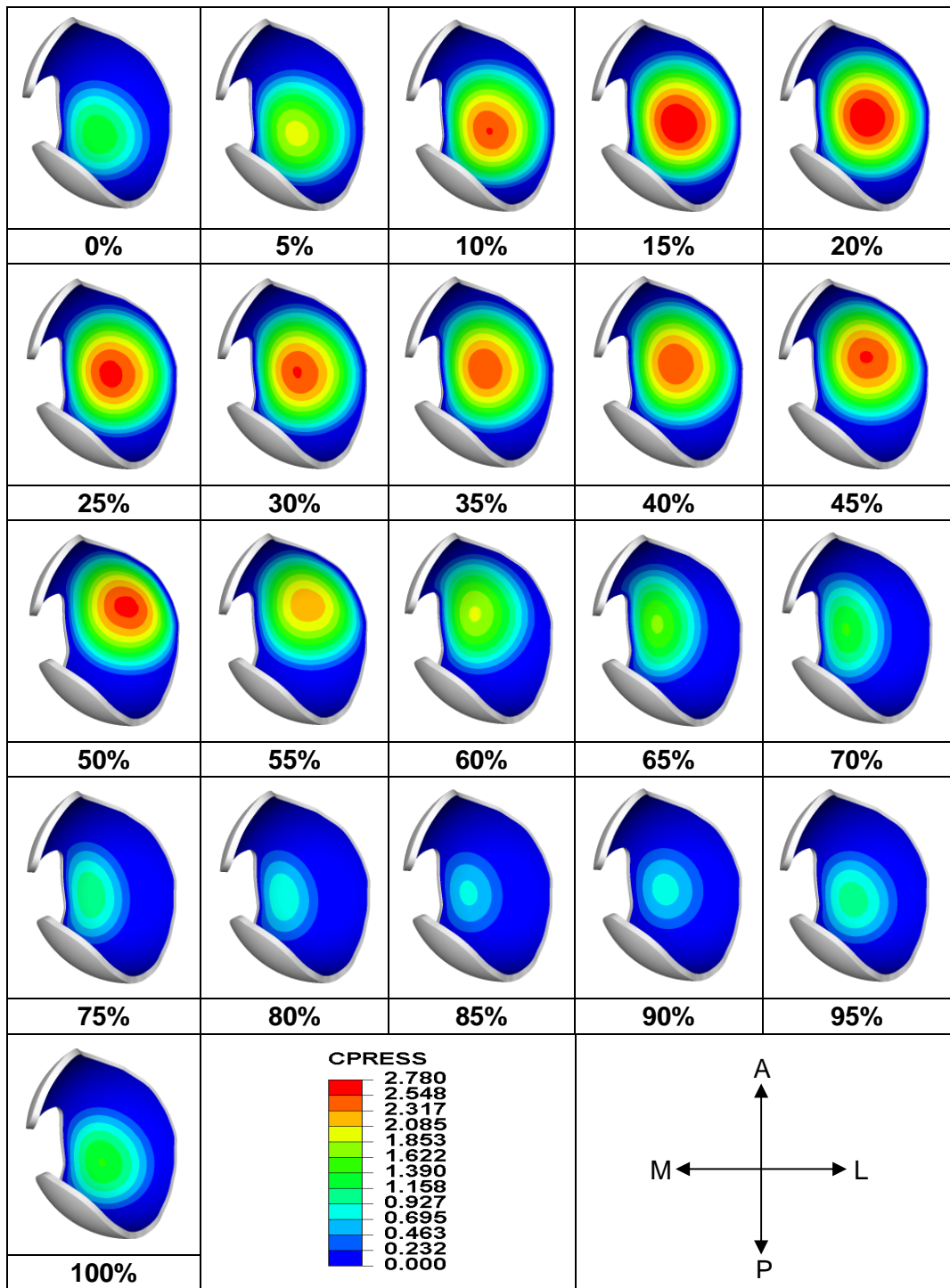


Figure 6.6 Contours of contact stresses (MPa) in acetabular cup during different phases of first cycle of normal walking (A – Anterior; P – Posterior; M – Medial; L – Lateral)

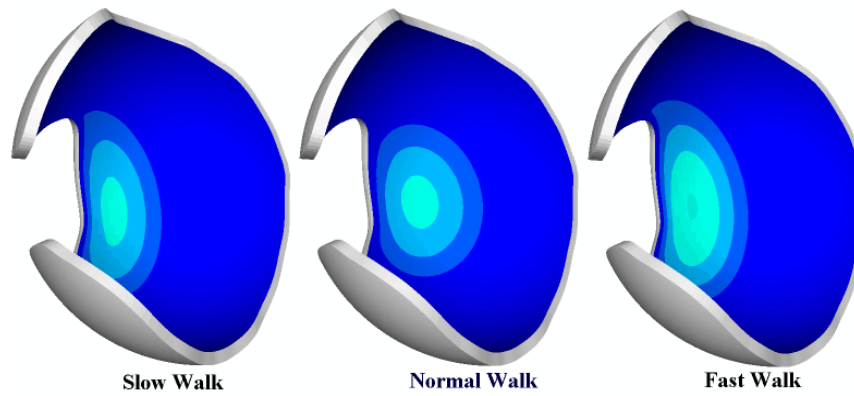


Figure 6.7 Contours of contact stresses at 84% of first walking cycle

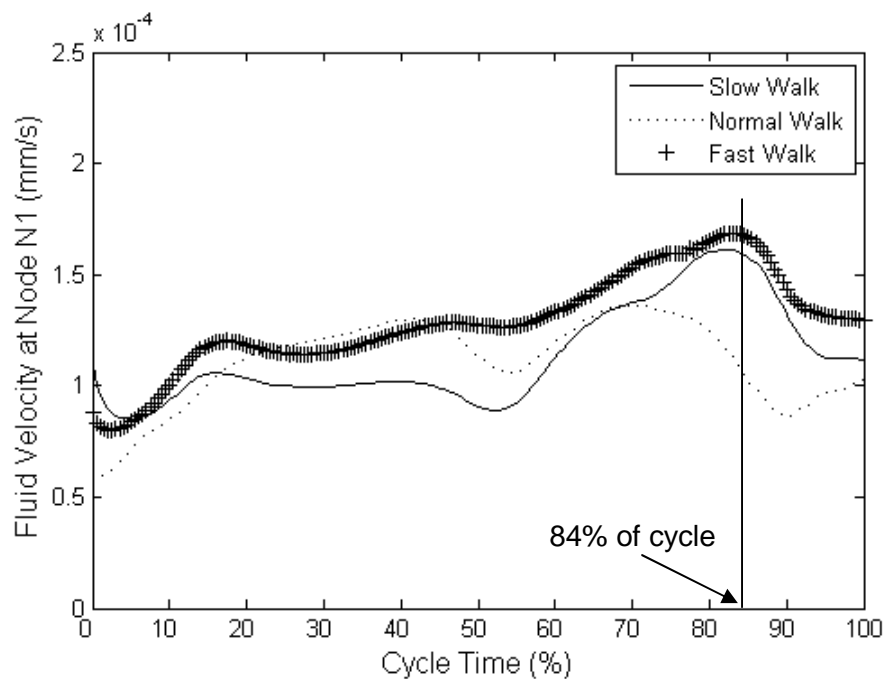


Figure 6.8 Fluid velocity at node N1 during first cycle of slow, normal and fast walking

The predictions of important parameters for all the activities that were analysed are listed in **Table 6-2** and **Table 6-3**. The predicted peak contact pressure, peak fluid pressure, contact area and total fluid load support for standing up and sitting down are shown in **Figure 6.9**. The variation of parameters for going down the stairs and climbing up the stairs is shown in **Figure 6.10** as a function of percentage cycle whereas the results for knee bending and standing on one leg are shown in **Figure 6.11**. The peak contact pressure, peak fluid pressure and acetabular contact area for different activities generally showed the same time-dependent trend as that of contact force. However, while going down the stairs and

in one-legged stance, the contact area variation was found to be somewhat deviating from that of the contact force (**Figure 6.10c**, **Figure 6.10d**, **Figure 6.11c** and **Figure 6.11d**). The variation of total fluid load support was different to that of the contact force for almost all activities except for some similarity in slow and fast walking (**Figure 6.4e**).

When void dependent permeability was used, the variations of all the parameters of interest remained similar to the predictions with constant permeability. The maximum difference with respect to constant permeability predictions was 3.87% in total fluid load support during standing up.

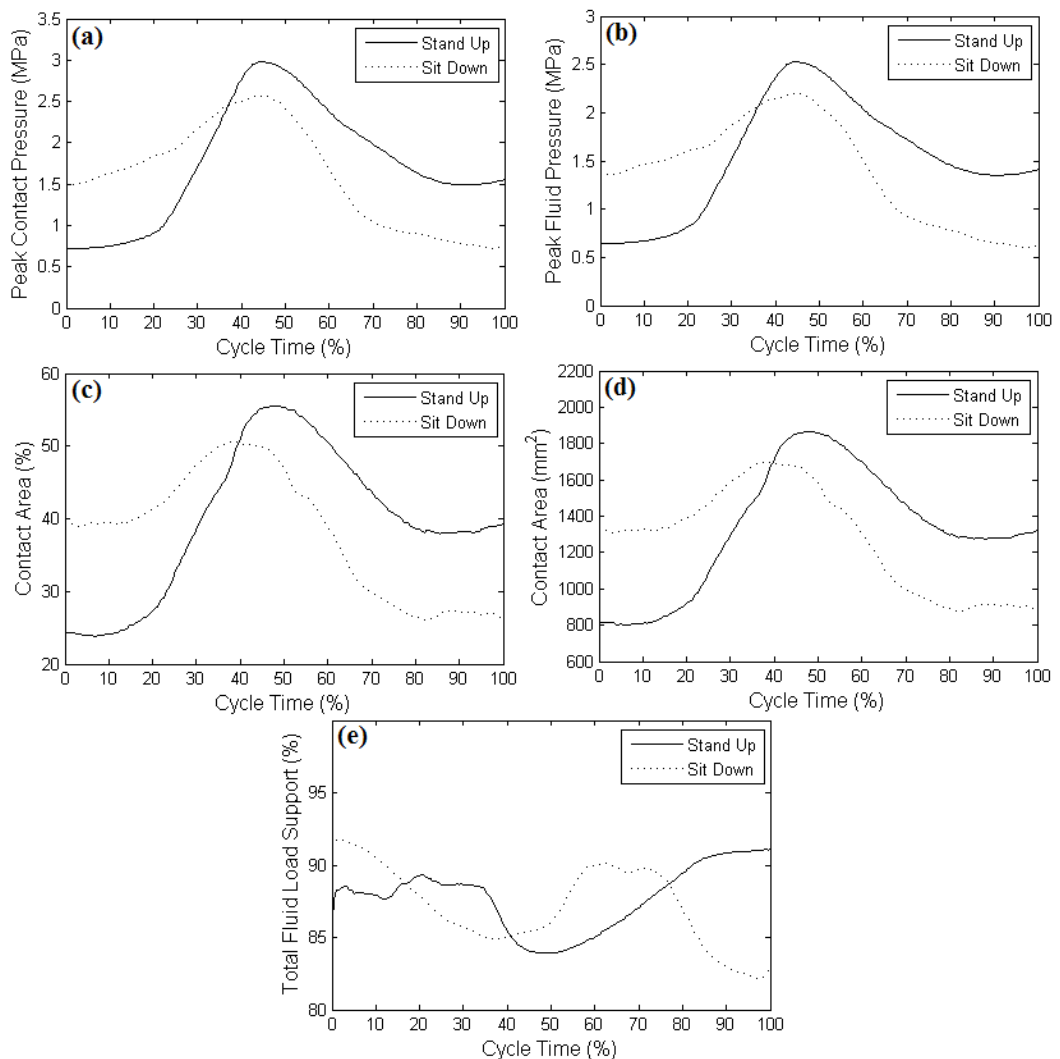


Figure 6.9 (a) Peak contact pressure, (b) peak fluid pressure, (c), (d) acetabular contact area and (e) total fluid load support during first cycle of standing up and sitting down

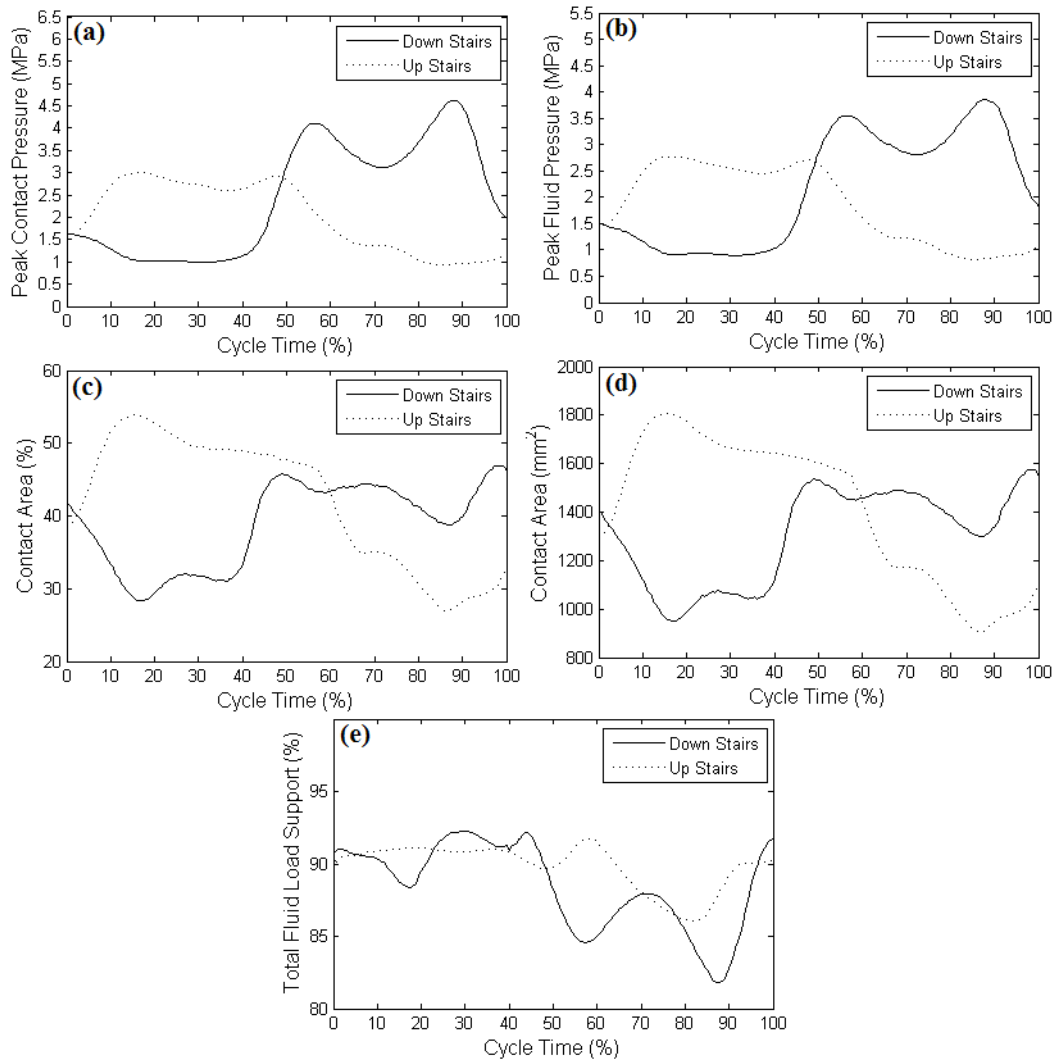


Figure 6.10 (a) Peak contact pressure, (b) peak fluid pressure, (c), (d) acetabular contact area and (e) total fluid load support during first cycle of going down stairs and climbing stairs

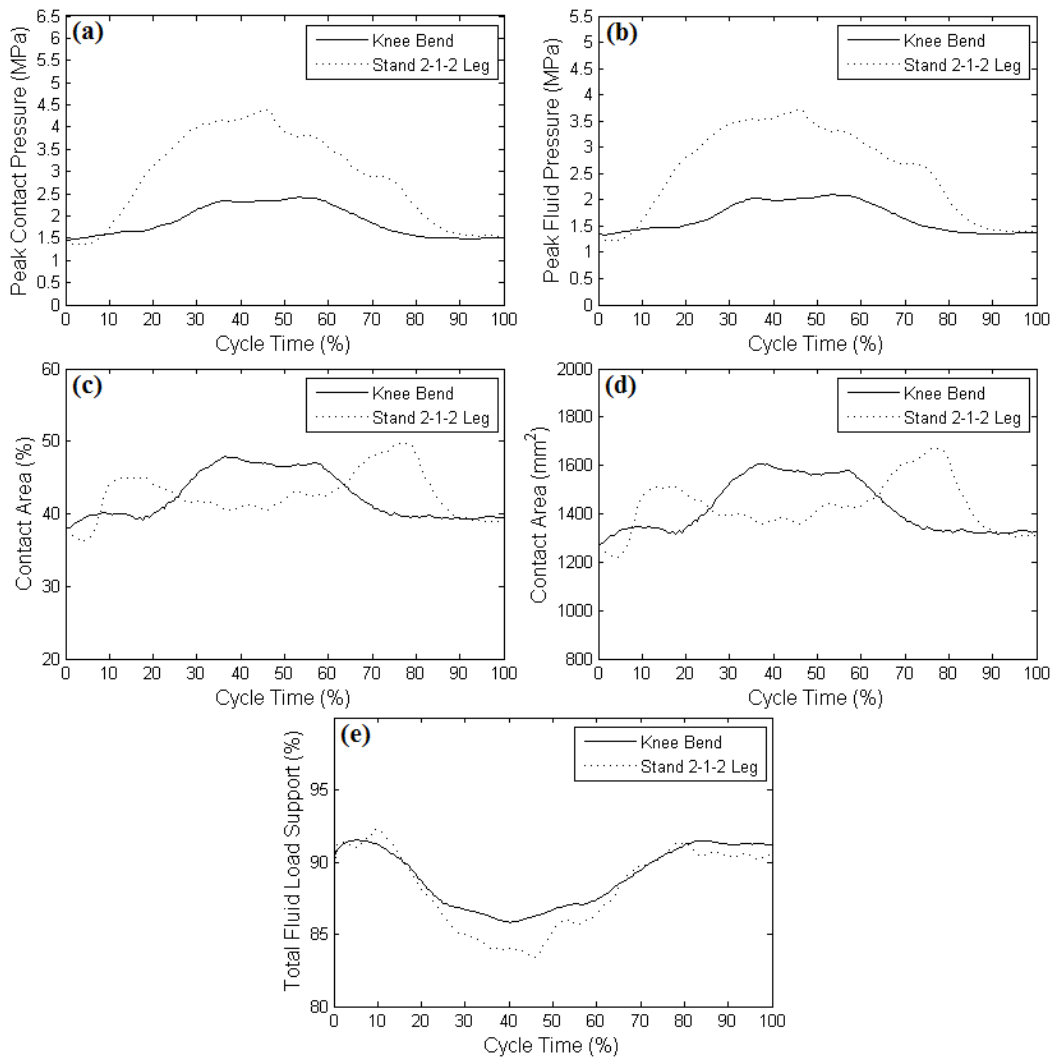


Figure 6.11 (a) Peak contact pressure, (b) peak fluid pressure, (c), (d) acetabular contact area and (e) total fluid load support during first cycle of knee bending and standing on one leg

6.4 Discussion

A limited number of FE/numerical studies of the contact mechanics of the hip joint exist. However, none of these studies have investigated the role played by interstitial fluid pressurization in the contact mechanics and tribology of the cartilage in a whole joint model. Therefore nine different activities of daily living were simulated to investigate the extent of effect that the fluid phase has in the tribological functioning of the hip joint after hemiarthroplasty.

It should be noted that the load vector in the first step was applied in

1 second. This was needed as a very high value of UTOL (100 MPa) was used in these formulations. A smaller value of the time step underestimated fluid pressure which could be improved by lowering UTOL at the expense of computational time. This high value of UTOL was found to be suitable through experimental validation discussed in **Chapter 4**. The instabilities usually associated with using a lower time step in poroelastic formulations (Vermeer and Verruijt, 1981; Ferronato *et al.*, 2001; ABAQUS., 2007; Stokes *et al.*, 2010) were not observed in the current study.

The variation of acetabular cartilage peak contact pressure followed that of contact force in all the activities of daily living as observed previously (Bachtar *et al.*, 2006). A similar correlation was observed by Park and colleagues with respect to hip joint forces (Park *et al.*, 1999) and ground reaction forces for the stance phase (Rydell, 1965; Park *et al.*, 1999). The peak contact pressure was maximal when going down the stairs just before toe-off. This was the most strenuous of all the activities investigated. Standing on one leg was the next demanding activity. In both these activities the corresponding contact areas were smaller and were on the lateral roof of the acetabulum. The contact stresses for descending stairs were found to be higher than those during stair ascent as has been also observed in clinical (McGibbon *et al.*, 1999) and analytical studies (Daniel *et al.*, 2008). The variation of peak fluid pressure also showed patterns similar to those of contact forces for all the activities of daily living.

The total fluid load support in all the activities was found to be around 90%. This reduced the load supported by the solid phase of the cartilage which would reduce the effective coefficient of friction (McCutchen, 1962; Macirowski *et al.*, 1994; Forster and Fisher, 1996; Ateshian *et al.*, 1998; Forster and Fisher, 1999; Krishnan *et al.*, 2004). This would then reduce the frictional shear stresses thus protecting the cartilage from wear. This fluid load support was high over most of the cycle for all the activities. The drop in the fluid load support was very small even after five cycles of normal walking. The migration of contact probably helped in rehydration of the cartilage thus maintaining high interstitial fluid pressurization (Pawaskar *et al.*, 2007; Katta *et al.*, 2009). It has been also hypothesised that the contact migrating faster than the diffusive velocity of the interstitial fluid ($\sim 10^{-4} - 10^{-6}$ mm/s) does not allow enough time for the fluid to flow to the regions of low pressure and may help in maintaining higher fluid pressurisation over longer time duration (Caligaris and Ateshian, 2008; Ateshian, 2009). It reduced only when the contact moved towards the edges of the acetabular cartilage. This was because, the acetabular labrum was not modelled in the present study and free flow was prescribed on the edges of the cartilage. Thus more fluid exudation occurred when the contact moved towards any edge. In the presence of the labrum which has

lower permeability than the cartilage (Ferguson *et al.*, 2000a), this edge effect will reduce. The anomaly seen in total fluid load support between 60% and 95% of the normal walking cycle in **Figure 6.4e** was due to the contact being slightly away from the medial edge as seen in **Figure 6.7**. This caused lesser fluid to exude from the edges in case of normal walking (**Figure 6.8**) and hence higher fluid load support was observed in this case (**Figure 6.4e**).

The contact area was generally small in spite of the conforming contacting surfaces. The contact areas for all activities did not exceed 55.59% which happened at 47.5% of the standing up cycle. The contact moved medially but slightly towards the posterior horn during this time. This was lower than that observed by Yoshida and colleagues (100% during walking and, going up and down the stairs) in their discrete element analysis study (Yoshida *et al.*, 2006). However, the clearance used by Yoshida *et al.* was not mentioned. Acetabular fit has been cited as an important parameter in the prevention of acetabular erosion (Harris *et al.*, 1975; Yamagata *et al.*, 1987). The current study used a radial clearance of 0.5 mm between the acetabular cartilage and the metallic prosthetic head which might have reduced the contact areas. The smallest contact area was 23.77% at 7% of the standing up cycle when the contact moved in the posterior horn of the acetabular cup. It should be noted that the commercial femoral head prostheses are available in increments between 1 and 2 mm (Kosashvili *et al.*, 2008). Thus a radial clearance of 0.5 mm represented the smallest realistic clearance for hemiarthroplasty for spherical acetabular cup assumption.

The acetabular cavity was assumed to be spherical in this study which is not the case in an anatomical joint. The non-spherical articular surface would, in turn, introduce variable clearance in the joint and adversely affect both the contact pressures and fluid load support. The total fluid load support in this case might be reduced if there was a greater area available for fluid exudation (as in higher clearances) or the permeability was increased (when water content increases as in case of OA) (McDevitt and Muir, 1976; Armstrong and Mow, 1982). This would then increase the coefficient of friction and hence frictional shear stresses. The increased contact stresses along with the increased shear stresses have the potential to induce cartilage fibrillation thus compromising the integrity of the hip joint in general and cartilage in particular. In OA joints in which the cartilage structure has already been compromised and diminished, higher local contact stresses might enhance this effect. However, it should be noted, that the long term survivorship has been shown in both unipolar (Wachtl *et al.*, 2003) and bipolar (Haidukewych *et al.*, 2002) hemiarthroplasties which may be due to higher fluid load support and lower contact stresses.

Contact area and peak contact pressure depended not only on the magnitude of the load but also on the location of the contact. For example, in standing on one leg, contact stresses were 3.65 MPa and 2.88 MPa for similar loads of 1937 N and 1935 N respectively during two different stages of the activity. However, in the first case the contact was near the lateral roof (contact area - 42.45%) whereas in the second case it was in the superior dome (contact area – 48.43%) where larger area was available for contact. The contact areas and their location also varied depending upon the activity. In most of the activities the contact was found in the superior dome of the acetabular cartilage as can be seen from **Table 6-2**. McGibbon and colleagues observed this frequent loading of the superior dome in their clinical hemiarthroplasty study which may explain cartilage degradation in this area (McGibbon *et al.*, 1999). The thickness of the cartilage has been hypothesized to vary with contact stresses (McGibbon *et al.*, 1999); the thickest cartilage is found antero-superiorly near lateral roof (Oberlander, 1977; von Eisenhart *et al.*, 1999). The concentration of stresses in the superior dome and near lateral roof seemed to support this hypothesis. Although the present study focused on hemiarthroplasty, these findings may also be related to the natural joint.

The values of contact pressure in general were however lower than those measured using endoprosthesis in hemiarthroplasty studies (Hodge *et al.*, 1986; Krebs *et al.*, 1991; McGibbon *et al.*, 1999; Park *et al.*, 1999). For example, in normal walking, peak contact pressure in the present study was 2.78 MPa during the stance phase as compared to clinical values of 5.5 MPa (Hodge *et al.*, 1989) and 3.69 MPa (Krebs *et al.*, 1991). Hodge and colleagues also reported a reduced peak pressure of 4.0 MPa after 36 months of surgery (Hodge *et al.*, 1989) during walking. Bachtar and colleagues have reported 5.5 MPa in their finite element study (Bachtar *et al.*, 2006). However, predictions in the current study were more in line with the mathematical/numerical models in which a spherical geometry was assumed for the acetabulum and femoral head (Genda *et al.*, 1995; Hipp *et al.*, 1999; Ipavec *et al.*, 1999). Ipavec and colleagues found a peak stress of 3 MPa during the stance phase of normal walking. In a discrete element model with spherical acetabular cartilage of uniform thickness, peak contact pressure of 3.26 MPa has been reported for normal walking (Yoshida *et al.*, 2006). It has been shown recently that both conchoid and spherical shapes underestimate peak contact stresses by nearly 50% and overestimate contact areas by around 25% when compared to subject-specific models (Anderson *et al.*, 2010). It should be noted that the study of failure is associated with material properties as well as level of stresses.

The use of void dependent permeability did not change the predictions

substantially in spite of large cartilage deformation (around 44% when maximum load of 2.6 times BW was applied during walking down the stairs). This may be due to a very low permeability of cartilage and a small variation in it due to corresponding small change in void ratio ($\sim 0.06\%$ of initial value).

One of the limitations of the current study was that the predictions were totally dependent on only one set of kinematic and force data (Bergmann, 2001). Thus some of the inferences may be purely due to the data being used and might not be a general trend, for example, the contact moving away from the medial edge in normal walking vis-à-vis slow and fast walking (**Figure 6.7**). Moreover, as mentioned above, a more realistic geometry of the acetabular cartilage needs to be considered to take into account the effect of variable clearance.

The contact stresses and fluid load support have been predicted for the hemiarthroplasty in the hip. Although the stresses were lower than in total joint replacement (Udofia *et al.*, 2007), currently it is not known how natural cartilage will respond to this level of cyclic stress over prolonged periods. Further experimental work is needed to understand the response of articular cartilage in the hip to this type of tribological and biomechanical demand. We have recently shown in the knee that at higher levels of contact stress and shear stress, failure of cartilage can occur (McCann *et al.*, 2009). Further experimental studies are needed in the hemiarthroplasty in the hip.

In conclusion, the present study showed that mean contact areas were generally only around 40% of the total potential contact area despite the surfaces being conforming. Certain activities could result in an increase in contact stresses and decrease in fluid load support consistent with the load. However, the fluid load support was high in most of the activities aiding in stress shielding of the cartilage matrix. This may explain the remarkable survival of articular cartilage in the hemiarthroplasty.

Chapter 7 Overall Discussion and Conclusions

7.1 FE modelling of Natural Hip Joint and Hemiarthroplasty

As human life expectancy increases due to better standards of living and as increasing numbers of young people engage themselves in sports which demands the highest level of fitness and more efficient and effective body movements; study of the biomechanics of human joints must encompass these extreme living conditions. The role played by the exceptional tribological properties of the joints, in their smooth functioning and at times in adverse conditions throughout the lifetime of an individual, has yet to be fully understood. Contact mechanics of joints has been found to have a direct influence on the structure and integrity of soft contacting tissues covering the articulating ends of the bones of the joint. To investigate these phenomena, the human hip joint has attracted a great deal of attention owing to its simplicity in geometry and because it is one of the joints in the body transmitting large loads (Dowson *et al.*, 1981a) and providing stability to the whole skeletal system. The hip joint is a diarthrodial joint with the femur and acetabulum as articulating components. The bearing surfaces of the femoral head and acetabular cavity (lunate surface) are covered with articular cartilage which has a very low coefficient of friction and wear rate. This is mainly attributed to interstitial fluid pressurisation of the cartilage under loading which forms the basis of biphasic lubrication.

Contact mechanics of hip joint have been studied analytically, numerically as well as clinically. *In vivo* clinical studies are invasive and hence change the natural joint structure. Analytical and numerical (e.g. finite element) studies, on the other hand, rely on anthropometric as well as gait data to predict joint forces and stresses without having to compromise the anatomy of the joint. However, finite element models of the anatomical hip joint are mostly simplified to a two-dimensional or axisymmetric configuration and hence do not represent the joint accurately. Moreover, three-dimensional hip studies model the articular cartilage as elastic/hyperelastic material and hence cannot investigate the role played by interstitial fluid in contact mechanics and tribology of the joint. There is a need to understand the mechanical, functional, structural and biochemical aspects of the joint in general and of articular cartilage in particular as they are important to the overall efficiency and efficacy in handling the complex loads and motions, and providing biphasic lubrication. Any changes to these due to various interventions

such as hemiarthroplasty in which femoral head is replaced by a rigid metallic prosthesis can have an adverse effect on the survivorship of the joint and the cartilage. It is, therefore, important to model the joint in three-dimensions to reflect its anatomy and include the biphasic nature of the cartilage in all analytical and numerical models. The current study thus aimed to develop the methodology to model contact mechanics and tribology of the natural hip joint as well as the one with hemiarthroplasty.

In contact mechanics modelling involving biphasic cartilage, the information about nodes/points in contact is essential to enforce surface fluid flow boundary conditions. However, in the case of joint contact simulation this information forms part of the solution and is not available a priori as the articulating surfaces are of different shapes and relative motion between them involves rolling as well as sliding. To do this, an algorithm proposed earlier (Pawaskar, 2006) was refined and extended to include three-dimensional elements in **Chapter 2**. The algorithm was used to find the nodes in contact and then assign fluid flow based on the fluid pressure difference on the opposite sides of the contact interface. This was true of two cartilages in contact, but in the case of a rigid metallic prosthesis in contact with acetabular cartilage, as in the case of hemiarthroplasty, the flow at contacting nodes was completely stopped. The non-contacting nodes in both these cases were prescribed free fluid flow. Subroutines available in ABAQUS (ABAQUS., 2007) were used to read the contact information and impose fluid flow boundary conditions as the simulation progressed. The predictions using this algorithm were verified against the established results (Warner, 2000; Federico *et al.*, 2004). An exceptionally good agreement was found between the predictions of contact and fluid pressures, solid stresses and fluid flow in the current study and those in the studies by Warner, and Federico and colleagues. The significance of the new algorithm was its generality and robustness and that it posed no restrictions on the type of elements used or on the geometry of the articulating surfaces in order to implement surface fluid flow conditions.

In the course of establishing three-dimensional modelling methodology, some of the parameters needed to be relaxed by trial and error, to avoid convergence problems. However, this did not affect the accuracy of the predicted contact parameters markedly. This was verified using two-dimensional axisymmetric and corresponding three-dimensional cup and ball models in case of natural hip joint model. Experimentally validation was carried for hemiarthroplasty model. Apart from the changes made to the parameters, cartilage was modelled as a neo-Hookean poro-hyperelastic material, for the most part of this study. This was to take into account the large deformations that might typically exist in the joint. As was done

with the contact detection algorithm, these changes needed to be either verified or experimentally validated.

Experimental validation of the natural joint with contact between two biphasic cartilages was beyond the scope of this project. The methodology was, therefore, first tested on a simple cup and ball model in **Chapter 3**. The previously verified methodology for the axisymmetric cartilage-cartilage model was used to compare the three-dimensional cup and ball model predictions. The contact detection algorithm proposed in **Chapter 2** was used in this study. The maximum difference in predictions of these simplified models was less than 2%. This verification confirmed that the aforementioned changes in parameters had a very negligible effect on the predictions of the three-dimensional model. It was, therefore, thought to be acceptable to apply the methodology to the natural hip joint.

The hemiarthroplasty model was experimentally validated using porcine acetabular hip joint as discussed in **Chapter 4**. The validation process was a two stage process; the material properties such as equilibrium elastic modulus and permeability were first derived using porcine acetabular pins and indentation tests. The least square method was then used to fit an FE deformation curve to the corresponding experimental curve giving the relevant properties. The material properties were converted to neo-Hookean material constants and were then used in the hemiarthroplasty model. Porcine hip joint models were created from μ CT images. The orientations and boundary conditions of the porcine acetabular cups in experimental tests were reproduced in FE models. Similar loads were applied in both cases. The contact detection algorithm of **Chapter 2** was also used in this case to impose surface fluid flow boundary conditions.

Contact stresses and contact areas in experimental and FE models were compared in order to confirm that the methodology used for FE modelling had a sound experimental footing. The peak contact stresses were very high (8.54 MPa was the lowest in experiments; 8.30 MPa in FE) in both cases whereas the maximum contact areas were 147.19 mm² and 175.11 mm² in experiments and FE models respectively. This was as expected due to the large variable local radial clearance that existed in these models. The maximum differences between experimental and FE peak contact stresses and contact areas were at 12.42% and 20.69% respectively. The location of stress distribution was mostly similar in both the cases. The fluid load support was around 80% which could not be experimentally verified as it was beyond the scope of this study.

There were however, several limitations to this study that have been explained in detail in **Section 4.4**. A thorough and more accurate approach needs to be developed in the future; e.g. alignment of the porcine acetabular cup model to

that of the actual cup was carried out by choosing three distinct non-linear points on the edge of the cup and then finding its coordinates using CMM. The registration blocks (Fischer *et al.*, 2001) could be used in the future. Despite these limitations, the FE models could reproduce experimental outcomes. This validation also confirmed, as in the case of natural hip joint, that the parameter relaxation did not substantially affect the predictions of the three-dimensional hemiarthroplasty model. The validated methodology was thus thought to be suitable to be applied to the model of hemiarthroplasty of the natural hip joint.

The methodology was first applied to the natural hip joint in **Chapter 3**. Acetabular cartilage was horseshoe shaped in this model. The clearance between acetabular and femoral cartilages was assumed to be 0.0 mm as would be the case in the natural hip joint (MR images of hip joint shows both the acetabular and femoral head cartilages as one with a little or no inter-articular gap (Naish *et al.*, 2006; Li *et al.*, 2008)).

A very high fluid load support (~94%) was predicted with peak contact stresses of around 2 MPa soon after loading. The lower peak contact stress was due to the spreading of the load over a larger area of approximately 83% of the total acetabular cartilage area available for contact. The highly conforming joint was also the cause for a very high fluid load support seen in this study.

When natural cartilage of the femoral head, has to be sacrificed for a variety of reasons, hemiarthroplasty is usually the intervention of choice. In this, a rigid metallic prosthesis articulates against the natural acetabular cartilage which may result in several complications such as acetabular erosion and protrusion. Despite this, the use of hemiarthroplasty is on the rise (Jain *et al.*, 2008) due to its conservative nature when compared to total hip replacement, lower cost, lower operating time and lower time required for post-operative rehabilitation. Two applications of hemiarthroplasty were thus investigated.

In **Chapter 5**, the effect of clearance between the acetabular cartilage and the femoral head prosthesis on fluid load support and contact mechanics of the hemiarthroplasty of human natural hip joint was investigated. The femoral head prosthesis was modelled as a solid with CoCr material properties and not as an analytical solid, in order to ensure the creation of a base model for future realistic studies. The use of analytical solid, however, does not affect predictions as the head is very rigid as compared to soft cartilage. Four increasing radial clearances were studied. Increasing the clearance was found to increase peak contact stresses and lower the total fluid load support due to decreasing conformity and contact area. Total fluid load support was high (~90) for all the clearances.

The second application of the experimentally validated hemiarthroplasty methodology was to investigate the role of interstitial pressurisation in the contact mechanics and tribology of the hip joint during activities of daily living such as walking, climbing stairs and so on (**Chapter 6**). The loading data was taken from Bergmann's study using an instrumented hip prosthesis (Bergmann, 2001).

The contact areas were generally small with a mean contact area of ~40% in all the activities despite congruent articulating surfaces. The peak contact stresses, in general, were lower (2.78 MPa during stance phase of normal walking) than those observed in clinical hemiarthroplasty studies (5.5 MPa) (Hodge *et al.*, 1986; Krebs *et al.*, 1991; McGibbon *et al.*, 1999; Park *et al.*, 1999) mainly due to the use of a spherical shaped acetabulum and femoral head in this study. Contact area and peak contact pressure were dependent on the magnitude of the load as well as on the location of the contact. A superior dome provided a larger contact area and hence lower contact stresses were observed. The contact in the lateral roof, on the other hand provided a smaller area thus increasing the contact stresses. Peak contact stresses and peak fluid pressures followed the variation of contact loads. Going down the stairs was the most strenuous activity followed by standing on one leg. In both these activities the peak pressures were observed in the lateral roof. On the other hand, during stance phase of normal walking, peak contact stress was lower and was in the superior dome. The fluid load support in all the activities was very high (~90%) and decreased a little after five cycles of normal walking. The fluid load support reduced only when the contact moved towards the free draining edges of the acetabular cartilage which possibly could be avoided by modelling acetabular labrum. Implementation of void dependent permeability did not alter the predictions substantially.

One of the limitations of this study was quasi-static implementation of gait cycles due to the limitations of the software (Abaqus Standard) that was used for analysis (ABAQUS., 2007). For dynamic analysis Abaqus Explicit could have to be used. However, it does not offer soils consolidation procedure which was needed for biphasic modelling. It may be worthwhile looking at alternative software with a possibility of implementing this.

The high fluid load support predicted in natural (**Chapter 3**) as well as hemiarthroplasty (**Chapter 5** and **Chapter 6**) joints (though it was slightly lower in hemiarthroplasty) would reduce the friction due to reduction in solid-to-solid contact which would in turn reduce the frictional shear stresses. Lower contact stresses would also have a similar effect. This combined reductions of contact and shear stresses perhaps protect the natural cartilages in both types of joints from erosion and might be the reason for their long term survivorship. In hemiarthroplasties this

has been observed in several clinical studies (Haidukewych *et al.*, 2002; Wachtl *et al.*, 2003).

The effect of altering the natural hip joint with hemiarthroplasty was to lower the fluid load support slightly. In subject-specific hemiarthroplasty hip joints investigated for validation in **Chapter 4**, the fluid load support was even lower. The contact stresses in the hemiarthroplasty joint were higher due to smaller contact areas. Lower fluid load support and higher contact stresses would result in an increase in frictional shear stresses in the hemiarthroplasty joint and may potentially be harmful to the structural integrity of the acetabular cartilage and may induce cartilage erosion. Increasing the clearance was found to be harmful to the cartilage in terms of both the fluid load support and contact stresses. The prosthesis head diameter is thus an important parameter to consider during hemiarthroplasty as has been previously discussed in **Section 1.7.3**. The importance of acetabular fit to cartilage degradation has been recognised previously (Yamagata *et al.*, 1987; Jeffery and Ong, 2000) which this study supported. The increase in contact stresses and wear with the decreasing conformity has also been shown experimentally (McCann *et al.*, 2009). Similar harmful effects could be experienced by the cartilage during activities which would frequently shift the contact towards edges offering lower contact areas and higher fluid exudation. Thus contact stresses were dependent not only on the magnitudes of the load but also on their locations along with the type of activity a person is undertaking.

The acetabular cavity and femoral head were spherical in both the natural as well as hemiarthroplasty joints models assumed in this study. Cartilages covering the lunate surface of the acetabular cavity and femoral head were of uniform thickness of 2 mm. On the other hand the validated porcine cup model was subject-specific. The effect of this idealised geometry was to decrease predicted contact stresses and increase contact areas as has been previously shown by Anderson and colleagues (Anderson *et al.*, 2010). Moreover, as seen in **Section 4.3**, the subject-specific porcine hemiarthroplasty hip joint also predicted lower total fluid load support (~80%) as compared to the idealised human hemiarthroplasty joint (~90%). This was due to more area available for fluid exudation in subject specific models because of larger variable local clearances. Human hip joint models need to be subject-specific in future and to achieve that, CT or MRI images of human hip cadavers along with cartilage will have to be used and converted to FE models.

An investigation of the long term sustainability of fluid pressurisation under prolonged static load was attempted in the hemiarthroplasty joint in **Chapter 5**. In these models, even after 600 seconds, the fluid load support did not decrease substantially. This could not be verified in the natural joint model in **Chapter 3**, due

to the difficulties in solution convergence arising from the soft contact formulation between two cartilages. Severe elemental distortions and overclosures were noticed which need to be addressed in the future. The hard contact formulation was not used in this case to avoid high residual forces and may also be worth looking at as a continuation of this study. The model was however, still beneficial in understanding the contact mechanics and tribology of the joint immediately after the load was applied. The distortion and overclosure problems need to be fixed before the model could be used for consolidation scenarios. Use of alternative software such as FEBio from the University of Utah which has been specifically written for problems in computational biomechanics (Maas *et al.*, 2009) could be looked into in the future.

In spite of these limitations, the use of biphasic cartilage in the models discussed made it possible to investigate fluid load support in a three-dimensional anatomical hip joint model (normal and hemiarthroplasty) and its influence on the tribology and contact mechanics of the joint. The stress shielding of the solid matrix of the cartilage due to high fluid load support would protect the cartilage from degradation by reducing solid-to-solid contact and in turn reducing frictional shear stresses. The total fluid load support in hemiarthroplasty was found to be lower (~91 %) compared to that in natural hip joint (~94 %) but was still high. This high interstitial fluid pressurisation might be the reason for the long term survival of cartilage in both the hemiarthroplasty as well as natural joint. However, interventions and design parameters such as head diameter as well as subject-specific geometries and gait patterns can all affect the magnitude of fluid load support.

7.2 Conclusions

To summarise, the major conclusions of this study were:

- 1) Successful methodologies were developed for three-dimensional models of natural and hemiarthroplasty hip joints. Contact dependent flow was also implemented. This allowed different applications to be investigated.
- 2) Fluid load support in both the natural hip joint as well as the one with hemiarthroplasty was very high (~90%) mainly due to the spherical geometry of the articulating surfaces as well as their congruence. This also reduced contact stresses and increased contact areas in these models.
- 3) In the subject-specific porcine hip joint model, the fluid load

support was lower (~80%) than in the models with idealised geometry but was still high. This was due to variable local clearances which would provide more area for fluid exudation. Local variable clearance also meant higher local contact stresses and lower contact areas.

- 4) The peak contact stresses increased with the increase in radial clearance in the hemiarthroplasty model. The corresponding contact areas and total fluid load support decreased at the same time. This was due to the decrease in the congruence of the joint. This can potentially cause cartilage erosion.
- 5) The contact areas in the hemiarthroplasty model were smaller despite the conforming joints. In activities of daily living mean contact areas were approximately ~40% of the area available for contact.
- 6) Contact areas and peak contact stresses depended not only on the magnitude of the load but also on their location and the type of activity undertaken. The superior dome of acetabulum provided larger contact areas and hence the contact stresses in this area were lower.
- 7) Peak contact stresses and peak fluid pressures mostly followed the variation of contact loads in activities of daily living.
- 8) Total fluid load support in all the activities was very high (~90%) and decreased only slightly during five cycles of normal walking. The fluid load support was lower when the contact moved towards the free draining edges of the acetabular cartilage. This could possibly be avoided by incorporating acetabular labrum in the model.

7.3 Promising Potential

The main predictions of this study were contact stresses, contact areas and total fluid load support. Biphasic lubrication has been hypothesised as an important phenomenon protecting the cartilage against friction and wear. The output of the current study (including deformations) could be used for investigating other types of lubrication such as elastohydrodynamic and self-generating lubrications.

Rigid body multi-body dynamics modelling is a very helpful tool in

investigating the kinematics and kinetics of the musculoskeletal system in a simplified way due to the assumption of absence of deformation. The results obtained in this study such as location of contact and contact areas could be used as inputs to develop realistic contact algorithms for rigid bodies (as are present in multi-body systems). For example, the coefficient of restitution, i.e. the ratio of velocities after and before an impact, can be derived from the force displacement curves in a finite element model without having to go through the rigorous and time consuming computations involved in FE modelling.

The models and methodologies proposed here can be used as a reference for future contact mechanics studies. In the current study, both the acetabulum and femoral head/femoral prosthesis were modelled as spherical. This could be treated in future as an idealised configuration for comparison with other geometrical shapes (such as ellipsoidal or conchoid) or subject specific models.

It should be noted that in the current study cartilage was modelled as an isotropic and homogeneous material with only compressive material properties. However, the collagen fibres oriented parallel to the cartilage surface are loaded in tension when the cartilage bulk is loaded in compression. The cartilage modulus in tension has been found to be around an order of magnitude higher than compressive modulus (Soltz and Ateshian, 2000; Ateshian *et al.*, 2003). This tension-compression non-linearity at the surface has been shown to increase the fluid load support, sometimes to as high as 98%, in unconfined compression (Soltz and Ateshian, 2000; Ateshian, 2009). It will be interesting to investigate the effect of tension-compression non-linearity on fluid load support in a three-dimensional model of the whole joint.

Moreover, an optimisation scheme could be devised based on the current study which would save time and predict the outcomes in a more efficient way. The optimisation would be akin to neural network where the network could be trained based on a wide variety of subject-specific data. The network should then be able to predict variables of interests in a relatively short time. This would help clinicians to make informed decisions in pre-operative planning and post-operative rehabilitation without having to wait for unreasonably long periods as those required for FE simulations.

References

- ABAQUS. Manuals, Version 6.7-1. Dassault Systemes., 2007, Suresnes Cedex, France.
- Adam, C., Eckstein, F., Milz, S., and Putz, R. The distribution of cartilage thickness within the joints of the lower limb of elderly individuals. *J Anat*, 1998. **193** (Pt 2): pp. 203-214.
- Adams, C., Ellis, B., Harris, M., Andersion, A., Peters, C., and Weiss, J. Effect of the acetabular labrum on cartilage contact stresses and load distribution in the hip. In: *56th Annual Meeting of the Orthopaedic Research Society*. 2010, New Orleans, LA, USA, **35**. Paper No.: 0306.
- Adams, D., and Swanson, S. A. V. Direct measurement of local pressures in the cadaveric human hip-joint during simulated level walking. *Annals of the Rheumatic Diseases*, 1985. **44**(10): pp. 658-666.
- Afoke, N., Byers, P., and Hutton, W. Contact pressures in the human hip joint. *J Bone Joint Surg Br*, 1987. **69-B**(4): pp. 536-541.
- Aigner, T., and McKenna, L. Molecular pathology and pathobiology of osteoarthritic cartilage. *Cellular and Molecular Life Sciences (CMLS)*, 2002. **59**(1): pp. 5-18.
- Altman, R. D. Ibuprofen, acetaminophen and placebo in osteoarthritis of the knee: A six-day double-blind study. *Arthritis and Rheumatism*, 1999. **42**(9): pp. 1995.
- Aminian, K., Robert, P., Jequier, E., and Schutz, Y. Estimation of speed and incline of walking using neural network. *Instrumentation and Measurement, IEEE Transactions on*, 1995. **44**(3): pp. 743-746.
- An, K. N., and Chao, E. Y. S. Kinematic analysis of human movement. *Annals of Biomedical Engineering*, 1984. **12**(6): pp. 585-597.
- Anderson, A. E., Ellis, B. J., Maas, S. A., Peters, C. L., and Weiss, J. A. Validation of hip joint contact pressures in a subject-specific finite element model. In: *53rd Annual Meeting of the Orthopaedic Research Society*. 2007, San Diego, CA, **32**. Poster No: 0621.
- Anderson, A. E., Ellis, B. J., Maas, S. A., Peters, C. L., and Weiss, J. A. Validation of finite element predictions of cartilage contact pressure in the human hip joint. *Journal of Biomechanical Engineering*, 2008. **130**(5): pp. 051008-10.
- Anderson, A. E., Ellis, B. J., Maas, S. A., and Weiss, J. A. Effects of idealized joint geometry on finite element predictions of cartilage contact stresses in

- the hip. *Journal of Biomechanics*, 2010. **43**(7): pp. 1351-1357.
- Anderson, A. E., Peters, C. L., Tuttle, B. D., and Weiss, J. A. Subject-specific finite element model of the pelvis: Development, validation and sensitivity studies. *Journal of Biomechanical Engineering*, 2005. **127**(3): pp. 364-373.
- Andriacchi, T. P., and Hurwitz, D. E. Gait biomechanics and the evolution of total joint replacement. *Gait & Posture*, 1997. **5**(3): pp. 256-264.
- Andriacchi, T. P., Ogle, J. A., and Galante, J. O. Walking speed as a basis for normal and abnormal gait measurements. *Journal of Biomechanics*, 1977. **10**: pp. 261 - 268.
- Armstrong, C. G., and Gardner, D. L. Thickness and distribution of human femoral head articular cartilage: Changes with age. *Ann Rheum Dis*, 1977. **36**(5): pp. 407-12.
- Armstrong, C. G., and Mow, V. C. Friction, lubrication and wear of synovial joints. In: *Scientific foundation of orthopaedics and traumatology*. Eds. Owen, R., Goodfellow, J., and Bullough, P. 1980, William Heinemann Medical Books Limited: London. pp. 223 - 232.
- Armstrong, C. G., and Mow, V. C. Variations in the intrinsic mechanical properties of human articular cartilage with age, degeneration, and water content. *Journal of Bone and Joint Surgery-American Volume*, 1982. **64**(1): pp. 88-94.
- Ateshian, G., Personal communication regarding "hemiarthroplasties defeat interstitial fluid pressurization in cartilage and promote greater friction than natural joints". *Clarification on poster no. 2120 at 56th Annual Meeting of the Orthopaedic Research Society*, 2010. To: Pawaskar, S. S., University of Leeds, Leeds, UK.
- Ateshian, G. A. A theoretical formulation for boundary friction in articular cartilage. *Journal of Biomechanical Engineering*, 1997. **119**(1): pp. 81-86.
- Ateshian, G. A. The role of interstitial fluid pressurization in articular cartilage lubrication. *Journal of Biomechanics*, 2009. **42**(9): pp. 1163-1176.
- Ateshian, G. A., Kwak, S. D., Soslowsky, L. J., and Mow, V. C. A stereophotogrammetric method for determining in situ contact areas in diarthrodial joints, and a comparison with other methods. *Journal of Biomechanics*, 1994a. **27**(1): pp. 111-124.
- Ateshian, G. A., Lai, W. M., Zhu, W. B., and Mow, V. C. An asymptotic solution for the contact of two biphasic cartilage layers. *Journal of Biomechanics*, 1994b. **27**(11): pp. 1347 - 1360.
- Ateshian, G. A., and Mow, V. C. eds. Friction, lubrication, and wear of articular cartilage and diarthrodial joints. In *Basic orthopaedic biomechanics and mechano-biology.*, eds. Mow, V. C., and Huiskes, R. Third ed. 2005,

- Lippincott Williams & Wilkins: Philadelphia. pp. 447 - 494.
- Ateshian, G. A., Soltz, M. A., Mauck, R. L., Basalo, I. M., Hung, C. T., and Lai, W. M. The role of osmotic pressure and tension-compression nonlinearity in the frictional response of articular cartilage. *Transport in Porous Media*, 2003. **50**(1-2): pp. 5-33.
- Ateshian, G. A., Soslowky, L. J., and Mow, V. C. Quantitation of articular surface topography and cartilage thickness in knee joints using stereophotogrammetry. *Journal of Biomechanics*, 1991. **24**(8): pp. 761-776.
- Ateshian, G. A., and Wang, H. A theoretical solution for the frictionless rolling contact of cylindrical biphasic articular cartilage layers. *Journal of Biomechanics*, 1995. **28**(11): pp. 1341 - 1355.
- Ateshian, G. A., and Wang, H. Rolling resistance of articular cartilage due to interstitial fluid flow. *Proceedings of the Institution of Mechanical Engineers, Part H (Journal of Engineering in Medicine)*, 1997. **211**: pp. 419 - 424.
- Ateshian, G. A., Wang, H. Q., and Lai, W. M. The role of interstitial fluid pressurization and surface porosities on the boundary friction of articular cartilage. *Journal of Tribology-Transactions of the ASME*, 1998. **120**(2): pp. 241-248.
- Athanasiou, K. A., Agarwal, A., and Dzida, F. J. Comparative study of the intrinsic mechanical properties of the human acetabular and femoral head cartilage. *Journal of Orthopaedic Research*, 1994. **12**(3): pp. 340-349.
- Atkinson, P. J., and Haut, R. C. Subfracture insult to the human cadaver patellofemoral joint produces occult injury. *Journal of Orthopaedic Research*, 1995. **13**(6): pp. 936-944.
- Bachtar, F., Chen, X., and Hisada, T. Finite element contact analysis of the hip joint. *Medical & Biological Engineering & Computing*, 2006. **44**(8): pp. 643-651.
- Balazs, E. A., Bloom, G. D., and Swann, D. A. Fine structure and glycosaminoglycan content of the surface layer of articular cartilage. *Fed Proc*, 1966. **25**(6): pp. 1813-1816.
- Balazs, E. A., Watson, D., Duff, I. F., and Roseman, S. Hyaluronic acid in synovial fluid .I. Molecular parameters of hyaluronic acid in normal and arthritic human fluids. *Arthritis and Rheumatism*, 1967. **10**(4): pp. 357-376.
- Barkmann, R., Dencks, S., Laugier, P., Padilla, F., Brixen, K., Ryg, J., Seekamp, A., Mahlke, L., Bremer, A., Heller, M., and Gluer, C. Femur ultrasound (femus) - first clinical results on hip fracture discrimination and estimation of femoral bmd. *Osteoporosis International*, 2009.
- Bay, B. K., Hamel, A. J., Olson, S. A., and Sharkey, N. A. Statically

- equivalent load and support conditions produce different hip joint contact pressures and periacetabular strains. *Journal of Biomechanics*, 1997. **30**(2): pp. 193-196.
- Bean, J. C., Chaffin, D. B., and Schultz, A. B. Biomechanical model calculation of muscle contraction forces: A double linear programming method. *Journal of Biomechanics*, 1988. **21**(1): pp. 59-66.
- Bell, C. J., Fisher, J., Ingham, E., Forsey, R., Thompson, J. I., and Stone, M. H. Tribology of therapeutic lubricants. In: *48th Annual Meeting of the Orthopaedic Research Society*. 2002, Dallas, Texas, **27**.
- Bell, C. J., Ingham, E., and Fisher, J. Influence of hyaluronic acid on the time-dependent friction response of articular cartilage under different conditions. *Proceedings of Institution of Mechanical Engineers - Part H*, 2006. **220**: pp. 23 - 31.
- Berend, M. E. Acetabular protrusion: A problem in depth. *Orthopedics*, 2008. **31**(9): pp. 895-6.
- Bergmann, G. Hip98. Free University, Berlin, 2001,
- Bergmann, G., Deuretzbacher, G., Heller, M., Graichen, F., Rohlmann, A., Strauss, J., and Duda, G. N. Hip contact forces and gait patterns from routine activities. *Journal of Biomechanics*, 2001. **34**(7): pp. 859-871.
- Bergmann, G., Graichen, F., and Rohlmann, A. Hip joint loading during walking and running, measured in two patients. *Journal of Biomechanics*, 1993. **26**(8): pp. 969-990.
- Bergmann, G., Graichen, F., and Rohlmann, A. Is staircase walking a risk for the fixation of hip implants? *Journal of Biomechanics*, 1995a. **28**(5): pp. 535-553.
- Bergmann, G., Graichen, F., and Rohlmann, A. Hip joint forces in sheep. *Journal of Biomechanics*, 1999. **32**(8): pp. 769-777.
- Bergmann, G., Graichen, F., and Rohlmann, A. Hip joint contact forces during stumbling. *Langenbeck's Archives of Surgery*, 2004. **389**(1): pp. 53-59.
- Bergmann, G., Graichen, F., Rohlmann, A., and Linke, H. Hip joint forces during load carrying. *Clinical Orthopaedics and Related Research*, 1997. **335**: pp. 190-201.
- Bergmann, G., Graichen, F., Siraky, J., Jendrynski, H., and Rohlmann, A. Multichannel strain gauge telemetry for orthopaedic implants. *Journal of Biomechanics*, 1988. **21**(2): pp. 169-176.
- Bergmann, G., Kniggenndorf, H., Graichen, F., and Rohlmann, A. Influence of shoes and heel strike on the loading of the hip joint. *Journal of Biomechanics*, 1995b. **28**(7): pp. 817-827.
- Bergmann, G., Siraky, J., Rohlmann, A., and Koelbel, R. A comparison of hip

- joint forces in sheep, dog and man. *Journal of Biomechanics*, 1984. **17**(12): pp. 907-909.
- Bhattacharyya, T., and Koval, K. J. Unipolar versus bipolar hemiarthroplasty for femoral neck fractures: Is there a difference? *J Orthop Trauma*, 2009. **23**(6): pp. 426-7.
- Binns, M. Stiffness of bipolar hip prostheses. *Injury*, 1989. **20**(5): pp. 287-290.
- Black, J. D., Matejczyk, M. B., and Greenwald, A. S. Reversible cartilage staining technique for defining articular weight-bearing surfaces. *Clinical Orthopaedics and Related Research*, 1981. **159**: pp. 265-267.
- Blewitt, N., and Mortimore, S. Outcome of dislocation after hemiarthroplasty for fractured neck of the femur. *Injury*, 1992. **23**(5): pp. 320-322.
- Bochner, R., Pellicci, P., and Lyden, J. Bipolar hemiarthroplasty for fracture of the femoral neck. Clinical review with special emphasis on prosthetic motion. *J Bone Joint Surg Am*, 1988. **70**(7): pp. 1001-1010.
- Bose, W., Miller, G., and Petty, W. Osteolysis of the acetabulum associated with a bipolar hemiarthroplasty. A late complication. *J Bone Joint Surg Am*, 1995. **77**(11): pp. 1733-1735.
- Brand, R. A. Joint contact stress: A reasonable surrogate for biological processes? *Iowa Orthopaedic Journal*, 2005. **25**: pp. 82 - 94.
- Brand, R. A., Crowninshield, R. D., Wittstock, C. E., Pedersen, D. R., Clark, C. R., and van Krieken, F. M. A model of lower extremity muscular anatomy. *Journal of Biomechanical Engineering*, 1982. **104**(4): pp. 304-310.
- Brand, R. A., Pedersen, D. R., Davy, D. T., Kotzar, G. M., Heiple, K. G., and Goldberg, V. M. Comparison of hip force calculations and measurements in the same patient. *The Journal of Arthroplasty*, 1994. **9**(1): pp. 45-51.
- Brand, R. A., Pedersen, D. R., and Friederich, J. A. The sensitivity of muscle force predictions to changes in physiologic cross-sectional area. *Journal of Biomechanics*, 1986. **19**(8): pp. 589-596.
- Braune, W., and Fischer, O. Ueber der schwerpunkt des menslicher koerpers . . . *Abh. d. Koenigl. Sachs. Gesellsch. Math. Phys. Cl.*, 1890. **26**: pp. 561.
- Brinckmann, P., Frobin, W., and Hierholzer, E. Stress on the articular surface of the hip joint in healthy adults and persons with idiopathic osteoarthritis of the hip joint. *Journal of Biomechanics*, 1981. **14**(3): pp. 149-156.
- Brittberg, M., Lindahl, A., Nilsson, A., Ohlsson, C., Isaksson, O., and Peterson, L. Treatment of deep cartilage defects in the knee with autologous chondrocyte transplantation. *N Engl J Med*, 1994. **331**(14): pp. 889-895.
- Brown, C. P., Nguyen, T. C., Moody, H. R., Crawford, R. W., and Oloyede, A. Assessment of common hyperelastic constitutive equations for describing normal and osteoarthritic articular cartilage. *Proceedings of the Institution of*

- Mechanical Engineers, Part H: Journal of Engineering in Medicine*, 2009. **223**(6): pp. 643-652.
- Brown, T. D., and DiGioia, A. M., III. A contact-coupled finite element analysis of the natural adult hip. *Journal of Biomechanics*, 1984. **17**(6): pp. 437 - 448.
- Brown, T. D., and Shaw, D. T. A technique for measuring instantaneous in vitro contact stress distributions in articular joints. *Journal of Biomechanics*, 1982. **15**(4): pp. 329-331.
- Brown, T. D., and Shaw, D. T. In vitro contact stress distributions in the natural human hip. *Journal of Biomechanics*, 1983. **16**(6): pp. 373 - 384.
- Caligaris, M., and Ateshian, G. A. Effects of sustained interstitial fluid pressurization under migrating contact area, and boundary lubrication by synovial fluid, on cartilage friction. *Osteoarthritis and Cartilage*, 2008. **16**(10): pp. 1220-1227.
- Caligaris, M., Canal, C. E., Ahmad, C. S., Gardner, T. R., and Ateshian, G. A. Investigation of the frictional response of osteoarthritic human tibiofemoral joints and the potential beneficial tribological effect of healthy synovial fluid. *Osteoarthritis and Cartilage*, 2009. **17**(10): pp. 1327-1332.
- Cao, L., Youn, I., Guilak, F., and Setton, L. A. Compressive properties of mouse articular cartilage determined in a novel micro-indentation test method and biphasic finite element model. *Journal of Biomechanical Engineering*, 2006. **128**(5): pp. 766-771.
- Carlson, K. L. Human hip joint mechanics : An investigation into the effects of femoral head endoprosthesis replacements using in vivo and in vitro pressure data. PhD Thesis, Mechanical Engineering, Massachusetts Institute of Technology. pp. 452.
- Carney, S. L., Billingham, M. E. J., Muir, H., and Sandy, J. D. Demonstration of increased proteoglycan turnover in cartilage explants from dogs with experimental osteoarthritis. *Journal of Orthopaedic Research*, 1984. **2**(3): pp. 201-206.
- Carrabba, M., and Sarzi-Puttini, P. Introduction: Osteoarthritis in the third millennium: A new era for an old disease? *Seminars in Arthritis and Rheumatism*, 2004. **34**(6, Supplement 2): pp. 1-2.
- Catani, F., Hodge, A., Mann, R. W., Ensini, A., and Giannini, S. The role of muscular co-contraction of the hip during movement. *Chir Organi Mov*, 1995. **80**(2): pp. 227-36.
- Cathcart, R. F. Shape of femoral head and preliminary results of clinical use of a non-spherical hip prosthesis. *Journal of Bone and Joint Surgery-American Volume*, 1971. **A 53**(2): pp. 397.

- Cathcart, R. F. Shape of normal femoral head and results from clinical use of more normally shaped non-spherical hip-replacement prostheses. *Journal of Bone and Joint Surgery-American Volume*, 1972. **A 54(7)**: pp. 1559.
- Chandler, R. F., Clauser, C. E., McConville, J. T., Reynolds, H. M., and Young, J. W. Investigation of inertia properties of the human body. *AMRL-TR-74-137*, 1975(DOT HS-801 430): pp. 1-169.
- Chandrasekar, C. R., Grimer, R. J., Carter, S. R., Tillman, R. M., Abudu, A., and Jeys, L. M. Unipolar proximal femoral endoprosthetic replacement for tumour: The risk of revision in young patients. *J Bone Joint Surg Br*, 2009. **91-B(3)**: pp. 401-404.
- Cheal, E. J., Spector, M., and Hayes, W. C. Role of loads and prosthesis material properties on the mechanics of the proximal femur after total hip arthroplasty. *Journal of Orthopaedic Research*, 1992. **10(3)**: pp. 405-422.
- Chiravambath, S., Simha, N. K., Namani, R., and Lewis, J. L. Poroviscoelastic cartilage properties in the mouse from indentation. *Journal of Biomechanical Engineering*, 2009. **131(1)**: pp. 011004-9.
- Cilingir, A. C., Ucara, V., and Kazana, R. Three-dimensional anatomic finite element modelling of hemi-arthroplasty of human hip joint. *Trends in Biomaterials & Artificial Organs*, 2007. **21(1)**: pp. 63 - 72.
- Cilingir, A. C., Ucara, V., Udofia, I. J., and Jin, Z. M. Biphasic finite element modelling of contact mechanics of hemi-arthroplasty of human hip joint. Part i: Metal on cartilage contact. *Trends in Biomaterials & Artificial Organs*, 2008. **22(1)**: pp. 41 - 53.
- Clarke, I. C. Articular cartilage: A review and scanning electron microscope study: 1. The interterritorial fibrillar architecture. *J Bone Joint Surg Br*, 1971. **53-B(4)**: pp. 732-750.
- Clarke, I. C. Role of ceramic implants. Design and clinical success with total hip prosthetic ceramic-to-ceramic bearings. *Clin Orthop Relat Res*, 1992(282): pp. 19-30.
- Clauser, C. E., McConville, J. T., and Young, J. W. Weight, volume and center of mass of segments of the human body. *AMRL-TR-69-70*, 1969: pp. 1-104.
- Coleman, S. H., Bansal, M., Cornell, C. N., and Sculco, T. P. Failure of bipolar hemiarthroplasty: A retrospective review of 31 consecutive bipolar prostheses converted to total hip arthroplasty. *Am J Orthop*, 2001. **30(4)**: pp. 313-9.
- Cook, S., Thomas, K., and Kester, M. Wear characteristics of the canine acetabulum against different femoral prostheses. *J Bone Joint Surg Br*, 1989. **71-B(2)**: pp. 189-197.
- Crowinshield, R. D., Brand, R. A., and Johnston, R. C. The effects of walking

- velocity and age on hip kinematics and kinetics. *Clin Orthop Relat Res*, 1978(132): pp. 140-4.
- Crowninshield, R. D., and Brand, R. A. A physiologically based criterion of muscle force prediction in locomotion. *Journal of Biomechanics*, 1981. **14**(11): pp. 793-801.
- Crowninshield, R. D., Johnston, R. C., Andrews, J. G., and Brand, R. A. A biomechanical investigation of the human hip. *Journal of Biomechanics*, 1978. **11**(1-2): pp. 75-85.
- Cunningham, D. M., and Brown, G. W. Two devices for measuring the forces acting on the human body during walking. *Proceedings of the Society for Experimental Stress Analysis*, 1952. **IX**(2): pp. 75 - 90.
- Dalldorf, P. G., Banas, M. P., Hicks, D. G., and Pellegrini, V. D. Rate of degeneration of human acetabular cartilage after hemiarthroplasty. *Journal of Bone and Joint Surgery-American Volume*, 1995. **77A**(6): pp. 877-882.
- Dalstra, M., and Huiskes, R. Load transfer across the pelvic bone. *Journal of Biomechanics*, 1995. **28**(6): pp. 715 - 724.
- Dalstra, M., Huiskes, R., and Vanerning, L. Development and validation of a three-dimensional finite element model of the pelvic bone. *Journal of Biomechanical Engineering-Transactions of the ASME*, 1995. **117**(3): pp. 272-278.
- Damsgaard, M., Rasmussen, J., Christensen, S. T., Surma, E., and de Zee, M. Analysis of musculoskeletal systems in the anybody modeling system. *Simulation Modelling Practice and Theory SIMS 2004*, 2006. **14**(8): pp. 1100-1111.
- Daniel, M., Antolic, V., Igljic, A., and Kralj-Igljic, V. Determination of contact hip stress from nomograms based on mathematical model. *Medical Engineering & Physics*, 2001. **23**(5): pp. 347-357.
- Daniel, M., Igljic, A., and Kralj-Igljic, V. The shape of acetabular cartilage optimizes hip contact stress distribution. *Journal of Anatomy*, 2005. **207**(1): pp. 85-91.
- Daniel, M., Igljic, A., and Kralj-Igljic, V. Hip contact stress during normal and staircase walking: The influence of acetabular anteversion angle and lateral coverage of the acetabulum. *J Appl Biomech*, 2008. **24**(1): pp. 88-93.
- D'Arcy, J., and Devas, M. Treatment of fractures of the femoral neck by replacement with the thompson prosthesis. *J Bone Joint Surg Br*, 1976. **58-B**(3): pp. 279-286.
- Davies, D. V. Synovial fluid as a lubricant. *Fed Proc*, 1966. **25**(3): pp. 1069 - 1076.
- Davies, D. V., Barnett, C. H., Cochrane, W., and Palfrey, A. J. Electron

- microscopy of articular cartilage in the young adult rabbit. *Ann Rheum Dis*, 1962. **21**: pp. 11-22.
- Davis, W. H., Lee, S. L., and Sokoloff, L. Proposed model of boundary lubrication by synovial-fluid - structuring of boundary water. *Journal of Biomechanical Engineering-Transactions of the Asme*, 1979. **101**(3): pp. 185-192.
- Davy, D., Kotzar, G., Brown, R., Heiple, K., Goldberg, V., Berilla, J., and Burstein, A. Telemetric force measurements across the hip after total arthroplasty. *J Bone Joint Surg Am*, 1988. **70**(1): pp. 45-50.
- Day, W. H., Swanson, S. A. V., and Freeman, M. A. R. Contact pressures in the loaded human cadaver hip. *J Bone Joint Surg Br*, 1975. **57-B**(3): pp. 302-313.
- Devas, M., and Hinves, B. Prevention of acetabular erosion after hemiarthroplasty for fractured neck of femur. *J Bone Joint Surg Br*, 1983. **65-B**(5): pp. 548-551.
- Dintenfass, L. Lubrication in synovial joints - a theoretical analysis - a rheological approach to the problems of joint movements and joint lubrication. *Journal of Bone and Joint Surgery-American Volume*, 1963. **45**(6): pp. 1241-1256.
- Donahue, T. L., Hull, M. L., Rashid, M. M., and Jacobs, C. R. A finite element model of the human knee joint for the study of tibio-femoral contact. *Journal of Biomechanical Engineering*, 2002. **124**(3): pp. 273-280.
- Donzelli, P. S., and Spilker, R. L. A contact finite element formulation for biological soft hydrated tissues. *Computer Methods in Applied Mechanics and Engineering*, 1998. **153**: pp. 63-79.
- Donzelli, P. S., Spilker, R. L., Ateshian, G. A., and Mow, V. C. Contact analysis of biphasic transversely isotropic cartilage layers and correlations with tissue failure. *Journal of Biomechanics*, 1999. **32**(10): pp. 1037-1047.
- Dostal, W. F., and Andrews, J. G. A three-dimensional biomechanical model of hip musculature. *Journal of Biomechanics*, 1981. **14**(11): pp. 803-807, 809-812.
- Dowson, D. Modes of lubrication in human joints. *ARCHIVE: Proceedings of the Institution of Mechanical Engineers, Conference Proceedings 1964-1970 (vols 178-184), Various titles labelled Volumes A to S*, 1966. **181**(3J): pp. 45 - 54.
- Dowson, D. Basic tribology. In: Introduction to the biomechanics of joints and joint replacement. Eds. Dowson, D., and Wright, V. 1981, Mechanical Engineering Publications Ltd.: London. pp. 49 - 60.
- Dowson, D., and Jin, Z. M. Micro-elastohydrodynamic lubrication of synovial

- joints In: *Biomechanics of Osteoarthritis. 1986 Annual Conference on Growing Points on the Biomechanics of Human Joints, Jan. 1986. Engineering in Medicine.* 1986, Leeds, UK, **15**: pp. 63 - 65.
- Dowson, D., Seedhom, B. B., and Johnson, G. R. Bio-mechanics of the lower limb. In: *An introduction to the bio-mechanics of joints and joint replacement.* Eds. Dowson, D., and Wright, V. 1981a, Mechanical Engineering Publications Ltd.: London. pp. 68 - 84.
- Dowson, D., Unsworth, A., Cooke, A. F., and Gvozdanovic, D. Lubrication of joints. In: *An introduction to the bio-mechanics of joints and joint replacement.* Eds. Dowson, D., and Wright, V. 1981b, Mechanical Engineering Publications Ltd.: London. pp. 120-145.
- Drake, R. L., Vogl, W., and Mitchell, A. W. M. *Gray's anatomy for students.* 1st ed. 2005, Elsevier Churchill Livingstone: Toronto. pp. 1058.
- Drinker, H., and Murray, W. The universal proximal femoral endoprosthesis. A short-term comparison with conventional hemiarthroplasty. *J Bone Joint Surg Am*, 1979. **61**(8): pp. 1167-1174.
- Duda, G. N., Schneider, E., and Chao, E. Y. S. Internal forces and moments in the femur during walking. *Journal of Biomechanics*, 1997. **30**(9): pp. 933-941.
- Eberhardt, A. W., Keer, L. M., Lewis, J. L., and Vithoontien, V. An analytical model of joint contact. *Journal of Biomechanical Engineering-Transactions of the ASME*, 1990. **112**(4): pp. 407-413.
- Eberhardt, A. W., Lewis, J. L., and Keer, L. M. Normal contact of elastic spheres with two elastic layers as a model of joint articulation. *Journal of Biomechanical Engineering*, 1991a. **113**(4): pp. 410-417.
- Eberhardt, A. W., Lewis, J. L., and Keer, L. M. Contact of layered elastic spheres as a model of joint contact: Effect of tangential load and friction. *Journal of Biomechanical Engineering-Transactions of the ASME*, 1991b. **113**(1): pp. 107-108.
- Eckstein, F., vonEisenhartRothe, R., Landgraf, J., Adam, C., Loehe, F., MullerGerbl, M., and Putz, R. Quantitative analysis of incongruity, contact areas and cartilage thickness in the human hip joint. *Acta Anatomica*, 1997. **158**(3): pp. 192-204.
- Edwards, J. Physical characteristics of articular cartilage. *ARCHIVE: Proceedings of the Institution of Mechanical Engineers, Conference Proceedings 1964-1970 (vols 178-184), Various titles labelled Volumes A to S*, 1966. **181**(3J): pp. 16-24.
- Elftman, H. Forces and energy changes in the leg during walking. *Am J Physiol*, 1939. **125**(2): pp. 339-356.

- Elmore, S. M., Sokoloff, L., Norris, G., and Carmeci, P. Nature of "imperfect" elasticity of articular cartilage. *Journal of Applied Physiology*, 1963. **18**(2): pp. 393-396.
- English, T. A., and Kilvington, M. In vivo records of hip loads using a femoral implant with telemetric output (a preliminary report). *Journal of Biomedical Engineering*, 1979. **1**(2): pp. 111-115.
- Eyre, D. R., McDevitt, C. A., Billingham, M. E., and Muir, H. Biosynthesis of collagen and other matrix proteins by articular cartilage in experimental osteoarthritis. *Biochem. J.*, 1980. **188**(3): pp. 823-837.
- Federico, S., La Rosa, G., Herzog, W., and Wu, J. Z. Effect of fluid boundary conditions on joint contact mechanics and applications to the modeling of osteoarthritic joints. *Journal of Biomechanical Engineering*, 2004. **126**(2): pp. 220-225 (Erratum in *Journal of Biomechanical Engineering*, 2005, **127**(1), pp. 208-209).
- Ferguson, S. J., Bryant, J. T., Ganz, R., and Ito, K. The influence of the acetabular labrum on hip joint cartilage consolidation: A poroelastic finite element model. *Journal of Biomechanics*, 2000a. **33**(8): pp. 953-960.
- Ferguson, S. J., Bryant, J. T., Ganz, R., and Ito, K. The acetabular labrum seal: A poroelastic finite element model. *Clinical Biomechanics*, 2000b. **15**(6): pp. 463-468.
- Ferguson, S. J., Bryant, J. T., Ganz, R., and Ito, K. Comments on the influence of the acetabular labrum on hip joint cartilage consolidation: A poroelastic finite element model - response. *Journal of Biomechanics*, 2002. **35**(1): pp. 151-152.
- Ferguson, S. J., Bryant, J. T., Ganz, R., and Ito, K. An in vitro investigation of the acetabular labral seal in hip joint mechanics. *Journal of Biomechanics*, 2003. **36**: pp. 171-178.
- Ferronato, M., Gambolati, G., and Teatini, P. Ill-conditioning of finite element poroelasticity equations. *International Journal of Solids and Structures*, 2001. **38**(34-35): pp. 5995-6014.
- Finlay, J. B., Bourne, R. B., Landsberg, R. P. D., and Andrae, P. Pelvic stresses in vitro--i. Malsizing of endoprostheses. *Journal of Biomechanics*, 1986. **19**(9): pp. 703-714.
- Fischer, K. J., Manson, T. T., Pfaeffle, H. J., Tomaino, M. M., and Woo, S. L.-Y. A method for measuring joint kinematics designed for accurate registration of kinematic data to models constructed from ct data. *Journal of Biomechanics*, 2001. **34**(3): pp. 377-383.
- Forster, H., and Fisher, J. The influence of loading time and lubricant on the friction of articular cartilage. *Proceedings of Institution of Mechanical*

- Engineers. Part H - Journal of Engineering in Medicine*, 1996. **210**(2): pp. 109-119.
- Forster, H., and Fisher, J. The influence of continuous sliding and subsequent surface wear on the friction of articular cartilage. *Proceedings of Institution of Mechanical Engineers - Part H*, 1999. **213**: pp. 329 - 345.
- Forster, H., Fisher, J., Dowson, D., and Wright, V. The effect of stationary loading on the friction and boundary lubrication of articular cartilage in the mixed lubrication regime. In: *Proceedings of the 21st Leeds/Lyon Symposium on Tribology, Lubrication and Lubricants*. (Eds. Dowson, D., Taylor, C. M., Childs, T. H. C., and Dalmaz, G.) 1995, Leeds, **30**: pp. 71 - 84 (Elsevier Science, Amsterdam, 1995).
- Fraysse, F., Dumas, R., Cheze, L., and Wang, X. Comparison of global and joint-to-joint methods for estimating the hip joint load and the muscle forces during walking. *Journal of Biomechanics*, 2009. **42**(14): pp. 2357-2362.
- FUJIFILM Recording Media GmbH. How to use: Prescale can measure pressure and visualize pressure range. In. <http://www.fujifilm-prescale.eu/index.php?page=How%20to%20use>, Accessed on 25/01/2010.
- Gebhard, J. S., Amstutz, H. C., Zinar, D. M., and Dorey, F. J. A comparison of total hip-arthroplasty and hemiarthroplasty for treatment of acute fracture of the femoral-neck. *Clinical Orthopaedics and Related Research*, 1992(282): pp. 123-131.
- Genda, E., Konishi, N., Hasegawa, Y., and Miura, T. A computer-simulation study of normal and abnormal hip-joint contact pressure. *Archives of Orthopaedic and Trauma Surgery*, 1995. **114**(4): pp. 202-206.
- Georgiou, G., Siapkara, A., Dimitrakopoulou, A., Provelengios, S., and Dounis, E. Dissociation of bipolar hemiarthroplasty of the hip after dislocation: A report of five different cases and review of literature. *Injury*, 2006. **37**(2): pp. 162-168.
- Ghadially, F. N., Yong, N. K., and Lalonde, J. M. A transmission electron microscopic comparison of the articular surface of cartilage processed attached to bone and detached from bone. *J Anat*, 1982. **135**(Pt 4): pp. 685-706.
- Gleghorn, J. P., Jones, A. R. C., Flannery, C. R., and Bonassar, L. J. Boundary mode lubrication of articular cartilage by recombinant human lubricin. *Journal of Orthopaedic Research*, 2009. **27**(6): pp. 771-777.
- Goldhill, V. B., Lyden, J. P., Cornell, C. N., and Bochner, R. M. Bipolar hemiarthroplasty for fracture of the femoral neck. *J Orthop Trauma*, 1991. **5**(3): pp. 318-24.
- Goldsmith, A. A. J., Hayes, A., and Clift, S. E. Modelling the response of

- biomaterials and soft, hydrated biological tissues using soils consolidation theory. In: *ABAQUS User's Conference*. 1995, Paris, France: pp. 305 - 319.
- Goldsmith, A. A. J., Hayes, A., and Clift, S. E. Application of finite elements to the stress analysis of articular cartilage. *Medical Engineering and Physics*, 1996. **18**(2): pp. 89 - 98.
- Graindorge, S., Ferrandez, W., Jin, Z., Ingham, E., Grant, C., Twigg, P., and Fisher, J. Biphasic surface amorphous layer lubrication of articular cartilage. *Medical Engineering & Physics*, 2005. **27**(10): pp. 836-844.
- Graindorge, S., Ferrandez, W., Jin, Z. M., Ingham, E., and Fisher, J. The natural synovial joint: A finite element investigation of biphasic surface amorphous layer lubrication under dynamic loading conditions. *Proceedings of the Institution of Mechanical Engineers Part J-Journal of Engineering Tribology*, 2006. **220**(J8): pp. 671-681.
- Gray, H. Anatomy of the human body. In, 'Ed.' Lewis, W. H. www.bartleby.com/107/, Accessed on 04/07/2007. Lea & Febiger, 1918: Philadelphia.
- Greenwald, A. S., and Haynes, D. W. Weight-bearing areas in the human hip joint. *J Bone Joint Surg Br*, 1972. **54-B**(1): pp. 157-163.
- Greenwald, A. S., and O'Connor, J. J. The transmission of load through the human hip joint. *Journal of Biomechanics*, 1971. **4**: pp. 507 - 528.
- Grosland, N. M., Shivanna, K. H., Magnotta, V. A., Kallemeyn, N. A., DeVries, N. A., Tadepalli, S. C., and Lisle, C. Ia-femesh: An open-source, interactive, multiblock approach to anatomic finite element model development. *Computer Methods and Programs in Biomedicine*, 2009. **94**(1): pp. 96-107.
- Gu, D., Chen, Y., Dai, K., Zhang, S., and Yuan, J. The shape of the acetabular cartilage surface: A geometric morphometric study using three-dimensional scanning. *Medical Engineering & Physics*, 2008. **30**(8): pp. 1024-1031.
- Guilak, F., Ratcliffe, A., Lane, N., Rosenwasser, M. P., and Mow, V. C. Mechanical and biochemical changes in the superficial zone of articular cartilage in canine experimental osteoarthritis. *J Orthop Res*, 1994. **12**(4): pp. 474-84.
- Guo, J. J., Yang, H., Yang, T., and Tang, T. Disassembly of cemented bipolar prosthesis of the hip. *Orthopedics*, 2008. **31**(8): pp. 813.
- Hadley, N. A., Brown, T. D., and Weinstein, S. L. The effects of contact pressure elevations and aseptic necrosis on the long-term outcome of congenital hip dislocation. *Journal of Orthopaedic Research*, 1990. **8**(4): pp. 504 - 513.
- Haidukewych, G. J., Israel, T. A., and Berry, D. J. Long-term survivorship of

- cemented bipolar hemiarthroplasty for fracture of the femoral neck. *Clin Orthop Relat Res*, 2002(403): pp. 118-26.
- Hak, D. J., Hamel, A. J., Bay, B. K., Sharkey, N. A., and Olson, S. A. Consequences of transverse acetabular fracture malreduction on load transmission across the hip joint. *J Orthop Trauma*, 1998. **12**(2): pp. 90-100.
- Hale, J. E., James Rudert, M., and Brown, T. D. Indentation assessment of biphasic mechanical property deficits in size-dependent osteochondral defect repair. *Journal of Biomechanics*, 1993. **26**(11): pp. 1319-1325.
- Harris, M. D., Anderson, A. E., Ellis, B. J., A.; M. S., C.; J. S., Peters, C. L., J.; G., and Weiss, J. A. Finite element prediction of cartilage contact pressures in normal human hips. In: *55th Annual Meeting of the Orthopaedic Research Society*. 2009, Las Vegas, NV, **34**. Poster No.: 2197.
- Harris, W. H., Rushfeldt, P. D., Carlson, D. E., Scholler, J.-M., and Mann, R. W. Pressure distribution in the hip and selection of hemiarthroplasty. *Proc. Hip Soc.*, 1975. **3**: pp. 93 - 102.
- Harrison, M. H. M., Schajowicz, F., and Trueta, J. Osteoarthritis of the hip: A study of the nature and evolution of the disease. *J Bone Joint Surg Br*, 1953. **35-B**(4): pp. 598-626.
- Hatze, H. A mathematical model for the computational determination of parameter values of anthropomorphic segments. *Journal of Biomechanics*, 1980. **13**(10): pp. 833-843.
- Hayes, W. C., and Bodine, A. J. Flow-independent viscoelastic properties of articular cartilage matrix. *Journal of Biomechanics*, 1978. **11**(8-9): pp. 407-419.
- Hayes, W. C., and Mockros, L. F. Viscoelastic properties of human articular cartilage. *Journal of Applied Physiology*, 1971. **31**(4): pp. 562-568.
- Heller, M. O., Bergmann, G., Deuretzbacher, G., Dürselen, L., Pohl, M., Claes, L., Haas, N. P., and Duda, G. N. Musculo-skeletal loading conditions at the hip during walking and stair climbing. *Journal of Biomechanics*, 2001. **34**(7): pp. 883-893.
- Herzog, W., Diet, S., Suter, E., Mayzus, P., Leonard, T. R., Muller, C., Wu, J. Z., and Epstein, M. Material and functional properties of articular cartilage and patellofemoral contact mechanics in an experimental model of osteoarthritis. *Journal of Biomechanics*, 1998. **31**(12): pp. 1137-1145.
- Higginson, G. R., and Unsworth, A. The lubrication of natural joints. In: *Tribology of natural and artificial joints*. Ed. Dumbleton, J. H. 1981, Elsevier: Amsterdam. pp. 47 - 73.
- Hills, B. A. Oligolamellar lubrication of joints by surface-active phospholipid. *Journal of Rheumatology*, 1989. **16**(1): pp. 82-91.

- Hills, B. A. Boundary lubrication in vivo. *Proceedings of the Institution of Mechanical Engineers. Part H-Journal of Engineering in Medicine*, 2000. **214**(H1): pp. 83-94.
- Hills, B. A., and Crawford, R. W. Normal and prosthetic synovial joints are lubricated by surface-active phospholipid: A hypothesis. *The Journal of Arthroplasty*, 2003. **18**(4): pp. 499-505.
- Hipp, J. A., Sugano, N., Millis, M. B., and Murphy, S. B. Planning acetabular redirection osteotomies based on joint contact pressures. *Clin Orthop Relat Res*, 1999(364): pp. 134-43.
- Hochberg, M. C., and Dougados, M. Pharmacological therapy of osteoarthritis. *Best Practice & Research Clinical Rheumatology*, 2001. **15**(4): pp. 583-593.
- Hodge, W., Carlson, K., Fijan, R., Burgess, R., Riley, P., Harris, W., and Mann, R. Contact pressures from an instrumented hip endoprosthesis. *J Bone Joint Surg Am*, 1989. **71**(9): pp. 1378-1386.
- Hodge, W. A., Fijan, R. S., Carlson, K. L., Burgess, R. G., Harris, W. H., and Mann, R. W. Contact pressures in the human hip joint measured in vivo. *Proceedings of the National Academy of Sciences of the United States of America*, 1986. **83**(9): pp. 2879-2883.
- Holmes, M. H. A theoretical-analysis for determining the nonlinear hydraulic permeability of a soft-tissue from a permeation experiment. *Bulletin of Mathematical Biology*, 1985. **47**(5): pp. 669-683.
- Holmes, M. H. Finite deformation of soft-tissue - analysis of a mixture model in uniaxial compression. *Journal of Biomechanical Engineering-Transactions of the ASME*, 1986. **108**(4): pp. 372-381.
- Holmes, M. H., Lai, W. M., and Mow, V. C. Singular perturbation analysis of the nonlinear, flow-dependent compressive stress relaxation behavior of articular cartilage. *Journal of Biomechanical Engineering*, 1985. **107**(3): pp. 206-218.
- Holmes, M. H., and Mow, V. C. The nonlinear characteristics of soft gels and hydrated connective tissues in ultrafiltration. *Journal of Biomechanics*, 1990. **23**(11): pp. 1145-1156.
- Hori, R. Y., and Mockros, L. F. Indentation tests of human articular cartilage. *Journal of Biomechanics*, 1976. **9**(4): pp. 259-268.
- Hou, J. S., Holmes, M. H., Lai, W. M., and Mow, V. C. Boundary-conditions at the cartilage-synovial fluid interface for joint lubrication and theoretical verifications. *Journal of Biomechanical Engineering-Transactions of the ASME*, 1989. **111**(1): pp. 78-87.
- Hou, J. S., Mow, V. C., Lai, W. M., and Holmes, M. H. An analysis of the squeeze-film lubrication mechanism for articular cartilage. *Journal of*

- Biomechanics*, 1992. **25**(3): pp. 247-259.
- Hurley, M., and Walsh, N. Physical, functional and other non-pharmacological interventions for osteoarthritis. *Best Practice & Research Clinical Rheumatology*, 2001. **15**(4): pp. 569-581.
- Huyghe, J. M., and Janssen, J. D. Quadriphasic mechanics of swelling incompressible porous media. *International Journal of Engineering Science*, 1997. **35**(8): pp. 793-802.
- Iglic, A., Antolic, V., and Srakar, F. Biomechanical analysis of various operative hip joint rotation center shifts. *Archives of Orthopaedic and Trauma Surgery*, 1993a. **112**(3): pp. 124-126.
- Iglic, A., Daniel, M., Kralj-Iglic, V., Antolic, V., and Jaklic, A. Peak hip-joint contact stress in male and female populations. *Journal of Musculoskeletal Research*, 2001. **5**(1): pp. 17 - 21.
- Iglic, A., Iglic, V. K., Antolic, V., Srakar, F., and Stanic, U. Effect of the periacetabular osteotomy on the stress on the human hip joint articular surface. *IEEE Transactions on Rehabilitation Engineering*, 1993b. **1**(4): pp. 207-212.
- Iglic, A., Kralj-Iglic, V., Daniel, M., and Macek-Lebar, A. Computer determination of contact stress distribution and size of weight bearing area in the human hip joint. *Comput Methods Biomech Biomed Engin*, 2002. **5**(2): pp. 185-92.
- Iglic, A., Srakar, F., and Antolic, V. Influence of the pelvic shape on the biomechanical status of the hip. *Clinical Biomechanics*, 1993c. **8**(4): pp. 223-224.
- Ikeuchi, K. The role of synovial fluid in joint lubrication In: *Proceedings of the 21st Leeds/Lyon Symposium on Tribology, Lubrication and Lubricants*. (Eds. Dowson, D., Taylor, C. M., Childs, T. H. C., and Dalmaz, G.) 1995, **30**: pp. 65 - 69 (Elsevier Science, Amsterdam).
- Ilfeld, F. W. Hemiarthroplasty of the hip. *Calif Med*, 1953. **78**(2): pp. 118-20.
- Ipavec, M., Brand, R. A., Pedersen, D. R., Mavcic, B., Kralj-Iglic, V., and Iglic, A. Mathematical modelling of stress in the hip during gait. *Journal of Biomechanics*, 1999. **32**(11): pp. 1229-1235.
- Jain, N. B., Losina, E., Ward, D. M., Harris, M. B., and Katz, J. N. Trends in surgical management of femoral neck fractures in the united states. *Clinical Orthopaedics and Related Research*, 2008. **466**(12): pp. 3116-3122.
- James, S. E., and Gallannaugh, S. C. Bi-articular hemiarthroplasty of the hip: A 7-year follow-up. *Injury*, 1991. **22**(5): pp. 391-393.
- Jeffery, J. A., and Ong, T. J. Femoral head measurement in hemiarthroplasty: Assessment of interobserver error using 3 measuring systems. *Injury*, 2000.

- 31(3)**: pp. 135-138.
- Jensen, R. K. Estimation of the biomechanical properties of three body types using a photogrammetric method. *Journal of Biomechanics*, 1978. **11(8-9)**: pp. 349-358.
- Jin, Z. M., Dowson, D., and Fisher, J. Analysis of fluid film lubrication in artificial hip joint replacements with surfaces of high elastic modulus. *Proceedings of the Institution of Mechanical Engineers Part H-Journal of Engineering in Medicine*, 1997. **211(3)**: pp. 247-256.
- Jin, Z. M., Pickard, J. E., Forster, H., Ingham, E., and Fisher, J. Frictional behaviour of bovine articular cartilage. *Biorheology*, 2000. **37(1 - 2)**: pp. 57 - 63.
- Johnston, R., Brand, R., and Crowninshield, R. Reconstruction of the hip. A mathematical approach to determine optimum geometric relationships. *J Bone Joint Surg Am*, 1979. **61(5)**: pp. 639-652.
- Jonsson, K., Buckwalter, K., Helvie, M., Niklason, L., and Martel, W. Precision of hyaline cartilage thickness measurements. *Acta Radiol*, 1992. **33(3)**: pp. 234-9.
- Katta, J. Self-assembling peptide networks for treatment of cartilage degenerative diseases. PhD Thesis, Institute of Biological and Medical Engineering, School of Mechanical Engineering, University of Leeds. pp. 235.
- Katta, J., Jin, Z., Ingham, E., and Fisher, J. Effect of nominal stress on the long term friction, deformation and wear of native and glycosaminoglycan deficient articular cartilage. *Osteoarthritis and Cartilage*, 2009. **17(5)**: pp. 662-668.
- Katta, J., Pawaskar, S. S., Jin, Z. M., Ingham, E., and Fisher, J. Effect of load variation on the friction properties of articular cartilage. *Proc. Instn Mech. Engrs, Part J: J Engineering Tribology.*, 2007. **221(J3)**: pp. 175 - 181.
- Keenan, K. E., Kourtis, L. C., Besier, T. F., Lindsey, D. P., Gold, G. E., Delp, S. L., and Beaupre, G. S. New resource for the computation of cartilage biphasic material properties with the interpolant response surface method. *Computer Methods in Biomechanics and Biomedical Engineering*, 2008(1): pp. 1 - 8.
- Kelkar, R., and Ateshian, G. A. Contact creep response between a rigid impermeable cylinder and a biphasic cartilage layer using integral transforms. In: *1995 Bioengineering Conference*. (Eds. Hochmuth, R. M., Langrana, N. A., and Hefly, M. S.) 1995, New York, (ASME).
- Keller, M., and Nijs, E. The role of radiographs and us in developmental dysplasia of the hip: How good are they? *Pediatric Radiology*, 2009.

- 39**(Suppl 2): pp. 211-215.
- Kempson, G. E. Mechanical properties of articular cartilage. In: Adult articular cartilag. Ed. Freeman, M. A. R. 1979, Tunbridge Wells, Eng. : Pitman Medical: London.
- Kempson, G. E., Freeman, M. A. R., and Swanson, S. A. V. The determination of a creep modulus for articular cartilage from indentation tests on the human femoral head. *Journal of Biomechanics*, 1971. **4**(4): pp. 239-250.
- Kim, Y. H., Cho, T. J., Park, S., Lee, D. Y., Yoo, W. J., and Choi, I. H. Contact pressure and its distribution at the hip joint after flexion-valgization femoral osteotomy for slipped capital femoral epiphysis. In: *53rd Annual Meeting of the Orthopaedic Research Society*. 2007, San Diego, CA, **32**. Poster No: 1775.
- Kofoed, H., and Kofod, J. Moore prosthesis in the treatment of fresh femoral neck fractures : A critical review with special attention to secondary acetabular degeneration. *Injury*, 1983. **14**(6): pp. 531-540.
- Konishi, N., and Mieno, T. Determination of acetabular coverage of the femoral head with use of a single anteroposterior radiograph. A new computerized technique. *J Bone Joint Surg Am*, 1993. **75**(9): pp. 1318-1333.
- Konrath, G. A., Hamel, A. J., Olson, S. A., Bay, B., and Sharkey, N. A. The role of the acetabular labrum and the transverse acetabular ligament in load transmission in the hip. *J Bone Joint Surg Am*, 1998. **80**(12): pp. 1781-8.
- Korhonen, R. K., Laasanen, M. S., Töyräs, J., Rieppo, J., Hirvonen, J., Helminen, H. J., and Jurvelin, J. S. Comparison of the equilibrium response of articular cartilage in unconfined compression, confined compression and indentation. *Journal of Biomechanics*, 2002. **35**(7): pp. 903-909.
- Kosashvili, Y., Backstein, D., Safir, O., Ran, Y., Loebenberg, M. I., and Ziv, Y. B. Hemiarthroplasty of the hip for fracture--what is the appropriate sized femoral head. *Injury*, 2008. **39**(2): pp. 232-237.
- Kotzar, G. M., Davy, D. T., Goldberg, V. M., Heiple, K. G., Berilla, J., Jr., K. G. H., Brown, R. H., and Burstein, A. H. Telemeterized in vivo hip joint force data: A report on two patients after total hip surgery. *Journal of Orthopaedic Research*, 1991. **9**(5): pp. 621-633.
- Krebs, D. E., Elbaum, L., Riley, P. O., Hodge, W. A., and Mann, R. W. Exercise and gait effects on in vivo hip contact pressures. *PHYS THER*, 1991. **71**(4): pp. 301-309.
- Krebs, D. E., Robbins, C. E., Lavine, L., and Mann, R. W. Hip biomechanics during gait. *J Orthop Sports Phys Ther*, 1998. **28**(1): pp. 51-9.
- Krishnan, R., Kopacz, M., and Ateshian, G. A. Experimental verification of the role of interstitial fluid pressurization in cartilage lubrication. *J Orthop*

- Res*, 2004. **22**(3): pp. 565-70.
- Kumagai, M., Kim, Y. H., Inoue, N., Genda, E., Hua, K., Liang, B. T. L., Koo, T., and Chao, E. Y. S. 3-d dynamic hip contact pressure distribution in daily activities. In: *2003 Summer Bioengineering Conference*. 2003, Key Biscayne, Florida, USA: pp. 53-54.
- Kurrat, H. J., and Oberlander, W. The thickness of the cartilage in the hip joint. *J Anat*, 1978. **126**(Pt 1): pp. 145-55.
- Kurtz, S. M., and Devine, J. N. Peek biomaterials in trauma, orthopedic, and spinal implants. *Biomaterials*, 2007. **28**(32): pp. 4845-4869.
- Kwan, M. K. Finite deformational theory for a nonlinearly permeable biphasic medium. PhD Thesis, Rensselaer Polytechnic Institute.
- Kwan, M. K., Lai, W. M., and Mow, V. C. Fundamentals of fluid transport through cartilage in compression. *Annals of Biomedical Engineering*, 1984. **12**(6): pp. 537-558.
- Kwan, M. K., Lai, W. M., and Mow, V. C. A finite deformation theory for cartilage and other soft hydrated connective tissues - i. Equilibrium results. *Journal of Biomechanics*, 1990. **23**(2): pp. 145 - 155.
- Kyomoto, M., Moro, T., Saiga, K.-i., Miyaji, F., Kawaguchi, H., Takatori, Y., Nakamura, K., and Ishihara, K. Biocompatible polymer layer on co-cr-mo surface for hemi-arthroplasty prevents degeneration of cartilage. In: *56th Annual Meeting of the Orthopaedic Research Society*. 2010, New Orleans, LA, USA, **35**. Poster No.: 2252.
- Lai, W. M., Hou, J. S., and Mow, V. C. A triphasic theory for the swelling and deformation behaviors of articular cartilage. *Journal of Biomechanical Engineering*, 1991. **113**(3): pp. 245-258.
- Lai, W. M., and Mow, V. C. Drag-induced compression of articular-cartilage during a permeation experiment. *Biorheology*, 1980. **17**(1-2): pp. 111-123.
- Lai, W. M., Mow, V. C., and Roth, V. Effects of non-linear strain-dependent permeability and rate of compression on the stress behavior of articular cartilage. *Journal of Biomechanical Engineering-Transactions of the ASME*, 1981. **103**(2): pp. 61-66.
- Lane, J. M., and Weiss, C. Review of articular cartilage collagen research. *Arthritis & Rheumatism*, 1975. **18**(6): pp. 553-562.
- Lee, H.-H., Lo, Y.-C., Lin, L.-C., and Wu, S.-S. Disassembly and dislocation of a bipolar hip prosthesis. *Journal of the Formosan Medical Association*, 2008. **107**(1): pp. 84-88.
- Lei, F., and Szeri, A. Z. Inverse analysis of constitutive models: Biological soft tissues. *Journal of Biomechanics*, 2007. **40**(4): pp. 936-940.
- Lester, G., McGowan, J., Panagis, J., Serrate-Sztejn, S., Tyree, B., Brandt, K.

- D., Goldberg, V. M., Hochberg, M. C., Klippel, J., and Moskowitz, R. Handout on health: Osteoarthritis. In Health Topics. <http://www.niams.nih.gov/hi/topics/arthritis/oahandout.htm>, Accessed on 19/03/2007. National Institute of Arthritis and Musculoskeletal and Skin Diseases, National Institutes of Health.: Bethesda, Maryland, USA.
- Levine, B. R., Meere, P. A., Di Cesare, P. E., and Zuckerman, J. D. Hip fractures treated by arthroplasty. In: The adult hip. 2nd ed. II. Eds. Callaghan, J. J., Rosenberg, A. G., and Rubash, H. E. 2007, Lippincott Williams & Wilkins: Philadelphia, PA, USA. pp. 1187 - 1210.
- Lewis, P. R., and McCutchen, C. W. Mechanism of animal joints: Experimental evidence for weeping lubrication in mammalian joints. *Nature*, 1959. 184: pp. 1285.
- Li, W., Abram, F., Beaudoin, G., Berthiaume, M. J., Pelletier, J. P., and Martel-Pelletier, J. Human hip joint cartilage: Mri quantitative thickness and volume measurements discriminating acetabulum and femoral head. *IEEE Trans Biomed Eng*, 2008. **55**(12): pp. 2731-40.
- Linn, F. C., and Sokoloff, L. Movement and composition of interstitial fluid of cartilage. *Arthritis & Rheumatism*, 1965. **8**(4): pp. 481-494.
- Lipshitz, H., Etheredge, R., 3rd, and Glimcher, M. J. In vitro wear of articular cartilage. *The Journal Of Bone And Joint Surgery. American Volume*, 1975. **57**(4): pp. 527-534.
- Lipshitz, H., Etheredge, R., and Glimcher, M. Changes in the hexosamine content and swelling ratio of articular cartilage as functions of depth from the surface. *J Bone Joint Surg Am*, 1976. **58**(8): pp. 1149-1153.
- Lipshitz, H., and Glimcher, M. J. In vitro studies of the wear of articular cartilage ii. Characteristics of the wear of articular cartilage when worn against stainless steel plates having characterized surfaces. *Wear*, 1979. **52**(2): pp. 297-339.
- Liu, F., Udofia, I., Jin, Z., Hirt, F., Rieker, C., Roberts, P., and Grigoris, P. Comparison of contact mechanics between a total hip replacement and a hip resurfacing with a metal-on-metal articulation. *Proceedings of the Institution of Mechanical Engineers, Part C: Journal of Mechanical Engineering Science*, 2005. **219**(7): pp. 727-732.
- Livermore, J., Ilstrup, D., and Morrey, B. Effect of femoral head size on wear of the polyethylene acetabular component. *J Bone Joint Surg Am*, 1990. **72**(4): pp. 518-528.
- Maas, S. A., Ellis, B. J., Rawlins, D. S., and Weiss, J. A., A comparison of febio, abaqus, and nuke3d results for a suite of verification problems. 2009, Scientific Computing and Imaging Institute, University of Utah: Salt Lake

- City, UT 84112 USA. p. 8.
- MacConaill, M. A. The movements of bones and joints. *J Bone Joint Surg Br*, 1951. **33-B(2)**: pp. 251-257.
- Macirowski, T., Tepic, S., and Mann, R. W. Cartilage stresses in the human hip joint. *Journal of Biomechanical Engineering-Transactions of the Asme*, 1994. **116(1)**: pp. 10 - 18.
- Mak, A. F. The apparent viscoelastic behavior of articular-cartilage - the contributions from the intrinsic matrix viscoelasticity and interstitial fluid-flows. *Journal of Biomechanical Engineering-Transactions of the ASME*, 1986. **108(2)**: pp. 123-130.
- Mankin, H., and Thrasher, A. Water content and binding in normal and osteoarthritic human cartilage. *J Bone Joint Surg Am*, 1975. **57(1)**: pp. 76-80.
- Maroudas, A. Hyaluronic acid films. *ARCHIVE: Proceedings of the Institution of Mechanical Engineers, Conference Proceedings 1964-1970 (vols 178-184), Various titles labelled Volumes A to S*, 1966. **181(3J)**: pp. 122 - 124.
- Martin, P. E., Mungiole, M., Marzke, M. W., and Longhill, J. M. The use of magnetic resonance imaging for measuring segment inertial properties. *Journal of Biomechanics*, 1989. **22(4)**: pp. 367-369, 371-376.
- Matsuda, Y., and Yamamuro, T. Metallosis due to abnormal abrasion of the femoral head in bipolar hip prosthesis. Implant retrieval and analysis in six cases. *Med Prog Technol*, 1994. **20(3-4)**: pp. 185-9.
- Matsuo, A., Jingushi, S., Nakashima, Y., Yamamoto, T., Mawatari, T., Noguchi, Y., Shuto, T., and Iwamoto, Y. Transposition osteotomy of the acetabulum for advanced-stage osteoarthritis of the hips. *Journal of Orthopaedic Science*, 2009. **14(3)**: pp. 266-273.
- Mavcic, B., Pompe, B., Antolic, V., Daniel, M., Igljic, A., and Kralj-Igljic, V. Mathematical estimation of stress distribution in normal and dysplastic human hips. *Journal of Orthopaedic Research*, 2002. **20(5)**: pp. 1025-1030.
- Maxian, T. A., Brown, T. D., and Weinstein, S. L. Chronic stress tolerance levels for human articular cartilage: Two nonuniform contact models applied to long-term follow-up of cdh. *Journal of Biomechanics*, 1995. **28(2)**: pp. 159-166.
- McCann, L., Ingham, E., Jin, Z., and Fisher, J. An investigation of the effect of conformity of knee hemiarthroplasty designs on contact stress, friction and degeneration of articular cartilage: A tribological study. *Journal of Biomechanics*, 2009. **42(9)**: pp. 1326-1331.
- McCann, L., Udofia, I., Ingham, E., Jin, Z., and Fisher, J. The importance of contact stress in knee hemiarthroplasty design: A tribological simulation. In: *Journal of Biomechanics, 16th Congress, European Society of Biomechanics*.

- (Eds. Huiskes, R., and Guilak, F.) 2008, Lucerne, Switzerland, **41**: pp. S268, Presentation O-265.
- McCutchen, C. W. Mechanism of animal joints: Sponge-hydrostatic and weeping bearings. *Nature*, 1959. 184: pp. 1284 - 1285.
- McCutchen, C. W. The frictional properties of animal joints. *Wear*, 1962. **5**(1): pp. 1 - 17.
- McCutchen, C. W. Boundary lubrication by synovial fluid: Demonstration and possible osmotic explanation. *Fed Proc*, 1966. **25**(3): pp. 1061-1068.
- McDevitt, C., and Muir, H. Biochemical changes in the cartilage of the knee in experimental and natural osteoarthritis in the dog. *J Bone Joint Surg Br*, 1976. **58-B**(1): pp. 94-101.
- McGibbon, C. A., Krebs, D. E., Trahan, C. A., Trippel, S. B., and Mann, R. W. Cartilage degeneration in relation to repetitive pressure : Case study of a unilateral hip hemiarthroplasty patient. *The Journal of Arthroplasty*, 1999. **14**(1): pp. 52-58.
- Meachim, G. Cartilage breakdown. In: Scientific foundation of orthopaedics and traumatology. Eds. Owen, R., Goodfellow, J., and Bullough, P. 1980, William Heinemann Medical Books Limited: London. pp. 290 - 296.
- Menschik, F. The hip joint as a conchoid shape. *Journal of Biomechanics*, 1997. **30**(9): pp. 971-973.
- Miyayama, Y., Fukubayashi, T., and Kurosawa, H. Contact study of the hip joint. *Archives of Orthopaedic and Trauma Surgery*, 1984. **103**(1): pp. 13-17.
- Morrell, K. C., Hodge, W. A., Krebs, D. E., and Mann, R. W. Corroboration of in vivo cartilage pressures with implications for synovial joint tribology and osteoarthritis causation. *Proceedings of the National Academy of Sciences of the United States of America*, 2005. **102**(41): pp. 14819-14824.
- Mow, V. C. Role of lubrication in biomechanical joints. *Journal of Lubrication Technology-Transactions of the Asme*, 1969. **91**(2): pp. 320-328.
- Mow, V. C., Ateshian, G. A., and Spilker, R. L. Biomechanics of diarthrodial joints: A review of twenty years of progress. *Journal of Biomechanical Engineering - Transactions of the ASME*, 1993. **115**(4B): pp. 460-467.
- Mow, V. C., Gibbs, M. C., Lai, W. M., Zhu, W. B., and Athanasiou, K. A. Biphasic indentation of articular cartilage - ii. A numerical algorithm and an experimental study. *Journal of Biomechanics*, 1989. **22**(8/9): pp. 853 - 861.
- Mow, V. C., Holmes, M. H., and Lai, W. M. Fluid transport and mechanical properties of articular cartilage: A review. *Journal of Biomechanics*, 1984. **17**(5): pp. 377 - 394.
- Mow, V. C., and Huiskes, R. eds. Basic orthopaedic biomechanics and

- mechano-biology. In Third ed. 2005, Lippincott Williams & Wilkins: Philadelphia. pp. 720.
- Mow, V. C., and Hung, C. T. Biomechanics of articular cartilage. In: Basic biomechanics of the musculoskeletal system. 3rd ed. Eds. Nordin, M., and Frankel, V. H. 2001, Lippincott Williams & Wilkins: Philadelphia, PA, USA. pp. 60-101.
- Mow, V. C., Kuei, S. C., Lai, W. M., and Armstrong, C. G. Biphasic creep and stress relaxation of articular cartilage in compression: Theory and experiments. *Transactions of ASME, Journal of Biomechanical Engineering*, 1980. **102**(1): pp. 73-84.
- Mow, V. C., and Lai, W. M. The optical sliding contact analytical rheometer (oscar) for flow visualization at the articular surface In: *1979 Advances in Bioengineering. Winter Annual Meeting of the American Society of Mechanical Engineers, 2-7 Dec. 1979*. 1979, New York, USA: pp. 97-99 (ASME).
- Mow, V. C., and Lai, W. M. Recent developments in synovial joint biomechanics. *SIAM Review*, 1980. **22**(3): pp. 275 - 317.
- Mow, V. C., Lai, W. M., and Redler, I. Some surface characteristics of articular cartilage--i. A scanning electron microscopy study and a theoretical model for the dynamic interaction of synovial fluid and articular cartilage. *Journal of Biomechanics*, 1974. **7**(5): pp. 449-456.
- Mow, V. C., Ratcliffe, A., and Poole, A. R. Cartilage and diarthrodial joints as paradigms for hierarchical materials and structures. (review). *Biomaterials*, 1992. **13**(2): pp. 67 - 97.
- Muehleman, C., and Arsenis, C. H. Articular cartilage. Part ii. The osteoarthritic joint. *J Am Podiatr Med Assoc*, 1995. **85**(5): pp. 282-286.
- Muir, H., Bullough, P., and Maroudas, A. The distribution of collagen in human articular cartilage with some of its physiological implications. *J Bone Joint Surg Br*, 1970. **52-B**(3): pp. 554-563.
- Mulder, L., Koolstra, J. H., Toonder, J. M. d., and Eijden, T. M. v. Relationship between tissue stiffness and degree of mineralization of developing trabecular bone. *Journal of Biomedical Materials Research Part A*, 2008. **84A**(2): pp. 508-515.
- Mungiole, M., and Martin, P. E. Estimating segment inertial properties: Comparison of magnetic resonance imaging with existing methods. *Journal of Biomechanics*, 1990. **23**(10): pp. 1039-1046.
- Naish, J. H., Xanthopoulos, E., Hutchinson, C. E., Waterton, J. C., and Taylor, C. J. Mr measurement of articular cartilage thickness distribution in the hip. *Osteoarthritis and Cartilage*, 2006. **14**(10): pp. 967-973.

- Nakanishi, K., Tanaka, H., Sugano, N., Sato, Y., Ueguchi, T., Kubota, T., Tamura, S., and Nakamura, H. Mr-based three-dimensional presentation of cartilage thickness in the femoral head. *European Radiology*, 2001. **11**(11): pp. 2178-2183.
- Nakano, T., and Aherne, F. X. Morphology and water and lipid contents of stifle menisci of growing swine. *Can J Vet Res*, 1992. **56**(2): pp. 165-7.
- Oberlander, W. The stress of the human hip joint. Vii. The distribution of cartilage thickness in the acetabulum and its functional explanation. *Anatomy and Embryology*, 1977. **150**(2): pp. 141-153.
- Oloyede, A., and Broom, N. D. Is classical consolidation theory applicable to articular cartilage deformation? *Clinical Biomechanics*, 1991. **6**(4): pp. 206-212.
- Olsen, S., and Oloyede, A. A finite element analysis methodology for representing the articular cartilage functional structure. *Computer Methods in Biomechanics & Biomedical Engineering*, 2002. **5**(6): pp. 377 - 386.
- Ong, B. C., Maurer, S. G., Aharonoff, G. B., Zuckerman, J. D., and Koval, K. J. Unipolar versus bipolar hemiarthroplasty: Functional outcome after femoral neck fracture at a minimum of thirty-six months of follow-up. *J Orthop Trauma*, 2002. **16**(5): pp. 317-22.
- Orford, C. R., and Gardner, D. L. Ultrastructural histochemistry of the surface lamina of normal articular cartilage. *The Histochemical Journal*, 1985. **17**(2): pp. 223-233.
- Orford, C. R., Gardner, D. L., and O'Connor, P. Ultrastructural changes in dog femoral condylar cartilage following anterior cruciate ligament section. *J Anat*, 1983. **137** (Pt 4): pp. 653-63.
- Orthopaedics Developmental dysplasia of the hip. In Orthopaedics. <http://www.lpch.org/DiseaseHealthInfo/HealthLibrary/orthopaedics/ddh.html>, Accessed on 19/03/2007. Lucile Packard Children's Hospital at Stanford: Palo Alto, California.
- Palastanga, N., Field, D., and Soames, R. The lower limb. In: Anatomy and human movement: Structure and function. 5th ed. 2006, Elsevier: Philadelphia. pp. 235 - 470.
- Park, S., Krebs, D. E., and Mann, R. W. Hip muscle co-contraction: Evidence from concurrent in vivo pressure measurement and force estimation. *Gait & Posture*, 1999. **10**(3): pp. 211-222.
- Park, S., Krishnan, R., Nicoll, S. B., and Ateshian, G. A. Cartilage interstitial fluid load support in unconfined compression. *Journal of Biomechanics*, 2003. **36**: pp. 1785 - 1796.
- Parker, M. J., Khan, R. J. K., Crawford, J., and Pryor, G. A. Hemiarthroplasty

- versus internal fixation for displaced intracapsular hip fractures in the elderly: A randomised trial of 455 patients. *J Bone Joint Surg Br*, 2002. **84-B(8)**: pp. 1150-1155.
- Parsons, J. R., and Black, J. The viscoelastic shear behavior of normal rabbit articular cartilage. *Journal of Biomechanics*, 1977. **10(1)**: pp. 21-29.
- Patil, S., Mohammed, A., and Meek, R. Explant removal of a well fixed resurfacing acetabular component. *J Bone Joint Surg Br*, 2008. **90-B(SUPP_III)**: pp. 547.
- Paul, J. P. Biomechanics. The biomechanics of the hip-joint and its clinical relevance. *Proc R Soc Med*, 1966. **59(10)**: pp. 943-8.
- Paul, J. P. Forces transmitted by joints in the human body. *Proceedings of the Institution of Mechanical Engineers*, 1967. **181(3J)**: pp. 8-15.
- Paul, J. P. The effect of walking speed on the force actions transmitted at the hip and knee joints. *Proc R Soc Med.*, 1970. **63(2)**: pp. 200–202.
- Paul, J. P. Force actions transmitted by joints in the human body. *Proceedings of the Royal Society of London. Series B, Biological Sciences*, 1976. **192(1107)**: pp. 163-172.
- Pawaskar, S. S. Contact mechanics modelling of articular cartilage and applications. MSc Thesis, Institute of Biological and Medical Engineering, School of Mechanical Engineering, University of Leeds. pp. 133.
- Pawaskar, S. S., Jin, Z. M., and Fisher, J. Modelling of fluid support inside articular cartilage during sliding. *Proc. Instn Mech. Engrs, Part J: J Engineering Tribology.*, 2007. **221(J3)**: pp. 165 - 174.
- Pedersen, D. R., Brand, R. A., and Davy, D. T. Pelvic muscle and acetabular contact forces during gait. *Journal of Biomechanics*, 1997. **30(9)**: pp. 959-965.
- Peltier, L. F. A history of hip surgery. In: The adult hip. I. Eds. Callaghan, J. J., Rosenberg, A. G., and Rubash, H. E. 2007, Lippincott Williams & Wilkins: Philadelphia, PA, USA. pp. 3-31.
- Penrod, D. D., Davy, D. T., and Singh, D. P. An optimization approach to tendon force analysis. *Journal of Biomechanics*, 1974. **7(2)**: pp. 123-129.
- Persson, B. N. J. Sliding friction. Second ed. 2000, Springer-Verlag: Berlin. pp. 515.
- Phillips, T. The bateman bipolar femoral head replacement. A fluoroscopic study of movement over a four-year period. *J Bone Joint Surg Br*, 1987. **69-B(5)**: pp. 761-764.
- Phillips, T. Thompson hemiarthroplasty and acetabular erosion. *J Bone Joint Surg Am*, 1989. **71(6)**: pp. 913-917.
- Pickard, J., Ingham, E., Egan, J., and Fisher, J. Investigation into the effect of

- proteoglycan molecules on the tribological properties of cartilage joint tissues. *Proceedings of the Institution of Mechanical Engineers, Part H: Journal of Engineering in Medicine*, 1998. **212**(3): pp. 177-182.
- Pollo, F. E. Bracing and heel wedging for unicompartmental osteoarthritis of the knee. *Am J Knee Surg*, 1998. **11**(1): pp. 47-50.
- Quiñonez, A. F., Fisher, J., and Jin, Z. M. A steady-state elastohydrodynamic lubrication model aimed at natural hip joints with physiological loading and anatomical position. *Proceedings of the Institution of Mechanical Engineers, Part J: Journal of Engineering Tribology*, 2008. **222**(3): pp. 503-512.
- Qvist, P., Bay-Jensen, A.-C., Christiansen, C., Dam, E. B., Pastoureau, P., and Karsdal, M. A. The disease modifying osteoarthritis drug (dmoad): Is it in the horizon? *Pharmacological Research*, 2008. **58**(1): pp. 1-7.
- Radin, E. L. Synovial fluid as a lubricant. *Arthritis & Rheumatism*, 1968. **11**(5): pp. 693-695.
- Radin, E. L. M. D., Ehrlich, M. G. M. D., Chernack, R. B. S., Abernethy, P. M. S., Paul, I. L. S. D., and Rose, R. M. S. D. Effect of repetitive impulsive loading on the knee joints of rabbits. *Clinical Orthopaedics & Related Research*, 1978. **131**: pp. 288-293.
- Rajan, V., Caligaris, M., Hung, C., Ahmad, C., and Ateshian, G. Hemiarthroplasties defeat interstitial fluid pressurization in cartilage and promote greater friction than natural joints. In: *56th Annual Meeting of the Orthopaedic Research Society*. 2010, New Orleans, LA, USA, **35**. Poster No.: 2120.
- Rapperport, D. J., Carter, D. R., and Shcurman, D. J. Contact finite-element stress-analysis of the hip-joint. *Journal of Orthopaedic Research*, 1985. **3**(4): pp. 435-446.
- Rasmussen, J., Damsgaard, M., and Voigt, M. Muscle recruitment by the min/max criterion -- a comparative numerical study. *Journal of Biomechanics*, 2001. **34**(3): pp. 409-415.
- Ratcliffe, A., Beauvais, P. J., and Saed-Nejad, F. Differential levels of synovial fluid aggrecan aggregate components in experimental osteoarthritis and joint disuse. *Journal of Orthopaedic Research*, 1994. **12**(4): pp. 464-473.
- Recnik, G., Kralj-Iglic, V., Iglic, A., Antolic, V., Kramberger, S., Rigler, I., Pompe, B., and Vengust, R. The role of obesity, biomechanical constitution of the pelvis and contact joint stress in progression of hip osteoarthritis. *Osteoarthritis and Cartilage*, 2009. **17**(7): pp. 879-882.
- Recnik, G., Kralj-Iglic, V., Iglic, A., Antolic, V., Kramberger, S., and Vengust, R. Higher peak contact hip stress predetermines the side of hip involved in idiopathic osteoarthritis. *Clinical Biomechanics*, 2007. **22**(10): pp. 1119-

1124.

- Redler, I., Mow, V. C., Zimny, M. L., and Mansell, J. The ultrastructure and biomechanical significance of the tidemark of articular cartilage. *Clin Orthop Relat Res*, 1975(112): pp. 357-62.
- Rhee, D. K., Marcelino, J., Baker, M. A., Gong, Y. Q., Smits, P., Lefebvre, V., Jay, G. D., Stewart, M., Wang, H. W., Warman, M. L., and Carpten, J. D. The secreted glycoprotein lubricin protects cartilage surfaces and inhibits synovial cell overgrowth. *Journal of Clinical Investigation*, 2005. **115**(3): pp. 622-631.
- Rizzo, M., and Pace, T. B. Premature failure of a hip hemiarthroplasty secondary to osteolysis and aseptic loosening. *Am J Orthop*, 2003. **32**(4): pp. 206-9.
- Roemhildt, M. L., Coughlin, K. M., Peura, G. D., Fleming, B. C., and Beynon, B. D. Material properties of articular cartilage in the rabbit tibial plateau. *Journal of Biomechanics*, 2006. **39**(12): pp. 2331-2337.
- Rohrle, H., Scholten, R., Sigolotto, C., Sollbach, W., and Kellner, H. Joint forces in the human pelvis-leg skeleton during walking. *Journal of Biomechanics*, 1984. **17**(6): pp. 409-424.
- Ruano-Ravina, A., and Jato Díaz, M. Autologous chondrocyte implantation: A systematic review. *Osteoarthritis and Cartilage*, 2006. **14**(1): pp. 47-51.
- Rushfeld, P. D., Mann, R. W., and Harris, W. H. Influence of cartilage geometry on the pressure distribution in the human hip joint. *Science*, 1979. **204**(4391): pp. 413-415.
- Rushfeldt, P. D., Mann, R. W., and Harris, W. H. Improved techniques for measuring in vitro the geometry and pressure distribution in the human acetabulum--i. Ultrasonic measurement of acetabular surfaces, sphericity and cartilage thickness. *Journal of Biomechanics*, 1981a. **14**(4): pp. 253-255.
- Rushfeldt, P. D., Mann, R. W., and Harris, W. H. Improved techniques for measuring in vitro the geometry and pressure distribution in the human acetabulum--ii. Instrumented endoprosthesis measurement of articular surface pressure distribution. *Journal of Biomechanics*, 1981b. **14**(5): pp. 315-323.
- Russell, M. E., Shivanna, K. H., Grosland, N. M., and Pedersen, D. R. Cartilage contact pressure elevations in dysplastic hips: A chronic overload model. *Journal of Orthopaedic Surgery and Research*, 2006. **1**: pp. 6.
- Rydell, N. Forces in the hip-joint: Part (ii) intravital measurements In: *Proceedings of a Symposium on Biomechanics and Related Bio-Engineering Topics*. (Ed. Kenedi, R. M.) 1965, Glasgow: pp. 351 - 357 (Symposium Publications Division, Pergamon Press, Oxford).

- Rydell, N. W. Forces acting on the femoral head-prosthesis. A study on strain gauge supplied prostheses in living persons. *Acta Orthopaedica Scandinavica*, 1966. **37**(Suppl 88): pp. 1-132.
- Sarfaty, O., and Ladin, Z. A video-based system for the estimation of the inertial properties of body segments. *Journal of Biomechanics*, 1993. **26**(8): pp. 1011-1016.
- Sarzi-Puttini, P., Cimmino, M. A., Scarpa, R., Caporali, R., Parazzini, F., Zaninelli, A., Atzeni, F., and Canesi, B. Osteoarthritis: An overview of the disease and its treatment strategies. *Seminars in Arthritis and Rheumatism*, 2005. **35**(1, Supplement 1): pp. 1-10.
- Schmidt, T. A., Gastelum, N. S., Nguyen, Q. T., Schumacher, B. L., and Sah, R. L. Boundary lubrication of articular cartilage: Role of synovial fluid constituents. *Arthritis & Rheumatism*, 2007. **56**(3): pp. 882-891.
- Schmidt, T. A., and Sah, R. L. Effect of synovial fluid on boundary lubrication of articular cartilage. *Osteoarthritis and Cartilage*, 2007. **15**(1): pp. 35-47.
- Schöllhorn, W. I. Applications of artificial neural nets in clinical biomechanics. *Clinical Biomechanics*, 2004. **19**(9): pp. 876-898.
- Seireg, A., and Arvikar, R. J. A mathematical model for evaluation of forces in lower extremities of the musculo-skeletal system. *Journal of Biomechanics*, 1973. **6**(3): pp. 313-322, IN19-IN20, 323-326.
- Seireg, A., and Arvikar, R. J. The prediction of muscular load sharing and joint forces in the lower extremities during walking. *Journal of Biomechanics*, 1975. **8**(2): pp. 89-102.
- Sekiya, J. K., Martin, R. L., and Lesniak, B. P. Arthroscopic repair of delaminated acetabular articular cartilage in femoroacetabular impingement. *Orthopedics*, 2009. **32**(9): pp. 692.
- Seller, P. C., Dowson, D., and Wright, V. The rheology of synovial fluid. *Rheologica Acta*, 1971. **10**(1): pp. 2-7.
- Sen, D., Alsousou, J., and Fraser, J. Painful hemiarthroplasty due to acetabular erosion: A new technique of treatment. *J Bone Joint Surg Br*, 2009. **91-B**(4): pp. 530-532.
- Setton, L. A., Elliott, D. M., and Mow, V. C. Altered mechanics of cartilage with osteoarthritis: Human osteoarthritis and an experimental model of joint degeneration. *Osteoarthritis and Cartilage*, 1999. **7**: pp. 2 - 14.
- Setton, L. A., Mow, V. C., Müller, F. J., Pita, J. C., and Howell, D. S. Mechanical properties of canine articular cartilage are significantly altered following transection of the anterior cruciate ligament. *Journal of Orthopaedic Research*, 1994. **12**(4): pp. 451-463.
- Setton, L. A., Zhu, W., and Mow, V. C. The biphasic poroviscoelastic

- behavior of articular cartilage: Role of the surface zone in governing the compressive behavior. *Journal of Biomechanics*, 1993. **26**(4-5): pp. 581-592.
- Shamoon, M., and Hochberg, M. C. The role of acetaminophen in the management of patients with osteoarthritis. *The American Journal of Medicine*, 2001. **110**(3, Supplement 1): pp. 46-49.
- Sharkey, P., Rao, R., Hozack, W., Rothman, R., and Carey, C. Conversion of hemiarthroplasty to total hip arthroplasty: Can groin pain be eliminated? *The Journal of arthroplasty*, 1998. **13**(6): pp. 627-630.
- Shepherd, D. E., and Seedhom, B. B. Thickness of human articular cartilage in joints of the lower limb. *Ann Rheum Dis*, 1999. **58**(1): pp. 27-34.
- Siemienski, A. Soft saturation, an idea for load sharing between muscles. Application to the study of human locomotion. In: *Proceedings of the Symposium "Biocomotion: a Century of Research Using Moving Pictures"*. (Eds. Cappozzo, A., Marchetti, M., and Tosi, V.) 1992, Promograph, Rome, Italy: pp. 293-303.
- Simon, W. H. Scale effects in animal joints. I. Articular cartilage thickness and compressive stress. *Arthritis & Rheumatism*, 1970. **13**(3): pp. 244-255.
- Simunek, Z., and Muir, H. Changes in the protein-polysaccharides of pig articular cartilage during prenatal life, development and old age. *Biochem J*, 1972. **126**(3): pp. 515-23.
- Smith, G. D., Knutsen, G., and Richardson, J. B. A clinical review of cartilage repair techniques. *J Bone Joint Surg Br*, 2005. **87-B**(4): pp. 445-449.
- Smith, S. L., Ash, H. E., and Unsworth, A. A tribological study of uhmwpe acetabular cups and polyurethane compliant layer acetabular cups. *Journal of Biomedical Materials Research*, 2000. **53**(6): pp. 710-716.
- Sokoloff, L. Elasticity of aging cartilage. *Federation Proceedings*, 1966. **25**(3): pp. 1089 - 1095.
- Soltz, M. A., and Ateshian, G. A. Experimental verification and theoretical prediction of cartilage interstitial fluid pressurization at an impermeable contact interface in confined compression. *Journal of Biomechanics*, 1998. **31**(10): pp. 927-934.
- Soltz, M. A., and Ateshian, G. A. A conewise linear elasticity mixture model for the analysis of tension-compression nonlinearity in articular cartilage. *Journal of Biomechanical Engineering*, 2000. **122**(6): pp. 576-586.
- Soreide, O., Skjaerven, R., and Alho, A. The risk of acetabular protrusion following prosthetic replacement of the femoral-head. *Acta Orthopaedica Scandinavica*, 1982. **53**(5): pp. 791-794.
- Soslowsky, L. J., Flatow, E. L., Bigliani, L. U., Pawluk, R. J., Ateshian, G. A., and Mow, V. C. Quantitation of in situ contact areas at the glenohumeral

- joint: A biomechanical study. *J Orthop Res*, 1992. **10**(4): pp. 524-34.
- Spilker, R. L., Suh, J. K., and Mow, V. C. A finite element analysis of the indentation stress-relaxation response of linear biphasic articular-cartilage. *Journal of Biomechanical Engineering-Transactions of the ASME*, 1992. **114**(2): pp. 191-201.
- Stanescu, R., and Leibovich, S. The negative charge of articular cartilage surfaces. An electron microscopic study using cationized ferritin. *J Bone Joint Surg Am*, 1982. **64**(3): pp. 388-398.
- Stansfield, B. W., Nicol, A. C., Paul, J. P., Kelly, I. G., Graichen, F., and Bergmann, G. Direct comparison of calculated hip joint contact forces with those measured using instrumented implants. An evaluation of a three-dimensional mathematical model of the lower limb. *Journal of Biomechanics*, 2003. **36**(7): pp. 929-936.
- Stewart, H. D., and Papagiannopoulos, G. Hemiarthroplasty: A progression in treatment? *J R Coll Surg Edinb*, 1986. **31**(6): pp. 345-350.
- Stockwell, R. A., and Scott, J. E. Distribution of acid glycosaminoglycans in human articular cartilage. 1967. **215**(5108): pp. 1376-1378.
- Stokes, I., Chegini, S., Ferguson, S., Gardner-Morse, M., Iatridis, J., and Laible, J. Limitation of finite element analysis of poroelastic behavior of biological tissues undergoing rapid loading. *Annals of Biomedical Engineering*, 2010.
- Sun, D. N., Gu, W. Y., Guo, X. E., Lai, W. M., and Mow, V. C. A mixed finite element formulation of triphasic mechano-electrochemical theory for charged, hydrated biological soft tissues. *International Journal for Numerical Methods in Engineering*, 1999. **45**(10): pp. 1375-1402.
- Swann, A. C., and Seedhom, B. B. Improved techniques for measuring the indentation and thickness of articular cartilage. *ARCHIVE: Proceedings of the Institution of Mechanical Engineers, Part H: Journal of Engineering in Medicine 1989-1996 (vols 203-210)*, 1989. **203**(38): pp. 143-150.
- Swann, D. A., Hendren, R. B., Radin, E. L., Sotman, S. L., and Duda, E. A. The lubricating activity of synovial fluid glycoproteins. *Arthritis and Rheumatism*, 1981. **24**(1): pp. 22-30.
- Swann, D. A., Radin, E. L., and Hendren, R. B. Lubrication of articular-cartilage by synovial-fluid glycoproteins. *Arthritis and Rheumatism*, 1979. **22**(6): pp. 665-666.
- Swann, D. A., Silver, F. H., Slayter, H. S., Stafford, W., and Shore, E. The molecular-structure and lubricating activity of lubricin isolated from bovine and human synovial-fluids. *Biochemical Journal*, 1985. **225**(1): pp. 195-201.
- Tortora, G. J., and Grabowski, S. R. Introduction to the human body: The

- essentials of anatomy and physiology. Sixth ed. 2004, John Wiley & Sons, Inc.: USA. pp. 619.
- Torzilli, P. A. Influence of cartilage conformation on its equilibrium water partition. *Journal of Orthopaedic Research*, 1985. **3**(4): pp. 473-483.
- Torzilli, P. A. Water content and equilibrium water partition in immature cartilage. *Journal of Orthopaedic Research*, 1988. **6**(5): pp. 766-769.
- Udofia, I., Liu, F., Jin, Z., Roberts, P., and Grigoris, P. The initial stability and contact mechanics of a press-fit resurfacing arthroplasty of the hip. *J Bone & Joint Surg Br*, 2007. **89-B**(4): pp. 549-556.
- van der Meulen, M. C. H., Beaupré, G. S., Smith, R. L., Giddings, V. L., Allen, W. A., Athanasiou, K. A., Zhu, C. F., Song, Y., Mandell, J. A., Poser, R. D., and Goodman, S. B. Factors influencing changes in articular cartilage following hemiarthroplasty in sheep. *Journal of Orthopaedic Research*, 2002. **20**(4): pp. 669-675.
- Verberne, G. A femoral head prosthesis with a built-in joint. A radiological study of the movements of the two components. *J Bone Joint Surg Br*, 1983. **65-B**(5): pp. 544-547.
- Verberne, G., Merkher, Y., Halperin, G., Maroudas, A., and Etsion, I. Techniques for assessment of wear between human cartilage surfaces. *Wear*, 2009. **266**(11-12): pp. 1216-1223.
- Vermeer, P. A., and Verruijt, A. An accuracy condition for consolidation by finite elements. *International Journal for Numerical and Analytical Methods in Geomechanics.*, 1981. **5**(1): pp. 1-14.
- Visible Human Project Full pelvis. In. http://www.nlm.nih.gov/research/visible/visible_human.html, Accessed on February 2005. National Library of Medicine - National Institutes of Health.
- von Eisenhart, R., Adam, C., Steinlechner, M., Müller-Gerbl, M., and Eckstein, F. Quantitative determination of joint incongruity and pressure distribution during simulated gait and cartilage thickness in the human hip joint. *Journal of Orthopaedic Research*, 1999. **17**(4): pp. 532-539.
- von Eisenhart-Rothe, R., Eckstein, F., Muller-Gerbl, M., Landgraf, J., Rock, C., and Putz, R. Direct comparison of contact areas, contact stress and subchondral mineralization in human hip joint specimens. *Anatomy and Embryology*, 1997. **195**(3): pp. 279-288.
- von Eisenhart-Rothe, R., Witte, H., Steinlechner, M., Muller-Gerbl, M., Putz, R., and Eckstein, F. Quantitative determination of the contact pressure distribution in the hip joint during gait. *Der Unfallchirurg*, 1999. **V102**(8): pp. 625-631.
- Wachtl, S. W., Jakob, R. P., and Gautier, E. Ten-year patient and prosthesis

- survival after unipolar hip hemiarthroplasty in female patients over 70 years old. *The Journal of Arthroplasty*, 2003. **18**(5): pp. 587-591.
- Wagner, H. Surface replacement arthroplasty of the hip. *Clin Orthop Relat Res*, 1978(134): pp. 102-30.
- Walker, P. S., Dowson, D., Longfield, M. D., and Wright, V. "boosted lubrication" in synovial joints by fluid entrapment and enrichment. *Annals of the Rheumatic Diseases*, 1968. **27**(6): pp. 512-520.
- Walker, P. S., Sikorski, J., Dowson, D., Longfield, M. D., Wright, V., and Buckley, T. Behaviour of synovial fluid on surfaces of articular cartilage. A scanning electron microscope study. *Ann Rheum Dis*, 1969. **28**(1): pp. 1-14.
- Wan, L., de Asla, R. J., Rubash, H. E., and Li, G. Determination of in-vivo articular cartilage contact areas of human talocrural joint under weight bearing conditions. *Osteoarthritis and Cartilage*, 2006. **14**(12): pp. 1294-1301.
- Wang, A., Lin, R., Polineni, V. K., Essner, A., Stark, C., and Dumbleton, J. H. Carbon fiber reinforced polyether ether ketone composite as a bearing surface for total hip replacement. *Tribology International*, 1998. **31**(11): pp. 661-667.
- Wang, M.-J., Wu, W.-Y., Lin, K.-C., Yang, S.-N., and Lu, J.-M. Automated anthropometric data collection from three-dimensional digital human models. *The International Journal of Advanced Manufacturing Technology*, 2007. **32**(1): pp. 109-115.
- Warner, M. D. Finite element biphasic modelling of articular cartilage: An investigation into crystal induced damage. PhD Thesis, University of Bath. pp. 177.
- Warner, M. D., Taylor, W. R., and Clift, S. E. Finite element biphasic indentation of cartilage: A comparison of experimental indenter and physiological contact geometries. *Proceedings of Institution of Mechanical Engineers - Part H*, 2001a. **215**: pp. 487-496.
- Warner, M. D., Taylor, W. R., and Clift, S. E. A method for determining contact between a non-porous surface and articular cartilage in a biphasic fe model. In: *Computer Methods in Biomechanics and Biomedical Engineering – 3*. (Eds. Middleton, J., Shrive, N. G., and Pande, G. N.) 2001b, Lisbon, Portugal: pp. 207-212 (Gordon and Breach Science Publishers, Amsterdam).
- Weinrauch, P. C. L., Moore, W. R., Shooter, D. R., Wilkinson, M. P. R., Bonrath, E. M., Dedy, N. J., McMeniman, T. J., Jabur, M. K. A., Whitehouse, S. L., and Crawford, R. W. Early prosthetic complications after unipolar hemiarthroplasty. *ANZ Journal of Surgery*, 2006. **76**(6): pp. 432-435.

- Weiss, C., Rosenberg, L., and Helfet, A. J. An ultrastructural study of normal young adult human articular cartilage. *J Bone Joint Surg Am*, 1968. **50**(4): pp. 663-674.
- Whittaker, R. P., Abeshaus, M. M., Scholl, H. W., and Chung, S. M. K. Fifteen years' experience with metallic endoprosthesis replacement of the femoral head for femoral neck fractures. *The Journal of Trauma*, 1972. **12**(9): pp. 799-806.
- Wiberg, G. Studies on dysplastic acetabula and congenital subluxation of the hip joint; with special reference to the complication of osteoarthritis. *Acta Chir Scandinavica*, 1939. **83** (Supplement 58).
- Wilkins, J. Proteolytic destruction of synovial boundary lubrication. 1968. **219**(5158): pp. 1050-1051.
- Williams, R. J., III, Ranawat, A. S., Potter, H. G., Carter, T., and Warren, R. F. Fresh stored allografts for the treatment of osteochondral defects of the knee. *J Bone Joint Surg Am*, 2007. **89**(4): pp. 718-726.
- Wu, J. Z., and Herzog, W. Finite element simulation of location- and time-dependent mechanical behavior of chondrocytes in unconfined compression tests. *Annals of Biomedical Engineering*, 2000. **28**(3): pp. 318-330.
- Wyler, A., Bousson, V., Bergot, C., Polivka, M., Leveque, E., Vicaut, E., and Laredo, J.-D. Comparison of mr-arthrography and ct-arthrography in hyaline cartilage-thickness measurement in radiographically normal cadaver hips with anatomy as gold standard. *Osteoarthritis and Cartilage*, 2009. **17**(1): pp. 19-25.
- Xi, J., Hu, X., and Jin, Y. Shape analysis and parameterized modeling of hip joint. *Journal of Computing and Information Science in Engineering*, 2003. **3**(3): pp. 260-265.
- Yamagata, M., Chao, E. Y., Ilstrup, D. M., Melton III, L. J., Coventry, M. B., and Stauffer, R. N. Fixed-head and bipolar hip endoprostheses: A retrospective clinical and roentgenographic study. *The Journal of Arthroplasty*, 1987. **2**(4): pp. 327-341.
- Yang, T. A three-dimensional biphasic finite element formulation for hydrated soft tissue. PhD Thesis, Mechanical, Aeronautical and Nuclear Engineering, Rensselaer Polytechnic Institute. pp. 164.
- Yang, T., and Spilker, R. L. A lagrange multiplier mixed finite element formulation for three-dimensional contact of biphasic tissues. *Journal of Biomechanical Engineering*, 2007. **129**(3): pp. 457-471.
- Yao, J. Q., and Seedhom, B. B. A new technique for measuring contact areas in human joints - the "3s technique". *Proceedings of the Institution of Mechanical Engineers, Part H: Journal of Engineering in Medicine*, 1991.

205(28): pp. 69-72.

- Yoshida, H., Faust, A., Wilckens, J., Kitagawa, M., Fetto, J., and Chao, E. Y.-S. Three-dimensional dynamic hip contact area and pressure distribution during activities of daily living. *Journal of Biomechanics*, 2006. **39**(11): pp. 1996-2004.
- Yoshida, H., Kobayashi, K., Sakamoto, M., and Tanabe, Y. Determination of joint contact area using mri. *Japanese Journal of Radiological Technology*, 2009. **65**(10): pp. 1407-14.
- Young, J. W., Chandler, R. F., Snow, C. C., Robinette, K. M., Zehner, G., F., and Lofberg, M., S. Anthropometric and mass distribution characteristics of the adult female. *FAA-AM-83-16*, 1983: pp. 1-110.

Appendix A Sample Input Files

A.1 Natural Hip Joint

```

*****
**A typical input file for the natural hip joint
*****
*Heading
*Preprint, echo=NO, model=NO, history=NO, contact=YES
*constraint controls, print=yes
*FILE FORMAT, ZERO INCREMENT, ASCII
**
*Restart, write, frequency=1
*****
*INCLUDE, INPUT=G:\PhD_FE\3D_Models\natural_joint\final\pel.geom
*INCLUDE, INPUT=G:\PhD_FE\3D_Models\natural_joint\final\pel_cart_finer.geom
**
*INCLUDE, INPUT=G:\PhD_FE\3D_Models\natural_joint\final\fem_cart_00.geom
*INCLUDE, INPUT=G:\PhD_FE\3D_Models\natural_joint\final\femurBall20.geom
**
*****
**
*TIE, NAME=FEM_CART, TIED NSET=N_BOT_2, ADJUST=YES,
TYPE=SURFACE TO SURFACE
S_CART_FEM, S_FEM_BALL
**
*TIE, NAME=PEL_CART, TIED NSET=N_BOT, ADJUST=NO, TYPE=SURFACE
TO SURFACE
S_CART_PEL, S_PEL
**
*****
**
** MATERIALS
**
**
*MATERIAL, NAME=MTL_CORT
*ELASTIC
17.0E3, 0.3
**
*MATERIAL, NAME=MTL_CANCL_PEL
*ELASTIC
0.07E3, 0.2
**
*MATERIAL, NAME=MTL_SUBCHOND_PEL
*ELASTIC
2.0E3, 0.3
**
*Material, name=MTL_PORO_HYPERELASTIC
*Hyperelastic, neo hooke
0.265019, 5.47522
*Permeability, specific=1.

```

```

0.000983,4.
**
**
*INITIAL CONDITIONS, TYPE=RATIO
N_CART, 4.0
N_CART_2, 4.0
**
** -----
**
**
** INTERACTION PROPERTIES
**
*Surface Interaction, name=IntProp-1
1.,
*Friction
0.,
**
** SURFACE BEHAVIOR, PRESSURE-OVERCLOSURE=EXPONENTIAL
0.01, 0.01
**
**
** CONSTRAINT CONTROLS, NO CHECKS
**
** INTERACTIONS
**
** Interaction: Int-1
** Contact Pair, interaction=IntProp-1, small sliding, type=surface to surface
S_CART, S_CART_2
**
** Clearance, Master=S_CART_2, Slave=S_CART, value=0.0
**
** -----
**
** STEP: LOAD_Y
**
*Step, name=LOAD_000_Y, nlgeom=YES, inc=10000, amplitude=RAMP
Apply load Y
**Soils, consolidation, end=PERIOD, utol=100, stabilize
1, 1, 1e-15, 1
**
*****
*Boundary, op=new
**
**
N_PEL_HOLD, PINNED
**
**
N_FEM_BALL, 1, 1
N_FEM_BALL, 3, 3
**
**
** Name: CART_SIDE Type: Pore pressure
*Boundary, op=new
N_CART_SIDE, 8, 8
N_CART_SIDE_2, 8, 8
**

```

```

*****
** LOADS
**
** Name: N_LOAD  Type: Concentrated force
**
** *Cload, op=NEW
N_F_CENTRE, 2, 2000
**
**
** *SFLOW
S_CART, QNU
S_CART_2, QNU
S_CART_PEL, QD, 0.0
S_CART_FEM, QD, 0.0
**
** *CONTROLS, PARAMETERS=TIME INCREMENTATION
,,,,30,,
,,,,,
,,,,,
****
** *CONTROLS, PARAMETERS=FIELD, FIELD=PORE FLUID PRESSURE
10000,1,,,,,
,,
** *CONTROLS, PARAMETERS=FIELD, FIELD=DISPLACEMENT
10000,1,,,,,
,,
**
** *Controls, parameters=constraints
,,1,1,,
****
,,,,,
**
*****
** OUTPUT REQUESTS
**
** *Restart, write, frequency=0
**
** *FIELD OUTPUT: F-Output-1
**
** *Output, field
** *Node Output
CF, POR, RF, U, VF
** *Element Output, directions=YES
FLUVR, FLVEL, S
** *Contact Output
CSTRESS,
**
** *CONTACT FILE, SLAVE=S_CART, FREQUENCY=1, NSET=N_TOP
CSTRESS
** *CONTACT FILE, SLAVE=S_CART, FREQUENCY=1, NSET=N_TOP
CFN, CFS, CFT, CAREA
**
**
** *NODE FILE, FREQUENCY=1, NSET=N_TOP
POR, COORD, U
**
** *NODE FILE, FREQUENCY=1, NSET=N_TOP_2

```

POR, COORD, U

**

*Output, history, frequency=10

*Contact Output

CFN, CFS, CFT, CAREA

*Energy Output

ALLIE, ALLSD

**

*End Step

**

A.2 Hip Joint with Hemiarthroplasty

```

*****
**A typical input file for the natural hip joint
*****
*Heading
*Preprint, echo=NO, model=NO, history=NO, contact=YES
*constraint controls, print=yes
*FILE FORMAT, ZERO INCREMENT, ASCII
**
*Restart, write, frequency=1
*****
*INCLUDE, INPUT=G:\PhD_FE\3D_Models\gait_analysis\final_files\pel.geom
*INCLUDE, INPUT=G:\PhD_FE\3D_Models\gait_analysis\final_files\pel_cart.geom
**
**INCLUDE, INPUT=G:\PhD_FE\3D_Models\gait_analysis\final_files\IND_3D.geom
*INCLUDE,
INPUT=G:\PhD_FE\3D_Models\gait_analysis\final_files\femurBall05.geom
*****
*TIE, NAME=PEL_CART, TIED NSET=N_BOT, ADJUST=NO, TYPE=SURFACE
TO SURFACE
S_CART_PEL, S_PEL
**
*****
**
** MATERIALS
**
**
*MATERIAL, NAME=MTL_CORT
*ELASTIC
17.0E3, 0.3
**
*MATERIAL, NAME=MTL_CANCL_PEL
*ELASTIC
0.07E3, 0.2
**0.5E3, 0.2
**
*MATERIAL, NAME=MTL_SUBCHOND_PEL
*ELASTIC
2.0E3, 0.3
**
*MATERIAL, NAME=MTL_COCHR
*ELASTIC
2.2E5, 0.3
**
*Material, name=MTL_PORO_HYPERELASTIC
*Hyperelastic, neo hooke
0.265019, 5.47522
*Permeability, specific=1.
0.000983,4.
**
**
*INITIAL CONDITIONS, TYPE=RATIO
N_CART, 4.0
** -----

```

```

**
**
** INTERACTION PROPERTIES
**
*Surface Interaction, name=IntProp-1
1.,
*Friction
0.,
**
**
** CONSTRAINT CONTROLS, NO CHECKS
**
** INTERACTIONS
**
** Interaction: Int-1
** Contact Pair, interaction=IntProp-1, small sliding
S_CART, S_FEM_BALL
**
** Clearance, Master=S_FEM_BALL, Slave=S_CART, value=0.5
**
** -----
**
** STEP: INITIAL CONTACT
**
** Step, name=IniCont_X, nlgeom=YES, amplitude=RAMP, inc=10000
Initiate Contact X
**Static
1, 1, 1e-15, 1,
*****
**Boundary, op=NEW
**
N_PEL_HOLD, PINNED
**
**
N_FEM_BALL, 2, 2
N_FEM_BALL, 3, 3
**
*****
**
N_FEM_BALL, 1, 1, -0.36
**
**End Step
** -----
**
** STEP: INITIAL CONTACT
**
** Step, name=IniCont_Y, nlgeom=YES, amplitude=RAMP, inc=10000
Initiate Contact Y
**Static
1, 1, 1e-15, 1,
*****
**Boundary, op=NEW
**
N_PEL_HOLD, PINNED
**
N_FEM_BALL, 3, 3

```

```

**
*Boundary, op=new, fixed
N_FEM_BALL, 1, 1
**
**
*****
**
*Boundary, op=NEW
N_FEM_BALL, 2, 2, 0.36
**
*End Step
** -----
**
** STEP: LOAD
**
*Step, name=LOAD_000, ngeom=YES, inc=10000, amplitude=RAMP
Apply load
*Soils, consolidation, end=PERIOD, utol=100, stabilize
1, 1, 0.100E-14, 1
**
*****
*Boundary, op=new
**
**
N_PEL_HOLD, PINNED
**
** Name: CART_SIDE Type: Pore pressure
*Boundary, op=new
N_CART_SIDE, 8, 8
**
*****
** LOADS
**
** Name: N_LOAD Type: Concentrated force
**
*Clod, op=NEW
N_F_CENTRE, 1, -167.42249000
N_F_CENTRE, 2, 584.53753000
N_F_CENTRE, 3, -227.37315000
**
**
*SFLOW
S_CART, QNU
S_CART_PEL, QD, 0.0
**
*CONTROLS, PARAMETERS=TIME INCREMENTATION
,,,,,30,,,
,,,,,
,,,,,
**
*CONTROLS, PARAMETERS=FIELD, FIELD=PORE FLUID PRESSURE
10000,0.1,,,,,
**
**
*CONTROLS, ANALYSIS=DISCONTINUOUS
**
**CONSTRAINT CONTROLS, NO CHECKS

```

** OUTPUT REQUESTS

**

**Restart, write, frequency=0

**

** FIELD OUTPUT: F-Output-1

**

*Output, field

*Node Output

CF, POR, RF, U

*Element Output, directions=YES

FLUVR, FLVEL, S

*Contact Output

CSTRESS,

**

*CONTACT FILE, SLAVE=S_CART, FREQUENCY=1, NSET=N_TOP
CSTRESS

*CONTACT FILE, SLAVE=S_CART, FREQUENCY=1, NSET=N_TOP
CFN, CFS, CFT, CAREA

**

**

*NODE FILE, FREQUENCY=1, NSET=N_TOP

POR, COORD, U

**

**

*Output, history, frequency=10

*Contact Output

CFN, CFS, CFT, CAREA

*Energy Output

ALLIE, ALLSD

**

*End Step

** -----

Appendix B Pseudo Code of FORTRAN User Subroutines

B.1 Cartilage Surface against Cartilage Surface

```

*****
C THIS PROGRAM IS WRITTEN BY SAINATH SHRIKANT PAWASKAR
C WRITTEN ON - 13/03/2006
C LAST MODIFIED ON - 16/02/2010
*****
SUBROUTINE URDFIL(LSTOP,LOVRWRT,KSTEP,KINC,DTIME,TIME)
C
C   INCLUDE 'ABA_PARAM.INC'
C
C   DIMENSION ARRAY(513), JRRAY(NPRECD,513),TIME(2)
C   EQUIVALENCE (ARRAY(1),JRRAY(1,1))
C *****
C DECLARATIONS
C
C DATA STRUCTURE WHICH STORES THE CONTACT AND OTHER
C INFORMATION ABOUT TWO SURFACES. THIS DATA STRUCTURE IS USED
C TO SHARE INFORMATION ACROSS TWO SUBROUTINES; URDFIL AND
C FLOW

TYPE ELE_DATA
SEQUENCE
DOUBLE PRECISION :: NODE_COORD(24)
DOUBLE PRECISION :: NEW_NODE_COORD(24)
DOUBLE PRECISION :: OPP_NODE_COORD(24)
DOUBLE PRECISION :: NEW_OPP_NODE_COORD(24)
DOUBLE PRECISION :: IPT_COORD(24)
DOUBLE PRECISION :: NEW_IPT_COORD(24)
DOUBLE PRECISION :: OPP_IPT_COORD(24)
DOUBLE PRECISION :: NEW_OPP_IPT_COORD(24)
DOUBLE PRECISION :: POR(8)
DOUBLE PRECISION :: OPP_POR(8)
DOUBLE PRECISION :: CPRESS(8)
DOUBLE PRECISION :: OPP_CPRESS(8)
DOUBLE PRECISION :: ELE_CAREA
DOUBLE PRECISION :: OPP_ELE_CAREA
DOUBLE PRECISION :: AVG_CPRESS
DOUBLE PRECISION :: OPP_AVG_CPRESS
DOUBLE PRECISION :: AVG_POR
DOUBLE PRECISION :: OPP_AVG_POR
DOUBLE PRECISION :: CPRESS_F
DOUBLE PRECISION :: POR_F
DOUBLE PRECISION :: ANGLE_X
DOUBLE PRECISION :: ANGLE_Y
DOUBLE PRECISION :: ANGLE_Z
DOUBLE PRECISION :: DUMMY(5)
INTEGER :: ELE_NUM
INTEGER :: OPP_ELE_NUM

```

```

INTEGER :: DUMMY2(22)
INTEGER :: NODE_NUM(8)
INTEGER :: OPP_NODE_NUM(8)
INTEGER :: IPT_NUM(8)
INTEGER :: OPP_IPT_NUM(8)
INTEGER :: IS_CONT(8)
INTEGER :: OPP_IS_CONT(8)
END TYPE ELE_DATA

```

```

TYPE (ELE_DATA) :: K_ELE_DETAILS(12000)

```

```

COMMON K_ELE_DETAILS

```

```

PARAMETER (THRESHOLD_CSTRESS=0.0D-7)
PARAMETER (THRESHOLD_DIST=0.0D-7)

```

```

C ONLY FOR CART CART MODELS

```

```

PARAMETER (THRESHOLD_PRESS_PLUS_CPRESS=1.0D-4)

```

```

*****

```

```

C OTHER DECLARATIONS

```

```

CHARACTER*80 K_NODE_SET

```

```

CHARACTER*80 SURFACE_N_SET, THIS_SURF, IS_CART_CART

```

```

...

```

```

C TEMPORARY DATA STRUCTURE TO STORE INFORMATION ABOUT THE
MASTER SURFACE

```

```

C THESE VALUES ARE THEN TRANSFERRED TO MAIN DATA STRUCTURE

```

```

TYPE OPP_ELE_DATA

```

```

SEQUENCE

```

```

DOUBLE PRECISION :: NODE_COORD(24)

```

```

DOUBLE PRECISION :: NEW_NODE_COORD(24)

```

```

DOUBLE PRECISION :: POR(8)

```

```

DOUBLE PRECISION :: DUMMY1(16)

```

```

INTEGER :: ELE_NUM

```

```

INTEGER :: DUMMY2(7)

```

```

INTEGER :: NODE_NUM(8)

```

```

INTEGER :: IS_CONT(8)

```

```

END TYPE OPP_ELE_DATA

```

```

TYPE (OPP_ELE_DATA) :: K_OPP_ELE_DETAILS(12000)

```

```

...

```

```

*****

```

```

C INITIALIZATION

```

```

IS_CART_CART = 'Y'

```

```

LSTOP = 0

```

```

LOVRWRT = 1

```

```

LOP = 0

```

```

K_NODE_SET = 'NOT_N_TOP'

```

```

THIS_SURF = 'N_S_CART'

```

```

*****

```

```

NO_OF_NODES = 4
NO_OF_ELEMENTS = 12000
NO_OF_DIM = 3
*****
DO K1=1,999999
  IF(KSTEP .EQ. 1 .AND. KINC. EQ. 1) THEN
    LSTOP = 0
  END IF
  CALL DBFILE(LOP,ARRAY,JRCD)
  IF (JRCD .NE. 0) GO TO 110

  KEY=JRRAY(1,2)
*****
** KEY 1501 CONTAINS SURFACE DEFINITIONS

  IF(KEY .EQ. 1501) THEN
    Identify the contact surfaces and initialise relevant variable
    accordingly

*****
** KEY 1502 CONTAINS SURFACE FACET INFORMATION CORRESPONDING
TO KEY 1501
  ELSE IF(KEY .EQ. 1502) THEN
    Retrieve elements and nodes making up the contact surfaces and
    store them in corresponding variables

*****
  ELSE IF(KEY .EQ. 1911) THEN
    Identify the set names of the nodes making up contact surfaces

*****
** KEY 108 CONTAINS PORE PESSURE AT EACH NODE
C FIRST CARTILAGE
  ELSE IF(KEY .EQ. 108 .AND. SURFACE_N_SET .EQ. 'N_TOP') THEN
    Access and store the slave surface nodal pore pressure values in
    respective variables. Also record the maximum pore pressure on
    the slave surface and the node at which it is occurring

*****
C SECOND CARTILAGE
  ELSE IF(KEY .EQ. 108 .AND. SURFACE_N_SET .EQ. 'N_TOP_2') THEN
    Access and store the master surface nodal pore pressure values in
    respective variables

*****
** KEY 107 CONTAINS CO-ORDINATES OF EACH NODE
C FIRST CARTILAGE
  ELSE IF(KEY .EQ. 107 .AND. SURFACE_N_SET .EQ. 'N_TOP') THEN
    Access and store the slave surface nodal coordinates

*****
C SECOND CARTILAGE
  ELSE IF(KEY .EQ. 107 .AND. SURFACE_N_SET .EQ. 'N_TOP_2') THEN
    Access and store the master surface nodal coordinates

*****

```

```

** KEY 1503 CONTAINS CONTACT OUTPUT REQUEST DEFINITION
  ELSE IF(KEY .EQ. 1503) THEN
C FIRST CARTILAGE
  IF(ARRAY(6) .EQ. 'N_TOP') THEN
    Flag the beginning of the slave surface contact information

*****
** KEY 1504 CONTAINS NODE NUMBER IN CONTACT SURFACE
C FIRST CARTILAGE
  ELSE IF(KEY .EQ. 1504 .AND. K_NODE_SET .EQ. 'N_TOP') THEN
    Record the node number on the slave surface about which contact
    stress information will be printed in 'KEY 1511'

*****
** KEY 1511 CONTAINS CSTRESS VALUES
C FIRST CARTILAGE
  ELSE IF(KEY .EQ. 1511) THEN
    Access and store the slave surface nodal contact pressure values in
    respective variables. If contact pressure value is above the threshold,
    flag the node to be in contact otherwise not in contact. Also record
    the maximum contact pressure on the slave surface and the node at
    which it is occurring

*****
C SECOND CARTILAGE
C NO VALUES ARE PRINTED FOR MASTER SURFACE HENCE KEY 101 IS
USED
*****
** KEY 101 CONTAINS DISPLACEMENT VALUES FOR THE NODES
C FIRST CARTILAGE
  ELSE IF(KEY .EQ. 101 .AND. SURFACE_N_SET .EQ. 'N_TOP') THEN
    Record and add nodal displacement values to the slave surface node
    coordinates. Store these values in relevant variables. This is to be used
    only when NLGEOM is not used

*****
C SECOND CARTILAGE
  ELSE IF(KEY .EQ. 101 .AND. SURFACE_N_SET .EQ. 'N_TOP_2') THEN
    Record and add nodal displacement values to the master surface
    node coordinates. Store these values in relevant variables. This is to
    be used only when NLGEOM is not used

*****
C TOTAL CONTACT AREA
  ELSE IF(KEY .EQ. 1524) THEN
    Access and store contact area on the slave surface
  END IF
*****
120 CONTINUE
  END DO
110 CONTINUE

*****
C FIND THE POINTS IN CONTACT ON MASTER SURFACE

C OUTER LOOP IS OF MASTER SURFACE

  DO K21 = 1, NO_OF_ELEMENTS

```

DO K22 = 1, NO_OF_NODES

C FOR EACH NODE ON MASTER SURFACE SEARCH FOR THE NEAREST
NODES ON SLAVE SURFACE

DO K23 = 1, NO_OF_ELEMENTS

DO K24 = 1, NO_OF_NODES

**Calculate distances of slave surface nodes in X, Y and Z
direction from the master surface node under consideration.**

**Calculate the actual distance from those three distances. Find
2 closest nodes for 2D models and 4 nodes for 3D models**

END DO

END DO

C PASS COORDINATES OF CLOSEST SLAVE SURFACE NODES TO A
FUNCTION TO CALCULATE MASTER SURFACE NODE DISTANCE FROM
SLAVE SURFACE

CALL calcDist(PT1,PT2,PT3,PT4,PT5,NO_OF_DIM,DIST)

**Assume the node on the master surface to be in contact if its
distance from slave surface is smaller than the threshold. In some
curved surfaces and non-matching meshes, the master node may
not be exactly where slave surface node is. In this latter case, for
2D models, check if at least one closest slave node is in contact
(for 3D models check if at least two closest slave nodes are in
contact). If it is so, then the master surface node under consideration
is assumed to be in contact.**

END DO

END DO

C ASSIGN ATTRIBUTES OF THE MASTER SURFACE TO THE RESPECTIVE
ATTRIBUTES

C IN THE MAIN VARIABLE TO BE TRANSFERRED TO 'FLOW' SUBROUTINE
VIA

C COMMON BLOCK

C ASSUMPTION - SLAVE SURFACE WILL ATLEAST HAVE SAME NUMBER OF
ELEMENTS AS

C THAT OF MASTER SURFACE

C OUTER LOOP IS FOR SLAVE SURFACE

DO K_ELE_S = 1, NO_OF_ELEMENTS

DO K_NODE_S = 1, NO_OF_NODES

DO K_ELE_M = 1, NO_OF_ELEMENTS

DO K_NODE_M = 1, NO_OF_NODES

**Calculate the distances of the slave node from the master nodes.
Record the closest master surface node to the slave node under
consideration**

END DO

END DO

Assign the master surface node parameters to the corresponding variables in common block

END DO
END DO

C CALCULATE FLUID LOAD SUPPORT

DO K_EINDX = 1, NO_OF_ELEMENTS

For each element, calculate average the nodal pore pressure and nodal contact pressure values by taking sum of pressure values at all element nodes and dividing by number of nodes. Pass the nodal coordinates to the function to calculate elemental area.

CALL calcArea(PT1,PT2,PT3,PT4,NO_OF_DIM,AREA)

Calculate the contact force and fluid force on this element by multiplying the respective average pressure values with area. If contact force on an element is non-zero then count that element area towards the contact area. Calculate the normal vector direction of the element under consideration along which contact and fluid force will act

CALL calcAngles(PT1,PT2,PT3,PT4,NO_OF_DIM,ANG_X,ANG_Y,ANG_Z)

Resolve the contact and fluid forces in the three directions and sum the components in each direction

END DO

Calculate total contact force and total fluid force for the whole slave surface. The contact pressure in cartilage-cartilage models is effective pressure and hence fluid force needs to be added to contact force calculated here to get total contact force. In a rigid indenter/prosthesis against cartilage models, the contact pressure is total and no such addition is required.

Calculate total fluid load support by dividing fluid force by total contact force

RETURN
END

C#####
SUBROUTINE FLOW(H,SINK,U,KSTEP,KINC,TIME,NOEL,NPT,COORDS,
1JLTYP, SNAME)

C
INCLUDE 'ABA_PARAM.INC'

C
DIMENSION TIME(2), COORDS(3)
CHARACTER*80 SNAME

TYPE ELE_DATA
SEQUENCE

```

DOUBLE PRECISION :: NODE_COORD(24)
DOUBLE PRECISION :: NEW_NODE_COORD(24)
DOUBLE PRECISION :: OPP_NODE_COORD(24)
DOUBLE PRECISION :: NEW_OPP_NODE_COORD(24)
DOUBLE PRECISION :: IPT_COORD(24)
DOUBLE PRECISION :: NEW_IPT_COORD(24)
DOUBLE PRECISION :: OPP_IPT_COORD(24)
DOUBLE PRECISION :: NEW_OPP_IPT_COORD(24)
DOUBLE PRECISION :: POR(8)
DOUBLE PRECISION :: OPP_POR(8)
DOUBLE PRECISION :: CPRESS(8)
DOUBLE PRECISION :: OPP_CPRESS(8)
DOUBLE PRECISION :: ELE_CAREA
DOUBLE PRECISION :: OPP_ELE_CAREA
DOUBLE PRECISION :: AVG_CPRESS
DOUBLE PRECISION :: OPP_AVG_CPRESS
DOUBLE PRECISION :: AVG_POR
DOUBLE PRECISION :: OPP_AVG_POR
DOUBLE PRECISION :: CPRESS_F
DOUBLE PRECISION :: POR_F
DOUBLE PRECISION :: ANGLE_X
DOUBLE PRECISION :: ANGLE_Y
DOUBLE PRECISION :: ANGLE_Z
DOUBLE PRECISION :: DUMMY(5)
INTEGER :: ELE_NUM
INTEGER :: OPP_ELE_NUM
INTEGER :: DUMMY2(22)
INTEGER :: NODE_NUM(8)
INTEGER :: OPP_NODE_NUM(8)
INTEGER :: IPT_NUM(8)
INTEGER :: OPP_IPT_NUM(8)
INTEGER :: IS_CONT(8)
INTEGER :: OPP_IS_CONT(8)
END TYPE ELE_DATA

```

```

TYPE (ELE_DATA) :: K_ELE_DETAILS(12000)

```

```

COMMON K_ELE_DETAILS

```

```

*****

```

```

CHARACTER*80 CNOEL, CNPT
INTEGER :: NO_OF_NODES
INTEGER :: NO_OF_ELEMENTS
INTEGER :: NO_OF_DIM

```

```

PARAMETER (THRESHOLD_PRESS_DIFF=1.0D-1)

```

```

*****

```

```

NO_OF_NODES = 4
NO_OF_ELEMENTS = 12000
NO_OF_DIM = 3

```

```

*****

```

```

WRITE(CNOEL,*) NOEL
WRITE(CNPT,*) NPT

```

```

C S_CART IS A SLAVE SURFACE AND S_CART_2 IS A MASTER SURFACE; 'H'

```

IS A SEEPAGE COEFFICIENT and 'SINK' IS A SINK PORE PRESSURE

IF(SNAME .EQ. 'S_CART') THEN

Find the closets node to the integration point under consideration

IF(**node is not in contact**) THEN

IF(**pore pressure is greater than or equal to zero**) THEN

SINK = 0

H = 1

ELSE

SINK = 0

C MAKE H = 0; IF FLUID IS NOT TO FLOW INSIDE

H = 0

END IF

ELSE IF(**node is in contact**) THEN

Find the pressure difference of the current node and its opposite node. If this pressure difference is smaller than the threshold, assign it a zero value. Assign pore pressure of opposite node to be SINK pressure

IF(**pressure difference is zero**) THEN

C NO FLOW ACROSS THE CONTACT INTERFACE

C H = 0

H = 0

ELSE

C FLOW IN DECREASING PORE PRESSURE DIRECTION

C H = 1

H = 1

END IF

END IF

END IF

IF(SNAME .EQ. 'S_CART_2') THEN

Find the closets node to the integration point under consideration

IF(**node is not in contact**) THEN

IF(**pore pressure is greater than or equal to zero**) THEN

SINK = 0

H = 1

ELSE

SINK = 0

C MAKE H = 0; IF FLUID IS NOT TO FLOW INSIDE

H = 0

END IF

ELSE IF(**node is in contact**) THEN

Find the pressure difference of the current node and its opposite node. If this pressure difference is smaller than the threshold, assign it a zero value. Assign pore pressure of opposite node to be SINK pressure

IF(**pressure difference is zero**) THEN

C NO FLOW ACROSS THE CONTACT INTERFACE

C H = 0

H = 0

ELSE

C FLOW IN DECREASING PORE PRESSURE DIRECTION

```

C H = 1
      H = 1
      END IF
    END IF
  END IF

  RETURN
  END
C#####
C OTHER SUBROUTINES USED TO COMPUTE VARIOIUS VARIABLES

  subroutine calcArea(p1, p2, p3, p4, noOfDim, area)

c This subroutines calculates element surface area

  if(two dimensional axisymmetric model) then
    Calculate circular area with distance between two nodes as radius
  else if(three dimensional model) then
    Calculate area by dividing the quadrilateral into two triangles and then
    calculating individual triangle areas and adding them together
  end if

  return
  end

  subroutine calcAngles(p1, p2, p3, p4, noOfDim, angX, angY, angZ)

c This subroutine calculates the direction of normal vector

  if(two dimensional model) then
    Calculate first vector based on the coordinates of two nodes. Second
    vector is (0,0,1)
  else if(three dimensional model) then
    Calculate the two vectors based on the coordinates of three nodes
  end if

c Normal vector is the cross product of two diagonal vectors

  Calculate the magnitude and direction of the normal vector

  return
  end

  subroutine calcDist(p1, p2, p3, p4, p5, noOfDim, dist)

c This subroutines calculates the distance of one node from the surface formed by
other 4 nodes.

  if(two dimensional model) then
    Calculate first vector based on the coordinates of two nodes. Second
    vector is (0,0,1)
  else if(three dimensional model) then
    Calculate the two vectors based on the coordinates of three nodes
  end if

```

Calculate the magnitude and direction of the normal vector. From this calculate unit normal vector

Calculate vector from the coordinates of a node whose distance is being calculated and any of the four nodes making the surface

c Dot product of unit normal vector and vector formed last will give the distance

Calculate the distance

return
end

B.2 A rigid Impervious Surface against Cartilage Surface

The subroutines used in this case were similar to those given in **Section B.1** except for a few changes as stated here:

- 1) Details of only slave cartilage surface were kept as master was a rigid surface. This would make the data structure for the master surface redundant.
- 2) Surface fluid flow boundary conditions were imposed only on slave cartilage surface.
- 3) The contact stresses in this formulation were total and hence calculations for total fluid load support did not involve addition of contact and fluid pressures.

Appendix C Verification of Biphasic Jump Condition

Biphasic jump condition has been stated in **Equation (2.1)**. As mentioned in **Section 2.2.1**, when two cartilage surfaces are in contact, the jump condition is reduced to the form given in **Equation (2.2)**. According to this equation the flow of fluid is from the surface with higher fluid pressure towards the one with lower fluid pressure. However, due to the nature of problems analysed throughout this thesis, it was not possible to show this. Hence a two-dimensional plane strain model (ABAQUS., 2007), as shown in **Figure C.1** was created and analysed for three surface fluid flow conditions: free flow, no flow (sealed) and contact dependent flow. It should be noted that this model was created and analysed only to show fluid exchange between cartilages using the algorithm proposed in **Chapter 2**.

The model consisted of five elements with upper two (depicting upper cartilage) contacting the lower three (depicting lower cartilage). The size of each element was 1 mm x 1 mm. 4-node bilinear displacement and pore pressure plane strain (CPE4P) elements were used.

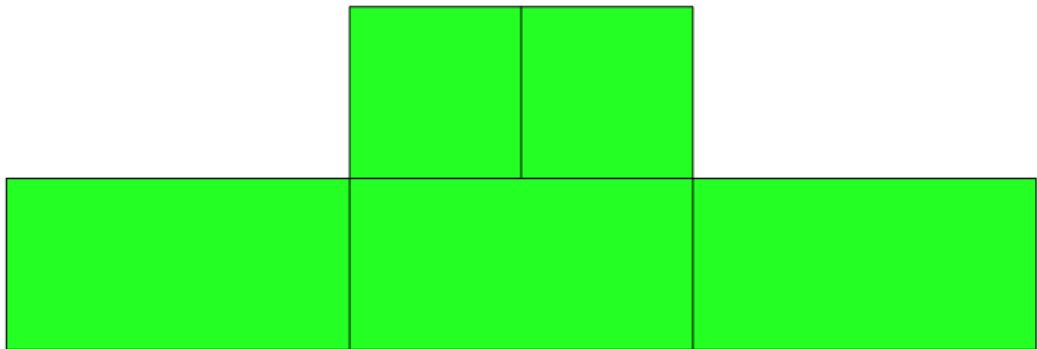


Figure C.1 Two-dimensional plane strain model of contact mechanics of poroelastic elements

The material properties used in the model are given in **Table C.1**. Elements were assigned 100 MPa of initial fluid pressure.

The bottom nodes of the lower three elements were constrained in both horizontal and vertical directions. The uppermost nodes of the upper two elements were constrained only in the horizontal direction. The surface made of upper elemental surfaces of lower three elements was made master whereas the surface

made of lower elemental surfaces of upper two elements was made slave. Contact was assumed to be frictionless and surface to surface contact was formulated. The surface fluid flow boundary conditions were imposed using algorithm proposed in **Chapter 2**. To implement all three surface flow conditions relevant changes were made only in the algorithm and model was not altered.

Table C.1 Material properties used in the biphasic jump condition model (ABAQUS., 2007 and Federico *et al.*, 2004)

Parameter	Value
Young's modulus, E	36×10^6 MPa
Poisson's ratio, ν	0.106
Permeability, k	1.0×10^{-16} m ⁴ /N.s
Void ratio, e	4.2 (approx. 80.75 % interstitial fluid)
Seepage coefficient, k_s	1 mm ³ /N.s – Flow 0 mm ³ /N.s – No flow

A uniformly distributed load (pressure) of 100 N/mm² was applied vertically downward on the uppermost elemental surfaces of the upper two elements. This load was applied in 1 second and was then maintained for further 300 seconds.

The fluid flow after 1 second of loading has been shown in **Figure C.2** for all three surface fluid flow boundary conditions. The difference in this flow was due to the different surface fluid flow boundary conditions assumed in three cases. In free flow condition (**Figure C.2a**), the fluid from the lower elements seemed to flow towards the upper elements. In this case, the fluid velocity was almost zero and was of the order 10^{-13} mm/s. This was as expected since free flow conditions did not offer any resistance to fluid flow. On the other hand, in sealed (**Figure C.2b**) and contact dependent flow (**Figure C.2c**), the magnitude of fluid velocity was of the order of 10^{-6} mm/s. When the surfaces were sealed, the fluid flowed away from these surfaces. However, as already discussed in **Chapter 2**, imposition of contact dependent surface fluid flow boundary conditions was the most realistic way of investigating contact mechanics problem involving cartilage. Moreover, it was the only model in the current analysis to show cartilage-to-cartilage fluid exchange. This was possible only because of the difference in surface fluid pressure, though, this difference was smaller than 1 Pa. Fluid flowed in both the directions based on the magnitude of pressure.

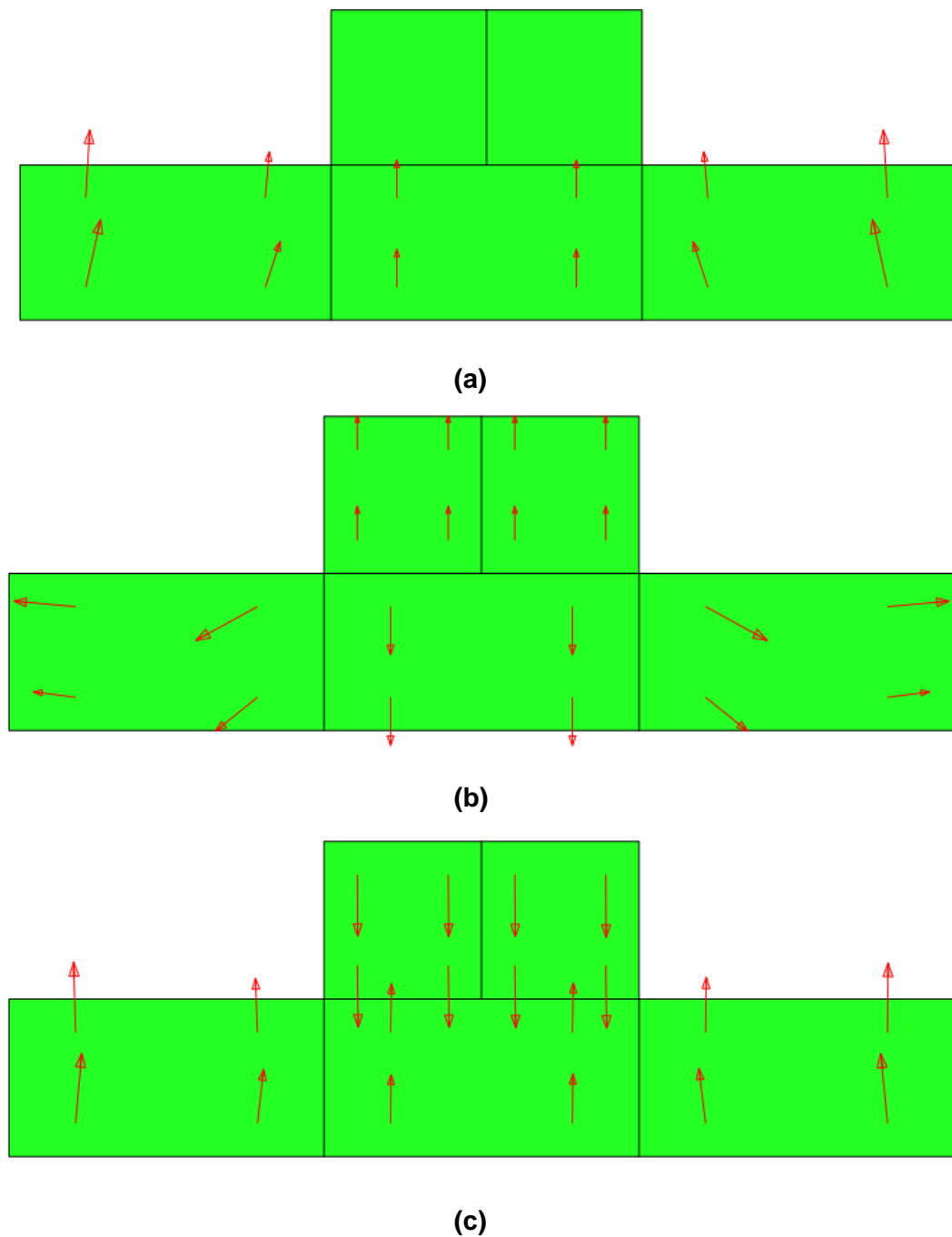


Figure C.2 Fluid velocity vectors after 1 second of loading for (a) free flow, (b) sealed surface flow and (c) contact dependent surface fluid flow conditions

The biphasic jump condition, in contact dependent model, worked as intended. This clearly showed that the contact detection and imposition of surface fluid flow based on that contact information as proposed in **Chapter 2** would allow cartilage to cartilage fluid exchange when the fluid pressures are different.

Appendix D Mesh Sensitivity Analysis

A series of meshes with increasing number of elements needs to be analysed before using any mesh for the final analysis. This ensures not only greater accuracy of solution but also helps avoid using unnecessarily dense mesh thus reducing simulation time.

In the models analysed in this thesis, mesh sensitivity analysis was carried to ensure that the difference in predictions between two consecutive meshes was always less than 5%. In this section, a typical mesh sensitivity analysis is discussed.

The model used for this has been discussed previously in **Section 2.2.2**. It should be noted that the final mesh used in the actual analysis was denser in the loaded region and coarser in non-loaded region to reduce simulation time further. However, the mesh used here was only for the purpose of discussing the concept of mesh sensitivity analysis and hence was kept uniform throughout the cartilage surface (**Figure D.1**) for ease of understanding. Moreover, as an example, only fluid pressure prediction is included in this discussion.

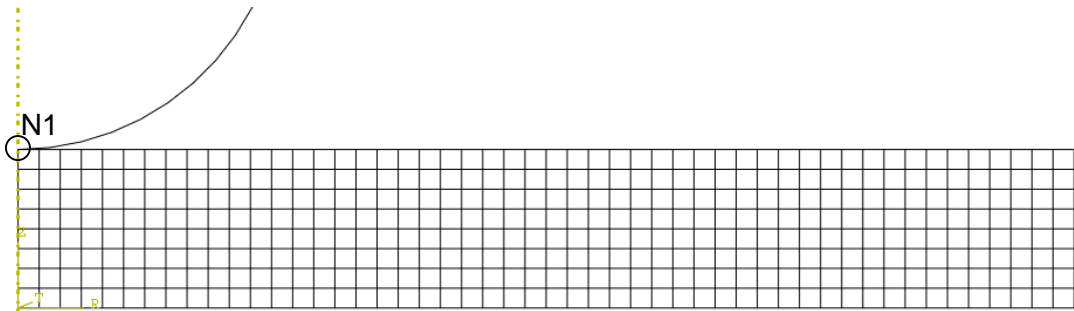


Figure D.1 First uniform mesh used for mesh sensitivity analysis discussion

The number of elements in the first mesh was 400. They were created by assigning seeds of 0.4 mm. This created elements of approximately 0.4 mm × 0.4 mm dimension. For the second mesh the seed was decreased to 0.3 mm. **Table D.1** shows the number of elements, fluid pressure prediction at the cartilage surface node on the axis of symmetry (node N1) and the percentage difference in predictions between consecutive meshes.

Table D.1 Predictions in mesh sensitivity analysis

Approximate Global Element Size (mm)	Total Number of Elements	Fluid Pressure at node N1 (MPa)	Error (%)
0.4	400	0.232	--
0.3	670	0.165	28.96
0.2	1500	0.174	5.78
0.1	6000	0.166	4.68
0.05	24000	0.165	0.43

As can be seen from **Table D.1**, the error in predictions between consecutive meshes reduced as the mesh was made finer. The error between fluid pressure predictions using the mesh with 1500 elements and 6000 elements was 4.68% and hence the latter mesh would be used. The mesh with 24000 elements predicted more accurate fluid pressure but this would come at a higher computational cost.

Appendix E Publications

E.1 Published

E.1.1 Journals

- 1) Pawaskar, S. S., Fisher, J., and Jin, Z., 2010, "Robust and General Method for Determining Surface Fluid Flow Boundary Conditions in Articular Cartilage Contact Mechanics Modeling," *Journal of Biomechanical Engineering*, 132(3), pp. 8 (031001).

E.1.2 Conferences

- 1) Stops, A., Pawaskar, S., Wilcox, R., and Jin, Z. Biphasic lubrication of cartilage modelled using a friction coefficient dependent on the instantaneous fluid load support. In: *The 18th Annual Symposium on Computational Methods in Orthopaedic Biomechanics*. 2010, Tulane University, College of Science and Engineering, New Orleans, LA, USA.
- 2) Pawaskar, S. S., Ingham, E., Fisher, J., and Jin, Z. M. Importance of clearance on contact mechanics of hemiarthroplasty in hip joints. In: *55th Annual Meeting of the Orthopaedic Research Society*. 2009, Las Vegas, NV, **34**. Poster No.: 2405.
- 3) Pawaskar, S.S., Jin, Z., Ingham, E., and Fisher, J. A novel, generic and robust approach to the contact analysis of articular cartilage. In *Journal of Biomechanics, 16th Congress, European Society of Biomechanics* (Eds. R. Huiskes and Guilak, F.), Lucerne, Switzerland, 2008, S302, Presentation O-299.

E.2 Under Review/Submitted

E.2.1 Journals

- 1) Pawaskar, S. S., Ingham, E., Fisher, J., and Jin, Z. Hemiarthroplasty of the hip joint with biphasic acetabular cartilage: Effect of clearance on fluid load support and contact mechanics. **Submitted**.

- 2) Pawaskar, S. S., Ingham, E., Fisher, J., and Jin, Z. Fluid load support and contact mechanics of hemiarthroplasty in the natural hip joint. **Submitted.**

E.3 To be Submitted

E.3.1 Journals/Conferences

- 1) Pawaskar, S. S., Ingham, E., Fisher, J., and Jin, Z. Experimental validation of hemiarthroplasty hip joint using porcine model. 2010. **To be submitted.**
- 2) Pawaskar, S. S., Ingham, E., Fisher, J., and Jin, Z. Contact mechanics and fluid load support in natural hip joint. 2010. **To be submitted.**